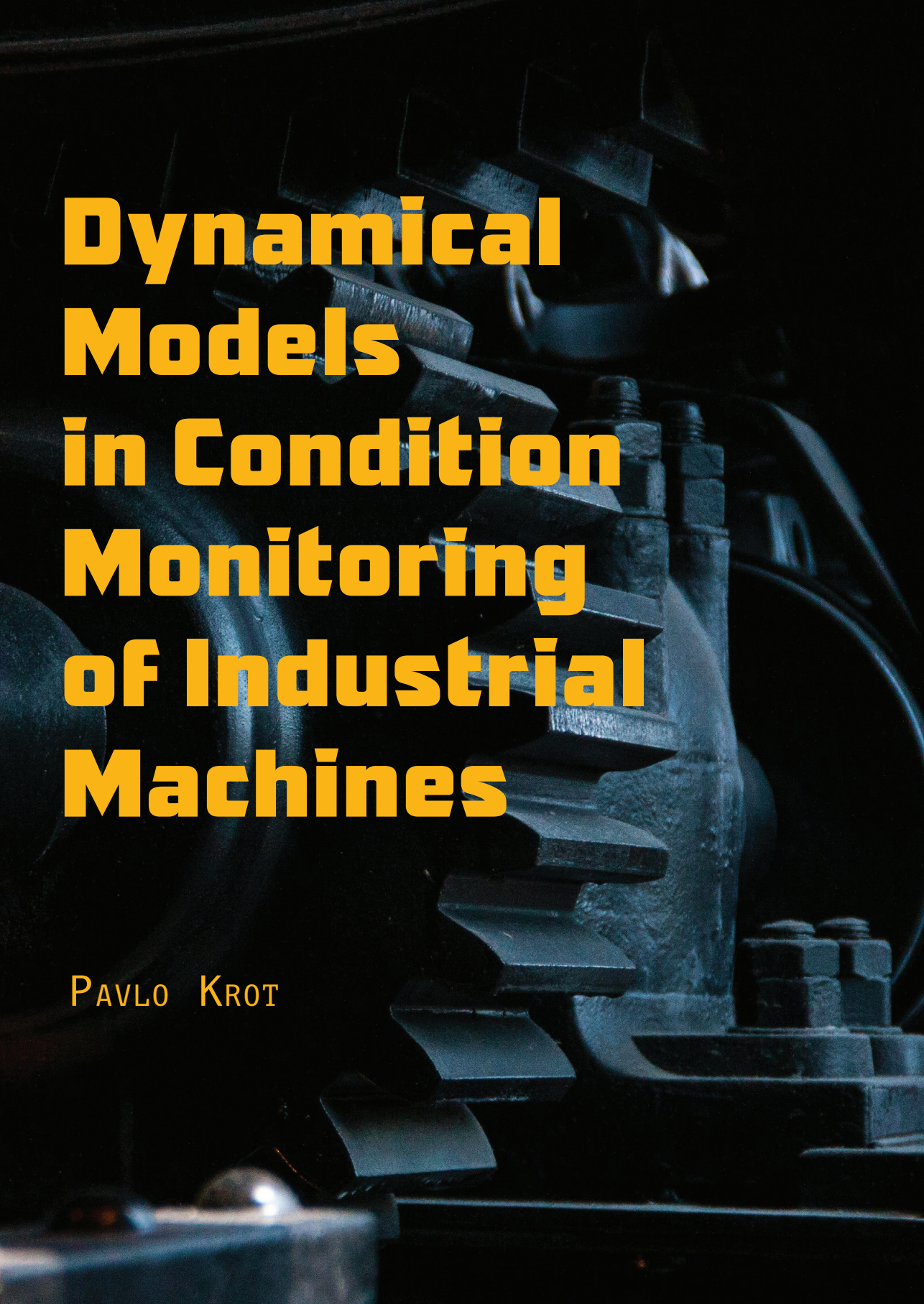

Dynamical Models in Condition Monitoring of Industrial Machines

Pavlo Krot

Pavlo Krot

Dynamical Models in Condition Monitoring of Industrial Machines

WUST Publishing House, Wrocław 2024

Reviewers
Łukasz Warguła
Piotr Przystałka

Editing and linguistic verification
Agnieszka Piasecka-Ceccato

Cover design
Dominika Osadców-Będkowska

Layout design and paging
Małgorzata Szafran
Janusz M. Szafran

WUST PUBLISHING HOUSE
Wybrzeże Wyspiańskiego 27, 50-370 Wrocław, Poland
https://www.oficyna.pwr.edu.pl
e-mail: oficwyd@pwr.edu.pl, zamawianie.ksiazek@pwr.edu.pl

ISBN 978-83-7493-279-0
DOI: 10.37190/PavloKrot2024

Print and binding
beta-druk, www.betadruk.pl

"The only things which went wrong were items we did not have a good simulation for."

Quote from the US Apollo space program

CONTENTS

ABBREVIATIONS

CAN – controller area network
CBM – condition-based maintenance
CMMS – computerised maintenance management systems
CRM – cold rolling mill
DCT – deep cryogenic treatment
DOF – degree of freedom
ECU – electronic control unit
ERP – enterprise resource planning
FEM – finite element model
FFT – fast Fourier transform
FM – frequency modulation
FRF – frequency response functions
HAGC – hydraulic automatic gauge control
HRM – hot rolling mill
HT – hauling truck
LHD – load-haul-dump vehicle
MMDS – multi-motor drive system
MTBF – mean time between failures
NDT – non-destructive testing
PHM – prognostics and health management
PM – predictive maintenance
PWM – pulse width modulation
RSM – reducing sizing mill
RUL – remaining useful life
SHM – structural health monitoring
TAF – torque amplification factor

ABSTRACT

This book contains results of the theoretical and experimental research of mining machines and rolling mills aimed at the development of new methods for their condition monitoring and vibration damping. Instead of the usually used data-driven methodology, the proposed approach is based on several known classes of dynamical models, of which some appropriate ones have been implemented for monitoring certain types of machines and technological processes.

The non-stationary operational regimes excite natural modes of vibrations in machines and transient signals are used for diagnosing wear of some elements, namely, angular backlashes in drivelines, radial clearances in the bearings, stiffness changes in structural elements and loosening of bolted joints.

In every case, a detailed modal analysis of machines' structures has been conducted to undermine the root causes of high dynamics and resonance phenomena. Linear systems of machines are assumed as reference points in diagnostic algorithms, while the nonlinear features are used for the detection of certain part condition deterioration and process control. Not only mechanical shocks and vibration but also hydraulic systems and structural steel properties are considered, and strength capacity is improved by the mathematical models.

The proposed approach allowed the development of efficient solutions for real dynamical problems, e.g. torsional loads monitoring and remaining useful life prediction in articulated underground vehicles, chatter vibration control in rolling mills of different types, sieving screens diagnostics, structure optimisation and control of hydraulic machines, enhancement of treated material quality.

The developed methods of condition monitoring and diagnostics are realized in online computerized automation and maintenance management systems implemented in different industrial plants.

By logical structure, the book is divided into several parts. Chapter 1 introduces in operational conditions and failure modes of investigated industrial machines. Chapter 2 represents state-of-the-art condition monitoring of different

heavy-duty machines. Chapter 3 describes the classes of dynamical models used in research and the particularities of their simulation. Chapter 4 represents applications of dynamical models in condition monitoring and analysis of industrial machines. Chapter 5 describes the developed instrumentation for torque and backlash measurement in the drivelines. Chapter 6 represents model-based methods of wear diagnostics in the units of industrial machines. Chapter 7 explains the developed approaches to technological process stability monitoring, dynamics control and active vibration damping in rolling mills and mining machines. Chapter 8 highlights the industrial applications of the developed automation systems. General conclusions are formulated at the end of the book.

The results represented in this book were obtained by the author previously on the rolling mills at the Z.I. Nekrasov Iron and Steel Institute of the National Academy of Sciences of Ukraine (Dnipro) and recently on the mining machines in the Faculty of Geoengineering, Mining and Geology of the Wroclaw University of Science and Technology in Poland. The author is very thankful to his colleagues from both institutions as well as to the plant staff for support in industrial trials and assistance in implementation of the developed systems.

The author believes that research results presented in this book will be useful for solving problems of dynamics reducing, real failures analysis and increasing durability of plants, condition monitoring and vibration damping in industrial machines with a complicated structure and severe loading.

1. INTRODUCTION

The main reasons limiting the productivity and overall efficiency of industrial machines are the sudden failures in the drivelines and other units from mechanical overloads, cyclic fatigue or operator errors, which cause durable downtimes of mechanical equipment.

World trends in the control systems development for large rotating units show that under conditions of constant intensification of production in terms of processing speed and level of loads, the boundaries between automated purely control systems and supervision systems, i.e. condition monitoring and diagnostics, over the equipment operation are gradually blurring. Since the reliability and efficiency of the entire continuous technological chain depend on the reliability of every unit.

Studies of mining and metallurgical equipment show that the total maintenance and repair costs over the life cycle will be 75% of the new machine's cost. The cost of equipment repair is about 20% of the cost of product manufacturing; therefore, service departments employ about 35% of the total number of personnel (except in the case of outsourcing). Implementing predictive maintenance results in a 25–30% reduction in maintenance costs, a 70–75% decrease in breakdowns and a 35–45% reduction in downtime along with many other benefits. Also, predictive maintenance saves about 8–12% over preventive maintenance, and up to 40% over reactive maintenance. In the case of emergency failures of large-scale elements of equipment, as a rule, several adjacent parts fail and some amount of product is lost. With the intensification of processing technologies, an increase in the cost of repair and maintenance of equipment is predicted, while poor maintenance strategies can reduce a plant's overall productive capacity by up to 20% [1].

Although modern ubiquitous digitising makes it possible to record numerous parameters of technological processes and machine operation, some important data on mechanical loads are still not available for sensing due to harsh working

conditions in mining and metallurgy. Especially difficult to monitor multibody systems when dynamical loads are quite different in the elements depending on machine design. Quickly increasing wear of elements and backlashes gaps opening under transient loading make the system nonlinear, and installing costly sensors in numerous couplings becomes inefficient. The traditional data-driven approach in diagnostics of machines can be combined with model-based condition monitoring, which assumes the creation of appropriate soft-sensors for observation of machine units where sensors are not installed. This approach is under development in this book and its application is illustrated by the examples from industrial applications.

The Computerised Maintenance Management Systems (CMMS) at enterprises of the mining and metallurgical industry, as a rule, solve individual tasks of forming a portfolio of orders for the purchase of spare parts and optimal planning of machine fleet renovation. Despite the obvious benefits of accumulating statistics on failures and Remaining Useful Life (RUL) of operation of individual elements of machines, such a function is implemented only in advanced examples of CMMS as an additional option. Although planning the procurement of large expensive equipment for drivelines (couplings, shafts, gears, spindles) can provide a significant share of cost savings on spare parts for large enterprises. At present, because of the lack of data on the RUL of the units and the high probability of sudden failures, the machines service departments are forced to keep in warehouses double sets of spare parts for the main units because the terms of unique parts supply can be up to several months or longer. The advantages of CMMS are obvious; however, up to 80% of all attempts at CMMS implementation fail and users do not use all the functions offered by the software [1].

Existing automated control systems make it possible to obtain and accumulate large amounts of information about the current parameters of the technological process and the loads of the equipment, mainly electric drives. This information is used primarily for its intended purpose in the process of regulation and control. The studies presented in this book are aimed at improving the methods of dynamic analysis and statistical calculations of loads, which make it possible to increase the efficiency of using the information accumulated in digital form to improve the operation of the equipment and the stability of the technology.

The use of science-intensive developments for the identification and modelling of technological and mechanical systems of mining machines and rolling mills extends the functionality of existing process control systems. Without sig-

nificant additional costs, it becomes possible to solve the problems of optimal control from the viewpoint of the minimum probability of equipment failures during operation based on new methods of load monitoring and wear diagnostics in multibody systems.

1.1. Operational conditions of mining and metallurgical plants

Global digitalization of industrial plants [2] promotes effective approaches to prognostics and health management (PHM) of machines [3, 4]. Data-driven techniques are developed for monitoring [5], online identification [6] and model-based diagnostics [7]. The main players in heavy industry machinery: Epiroc, Caterpillar, Primetals Technologies, SMS Siemag, Danieli, NKMZ and other independent IT companies propose the Computerized Maintenance Management Systems (CMMS) in the market, which can be integrated into Enterprise Resource Planning (ERP) systems [8]. The advanced function of remaining useful life (RUL) estimation, if included, is usually based on either failure statistics of certain parts or by special signal processing methods with a short horizon of failure prediction when a first-level alarm has been generated. Algorithms of failure prediction include machine health indicators composed of different parameters of vibration [9, 10].

Advanced methods of condition monitoring and vibration diagnostics systems developed for heavy machinery should account for non-stationary loads and speeds [11], be adaptive to variable working conditions [12, 13] and support the RUL prediction function [14, 15]. Implementation of CMMS on large-scale industrial machines is a long-lasting process because some parts have a mean time between failures (MTBF) of more than one year. Using similar elements from neighbouring machines for building models of RUL and failure prediction is not feasible because of different working conditions. Therefore, world steel manufacturers like Tata Steel and ArcelorMittal are developing their systems for specific equipment and processes [16, 17]. The major efforts are applied in cold rolling mills to chatter vibration monitoring, which affects output product quality [18].

Heavy industrial machines, e.g., hot rolling mills, are characterized by high torsional dynamics, correspondingly, torque monitoring systems are used, e.g., of ACIDA (VOITH) [19], KMT Telemetry [20] and some others [21], which are based on wireless telemetry and strain gauges installed on rotating shafts. Methods and

models are developed for torque signal processing for diagnostic purposes [22, 23] based on torsional modes analysis.

Although mechanical torque measurement systems are efficient for load monitoring, their implementation is limited to spindles with enough long service time, because mounting strain gauges is problematic on frequently replaced shafts. Therefore, some condition monitoring methods are developed based on electric motor current analysis [24, 25]. However, measurement of either electrical motor current or mechanical torque in only one point of multibody drivelines does not allow determining dynamic loads and RUL predicting in elements.

1.2. Failure modes of heavy-duty machines

Currently, raw material processing plants and steel manufacturers are facing a problem how to increase the reliability of existing heavy machines. The main elements of drivelines were not initially designed for such harsh working conditions and, in addition, undergo deterioration. The use of high-grade materials for different applications increases the cost of machines. The increase in reliability can be achieved by passive damping of excessive dynamic loads [26, 27], active torsional vibration control [28–30], load distribution [31], optimization of technology [32] and machine unit tuning [33]. Although some efficient methods and technologies are developed to increase the wear resistance of elements made of alloy steels, e.g., Deep Cryogenic Treatment (DCT), severe failures occur [34–36] in heavy-duty machines (Fig. 1.1).

The failures in the mining machines can cause severe consequences, especially in the underground mines. For example, the stoppage of multi-kilometres

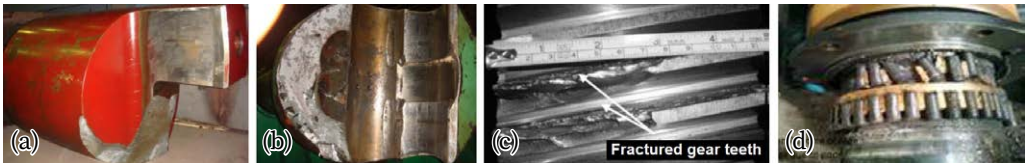

Fig. 1.1. The most critical failures in the drivelines:
(a) cracked cardan coupling due to high inclination angle [26]; (b) spindle head damaged by overload [26]; (c) gear teeth breakage due to shaft inclination [34];
(d) bearing jamming due to improper clearance [35]

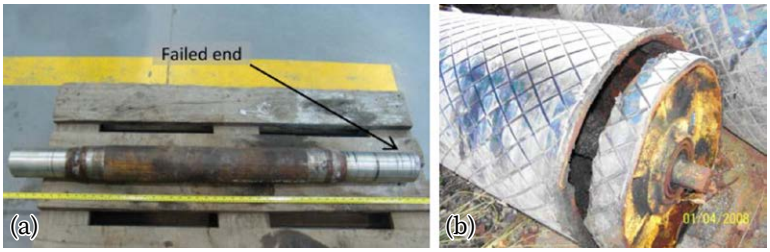

Fig. 1.2. The failures of belt conveyor elements:
(a) drive shaft damage [37]; (b) breakage of conveyor pulley due to fatigue [38]

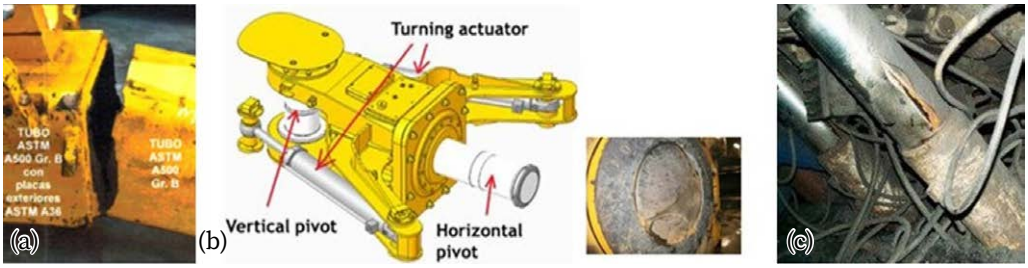

Fig. 1.3. The failures of underground mining machines:
(a) fatigue crack in drilling rig arm of mobile machine [39];
(b) breakage of horizontal pivot in the underground articulated vehicle [40];
(c) fracture of cylinder in a hydraulic roof support due to dynamic loading [41]

conveyors, urgent evacuation of mobile articulated vehicles, and the necessity of hydraulic cylinder replacement in powered roof support in a confined space, etc. (Figs. 1.2 and 1.3).

Deep underground mining machines and mechanisms are subjected to even more harsh environmental factors: high temperatures (up to +45°C) and humidity (above 90%), which lead to quick degradation of structural materials due to excessive corrosion and crack initiation even under protective coatings.

The vibrating machines are widely used in the separation of different fractions of materials in minerals processing enterprises (Fig. 1.4a). Sieving efficiency is greatly dependant on the trajectories of periodical motion of the particles and sieving decks. The key design parameters of the screening process are such as the vibrator drive power, synchronisation of unbalanced masses and oscil-

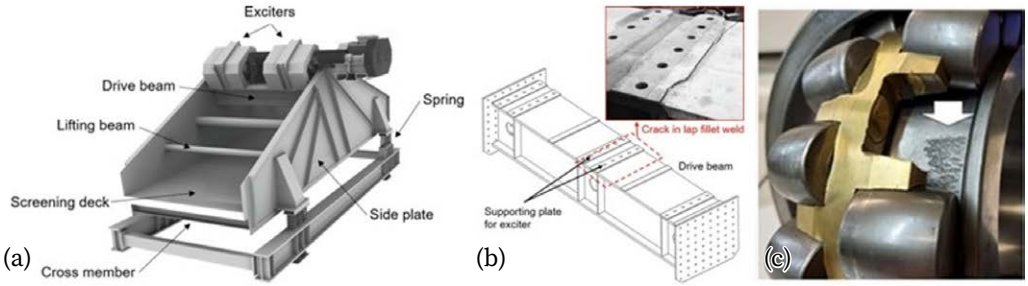

Fig. 1.4. (a) Vibrating screen; (b) fractured drive beam [42];
(c) damage of bearing in vibrator [43]

lation frequency as well as the stiffness of supporting springs. Deterioration of supporting springs (stiffness reduction and cracks) due to cyclic loading and fatigue are difficult to determine by visual inspection, static loading tests or non-destructive testing techniques. Structural elements with welded joints can also be damaged by cyclic fatigue. The beam for carrying unbalanced excitation drives is the most stressed element, whose fracture is shown in Figure 1.4b. Although only a special series of double-row tapered roller bearings are used in vibrating sieving screens, they are also subjected to damages, which affect the trajectory of motion (Fig. 1.4c).

Installation of fully new equipment is a rare case, while the maintenance staff needs computerized tools to predict abrupt failures and to share investments for replacement of spare parts and repairs planning. The most efficient way to detect hidden damages in the machines is their condition monitoring.

Based on numerous research projects conducted in different types of industrial plants, the author can state that angular and radial backlashes in the gearboxes and other elements of rotating machines are the most important parameters of their technical condition and the root cause of local defects and fatigue failures. Common world trends in Condition-Based Maintenance (CBM) and Predictive Maintenance (PM) require new approaches, which are based on adaptive models of complicated industrial plants and appropriate software for their implementation in practice.

2. STATE-OF-THE-ART CONDITION MONITORING OF INDUSTRIAL PLANTS

Every category of mining and steel processing machines has its specific features determined by their functions and technology, which require appropriate diagnostic procedures and methods of defect detection. Based on a literature review on condition monitoring and process control with different types of signals, the detailed classification of known methods and tools is given with an emphasis on specific methods applicable for non-stationary regimes of operation and harsh working conditions.

2.1. Classification of systems and methods

The most general schematic representation of the Condition-Based Maintenance (CBM) process is given in Figure 2.1. It consists of data acquisition, signals processing to obtain fault-related parameters and maintenance decision-making.

The diagnostic signals available for online acquisition are analysed in Table 2.1. This classification does not include the Non-Destructive Testing (NDT) techniques, e.g., Liquid Penetrate Inspection (LPI), Magnetic Particle Inspection (MPI), Eddy Current Testing (ECT), Ultrasonic Testing (UT), Radiography Testing (RT), Hardness Testing (HT), which can characterise materials properties and defects but require stoppage of rotating machines for a long time and manual operations for certain elements diagnostics.

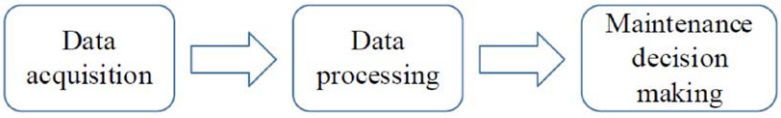

Fig. 2.1. General scheme of the condition-based maintenance process

Table 2.1. Data acquisition classification

Parameter	Advantages	Limitations	Sensors
Vibration	• Relatively low costs for multi-channel signal acquisition • Continuous measurement and processing • Detection of different faults • Close to components location • Wide frequency domain • Sensors durability	• Sensors on every shaft • Speed rotation sensors on shafts • High-cost laser sensors • Special skills for installing sensors • Sensitive to noise, speed and load variation	Accelerometers Proximeters Laser sensors
Electric motor current	• A non-intrusive method • Low-cost multi-channel acquisition • Easy implementation • No additional sensors • Detection of electrical motor faults	• Low sensitivity to damages in long drivelines • Less sensitive to weak fault features in bearings • Various harmonics from the power supply system	No special sensors
Acoustic emission	• Detecting small damages • Monitoring of large surfaces • Subsurface micro-damage detection • Method for friction condition monitoring	• Difficult signal processing • Huge raw data for storing • Signals attenuation and reflections • Internal noise interference • Relatively high costs	Special sensors Array of microphones
Temperature	• Simple amplitude alarms • Low costs and noise-resistant • Remote sensing method • One thermal image reflects the overall object condition	• Long time for heating up of damaged component • Sensitive to environment • Complicated processing of thermal images	Thermocouples Thermal imaging cameras IR sensors

Torque	• Non-invasive • Contains information about the whole driveline • Can detect many defects • The only method for resonance detection	• Can detect only defects in torsional elements • Sensors are complicated to install • Need telemetric data transfer modules	Strain gauges Telemetry modules
Oil/debris	• Close relationship with wear surface profile • Long persistence of information and powerful anti-interference capability	• Needs a closed-loop lubricating system • Difficult to identify damage to components made of the same metal	Special sensors and off-line analyzers
Image/Video	• Non-invasive • Low cost • Similar to human inspection • Applicable for drones • Thermal imaging applications	• Requires good lighting • More sensitive to dust • Difficult to identify internal damages • More complicated data processing	Standard or high-speed cameras

Vibration signals are the most widely used source of information in condition monitoring. Sensors (accelerometers) have comparatively low cost. However, installation of the required quantity may not be an economic solution for some applications, e.g., diagnostics of numerous bearings in the supporting idlers in the long belt conveyors. In this case, some non-contact methods based on image/video signals should be implemented [44].

Electric motor current is easy to implement in the case of automation system presence on the machine, e.g., electric motor equipped with a frequency converter and appropriate output ports for data collection. Otherwise, additional hardware is required, e.g., for the blast hole drilling machines [45]. Motor current is not suited for monitoring of bearings and bolted joints in the gearboxes.

Acoustic signals are susceptible to surrounding noise and require special sound sensors. They would be very efficient in the case of an array of microphones for the inspection of engines and defects localisation in machines with complicated internal structures when permanent sensors for temperature and vibration measurements are unavailable for installing.

Table 2.2. Methods of data processing

Domain	Technique	Advantages	Limitations
Time	Statistics analysis: • RMS • Peak factor • Kurtosis • Skewness • Impulse factor • Clearance	• Easy computation • Standardized alarm levels for certain classes of machines • Available for quick on-site inspection by simple devices • Some parameters are not sensitive to non-stationarity	• Difficulty in damage location • No standards for heavy machinery states • Sensitive to non-stationary • No damages classification • Not related to rotation speed
Time	Time--synchronous averaging	• Improved signal-to-noise ratio by eliminating asynchronous noise	• Shaft rotation signal required • Sensitive to non-stationarity
Time	Autoregressive moving average (ARMA)	• Applicable for different faults diagnostics • High sensitivity to condition change	• Time-consuming for trial and error determination of appropriate order of model • Needs adaptation to non-stationary conditions
Frequency	Power spectrum	• Pre-determined frequency band • Well-developed for analysis	• Lack of phase information • Non-Gaussian noise interference
Frequency	Higher order spectrum	• Suppression of Gaussian noise • Phase information retained • Nonlinear features detection	• High computation cost • Time-consuming calculation
Frequency	Cepstrum	• Extracting and simplifying for analysis of periodic components in the spectrum • Transmission path can be separated from the real signal	• Sensitive to background spectrum noise at an early stage of damage • Weak feature due to the average effect of FFT

Frequency	Envelope spectrum	• More fault-related information than in the original signal • Spectral and temporal representation of modulation • The most known and widely used technique for low rotation speed machinery	• No standards for the central frequency and bandwidth of the filtering
Time--frequency	Short-time Fourier transform (STFT)	• Analysis of time-varying spectrum components • Detection of resonances under varying speed	• Time-consuming calculation • Not suitable for signals non-stationary within the given window.
Time--frequency	Wigner–Ville distribution (WVD)	• High time-frequency resolution	• Not suitable for non-stationary signal
Time--frequency	Empirical mode decomposition (EMD)	• High resolution • Adaptive signal decomposition • No cross-term interference	• End effects • Sifting stop criterion • Mode mixing
Time--frequency	Ensemble empirical mode decomposition (EEMD)	• High time-frequency resolution • Adaptive signal decomposition • Suppressed mode-mixing	• Mode mixing cannot be eliminated completely • No standard method to choose the number of trails and the amplitude of noise
Time--frequency	Local mean decomposition (LMD)	• Instantaneous amplitude and frequency can be provided • Envelope error avoided • More than EMD information	• Mode mixing • End effects

Torque signals are especially useful in the multibody drivetrains of turbine units, rolling mills and other machines to detect dangerous amplitudes of torsional vibrations.

Temperature and oil/debris sensors are widely used in industry but can react with a delay on critical defects in the gearboxes or sliding bearings. Thermal imaging depends on machine surface emission and environmental conditions.

Different methods of data processing are analysed in Table 2.2. They are categorised by data domains with corresponding advantages and limitations. Time domain methods are less demanding to hardware and software but less sensitive to small defects. Frequency domain methods require additional operations of signal processing (filtering, windowing) to enhance signal/noise ratio. Methods in a time-frequency domain are used for the small defects detection and are usually implemented in the case of contradictory results of standard methods. Also, they are most suitable for non-stationary object monitoring.

2.2. Methods of decision-making in maintenance

The studies on machine fault prognosis of heavy industrial machines are much less represented in comparison with fault diagnosis methods because the mean time between failures (MTBF) can be quite long to accumulate reliable statistics for every important element of the machine. Moreover, working conditions of the mining and metallurgical machines may vary within the period of observation making it not reasonable for data comparison on similar parts.

The most widely used in condition monitoring is the group of standards ISO 10816-N [46], which give recommendations on ranges of averaged values of vibration velocity for the estimation of machine condition (Fig. 2.2). These charts vary according to types of machines (ISO standard parts: 1 – general machines, 2 – steam turbine and generators, 3 – critical machines, 4 – gas turbines, 5 – hydro turbines, 6 – reciprocating machinery, 7 – pumps, 8 – reciprocating compressors, 9 – gears, 21 – onshore wind turbines with gearbox). For instance, for Group 3 machines mounted on a rigid foundation, values of vibration velocity (mm/s) separating technical conditions are as follows: good – 2.3, satisfactory – 4.5, unsatisfactory – 7.1.

Standard ISO 7919-3:2009 [47] is based on shaft displacement (Fig. 2.3) where the allowable operation period is recommended but like the previous standard without the time until failure. There is no information allowing the assessment of the more or less probable date of critical failure. These both standards were revised and combined into ISO 20816 standard.

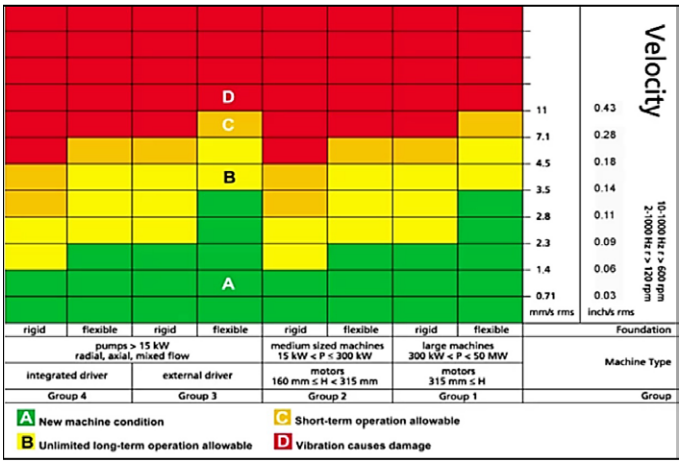

Fig. 2.2. Machine conditions as per ISO 10816 by bearing vibration velocity [46]

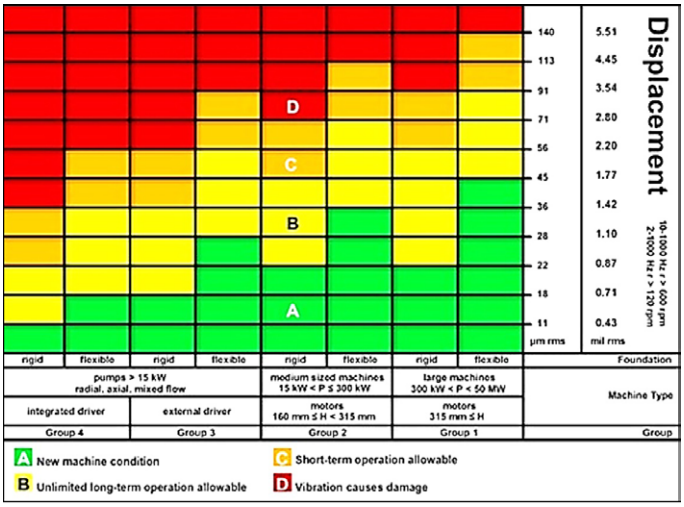

Fig. 2.3. Machine conditions as per ISO 7919-3:2009 by shaft displacement [47]

However, these standards are only applicable to machines working under stationary loading and constant speed of the drive. The transition between states corresponds to large differences in amplitude that can exceed 50%. The majority of mining machines and metallurgical equipment are not covered by these standards.

Approaches to decision-making in condition-based maintenance are discussed in [48–50] and summarized in Table 2.3. One of these approaches is model-based and has many advantages over the others. However, its implementation requires an exact understanding of the physical processes occurring in a certain machine and its units. Namely, this approach is assumed in this book and selected for implementation in practice.

Table 2.3. Prognosis methods in condition monitoring of machines

Approaches	Advantages	Limitations
Statistical	• Do not require condition monitoring • Information on similar machines enables longer-range forecast • Can be trained to recognize the types of faults	• Provide only general, overall estimates for the entire set of identical units
Model-based	• Can be highly accurate if the machine model is good • Require less data then data-driven approaches • Minimum set of parameters for monitoring	• Real-life systems are often too stochastic and complex to model • Simplifying assumptions needed • Various physics parameters needed
Data-driven	• Do not require assumption or empirical estimation of physics parameters • Do not require a priori knowledge	• Generally require a large amount of data to be accurate
Risk-based	• Do not require data monitoring and processing related to health indexes • Do not require a priori knowledge of failure statistics	• Require exact knowledge of possible consequences of failure • Require cost estimation of every failure

2.3. Mobile mining machines – articulated loaders and trucks

In mining enterprises, the main underground vehicles for material transportation are haul trucks (HT) and load-haul-dump (LHD) machines (Fig. 2.4). These vehicles are equipped with on-board monitoring systems that can collect any parameters from electronic control units (ECU) via CAN bus. Condition monitoring systems of underground mobile vehicles enable the collection of huge amounts

Fig. 2.4. Underground vehicles of KGHM ZANAM (Poland):
(a) haul truck (HT) CB4-24TB; (b) load-haul-dump (LHD) machine LKP-1601B

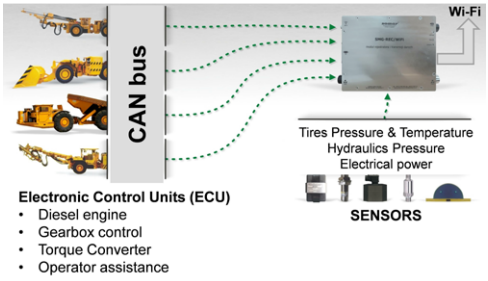

Fig. 2.5. Signals monitored in underground vehicles via CAN bus
and from additional sensors (modified from somar.com.pl)

of digital signals from different special-purpose sensors to prevent abrupt failures.

In addition, the monitoring systems can also include wireless channels of pressure and temperature measurement in tyres, as well as sensors of hydraulic pressure in loading/unloading/drilling mechanisms (Fig. 2.5). Due to a lack of real-time communication, data is locally acquired and recorded in special-purpose modules and then once per shift transferred by wireless channels to the main server on the surface. This is a typical procedure used for underground vehicles [51–53]. Methods of optimization of mining operations in a deep mine by tracking the dynamic loads using IoT sensors are proposed in [54].

Some underground vehicles work in remote control mode (controlled by operators outside the vehicle) or are even autonomously operated based on optical

sensors and other modern positioning technologies [55–57]. Therefore, simultaneously with the main parameters of vehicle operation, some additional parameters of external control actions and position can be determined and recorded [58]. Although the detection of operational cycles by underground truck positioning systems could seem like the simplest way to solve the problem, it requires huge investments in underground infrastructure and is not feasible for the majority of mining enterprises operated underground. In addition, methods of position data analysis are anyway needed in the case of changes in the location of truck unloading. Haulage cycle detection for wheeled transport in underground mines using neural networks is given in [59].

The general problem of classifying operating states for heavy underground trucks is an important task for logistics, maintenance planning and the estimation of transportation efficiency. Some approaches are known for on-surface vehicle monitoring, which are based on different types of sensors. A monitoring system based on the stationary magnetic sensor was developed in [60] for the detection, classification and recognition of passing vehicles using the improved support vector machine (SVM) method. A method of direct payload measurement by strain gauges mounted on the leaf springs of the suspension system of heavy vehicles was tested [61]. This method could also directly detect the loading-unloading events of underground trucks. However, measurements with strain gauges are complicated as they are sensitive to external impacts (uneven road surface, heavy truck manoeuvres), and their implementation is not feasible in the harsh underground environment. Virtual soft sensors are preferable for such tasks and eliminate the need for the installation of physical sensors.

The method of predicting heavy truck rollover speed was developed in [62] by combining a software application and acceleration sensors. The hybrid estimation strategy was developed in [63] using low-cost sensors to estimate the vehicle sideslip angle and the dynamics-based extended Kalman filter (DEKF) to adapt to changing tire-road conditions. However, these methods, besides the installation of additional sensors, presume knowledge of vehicle structure parameters and the chassis dynamic model, which may not be known or measured in underground haul trucks.

Understanding the external load applied to the machine is a critical issue for monitoring the vibrations of machines operated under non-stationary conditions [64]. The algorithmic method of classifying operational modes for online categorizing of vibration signals was proposed in [65]. Condition monitoring

of underground vehicles based on the statistics of engine temperature signals was considered in [66]. Here the problem is similar; however, the motivation is more process-oriented than condition-oriented. By identifying operational regimes, one can evaluate the production level, the efficiency of machine use, the operator's skills, etc. [67]. Statistical techniques of data segmentation and signal processing for operational regimes detection of underground vehicles were proposed in [68, 69]. Using signals from monitoring systems for the detection of operational cycles is considered for underground LHD machines [70, 71] and haul trucks [72]. The non-clustering method for the automatic selection of machine operational states was proposed in [73]. The method of Joint Approximation Diagonalization of Eigen-matrices (JADE) as one of the blind source separation techniques from the domain of Independent Component Analysis (ICA) was used in [74], where the authors analysed the working cycles of a haul truck. The ICA method is based on the assumption of statistical independence of original signals and the separation of only linear combinations of sources, but these conditions are not valid in our case. In addition, if two or more sources are perfectly Gaussian, they cannot be separated.

As an alternative approach for classifying vibration signals and operational states, neural networks can be used [75] as in many other applications. This approach is not considered for on-board monitoring systems of underground trucks because of the wide variation of working conditions from the nominal values of parameters. Besides, the high temperature and humidity of the air, along with the high intensity of shocks and vibrations result in mechanical damage to the sensors, connectors and cabling of monitoring systems in underground vehicles. It requires the development of fault-tolerant monitoring techniques and methods for online data processing to reduce false alarm signals and to detect specific machine operational events when some sensors are not available or fail.

One more issue is NaN/Null values in digital data. The problem of validating signals from sensors was mentioned in [76]. The authors highlighted the need for improving the robustness of algorithms for industrial applications and automatic validation of signals.

2.4. Stationary mining equipment – vibrating sieving screens

The various approaches to vibrating screens investigation and applied modifications of their structure and technological regimes tuning are overviewed

in [77, 78]. The assigned oscillating regimes of screens determine the diagnostics and monitoring methods. Two main classes of screens are known: resonant type and above resonance type. The resonance regime is desirable, however, its control is complicated because the sieving process is vulnerable to changes in bulk material thickness, particles distribution over the layer and their properties (fractional composition, material humidity and tendency to fracture) [79].

One of the ways to provide better sieving is to excite parametric vibration [80] and nonlinear oscillations with a broader frequency range [81]. However, drives with a constant frequency of excitation are the most used case in the industry. Separation of fine materials subjected to adhesion is achieved by increasing the excitation frequency.

The natural modes of screen motion and multiply particle trajectories are efficiently investigated by the finite and discrete elements methods [82]. However, these methods are very computer resources consuming in research and optimisation tasks. Besides, a detailed 3D model of a certain type of screen is required (not always available) as well as the design of particle configuration and statistical fractions distribution in the input flow. Therefore, a dynamical analysis of the vibrating screen as a rigid body filled with a bulk material can be conducted based on the reduced degree-of-freedom spring-mass models [83].

Supporting springs are the key elements because their stiffness influences the overall process and the particles' trajectory. Although air-filled or elastomer springs could be advantageous in operation, they may exhibit nonlinear behaviour [84], whereas steel springs have linear stiffness within a working range of deformation. Nevertheless, the side bending displacement of steel springs is nonlinearly related to vertical stiffness [85] that can result in specific dynamical effects.

To control spring stiffness and the dynamical characteristics of the system, authors in [86] proposed the use of shape memory alloy in the case of the resonant regime of vibrating screen for the fine-tuning of natural frequency. Standard springs made of alloy steels are subjected to corrosive wear and cyclic fatigue [87,88]. The most efficient remedy against failures of springs is the cryogenic treatment of high carbon and alloy steels [89].

Several vendors of condition monitoring systems are known in the market proposing options for vibrating machines. Some of those systems have specialised functions for sieving screen diagnostics, which are overviewed in [90].

- CONIQ (Schenck) is a condition monitoring system which can detect possible defects in the screen based on a six-dimensional vibration measurement using piezoelectric accelerometers and bearings temperature.
- FAG SmartCheck (Schaeffler) system monitors vibrations to recognise damages in a filled vibrating screen: settling of screen mats, loose springs, and spring breakage. Monitored parameters are vibrations, the temperature of bearings, speed of rotation, and screen load. Diagnostic methods include time series of vibration, envelope curve, speed, spectrum, and trend analysis.
- ScreenWatch (Check) (Metso) system is based on wireless self-powered sensors and detects a deviation in nominal screen motion caused by broken springs and damaged bearings, incorrect rotational speed and unbalanced masses settings.
- Copperhead (SKF) system monitors vibrating screen faults including gears, bearings, screen body and deck damage and overloading.
- IFM solutions for vibration screen/feeder monitoring.
- PCB IMI Sensors for monitoring vibratory screens and feeders.

All these systems are based on the standard algorithms of vibration monitoring aimed at the detection of local defects in the bearings. However, the falling copper ore is a source of random impulsive noise in vibration signals. Recording the pure signal of load supposes the use of strain sensors installed on the different elements [91] with appropriate wireless tools. Methods of driveline diagnostics with special instrumentation are not applicable in the case of springs. Also, the detection of defects by monitoring electrical drives is not feasible.

One of the specific features of vibrating machines is the continuous displacement of the most loaded zone on the outer race of rolling bearings of the vibrator shafts [92]. Only a special series of bearings are applicable in these machines. The stiffness of bearings housing should be equivalent in all directions to provide reliable and durable operation. Problems of rotor-bearing-housing system (RBHS) interactions based on the dynamic modelling method and including the additional excitation zone are investigated in [93].

The advanced methods are developed for vibration signal processing recorded on a hammer crusher [94], which includes stochastic impulsive components [95,96] having non-Gaussian distribution. Stochastic load analysis in vibrating screens is investigated in [97, 98], but the statistical approach is mainly implemented for analysis of particle distributions [99]. The diagnostics by the mul-

tibody nonlinear dynamical models is a quite suitable approach for diagnostic features derivation of vibrating screens including springs. In theory, the identification of the stiffness characteristics in multibody systems is conducted by combining experimental frequency response functions (FRF) and "inverse problem" solving. Several schemes were established and tested to determine joining stiffness in a set of elements, although only for linear stiffness estimation.

Algorithms of vibrating screen diagnosis based on the dynamical models are constructed in [100–102]. Assigned changes in spring stiffness have a small effect on amplitudes of vibration, and spring defects were hard to recognise under conditions of heavy-tailed noise. A method for damping spring failure diagnosis of a large vibrating screen based on a static deformation test is proposed in [103]. A detailed review of existing methods of vibrating screens diagnostics and own testing procedures are given in [104]. The influence of treated material and produced loads on screen vibration is analysed in [105, 106].

A phase space plot (PSP) is a graphical method in the analysis of nonlinear systems, which is rarely used in diagnostics [107, 108]. PSP is a trajectory in angular or linear coordinates and their derivatives. PSP is more efficient near the bifurcation points when the dynamical system is susceptible to a small change of parameters.

Taking into account the similar dynamic features of all systems with bilinear stiffness characteristics, the numerous methods developed for crack diagnostics in structural health monitoring of stressed bending beams or shafts and gears [109] can be considered in our case for failure diagnostics of spring defects. The estimates of damping and natural frequency are used as the diagnostic parameters in [110].

2.5. Dynamics and diagnostics of rolling mills

Wide strip hot rolling mills. The increasing production capacity of hot rolling mills due to higher speeds and strip thickness reduction leads to high torsional dynamics and resonant vibration problems. Some rolling practice methods can help to reduce the occurrence of such resonances but cannot eliminate them. There are some publications on the rolling mills' dynamics [111, 112], drivetrains parameters optimization [113], torsional vibration control [114], and backlashes compensation [115]. An extended state observer and linear quadratic-based speed controller are used to control drivetrain dynamics [116]. Due to the uncer-

Fig. 2.6. Multi-stand wide strip hot rolling mill

tainty and complexity of rolling parameters, a fuzzy neural network [117] and an extended Kalman filter [118] are used. The general view of such kind of rolling mills is shown in Figure 2.6.

The rolling mill drive control system includes automatic speed and current regulators (ASR, ACR). It was found that closing the outer loop could help or hurt damping just as in closing the inner loop. For a given inner loop, the greater the load inertia to motor inertia ratio corresponds to greater damping. In general, resonance control requires: reduced time lags; a stabilized inner loop; use of the work torque outer loop speed regulator [119].

Tuning of the motor speed and current regulators can help in improving the damping of the drive system. A significant increasing in damping by 50% to 100% of torsional vibration may be achieved by the additional control loop with feeding measured spindle torque into the drive current regulator. However, for such a method implementation a reliable telemetry torque sensor is required. In addition, speed-sensor ripple and sampling delays of the digital regulator limit the scope for method improvement [120].

In the analysis of electromechanical drives, it is common to choose only a first-order representation of the torsional elements between the motor and rolls. The analysis is often simplified by the neglect of mechanical system nonlinearities, the most important of which are backlash and torsional couplings having nonlinear stiffness. Usually, two lumped mass systems (motors and rolls) are used to describe torsional dynamics.

Authors of research [121] considered multibody models of drivetrain and stand. The properties of rolled metal as a nonlinear elastic-plastic element have been taken for the vertical and torsional chatter vibrations control. A detailed torsional model allowed describing nonsynchronous oscillations of spindles and the study of the higher modes with the opposite phases of the work rolls vibration.

The ABB Company reported high-performance converters with new features for torsional dynamics reducing: direct torque control (DTC), resonance frequency eliminator (RFE), backlash compensation, load shock elimination (LSE), and adaptive impact compensation (AIC). By applying newly developed control algorithms, the effect of backlash is reduced to almost nothing. When the system is being loaded, the produced torque keeps the backlash gaps closed, and when the system is idling, a more careful control algorithm is used, thus avoiding vibrations that could damage gearboxes [122].

The scope of dynamics research in this type of industrial machine covers the following:

- influence of weight balancing and angular position of spindles on dynamics;
- influence of torsional modes on driveline dynamics;
- drive acceleration ("soft start") for the backlashes closing.

Wire and rod hot rolling mills. During the last decades, modern wire and rod manufacturing technology has been developed toward high rolling speeds, a wide range of metal sections, and higher accuracy due to tension control [123]. The development of automated systems to control the rolled wire section is very important [124]. To meet these demands of the steel industry, producers of metallurgical equipment develop different types of Reducing Sizing Mills (RSM) such as Danieli (Kock's type with three rolls), Primetals Technologies (Morgan type two rolls blocks, see Fig. 2.7a), SMS (Sket type with two rolls) and several companies in Japan, India and China [125–127]. Some wire and rod rolling mills are also operated in Poland.

The RSM is usually installed between the finishing mills and laying head, where the material is coiled and cooled down rapidly to improve the internal microstructure of wire and rod and achieve the required mechanical properties. The final products in the RSM are of high accuracy by geometry, the dimensional tolerance is about ±0.10 mm. At the same time, the rising output speed of RSM up to 120–140 m/s is accompanied by increasing vibration amplitudes and subsequent cases of "cobbling" (Fig. 2.7b) due to axial instability of rolled material

Fig. 2.7. Reducing sizing mill (RSM): (a) gear driveline with a changeable structure; (b) cobbling accident in the mill caused by axial instability of hot rolled rod

when the uncontrolled loop grows up and quickly accumulate. This phenomenon is observed in any RSM, i.e., steel producers have a certain speed limit restricting overall productivity.

Experimental testing in RSM by torsional dynamics measurement with strain gauges and telemetry systems like in other types of machines with open drivelines is very problematic.

Stationary vibration monitoring systems with sensors installed on the housing may provide alarm signals to prevent abrupt failures of bearings [128, 129], but it is difficult to recognise elements in compact rolling blocks under variable speed and load. Hence, special methods of diagnostics are under development [130].

Some vendors patented the use of rotation speed sensors installed on the roller guides and rolls to monitor their faults [131, 132]. Methods of rolled rod

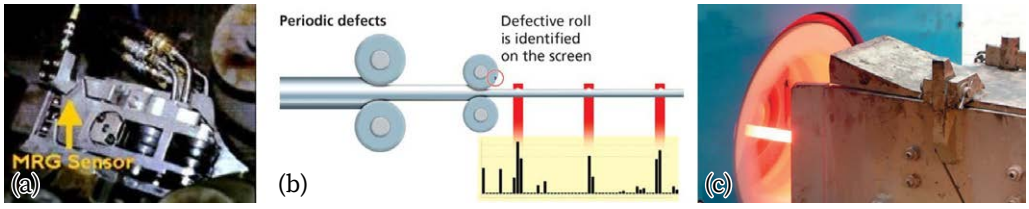

Fig. 2.8. Sensors used in RSM: (a) monitoring roller guide (Morgan); (b) in-line eddy current sensor Eddycheck of defects at up to 120 m/s (PRÜFTECHNIK NDT); (c) in-line laser measuring of rod section (ORBIS)

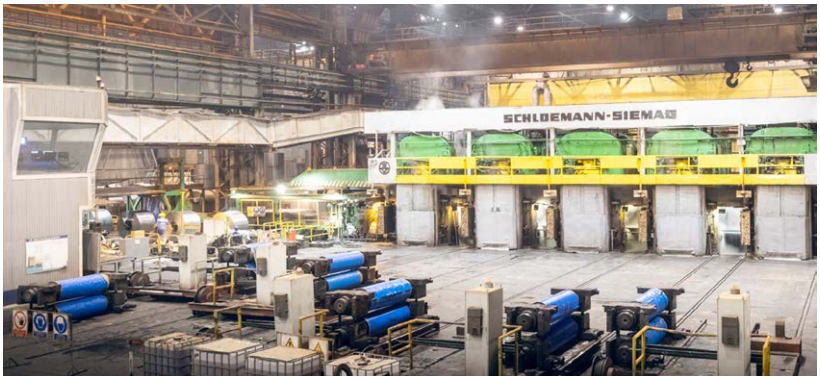

Fig. 2.9. The high-speed (up to 25–30 m/s) multi-stand tandem cold rolling mill

defects diagnostics (Fig. 2.8) and laying head vibrations damping are proposed [133]. Nevertheless, research on RSM dynamics, control and rolled metal oscillations for diagnostic purposes is still less represented [134–139]. That makes it necessary to implement mathematical modelling and analysis to discover reasons for wire and rod rolling instability at high speeds.

High-speed cold rolling mills. These are the powerful steel rolling machines combining many auxiliary mechanisms (coilers, welding units, strip accumulating stations), which form continuous processing lines. The tandem cold rolling mills consist of 46 stands (Fig. 2.9).

Fig. 2.10. Chatter marks: (a) in unstable boring operation [140];
(b) corrugation of rails [142]

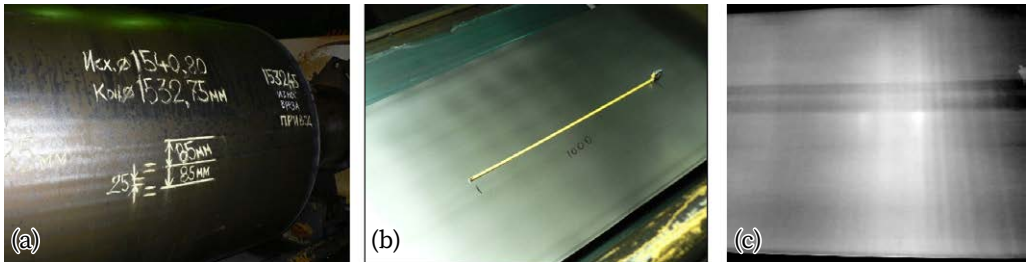

Fig. 2.11. Chatter marks: (a) on the backup roll; (b) on the strip (period 140 mm); (c) on the strip (period 20 mm)

High-frequency vibration or so-called "chatter" is a well-known phenomenon in the different types of industrial machines. As it is noted in [140–142], such vibrations are not a problem specific to only rolling mills. The periodic marks appear on the surface during grinding, drilling, and cutting operations and on the rails, where friction forces interact with the elastic "wheels-transmission--suspension" system (Fig. 2.10).

However, it is most important in the cold rolling mills where chatter vibration affects rolls and strip surfaces by periodic marks (Fig. 2.11) that may cause specific audible sounds or mill "roaring" even at half of the available speed. Depending on rolling conditions, the period of chatter marks may vary from 140 to 20 mm which corresponds to main mode frequencies of 100–120 Hz in the 3rd octave and 500–600 Hz in the 5th octave, respectively.

Nowadays, the only reliable method to reduce the amplitude of resonance vibration and to avoid strip breakages is the reduction of the rolling speed at the moment or before chatter excitation. In different mills, the required speed drop, which is enough for chatter cancelling before strip break, is about 50–250 m/min depending on the current level, mill type and rolling conditions. Such a method reduces the maximum speed available by mill design.

Frequent replacement of deteriorating mechanical components (spindles, couplings, gears, winding reels, tension rollers, bearings and rolls) may be applied only up to a certain extent when the maintenance costs begin to restrict the overall operational efficiency. Modern research and developments on chatter vibrations are carried out in several directions:

- permanent systems of vibration monitoring and diagnostics;
- passive and active vibration damping;

- non-contact detection of periodic marks;
- diagnostics of rolls grinding process and machines;
- optimisation of coolant supply in the contact zone;
- mill setup tuning and online control by vibration signals.

Among the companies proposing specialized chatter monitoring systems are Vold Solutions Automation (USA) with "QuartzMill", AMTRI (UK) with "AVAS", IAS – Industrial Automation Systems (Australia) with the "VIDAS chatter monitor", SMS Siemag (Germany) with the "MIDAS", iba AG (Germany) with ibaLogic based system.

Some companies implemented passive vibration dampers for the rolling mills (IAS, Asko and Dofasco) and in roll grinding machines (Vold Solutions Automation) as well as active vibration control systems (Primetals Technologies, SMS Siemag). Vibration recording for every coil and viewing spectrum amplitude in the different frequency ranges of mechanical elements are the most required functions in chatter monitoring systems. Such systems allow mill operators to keep mill speed as close as possible to the upper limit for current mill conditions. The most known method for chatter detection and strip break prevention is online spectrum analysis in certain frequency ranges including main mode frequency and giving the alarm signal for mill speed reduction when the spectrum amplitude overcomes the limit value (one or three levels). As the chatter amplitude arises quickly (less than 1.0 s) and the mill has a certain delay in reaction, operators try to set alarm levels as close as possible to the normal level. However, it frequently causes wrong alarm signals as the rolls and strip sizes are different from coil to coil.

According to the known publications and patents, there are no industrial systems which provide reliable early diagnostics and prediction of chatter excitation. The main problem in the high-speed cold rolling mills is in fact that standard Hydraulic Automatic Gauge Control (HAGC) systems with the cut frequency of control loops below 10–15 Hz are not able to control high-frequency oscillations of 100–200 Hz. The tuned mass dampers are not reliable because of the stochastic variation of the main natural modes of vibration. Therefore, active vibration control is proposed for chatter suppression [143, 144]. There are several approaches for active chatter damping:

- periodic force changing in HAGC cylinders through the fast servo-valves;
- periodic force generation in the hydraulics of backup rolls weight balancing;
- periodic force generation in the work rolls bending cylinders;
- safety valves in the hydraulic system of the rolling stand (one-time use).

The IAS Company (Australia) proposed a tunable damping device (VIP – Vibration Inhibition Piston) which is installed in the upper backup rolls balancing system. Designers reported that such devices allow an increase in mill speed by 25–30%. However, its implementation has certain issues. The efficiency of dampers directly depends on their ability to tune to the resonance frequency. In general, the main natural frequency varies insignificantly (±12 Hz). However, the chatter frequency in the rolling mill may vary in the wide range (±2025 Hz) or even more. Therefore dampers should be installed in the stand taking into account what mode of chatter (3^{rd} or 5^{th} octave) is targeted.

Some other kinds of vibration damping were proposed for dynamics reduction. In [145], an additional degree of freedom (DOF) has been introduced in the form of a controlled tension roller for phase shifting of tension vibration between stands of tandem mill for stability increase. The natural frequency of the supporting roller may be regulated by the stiffness or mass value and it should be a little bit more than the chatter frequency. Active damping may be realised by the actuation with an additional drive for tensioning roller vibration [146]. Such devices may be efficient as the strip tension is the elastic link providing stands' synchronization and vibration amplification in the tandem mill.

Testing of active chatter damping in one of the tandem mills showed that damping efficiency is restricted by the absence of reliable and exactly equal phase regulation in every actuator. Even a little phase divergence under control may cause an even worse situation in the mill dynamics. For example (Fig. 2.12), the ChatterBlock system of Primetals Technologies uses specially designed high-frequency servo valves. The AntiChatter system of SMS Group uses piezoelectric elements installed under the lower backup rolls [147]. Danieli Company patented a chatter control system that uses work rolls bending cylinders instead of the main large HAGC cylinders [148]. The efficiency of all above mentioned systems on the real mills has not been reported in the open sources. In any case, the vibration monitoring system is needed to produce input signals for actuators' control.

There are always clearances between the stand housing beams, which may cause chatter vibration. The resonance analysis of horizontal nonlinear vibrations of roll systems for cold rolling mills under double-frequency excitations is investigated in [149]. To struggle against the unstable horizontal beating of roll chocks, a special method is proposed [150], according to which the rolling process is controlled taking into account the dynamic changes in the horizontal forces

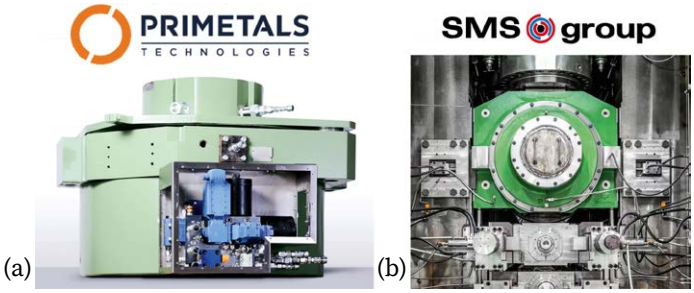

Fig. 2.12. Chatter active damping systems: (a) HAGC cylinder with high-frequency servo valves; (b) piezoelectric actuators in the stand

acting on the work rolls (WR). The method presumes the determination of many parameters in each stand: the roughness and diameters of the work and backup rolls (BUR), the static displacement of the work and backup rolls, the viscosity of the cooling fluid and friction coefficient. Further, based on calculation on the model, the regulated parameters are determined as required for roll stability. The application of this method in practice is associated with technical problems of unknown parameter measurement. In addition, when calculating the stability conditions, the work rolls bending forces are not taken into account, though they play a crucial role in the durability and vibration of bearings on the rolls.

Some companies (SMS Siemag, Danieli) proposed flat hydraulic cylinders for roll chocks pressing with constant force to the housing during rolling [151]. It prevents clearance opening and chocks horizontal vibration when the tension oscillation amplitude is too high. However, it was shown by experiments that critical rolling speed increases only by 10%. In addition, the restriction of the WR chocks' vertical motion worsens HAGC operating conditions. Also, this method may cause problems in thickness control as it restricts roll vertical motion. Patents [152–156] are aimed at chatter suppression by different methods.

Some works are known in the field of chaotic vibrations analysis in cold rolling [157]. Chaotic vibrations in metal cutting were also studied [158] and methods of friction instability early detection were developed for their active control [159]. However, the methods developed for metal processing machines are not applicable in the rolling mills. The essential complexities arise with the analysis of adjacent stands interaction in the rolling mills due to the regenerative mechanism of chatter excitation by means of the strip waviness induced in the previous

stands. This effect was considered by the deterministic models with a constant time delay [160, 161]. Also, the elastoplastic properties of the rolled strip and the damping ability of hardened metal have a great influence on chatter excitation that was investigated in [162–164].

2.6. Multi-motor drive systems (MMDS) of industrial plants

Possible problems in the multi-motor drive systems (MMDS) of industrial machines may appear from the mutual interaction when they are not synchronized. In this case, backlashes in the gears and high dynamic torques may affect overall durability and cause failures. In this relation, a method of control of the hot rolling mills is proposed [165]. Shock loads are reduced due to the automatic matching of speeds when the strip exits the preceding vertical stand and enters the horizontal stand. The dynamic torque and interaction of stands were investigated in [166, 167]. Results of experimental research showed the importance of this factor for reliability. A simplified synchronization system was implemented to solve this problem [168].

In recent years, the MMDS with digital control has been developed [169]. Measurements of torques using a telemetry system show that the ratio between the maximum dynamic value and steady-state level does not exceed 2.1, which is not a high value. Nevertheless, developers of this control system noted that additional play of gaps in the gearbox adversely affects the durability of mechanical components. To eliminate this drawback, they recommended installing individual thyristor converters and controlling each electric motor excitation by the difference signal of the motor armature currents. However, preliminary dynamic analysis of this drivetrain [170, 171] showed a possibility of high internal torsional dynamics due to parametric resonances. Studies related to parametric oscillations in MMDS are known for the platform rotation mechanism of bucket-wheel excavators [172], the tilting mechanism of steel processing converters [173, 174] and tumbling mills (Fig. 2.13), drives of tunnel boring machines [175] and long-wall shearer [176]. To prevent abrupt failures, advanced methods are designed for vibration diagnostics of the multi-motor planetary gear drive of the bucket wheel excavator [177].

The sources of parametrical excitation are investigated in different industrial machines [178–183]. Although the nature of parametric vibration is a well-known and investigated phenomenon, this problem remains a challenge for design-

Fig. 2.13. Industrial machines with multi-motor gear drives:
(a) bucket-wheel excavator; (b) tilting steel converter; (c) tumbling mill

ers. Some methods are proposed for gear profile modification and gears' phasing [172, 184] taking into account contact friction and transmission errors [185]. Those methods are applicable only at the design stage. During the operation, some elastic damping elements can be implemented in the shafts to reduce input impacts [186] that is not concerned with the internal dynamics of gearboxes. The diagnostic methods based on torsional dynamics monitoring [187], motor current signal processing and strain gauges telemetry tools [188] are not feasible due to low dynamics at the intermediate shafts. Equivalent load sharing in MMDS can be improved by the electric drive control [189–191] and active damping of torsional vibrations [192]. However, these methods are mainly applicable to two-mass drives (motor and load) and are not suitable for MMDS control. With the limited possibilities of load measurement inside the gearbox, mathematical models are widely used for dynamic simulation of gear drives [193, 194] including detailed modal analysis of geared drivelines [195]. Summarizing a wide scope of MMDS studies, we can note the following tasks: optimal control for equal load share between parallel drives; gears phasing; kinematic errors diagnostics; monitoring of mechanical loads by the electric drives parameters; and torsional vibrations damping.

2.7. Instrumentation for monitoring and diagnostics of industrial machines

The success of condition monitoring greatly depends on appropriately chosen sensors, signal transferring methods (via cable or wireless), signal conditioning and the quality of power supplied to the measurement modules. A detailed analysis of dynamic torque monitoring systems is given to understand their

applicability in different heavy-duty machines. Issues of bolt loosening detection and instrumentation for backlash measurement in the drivelines are considered.

2.7.1. Wireless torque meters

Online monitoring and diagnostic systems can be integrated into the automation system of the main equipment supplied by the producers. The most advanced systems are based on torsional torque meters developed, e.g., by BFI (Germany) and marketed by ACIDA (Voith) (Germany). Only a limited number of non-contact torque meter applications are known on rolling mills and mining machinery: Binsfeld (USA), Astech Electronics (UK), Transmission Dynamics (UK), and KMT (Germany).

Presently, the real-time condition monitoring and diagnostics of mining machines are among the most demanding and quickly expanding areas of research and development. Existing sensors and wireless data transmission technologies based on the Internet of Things (IoT) and cloud-computing approaches allow taking and storing huge measurement data in real time. Besides, the exponential growth of microcontroller processing power allows the creation of price-efficient measuring systems and provides the possibility to get insight into changes in the machine's dynamic state during its operation [196].

The creation of a well-suited mathematical model of the industrial plant helps in dynamical load controlling but can be difficult when it comes to the multibody geared drivetrains with non-smooth stiffness characteristics, which may cause complicated chaotic behaviour [197]. The models are not always able to reproduce all aspects of the real working conditions, especially for underground mining machines. That is why numerous trials are needed to verify models by the reliable wireless torque measuring system. On the other hand, there are obstacles related to a harsh environment, where mining machines are usually operated. Particularly, there is often no stable wireless connection underground. Moreover, the continuous repairs and replacement of damaged parts in the mining machines restrict significantly the possibility of torque sensor deployment. Installation of torque meters based on gauge sensors requires special skills and downtime of a machine or even the whole production line, e.g., long conveyors, which is generally undesirable. Therefore, a detailed analysis is conducted to figure out the functionality and design of torque meters.

Nowadays, the torsional vibration measurements on rotating shafts are used in the following applications [198]:

- automotive transmissions measurements;
- marine drivetrains with high-power diesel engines;
- oil and gas equipment, drilling rigs;
- turbines and generators in electric power stations;
- drivelines of rolling mills in steel processing plants;
- ore and coal drum mills, cement kilns in minerals processing.

The analysis of abrupt failures in heavy machinery, e.g., rolling mills or belt conveyor drives [199], shows that most of them are caused by one-time overloads from high torques. Torsional vibrations caused by internal resonances [200] or stick-slip friction-induced vibrations can lead to even more severe damage or deterioration in the drivelines due to accumulated fatigue cycles. Therefore, mechanical torque signal, if measured with special tools, is a profoundly informative diagnostic parameter for complicated planetary gearboxes [201], and reciprocating machines like diesel engines, pumps and compressors [202].

Measuring torque along with other parameters, such as electric drive current, allows the detection of operational cycles of machines, and compaction parameters of bulk materials briquetting. In parallel, angular clearances can be monitored in the drivetrain elements.

Although the monitoring of electrical drive currents allows estimating loads, their values are not strongly correlated with peak dynamic torques and have delays at higher natural modes above 10–20 Hz. In the case when the industrial plant is equipped with digitally controlled drives with a pass-band of 25–30 Hz, some procedures can be applied for DC motor armature current to extract the lowest natural modes for load monitoring. However, such a method is only applicable to a two-mass drivetrain layout "electric motor–working tool". In multibody powertrains with gearboxes, flywheels or other inertial components or synchronous AC motors, mechanical torques are not detectable directly by the motor current. One of the additional advantages of dynamic torque monitoring is the possibility of computing the remaining useful life (RUL) based on multibody models [203].

The examination of the consequences of torsional vibrations on machines, including pneumatic and hydraulic systems, enables a better understanding of the real operating parameters of the process. The analysis of down hole drilling vibration data is represented in [204]. Methodology and experimental verifica-

tion of a drilling system optimisation based on torsional vibration suppression are represented in [205]. The assessment method of reliability calculation for mine machines, e.g., belt conveyors, is shown in [206].

Classification of torque sensors. There are several features for the classification of torque meters shown in Figure 2.14. First, the principle of measurements determines how the system would be installed, and other parameters such as power supply, and methods of sensor installation. Accordingly, certain types of torque meters can be assigned for specific machines, e.g., mobile or stationary.

In the case of the mining industry, issues of permanent torque monitoring are the harsh environment and wireless connection stability. Moreover, there is an obstacle with a permanent power supply for sensors and shaft replacement caused by damage or failure. When it comes to higher torques, special calibration methods are needed.

Magneto-elastic sensors. The magneto-elastic effect has been used in sensors for a long time [207]. An example of a modern torque meter is shown in Figure 2.15, which is used in the testing of car transmissions and ship drives with internal combustion engines. The sensor detects changes in the permeability of ferromagnetic materials under the influence of tension and compression forces.

Piezoelectric sensors. The most common design of piezoelectric torque sensors available in the market include discs with measuring elements and plug-in bearings to take signals from the rotating shafts, which are connected with pin

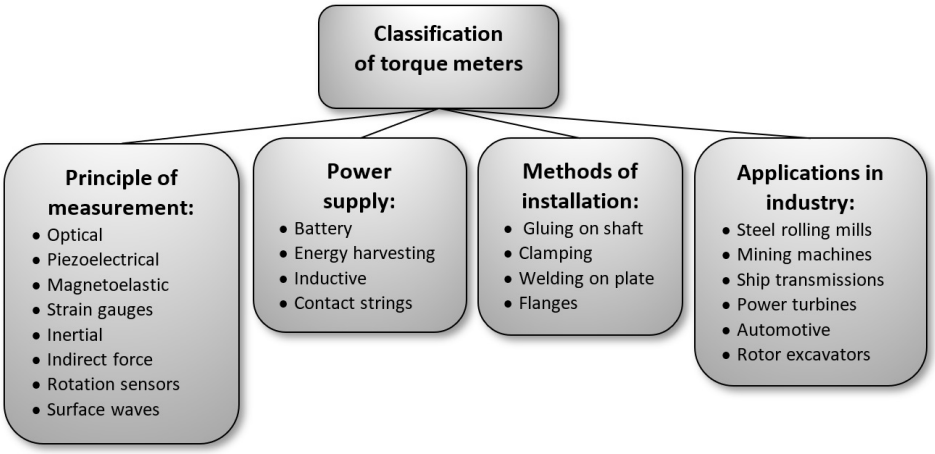

Fig. 2.14. Classification of torque meters

Fig. 2.15. Magneto-elastic torque sensor (ABB

or flange couplings (Fig. 2.16). Such meters are installed inside the transmissions of small machines or at the ends of shafts, which is practically not feasible in the drivelines of mining machines and rolling mills.

The torsional torque can also be measured with piezoelectric sensors due to the difference in angular displacements of two sections of the shaft. The magnitude of the torque is calculated by the known diameter of the shaft and its stiffness. A pre-tensioned (for backlash elimination) plate with a load measuring element or an inductive micro-displacement sensor that responds to angular displacements of the deformable shaft is mounted between two rigid clamps installed in different sections of the shaft (Fig. 2.17).

A measurement base of not more than 100–150 mm along the shaft is used since this affects the overall rigidity of the sensor. Due to the large diameters (300–900 mm) of shafts in rolling mills, they have small twist angles proportional to the effective torsional torques and require an increase in the measurement base, and this in turn reduces the rigidity of the design of the clamps and connecting beams of the sensor affected by the impact loads and transient vibrations. This design was once used in measurements on rolling mills but was abandoned in favour of

Fig. 2.16. Design of the torque sensors (PCB):
(a) disc; (b) bearing; (c) flange

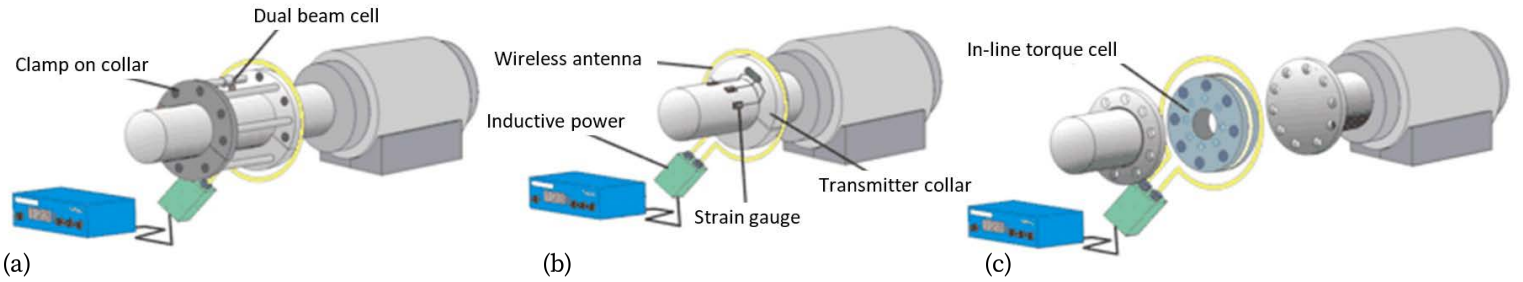

Fig. 2.17. Design of wireless torque sensors (Honeywell):
(a) clamps with micro-displacement sensor; (b) tensometers (strain gauges);
(c) in-shaft piezoelectric sensor

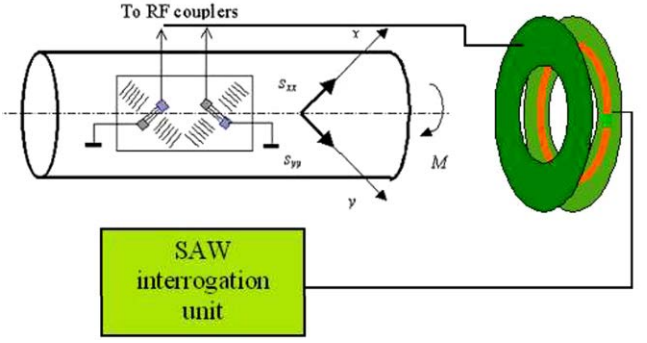

Fig. 2.18. Block diagram of the SAW torque sensor [208]

strain gauges. Most of the commercially available sensors of this type, as a rule, are used for precision measurement of relatively small torques (0.5...10 kN).

Wireless SAW sensors. Among the recent developments [208] is the torsional torque sensor based on two resonators operating on Surface Acoustic Waves (SAW) (Fig. 2.18). Resonators are mounted on a rotating shaft perpendicular to each other. When mechanical stresses occur, the operating frequency of the resonators is shifted in proportion to the magnitude of the torque. The resonators are connected to the measuring apparatus using transmitters. Recommended field – automotive applications. Advantages over known analogues: the inertia-free signal produced by the sensor and high sensitivity.

Inertial sensors. Historically, inertial sensors for measuring torques, or torsiographs, as they are called, have been used since the beginning of the 20th century to study ship propulsion systems with extended transmissions and internal combustion engines [209]. Later, sensors were equipped with telemetry data transmission from a rotating shaft, for example, the radio-torsiograph RT-660-02 developed in the Krylov State Research Center (Russia). Usually, these sensors measure the vibrations of a ship's transmission at the shaft end, relative to the flywheel. The sensitive element is a soft spiral spring between the end of the shaft and the flywheel, which maintains a constant rotational speed. Such devices have a non-uniform amplitude-frequency characteristic at frequencies up to 50–60 Hz (Fig. 2.19).

This allows their implementation in ship transmissions to identify resonant modes at higher shaft speeds, but not in low-speed shafts of mining machines and rolling mills, where the lowest natural frequencies are in the range of 10–20 Hz.

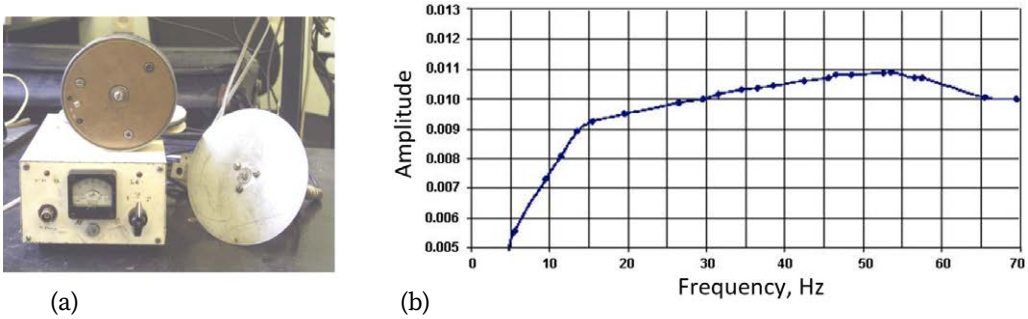

(a) (b)

Fig. 2.19. Radio-torsiograph RT-660-02: (a) general view;
(b) frequency response function

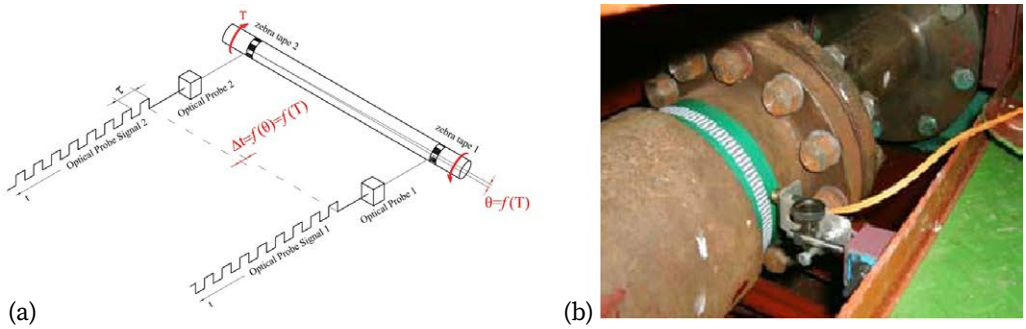

Fig. 2.20. Optical torque meter: (a) schematic diagram; (b) installation on the shaft

Some authors proposed MEMS inertial sensors installed on the shafts to measure torque ripples.

Optical sensors. Standard laser rotation sensors can be used as optical sensors, which measure the time intervals between successive pulses caused by the torsional vibrations of a given shaft section [210]. The optical measurement sensors (Fig. 2.20) are used on the shafts. The Brüel & Kjær (HBM) Company manufactures a serial torsiograph based on a laser vibrometer.

Instead of optical sensors, Hall sensors can also be used making measurements available inside the gearboxes, but with less angular accuracy. Similarly to the tension gauges method, the efficiency of torque measurement is determined by the correct choice of sensor positions. A single sensor should be installed in the place where the angular oscillations have maximum amplitudes, while the double sensors – in the main torsional node, i.e., maximum shaft deformation. Accordingly, special methods of signal processing are used.

This method of torsional deformation measurement has several limitations. The main sources of distortions of torsiograms recorded using optical sensors are as follows: sensor vibration and shaft beat; errors in the manufacture of tape "zebra"; errors when mounting the tape on the shaft. In addition, the sampling rate of the torque sensor signal depends on the drive rotation speed. A similar principle based on optical encoders is used for static torque metering in automotive steering systems.

Strain gauge sensors with wireless data transmission. A strain gauge, made of wire or foil, transforms mechanical force or deformation into an electrical signal. It is widely used in studies of machines, both on stationary parts and on

rotating shafts [211, 212]. The main advantage of strain gauges is their installation on the units without intrusion in the driveline. The disadvantage of using strain gauges in stationary monitoring systems is the slow drift of zero during the ageing of the adhesive composition, which can be compensated on the motor shaft with the signal of the electric motor current. Nevertheless, the analysis of known sensors for torque measurement and the experience of using them have shown that tension-resistive sensors are the most suitable primary transducers in harsh industrial conditions. To transmit signals from rotating shafts, several types of schemes are used:

- contacting strings and slip rings;
- movable rotor (shaft) and stationary stator (receiver antenna);
- transmitting via the radio channel using frequency (FM) or pulse (PWM) modulation;
- capacitive signal transmission.

Contact circuits are considered outdated due to large deviations in contact resistance. Among contactless circuits for use in rolling mills, the FM radio channel is the most acceptable. When using an inductive power supply to the sensor on a shaft, a circuit covering the shaft is simultaneously used as a receiving antenna. Therefore, the sensors cannot always be installed on spindles with large eccentricities. They are usually installed on cardan or gear spindles with small beating and long service time. The maximum distance to the shaft is no more than 50 mm. The schematic diagram of the monitoring system is shown in Figure 2.21. Data transmission from rotor to stator over the air gap occurs by a modulated signal, which is then normalized and sampled for storing in a computer.

Among mining machines, where it is needed to acquire torsional vibrations signals, are drilling rigs, load-haul-dump (LHD) vehicles and belt conveyor drives. Besides, the Measurement-While-Drilling (MWD) systems are successfully implemented in deep oil wells development. Dynamical changes in a power transmission line can be noticed implicitly through hydraulic oil pressure, vibrations or sudden changes in drill bit rotational speed. For a boom drill rig, although a considerable number of parameters are monitored now, torsional vibration signals are out of them. The drilling driveline is designed with standard components and there is no possibility of merely adding a torque sensor. On the other hand, torque is a crucial parameter, which can be used for chatter vibrations control and rock properties determination.

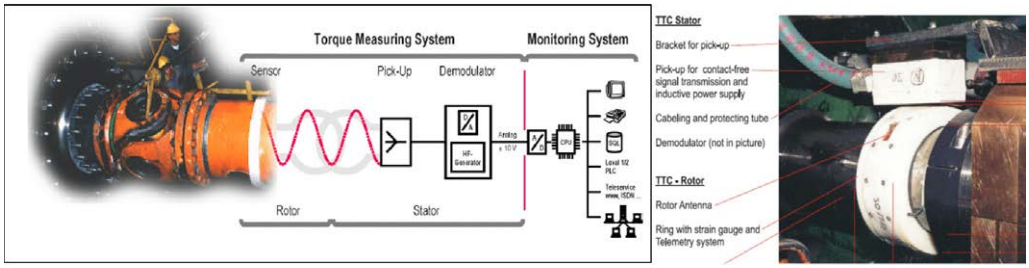

Fig. 2.21. Torque meters based on strain gauges and inductive power supply (ACIDA, VOITH)

Another fruitful example of torsional vibration monitoring is the underground Load-Haul-Dump (LHD) vehicles, which are exposed to intensive reversal loads of transmission and stoppages when the bucket is in the process of filling with bulk material. Their onboard monitoring systems can be improved by adding torque signals reflecting the condition of the powertrain without the need for numerous vibration sensors.

Torsional vibration measurements can be applied to the belt conveyor. Localization of the sensor is often chosen close to the motor, behind the clutch. Unfortunately, the continuous characteristics of belt conveyor work make the installation of measuring equipment limited.

2.7.2. Diagnostics of bolts loosening

Rolling bearings have a wide application in numerous industrial machines. Although bearings are the most standardized elements of transmissions, they are probably the most difficult-to-tune elements in the assembly units. Together with rotating shafts, bearings constitute a complex thermo-mechanical system, whose performance greatly depends on the radial and axial clearances. Any deviations of ring position caused by improper shaft installation, misalignment, or violation of shaft diameter tolerances may interrupt foreseen lubrication flows and homogeneous cooling that in turn provoke thermal deformations and reduction of bearing life. In addition, clearances may cause excessive dynamical loading in the case of gaps re-opening under non-stationary or reverse loading of a machine.

Therefore, clearances may be considered the most important operational parameters of drivelines because of their direct influence on bearing life and the overall reliability of rotating machines. Every producer of rolling bearings has a specification for axial and radial clearances. Neglecting the recommended maintenance rules, installation procedure, revision schedule, lubricant type and supply rate causes the majority of failures, even more than external loading. The influence of an oversized shaft diameter on the bearing life taken from work [213] is shown in Figure 2.22. This deviation in size can be caused, e.g., by the heating of the shaft itself or the bearings.

As it follows from the ISO Standard 5753-1981 (ANSI/AFBMA Standard 20), limits for clearances in the unmounted radial ball and roller bearings are categorised into five classes or groups: "Normal", "greater than Normal", (C3 suffix), "less than Normal" (C2) [214]. Class C3 is used to avoid too little internal bearing clearance in machine operation and is applied for mining and metallurgical machines.

One of the most important factors determining accurate clearances in bearings are the bolted joints that fasten the shaft and the bearings cover to the gearbox housing. The fundamental principle of bolted joints assumes that the designers of machines should predict their operational loads and avoid opening any joint contacted surfaces when forces are greatly increasing and additional com-

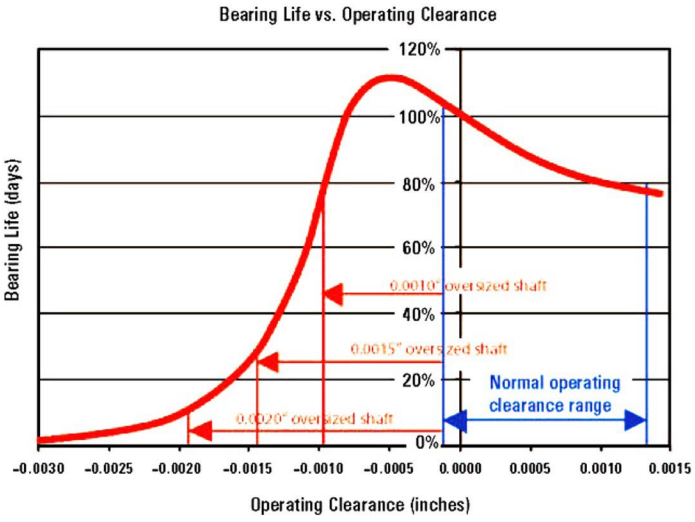

Fig. 2.22. Dependence of the bearing life on the operating clearance [213]

ponents of stresses (torsional, bending, shear) appear in the bolt shank [215]. The greater the preloading (limited by yield stress), the less chance of bolt failure. Although bolted joints preloading has great importance, their tightening torque is not always available for control during repairs and shaft replacement in the transmissions, especially for large-scale industrial plants where bolt diameters can reach 100–150 mm and even more. The metric bolts for heavy-duty gearboxes should have property classes 10.9 or 12.9 (ASTM F568M) and are made of alloy steels (Table 2.4).

Table 2.4. Classes, size ranges and mechanical properties of bolts

Class	Nominal size range, mm	Proof load, MPa	Min. yield strength, MPa	Min. tensile strength, MPa
10.9	5–100	830	940	1040
12.9	1.6–100	970	1100	1220

The strength and durability of high-grade bolt steels (40Cr, 30CrMnSi) are usually improved by quenching and tempering. The application of deep cryogenic treatment is recommended for important parts of industrial machines [216] but is rarely used in practice. An over-elastic pre-load of the screw-nut pair allows one to obtain a significantly higher load capacity, and a self-forming screw is proposed in this regard in [217] to achieve residual compressive stress at the thread root. However, the bolts of heavy-duty gearboxes of mining and metallurgical machines are subjected to fatigue damage due to frequent overloading beyond the allowed yield limits of steel parts.

Historically, direct measurements of installation clearances or the full wear (gap) in the elements of bearings in large-scale machines are conducted by lifting their heavy shafts with special mechanisms or cranes in workshops and then sticking calibrated probes into gaps. These methods require partial disassembly of the machines, for example, removing the end caps on gearbox shafts. This is a time-consuming operation and contributes to the bearings' damage and further reduction of the total life of machines.

The diagnosis of bolts loosening, not only in gearboxes but also in structural elements of buildings or bridges is a complicated scientific and engineering task taking into account the potentially huge number of bolted joints and the dramatic consequences of their loosening, which leads to unpredicted redistribution of internal loads between other bolts in joints.

There are several approaches to the health monitoring of bolted joints. They can be classified into two big groups: based on the use of local sensors or "smart bolts" and the modal analysis of the whole structure or machine. Local contact surface sensors, e.g., by electrical conductivity [218], tension stress measurement by ultrasonic waves [219], high-frequency acoustic emission of low-speed rotating machinery [220], using high-order harmonics and spectral sidebands [221], wave energy dissipation (WED) and vibroacoustic modulation (VAM) [222]. Sensing instrumentation also includes piezoelectric active sensing [223] using wearable sensors [224] and smart washers [225] based on lead zirconate titanate (PZT) transducers, which generate testing stress waves as the actuators. These methods can be supported by wireless data transfer technologies and remote data accumulation for large-scale civil and industrial critical structures.

The axial force reduction decreases the stiffness of the "bolt-nut" assembly leading to a shift in the characteristic peak frequency of the bending mode. A generation of acoustic emissions occurs due to the relative movement between the contacting elements of joints, e.g., the bolt shank within the clearance hole. Elongation of the bolt due to tensile stress is defined by the time-of-flight (TOF) of ultrasonic waves. The reliability of such methods may be high enough under laboratory conditions but they require more investments for additional sensors and their implementation in actual mining and metallurgical machines is complicated.

In recent years, visual image processing methods have gained popularity in bolts loosening diagnostics [226] using deep learning techniques [227], Hough transforms [228], support vector machine (SVM) [229], density-based spatial clustering of applications with noise (DBSCAN) [230], nonlinear system identification based on empirical mode decomposition [231] and convolutional neural networks (CNNs) [232]. A brief review of bolted joint monitoring is given in [233]. This subclass of methods allows an increase in the productivity of scheduled revisions on large-scale structures even in automatic mode by the drones equipped with cameras and embedded image processing methods. The reliability of such methods is greatly dependent on previous revisions, which are used as the reference points for nuts' position change detection. However, these methods cannot detect bolt creep or axial deformations if not accompanied by a change of nut or head position.

Another class of bolts loosening diagnostic methods uses system modal parameters. The decrease in bolt tightening influences various boundary conditions and can be detected by the changes in natural frequency, phase shift and

modal damping [234] due to less contact friction or stiffness. For example, vibration transmissibility function is determined as a more reliable parameter to identify the state of the joint while natural frequency and modal damping in lower modes appeared less reliable. Strain measurements are carried out using fibre Bragg-grating (FBG) sensors [235] and optimal tightening sequence is determined in multi-bolt connections [236]. Theoretical and experimental studies have been conducted for an assessment of modal properties for the detection of bolted joint degradation [237, 238].

Some methods of radial clearance diagnostics by vibration signals are given in [240, 241]. The effect of rolling bearing clearances is also investigated in nonlinear dynamic models. A simulation of truck transmission gearbox FEA in [242] showed that the loosening of one bolt varies the natural frequency in the 1637–2674 Hz range. Experimental research conducted in [243] on the flange plate joints of a wind turbine tower showed that the first-order phase difference parameter is more sensitive to the looseness of the bolts. A combination of FEA with vibration and impedance responses measurement of wind turbine tower for bolts loosening detection is given in [244]. FEM simulation is used in [245] for a lightning rod flange-bolt structure unit (FBSU) analysis. The authors in [246], considering a bolt as an axially stressed and clamped at both ends beam, proposed a simple method to determine the bolt tightness by natural frequencies and damping ratios in hammer impact tests, in particular, the first transverse natural frequency [247]. Damping ratios and nonlinearity in the bolt's frequency response were examined in [248], and the natural frequencies are found to be practically independent of the amplitude of hammer test impacts.

A more general multi-degree-of-freedom (MDOF) model is developed in [249] accounting not only for bolt tightening but also material or boundary nonlinearities in structures. Faults are detected with a second-order output spectrum (SOOS) and local tuning approach (LTA). A comprehensive overview of bolt tightening force measurement and loosening detection is presented in [250]. The authors in [251] demonstrated the implementation of an electronic stethoscope and a continuous wavelet transform (CWT) technique to process and display the transient responses of a bolted joint in a structure to detect loosening and enhance audible perception using audio output. In [252] the authors used instantaneous angular speed (IAS) measurements to analyse the size of local defects in bearings with clearance. Another example of bearing spalling defect diagnostics is given

in [253], where the authors estimate the duration of transient signals at the natural frequency caused by stiffness variation of the structure. The problem is that numerous tightening using uncontrolled torques make the distinction between elastic and plastic elongation difficult for a bolt of large diameter, while tolerance temperature compensation is required in assemblies of heavy-duty gearboxes of mining and metallurgical machines working under harsh conditions.

Some methods [254, 255] are accommodated to bearing condition monitoring under non-stationary working conditions using wavelets, bicoherence, spectral kurtosis and covariance, and high-order spectrum techniques to detect nonlinear features of the signals. Methods are developed for impulsive component extraction in the presence of non-Gaussian heavy-tailed noise due to stochastic impacts from mineral pieces [256–258].

The accuracy of vibration-based diagnosis depends on the reference values corresponding to a healthy condition. For serial machines, such references and alarm levels are determined by a group of similar mechanisms or on a new machine after running at a constant speed and nominal load level. The unique design of mining and metallurgical machines requires new approaches to determining reference values and alarm levels for health indicators.

2.7.3. Measurement of angular backlashes

The same as torque measurement, reliable diagnostics of wear (angular gaps) on rotating shafts is an important procedure of maintenance process in many heavy industries. Angular and radial clearances in the drivelines of various machines and mechanisms are the inevitable consequence of their functioning in transmitting torsion load from the engine to the working tools. Clearances, or backlashes, sustained within acceptable limits during operation play a positive role in allowing the installation of large-sized components and assemblies, adjusting possible distortions and displacements, providing lubricant access on all contacting surfaces and eliminating jamming parts, for example, with thermal expansion of bearing elements. However, with increased wear, gaps begin to play a negative role, especially when a cyclical or reversible load is applied to a machine, for example, metal entering the rolling stand. In precision instruments, gaps lead to measurement errors and positioning errors in actuators. As the overall dimensions of the machines increase and, accordingly, the transmitted torsional loads, clearances result in failures due to overloads.

The drivelines for mining and metallurgical machines consist of large inert torsional masses like rolls, gears, couplings and electric motors. During operation, all elements experience large static and dynamic torques and high specific contact loads, which contribute to the wear of the contacting surfaces. For example, bronze spindle pads wear of 5–6 mm happens in 1–3 weeks' time depending on the rotation speed and drive load. Therefore, the angular and radial gaps are the main parameters of the technical condition. In vehicles, the presence of backlash of the steering bodies and transmission also leads to emergencies during operation. The other defects can be considered a consequence of increased dynamic loads. The diagnosing of the open part and whole gaps is a challenging technical and scientific task.

Regulations of equipment maintenance. According to the rules of heavy machinery operation and ISO standards [259], total wear is considered as the parameter of maintenance. The open part of the angular gaps depends on the design features of the drivelines and machine operation modes. If the gaps are closed at the moment of loading and further under torsional oscillations, then the dynamics of the system are not dependable on wear. However, the maintenance staff is interested in the whole wear value (gear teeth thickness, size of slipper pads, etc.). There is a certain contradiction between operating rules and existing standards in diagnostics [260–264]. Known methods of vibration diagnostics in the steady mode of equipment are not suitable for measuring the total wear in the drivelines. When the driveline is loaded, gaps are closed, and at idle period, they are in an uncertain state, i.e., occasionally open under shaft rotations. Resolving this contradiction may be achieved by the following steps having quite different time scales.

- Development of diagnostic algorithms based on the dynamic models, which account for the open/total gap ratio and build functional relations between them and torques.
- Adaptation of existing maintenance rules from limiting total wear values to the maximum torques caused by the opened gaps, which are subject to diagnose.
- Continuous monitoring of loads in the equipment, converting accumulated data into mechanical stresses, comparing them with the strength and durability levels in elements, and assigning maintenance periods based on predicted remaining useful life (RUL).

Attempts to implement computerised systems for loading cycle accumulation and maintenance planning were undertaken quite a long time ago [265,

266] but with less success due to the lack of automation and reliable tools for torque measurement.

Methods and instrumentation for backlash measurement. The theoretical basement of nonlinear systems identification and backlashes analysis is given in [267–269]. However, there are a few experimental studies on the open gap behaviour in heavy industrial equipment and on the reduction of their influence on dynamics [270].

In practice, the use of standard sensors and vibration signals for diagnostics of gaps by known methods allows the wear determination only indirectly, by changing the surface geometry of the contacting parts (teeth, rings and rollers) causing shaft beating within gaps. Both at idle mode and under load, it is very difficult to identify accurately the absolute values of the gaps from the vibration signals. The use of special proximity sensors on the shafts, as in turbine units, is not feasible. The only method proposed for measuring clearances given in maintenance regulations is the thickness-calibrated probes or micrometres.

In automotive diagnostics, as well as in other industries, the basic principle of angular backlash measurement is the static fixation of one half of the coupling and the application of the moment to its second half for gap closing. The sensors can be either dial gauges or optical sensors similar to those used in laser shaft alignment. This principle is acceptable for small-sized machines, or if there are appropriate test benches. Under production conditions, it is desirable to perform diagnostics using electric drives. For this, inertial closure and opening of the gaps in transmissions can be used when reversing, accelerating and decelerating the machine drive.

Quite a lot of patents are devoted to the measurement of wear in mechanisms. According to the method [271], to determine the wear of the main transmission line of vehicles, the transmission is rotated sequentially in the acceleration and coasting modes. As a parameter characterizing the wear of teeth, the ratio of the maximum axial reaction to the average value of this variable in a slowing-down mode is taken. This method is not suitable for reverse gears where both sides of teeth have a certain wear. In [272], the authors provide a device for determining wear in friction pairs of a rolling stand (screw thread and thrust bearing). The device contains sensors of the angular position and displacement of the screws. The signals are recorded, and compared with previous values and thus the wear is determined. In the [273], a diagnostic method of the friction unit of an aircraft landing gear is given. The tested unit is affected by a compressive force,

the deformation is measured and the characteristic of the unit stiffness is built. The transition from one section to another is characterized by a fracture characteristic, the position of which determines the size of the gap in the friction unit. In work [274], to diagnose the wear of the stand linings and work roll chocks, an experimental assessment of the structural damping in the finishing stands of a wide-strip hot rolling mill was performed based on the *Q*-factor of the system in the transient mode of loading. The *Q*-factor (inverse of the damping coefficient) was determined by the formula:

$$Q = \pi \cdot N_e, \tag{2.1}$$

where N_e is the number of oscillations for which the amplitude decreases by $e \approx 2.73$ times.

The highest *Q*-factor of the order of 130–170, which means the maximum amplitude and duration of the oscillations, is determined in stand No. 11. According to the results of wear measurements, it was found that in this stand there was maximum wear compared to the rest of the stands, where the quality factor was about 20–50. The RMS vibration level in the idle mode was also the highest. Therefore, the *Q* can be considered a characteristic parameter of the wear. The quality factor was estimated in the horizontal, vertical and axial directions, thereby comparing this parameter the wear of various components can be estimated.

Methods and devices for contactless (telemetric) measurement of torsional vibrations on rotating shafts of various machines can also be implemented for diagnosing wear (angular gaps) in the drivelines since the torsional moment is highly sensitive to dynamics. For example, the method is known for diagnosing gaps by the time of a torsional shock pulse delay [275] measured in several points of the driveline. However, this method allows the diagnostics of only the open gap in the coupling.

There are known devices based on measuring the angular positions of transmission elements (angular gaps) based on selsynes (self-synchronized), optical and potentiometric sensors. To date, on the available data, those devices and diagnostic methods are not widely used for diagnostics on industrial machines due to the inconvenience of installing the sensors. Sensors, e.g., selsyn, should be installed at the ends of the shafts, which means they are not practical in reality. Optical sensors require precise calibration and enhanced protection against dust

and humidity. Encoders must be also installed at the ends of the shafts, which makes many elements inaccessible for diagnosing angular gaps.

2.8. Advantages and restrictions of model-based condition monitoring

The most general scheme of any machine exploitation is shown in Figure 2.23. Specific models are used at any stage of the machine's life cycle. At the stage of machine operation the control and diagnostic subsystems usually interact and exchange data.

The most difficult from the viewpoint of condition monitoring are systems where separate units, e.g., rolling stands or multi-drive conveyors, are connected through the rolled metal or the belt, and signals are highly interfered with by the adjacent units. However, namely for these machines, stationary systems give the greatest effect because scheduled observations with hand-held vibration collectors are not able to prevent failures.

For mining machines, only stationary systems can provide reliable failure detection before severe damages occur. Additional difficulties appear in mobile underground vehicles like load–haul–dampers, trucks or blast hole drilling machines. They need local acquisition and analysing systems because monitoring data upload to a central server is usually restricted to only one time per working shift (about 6 hours).

Limitations on the applicability of standard approaches to monitoring and diagnostics at heavy-duty machines are taken into account to some extent only

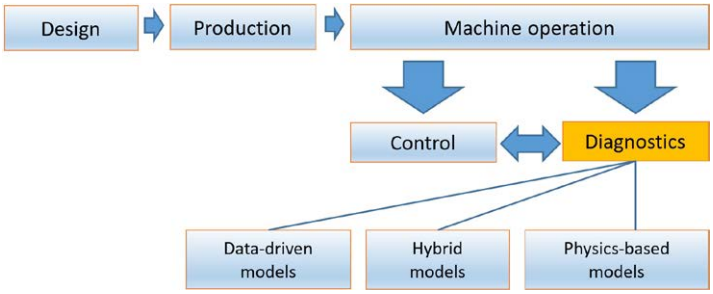

Fig. 2.23. The scheme of machine life cycle and model-based approaches in diagnostics

in some systems. For example, Tensor Systems Company (Australia) uses the "triggering", i.e., recording of vibration signals only in the steady-state stage after the completion of transient processes (capture-ejection of material) that narrows the system's capabilities to prevent equipment breakdowns namely during periods of maximum loading. Some systems use data acquisition that is synchronous with shaft revolutions, which is difficult to implement in the drives with multiple rotational speeds, such as mobile machines or reducing sizing mills with variable gear ratios or differential gears in some multi-stand tube rolling mills.

In this book, some special new methods of wear diagnostics are proposed, which are focused on the analysis of natural vibration frequencies of industrial machines, which are excited during transient modes of operation, which increases the noise immunity and reliability of the diagnostics.

The advantages of such an approach are as follows:

- different parts can be diagnosed where sensors are unavailable;
- alarm values can be derived by the linear model response;
- not only rotating parts of the machine can be monitored;
- can be highly accurate if the machine model is verified;
- required less information than data-driven approaches.

On the other side, this approach requires a good understanding of machine design and certain efforts for model parameter calculations and further adjusting by measurement data. However, once created, the dynamical model can be applied to the whole park of similar machines, e.g., underground frontal loaders, trucks or conveyor drives.

Based on the given above overview of condition monitoring in industrial machines, the main objectives of the scientific research represented in this book, are as follows:

- Development of a unified approach for implementation of reduced-order MDOF dynamical models in condition monitoring of heavy-duty industrial machines.
- Experimental investigation of operating regimes of industrial machines with specific loading and vibrations, analysis of failures and process instability.
- Selection of appropriate classes of dynamical models based on linear, nonlinear or parametric differential equations to describe various dynamic phenomena.

- Application of modal analysis of mechanical systems and selection of natural modes, which are most sensitive to wear (backlashes) and responsible for instabilities.
- Development based on computer simulations of the diagnostic parameters related to nonlinear features of mechanical systems for condition monitoring of machines.
- Design of instrumentation and sensors for direct measurements of dynamic torques and angular backlashes in drivelines of machines.
- Development of diagnostic methods for bolts loosening, bearings and supporting springs deterioration in industrial machines.
- Development methods of dynamics reduction and vibration control in industrial machines with high-pressure hydraulic systems, e.g., tubes testing rigs, mining roof supports and steel rolling mills.
- Dynamics analysis of MMDS systems concerning load equalisation and branched parts interaction, development recommendations for their design and control.
- Development methods of vibration control in industrial machines, which allow the reduction in dynamics and the improvement of product quality.
- Development methods of stochastic load representation and dynamic response calculation in nonlinear mechanical systems.
- Implementation of the developed dynamical models and methods of backlash diagnostics in the condition monitoring and control systems of the industrial plants.

3. CLASSES OF DYNAMICAL MODELS

To apply dynamical models in condition monitoring systems, it has to be created depending on machine design and the technological process where it is engaged. The class and order of these mathematical models should adequately reflect the main features of real objects. State variables are usually the subject of observation by the output measurable signals. Different classes of dynamical models used for condition monitoring of industrial machines are represented.

3.1. Linear models with lumped spring-mass parameters and damping

The standard matrix form of differential equations of a torsional linear system is as follows:

$$[J]\{\ddot{A}(t)\}+[C]\{\dot{A}(t)\}+[K]\{A(t)\}=\{M(t)\}, \tag{3.1}$$

where [*J*] – matrix of rotating inertias; [*C*] – matrix of damping coefficients; [*K*] – matrix of stiffnesses; {*A*(t)} – vector of angular coordinates; {*M*(t)} – vector of forcing torques. The stiffness and inertial parameters of the dynamic model are calculated as follows.

The torsional stiffness of the gear coupling (N m/rad):

$$K_g=\frac{b\cdot d_w^2\cdot\cos^2\alpha_w}{4\cdot k\cdot 10^{-11}}, \tag{3.2}$$

where b – is the width of the mesh; d_w – is the pitch diameter; α_w – pressure angle; k – coefficient of the gear type (k = 3.6 – bevel and helical, k = 6.0 – spur gear).

The stiffness of the cylindrical shaft (N m/rad) is determined by the formula:

$$K_c=\frac{\pi\cdot d^4\cdot G}{32\cdot l}, \tag{3.3}$$

where $G = 8 \times 10^{10}$ MPa is the shear modulus of the shaft material; d – shaft diameter, m; l – length of the shaft section, m.

The moment of inertia of the cylindrical element (kg m^2) is determined by the formula:

$$J = \frac{\pi \cdot d^4 \cdot \rho \cdot l}{32}, \tag{3.4}$$

where d – shaft diameter, m; ρ – shaft material density, kg/m^3.

In the drivelines with gearboxes, the parameters are reduced from the high-speed shaft to the low-speed shaft by the square the gear ratio of the transmission ($i^2 = z_1 / z_2$, where z_1, z_2 is the number of teeth of the driving and driven gear). Physical parameters calculated by the parts drawings and damping factors are then verified by the measurements of transient processes and assessment of their decrements of oscillations.

Frequency Response Functions (FRF) of multibody systems. The FRF-based dynamical systems analysis is widely used in control theory, but can also be efficiently applied to mechanical systems dynamics analysis. The examples of the FRF method use for dynamical systems optimisation are given in [276].

In this research, the FRF-based approach is used to describe and study dynamical processes in industrial machines of different types by representing them as a whole system with a treated material. The advantages of this method for multi-degree-of-freedom (MDOF) systems are as follows:

- FRF is directly derived from equations of motion and allows calculating the amplitudes and phases for each of the natural vibration modes for systems with an arbitrary structure.
- Convenient calculation of response in MDOF systems with multiple inputs-outputs and interconnections between elements, which is a typical case for industrial machines.
- FRFs are the most efficient in the dynamic analysis of MDOF systems for condition monitoring and diagnostics when processing vibration signals in real time.
- Allows accounting in analytical form the damping to optimise and analyse the MDOF systems, including the electric drive, control system, hydraulics and mechanical elements.
- Allows statistical calculations of the dynamic system response when the spectrum of input is known or analytically assigned and allows obtaining distributions of loads and vibrations produced by random inputs.

- Allows certain extensions for nonlinear systems dynamic analysis.

The MDOF mechanical system of machine driveline described by the system of second-order linear differential equations with damping can be investigated using the Laplace transform. The FRF for a single channel is the ratio of the Laplace transform of the output $Y(j\omega)$ to the input impact $X(j\omega)$ supposing that the input varies with different frequencies:

$$W\left(j\omega\right)=\frac{Y\left(j\omega\right)}{X\left(j\omega\right)}. \tag{3.5}$$

In mechanics, the expression inverse to the FRF has the meaning of dynamic stiffness with the dimension [force (perturbation) / deformation (response)]. Modal analysis of the dynamic system can be fulfilled by the amplitude and phase FRFs, which are defined as:

$$A\left(\omega\right)=\sqrt{P^2\left(\omega\right)+Q^2\left(\omega\right)}; \tag{3.6}$$

$$\varphi\left(\omega\right)=arctg\frac{Q\left(\omega\right)}{P\left(\omega\right)}, \tag{3.7}$$

where $P(\omega)$, $Q(\omega)$–are the real and imaginary parts of the complex FRF.

When analysing the torsional system of the machine, the FRF is built for each part where the torque in the elastic shaft is considered as the response, and the loading torque is admitted as the input impact:

$$W_{ij}\left(j\omega\right)=\frac{T_{ij}\left(j\omega\right)}{T_0\left(j\omega\right)}=\frac{b_{k-1}^{2(k-1)}\left(j\omega\right)+\ldots+b_1^2\left(j\omega\right)+b_0}{a_k^{2k}\left(j\omega\right)+\ldots+a_1^2\left(j\omega\right)+a_0}=\frac{\Delta_{ij}\left(j\omega\right)}{\Delta\left(j\omega\right)}, \tag{3.8}$$

where $T_{ij}(j\omega)$ – torque in elastic coupling between masses i and j; $T_0(j\omega)$ – input load torque on rolls; a_i, b_j – coefficients of characteristic polynomial functions; k – order of the system; $\Delta_{ij}(j\omega)$, $\Delta(j\omega)$ – determinants of the system. The numerator is the determinant, where the corresponding column is replaced with the column of the right parts of equations, and the denominator is the general determinant composed of coefficients of the left parts of a system.

It is possible additionally to consider damping when calculating the modes of the driveline oscillations. When a velocity dependant linear damping is introduced into the system, the FRF becomes a complex function, since in the diagonal elements, in addition to the squares of the frequency, terms appear with the first power of the complex frequency.

The use of FRF allows without integration the obtainment of the response at various points. Since the dynamic characteristics of the system are related by the Fourier transform, it is always possible to return from the frequency domain to the time domain by the transition function, which is performed by the expression:

$$h(t) = P(0) + \frac{2}{\pi}\int_0^{\infty} \frac{Q(\omega)\,\cos(\omega t)}{\omega} d\omega . \tag{3.9}$$

With a random input load due to changes, e.g. in friction and rolled metal temperature, the spectrum of the output response $S_{ij}(j\omega)$ in each point of the driveline can be calculated as the product of the square of the corresponding FRF $W_{ij}(j\omega)$ and input load spectrum $S_0(j\omega)$:

$$S_{ij}(j\omega) = \left|W_{ij}(j\omega)\right|^2 \; S_0(j\omega). \tag{3.10}$$

In the case of mining and metallurgical processes, based on this formula, the spectrum of the dynamical response of stochastically loaded machines can be determined.

Modal analysis of MDOF mechanical systems. Since the dynamic behaviour of industrial machines greatly depends on vibration modes, their modal analysis is required for diagnostic purposes. If we consider undamped free vibrations without external excitation, the equation of linear system motion can be represented as follows:

$$[M]\{\ddot{x}\} + [K]\{x\} = 0. \tag{3.11}$$

In modal analysis, the structure is assumed to be linear, and therefore, the response is assumed to be the harmonic functions:

$$\{x\} = \{\varphi_i\}\cos(\omega_i t), \tag{3.12}$$

where φ_i is the mode shape (eigenvector); ω_i is the natural frequency of the mode i. By substituting the values of the response in the equation of motion, it can be written as follows:

$$-\omega_i^2 [M]\{\varphi_i\}\cos(\omega_i t) + [K]\{\varphi_i\}\cos(\omega_i t) = 0 \; . \tag{3.13}$$

The solution $\varphi_i = 0$ is not meaningful, and ω_i needs to be solved as:

$$\left(-\omega_i^2 \left[M\right] + \left[K\right]\right)\left\{\varphi_i\right\} = 0. \tag{3.14}$$

By solving this algebraic equation, we obtain natural frequencies and mode shapes.

3.2. Nonlinear models with piecewise stiffness characteristics

The piecewise linear approximations of different kinds of backlashes occurring in the industrial equipment are given in [277] and shown in Figure 3.1, where the following notation is used: F – force (torque), δ – generalized coordinate of motion (deformation). Function like in Figure 3.1a describes clearance with a dead zone in the driveline couplings caused by wear or assembly errors (both positive and negative δ). In general, transient process calculation supposes that the opened part of gap b may not be equal to a closed part a (the whole gap is $a + b$). Figure 3.1b describes the "softening" stiffness function for bearings, housing and bolting (positive δ). The fracture point means stiffness decreases when a gap is opening between the gearbox housing and bearing cover under the action of severe shock vibrations. Some safety couplings may have the same characteristics, which are frequently installed in the drivelines to prevent overloading in other parts. A positive part of the "hardening" function in Figure 3.1c may correspond to the vertical stiffness of the rolling stand where the fracture point of characteristics corresponds to closing existing clearances under applied load, above which only machine parts deformations constitute the overall rigidity in a certain direction.

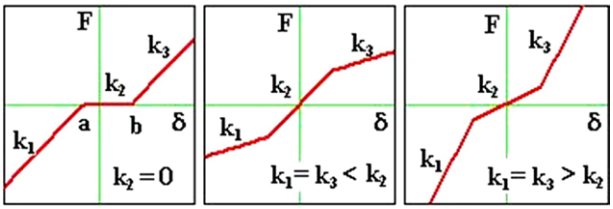

Fig. 3.1. Piecewise linear non-smooth stiffness in the industrial machines: (a) dead zone (backlash); (b) softening; and (c) hardening characteristics

Smoothening functions. Backlashes are described by a non-analytical and non-differentiable discontinuous function of logical type (see below), which worsens model numerical simulations. Therefore, some smoothening functions are analysed and issues of their implementation are discussed in [278]. They are as follows and shown in Figure 3.2:
logical:

$$g_1(\delta)=\begin{cases} k_3(\delta-b)+k_2 b \Rightarrow b<\delta \\ k_2\delta \Rightarrow -a\le\delta\le b \\ k_1(\delta+a)-k_2 a \Rightarrow \delta<-a \end{cases}; \tag{3.15}$$

polynomial:

$$g_2(\delta)=a_1\cdot\delta+a_2\cdot\delta^2+a_3\cdot\delta^3; \tag{3.16}$$

arc-tangent:

$$g_3(\delta)=\delta\cdot a_0\cdot\arctan(\sigma\cdot|\delta|); \tag{3.17}$$

hyperbolic-tangent:

$$g_4(\delta)=\delta\cdot a_0\cdot\tanh(\sigma\cdot|\delta|). \tag{3.18}$$

Adjusting the approximating functions $g_1(\delta)$–$g_4(\delta)$ is carried out by the following parameters a_0, a_1, a_2, a_3, σ. Regardless of the flexibility of such functions, there are certain restrictions for their implementation. Only small dimensionless values of gaps (0.01–0.1) and stiffness (10–100) combinations are available for accurate approximation. Otherwise, scaling factors for the transition to model parameters should be introduced to get acceptable accuracy.

A linear component (a_1) in $g_1(\delta)$ is responsible for gap size, while the cubic component (a_3) is for stiffness approximation. The values $a_1 < 0.01$ do not affect curvature near the zero point. A square component (a_2) gives a possibility of simulating with a polynomial $g_2(\delta)$ function the asymmetry in gap opening conditions (it corresponds to $a \neq b$ in $g_1(\delta)$). Coupling preloading conditions are also available due to square component (a_2) in $g_2(\delta)$ when the symmetry point is shifted beyond the initial point of coordinates. However, when $a_2 > \sqrt{3\cdot a_1 a_3}$ or

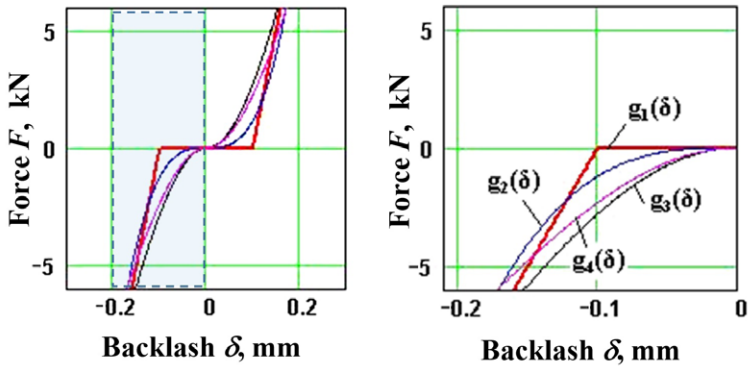

Fig. 3.2. Approximation of non-smooth stiffness characteristic with continuous functions

$a_1 < 0$, two points – maximum and minimum – appear in the $g_2(\delta)$ graph instead of one saddle point. That has to be taken into account during parameter tuning.

Every coupling in the driveline with its unique gap and stiffness values requires a special function for approximation. Right function choice depends not only on gap and stiffness values but is also related to actual torque amplitudes. For example, polynomial type function $g_2(\delta)$ is more accurate near the fraction points of the stiffness curve (within the $\pm 2(a + b)$ range), then, it crosses the original function $g_1(\delta)$ and begins to deviate significantly from it. On the other hand, the arc-tangent $g_3(\delta)$ and hyperbolic $g_4(\delta)$ functions (they are similar in behaviour) are more accurate for large amplitudes far from fracture points (beyond the $\pm 2(a + b)$ range). Therefore, there are no general recommendations for any cases.

The interaction of a_0 and σ is not fully understood and actual limits have not yet been determined definitely. For sure, a smaller σ value corresponds to smaller stiffness, but a smaller a_0 fits a larger gap. The larger the σ value, the closer the approximated $g_3(\delta)$, $g_4(\delta)$ curve to the original piecewise linear function $g_1(\delta)$.

Analysis of approximation functions in the frequency domain. The effect of smoothening functions on the frequency response of an oscillator with clearance nonlinearity was investigated in [278]. The nonlinear identification through feedback outputs (NIFO) technique was also used in [279] to estimate the nominal linear FRFs for the SDOF system using three different generating functions to describe the modulation in frequency response: $\Delta y^{p+(n/m)}$, where Δy is the relative motion across the nonlinear element, n and m are integers such that $m > n$. To

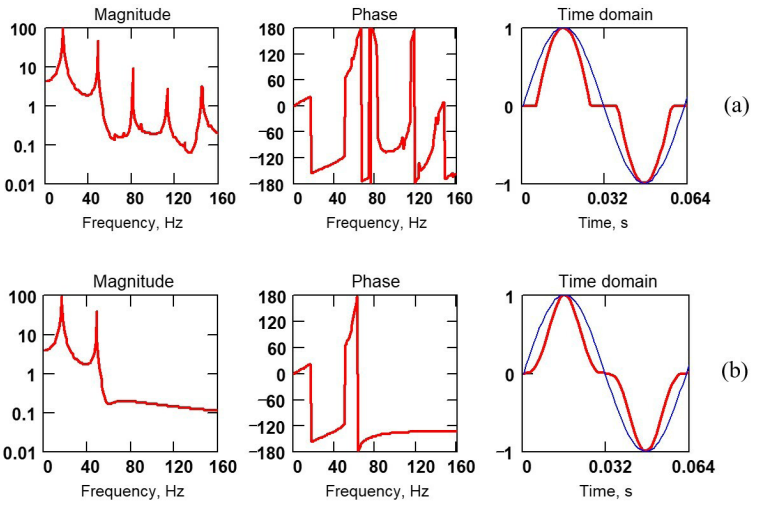

Fig. 3.3. FRF (magnitude and phase) and time domain signal for:
(a) logical g_1; (b) polynomial g_2 functions

estimate the influence of different approximation functions (g_1–g_4) on FRF, calculations were carried out on an SDOF system (Fig. 3.3).

The piecewise functions generate more harmonics and an irregular phase spectrum. The same output exhibits g_3 and g_4 functions (not shown). The polynomial function gives only two harmonics in FRF and a clearer phase portrait. Again, it depends on actual amplitudes of torque and gap value. The more trajectory lays beyond the stiffness fracture points, the less influence of nonlinearities that coincides with experimental results.

Research on the non-smooth characteristics of backlashes with analytic functions showed that this approach has no effect on peak values of dynamical response, but has some restrictions on parameters and produces additional high harmonics in the frequency domain. Therefore, based on the results of calculations, in numerical simulations of the nonlinear dynamical models, backlashes are usually described with the following expression:

$$M_{ij}\left(z_{ij}\right)=\begin{cases}K_{ij}\cdot\left(z_{ij}+k_{\Delta_{ij}}\Delta_{ij}\right), z_{ij}\le -k_{\Delta_{ij}}\Delta_{ij}\\ K_{ij}\cdot\left(z_{ij}-\left(1-k_{\Delta_{ij}}\right)\Delta_{ij}\right), z_{ij}\ge\left(1-k_{\Delta_{ij}}\right)\Delta_{ij},\\ 0, \text{otherwise}\end{cases} \tag{3.19}$$

where M_{ij} – elastic torques (N m); K_{ij} – stiffness in coupling (N m/rad); $z_{ij} = (\varphi_i - \varphi_j)$ – angular deformation of shaft or gear coupling (rad); Δ_{ij} – full backlash in coupling (rad); $k_{\Delta_{ij}}$ – coefficient of initial gap state, which equals 0 for fully opened gap, and 1 when it is closed. This parameter, e.g., $k_{\Delta_{ij}} = 0.80$, means that 20% of full backlash is opened at the moment of load application.

When torque is at the zero levels, backlashes open in the couplings with subsequent shocks until closing. Periodic changes of stiffness from a high average value up to zero are dynamically equivalent to a depth of modulation value $\mu = 1$. This factor increases driveline susceptibility to parametric excitation that belongs to another class of dynamical models.

3.3. Models with time-variable parameters

Periodic changes in the stiffness lead to a change in the natural frequencies of the system and, by their nature, are parametric perturbations. Even small changes in these parameters under certain conditions, depending on the ratio of damping and disturbance, on the one hand, can cause increased oscillations in the mill, and on the other hand, these oscillations are important diagnostic signs, as they directly depend on the conditions of contact interaction in gearing in the focus of deformation.

For a two-mass system with one generalized variable, parametrically excited oscillations are described by the Mathieu equation:

$$\frac{d^2\varphi}{dt^2} + 2\zeta\dot{\varphi} + \omega_0^2\left[1 + 2\mu\cos\left(\omega_1 t + \psi\right)\right]\varphi = 0, \tag{3.20}$$

where $\mu = \Delta\omega_0/\omega_1$ – the relative change in the natural frequency ω_0 or the depth of modulation; ω_1 – the frequency of parameter pulsation; ζ – damping factor.

The standard form of the Mathieu equation can be obtained by substitution of variables:

$$\varphi = e^{-\zeta t}q;\ \omega_1 t + \psi = 2\tau;\ \omega_0^2 = a\frac{\omega_1^2}{4};\ \mu = \frac{\varepsilon}{a}. \tag{3.21}$$

After subsequent substitution of these terms into the original equation, we obtain:

$$\frac{d^2q}{d\tau^2} + \left[a + 2\varepsilon\cos\left(2\tau\right)\right]q = 0. \tag{3.22}$$

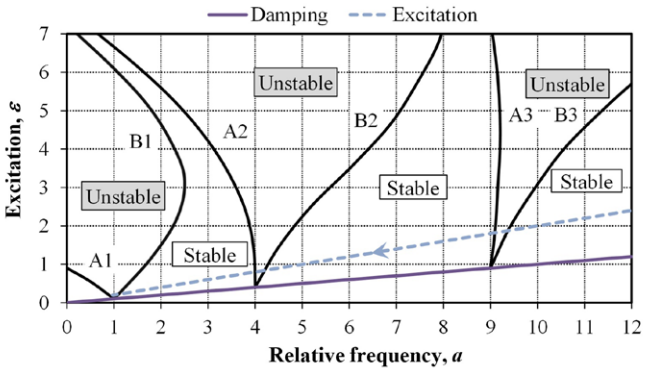

Fig. 3.4. Ince-Strutt diagram of a parametrically excited system
(excitation $m = 0.20$; damping $2d = 0.10$)

Solutions of this equation are special polynomials, which determine the stability regions of the system on the Ince-Strutt diagram (Fig. 3.4) in coordinates (a, ε).

The diagram is symmetrical about the axis a, since the sign of ε in equation does not matter [280]. The more damping and less disturbance, the more stable the system. For a multibody system, a stability diagram is analysed for each natural frequency and perturbation frequency.

With an unlimited increase in the frequency of the disturbance ω_1, the imaging point with abscissa $a = (2\omega_0/\omega_1)^2$ and ordinate $\varepsilon = \mu$ moves along the dashed line to the origin of coordinates (Fig. 3.4), where μ – tangent of inclination angle.

The condition for an unlimited increase in the oscillation amplitude, i.e. the occurrence of parametric resonance, at an arbitrarily small value of the parameter pulsation (points on the axis a of the diagram) is:

$$n_\omega = \frac{2\omega}{\omega} = 1, 2, 3. \tag{3.23}$$

At a significant depth of the parameter's pulsation, resonance may occur when the ratios of frequencies lay in a certain interval within unstable areas around the integer values of the ratio. The larger the pulsation value, the wider these areas are. Therefore, the frequency detuning from parametric resonance is more difficult than from usual resonance with external excitation, since the region of instability can be spread by a confidence interval for calculating the average natural frequency.

The linear damping in the system only narrows the instability regions slightly but is not capable of limiting the increase in the amplitudes of oscillations in the unstable areas of the diagram. Under the action of nonlinear viscous forces of resistance, the oscillation amplitudes are limited. The approximate value of the coefficient μ, at which resonance of the order n_ω is possible, is determined by the relation [280]:

$$\mu \approx \left(\frac{\delta}{\pi}\right)^{1/n_\omega}, \tag{3.24}$$

where δ – the decrement of natural vibrations. Oscillations can develop only above the solid line in Figure 3.4 with the tangent of inclination angle 2δ.

3.4. Models with random parameters and stochastic loading

Two types of uncertainties are encountered in heavy industrial machines: random parameters and stochastic external loading [281]. Backlashes as the factors of stiffness parameters uncertainty and other nonlinearities, can cause chaotic responses in mechanical systems [282, 283]. The analysis of stochastic loading is required for many kinds of heavy industrial equipment, e.g., vibrating screens, crushers, drilling rigs, and long-wall shearers where stochastic loading acts due to unpredictable material parameters and inclusions [284]. Different methods have been developed for random systems analysis: stochastic finite element techniques; random matrix theory and transfer matrixes.

The angular and radial backlashes make a drivetrain essentially a nonlinear multibody system. Drivetrain peak torque $M_{\max}$ produced by input static load M_{st} can be described by a polynomial function:

$$M_{\max}\left(M_{st}\right) = a_0 + a_1 \cdot M_{st} + a_2 \cdot M_{st}^2, \tag{3.25}$$

and corresponding nonlinear function of Torque Amplification Factor ($TAF = M_{\max}/M_{st}$):

$$TAF\left(M_{st}\right) = \frac{a_0}{M_{st}} + a_1 + a_2 \cdot M_{st}, \tag{3.26}$$

where a_i – constants (vary in time of machine operation) describing drivetrain design and machine technical condition; M_{st} – applied torque. Constant a_0 describes

drivetrain losses, a_1 summarizes the design features of a linear system (without wear) and a_2 takes into account nonlinear properties (wear). Coefficient a_1 can be interpreted as TAF for the linear system, which is constant and only depends on the spring-mass parameters and input load rate. System damping principally affects the transient process duration and has an insignificant effect on peak value.

Parameters of alpha-stable distribution $S(\alpha, \beta, \sigma; \mu)$ of impulsive force, which exists in many industrial machines, depends on treated bulk material fraction, the speed of specific loading and geometry of contacting bodies. Simulation of stochastic components in the dynamic model is available based on formulas from [285]:

for $\alpha \neq 1$

$$X = S_{\alpha,\beta} \times \frac{\sin\left(\alpha\left(V + B_{\alpha,\beta}\right)\right)}{\left(\cos V\right)^{1/\alpha}} \times \left(\frac{\cos\left(V - \alpha\left(V + B_{\alpha,\beta}\right)\right)}{W} \right)^{(1-\alpha)/\alpha} + \mu; \quad (3.27)$$

$$S_{\alpha,\beta} = \sigma \times \left[1 + \left(\beta \tan\frac{\pi\alpha}{2} \right)^2 \right]^{1/2\alpha}; \; B_{\alpha,\beta} = \frac{\arctan\left(\beta \tan\frac{\pi\alpha}{2} \right)}{\alpha}; \quad (3.28)$$

for $\alpha = 1$

$$X = \sigma \times \frac{2}{\pi} \left[\left(\frac{\pi}{2} + \beta V \right) \tan V - \beta \log\left(\frac{\frac{\pi}{2} W \cos V}{\frac{\pi}{2} + \beta V} \right) \right] + \frac{2}{\pi} \beta\sigma \log\sigma + \mu, \quad (3.29)$$

where $V(x) = \pi U - \pi/2$ – uniform distribution $U(-\pi/2, \pi/2)$; $W(x) = \lambda \exp(-\lambda x)$ – exponential distribution with the mean $1/\lambda = 1$; $\alpha \in [0, 2]$ – stability parameter; $\beta \in [-1, 1]$ – skewness; $\sigma > 0$ – scale factor; and $\mu \in R$ – mean location.

To account for the stochastic and periodic perturbations of contact friction, the approach is used from the work [286], where the concept of "effective friction coefficient" is proposed, which, by analogy with the mechanics of vibrational transportation, is defined by the following expressions:

$$f_S = f \cdot \left(1 - \frac{\Phi_0}{f \cdot N} \right); \quad (3.30)$$

$$f_s = f \cdot \sqrt{1 - \left(\frac{\Phi_0}{f \cdot N} \right)^2}; \quad (3.31)$$

$$f_N = f \cdot \left(1 - \frac{\Phi_0}{N}\right), \tag{3.32}$$

where f is the initial coefficient of friction without vibrations of contacting bodies; N – normal force; F_0 – the amplitude value of the variable force $F = F_0 \sin(\omega t)$. Formulas (3.30) and (3.31) are used to calculate tangential forces parallel and perpendicular to displacement, while (3.32) describes normal forces, perpendicular to the contacting surface. Worth emphasising that the term "effective friction coefficient" should not be identified with a change in physical friction coefficient under vibration, but only with a change in the proportionality of the tangent friction forces when the load is applied to the bodies.

In the case of eccentricity e of the rotating elements, the amplitude of periodical force:

$$F_0 = m_0 \cdot e \cdot \omega^2, \tag{3.33}$$

where m_0 e – the static moment of imbalance; ω – shaft rotational speed.

For example, with normal forces fluctuations of ±5% and rolled strip tensions of ±15%, the friction coefficient nonlinearly (in proportion to ω^2) decreases by up to 30% with increasing the rotation speed. At a certain speed, a steady state condition ($\alpha < 2\beta$, where α is the contact angle, β is the friction angle) may be violated, which will cause instability in the contact zone.

3.5. Model of electric drive

The dynamical model of the direct current (DC) drive with independent excitation is considered, which is frequently used in speed-regulated industrial machines. The reference value of speed is supplied by the voltage value in the first control zone without changing the magnetic flux of the excitation. In this case, the equations of DC motor motion are as follows:

$$\frac{di_a}{dt} = \left(U_a - i_a R_a - e_a - U_b\right) / L_a; \tag{3.34}$$

$$\frac{d_m}{dt} = \left(\left(M_e - M\right) - K_f \omega_m\right) / J, \tag{3.35}$$

where ω_m – rotational speed (rpm); $M_e = K_m \Phi i_a$ – electric torque (N m); M – load torque on the motor shaft (N m); $e_a = K_e \Phi \omega_m$ – electromotive force (EMF) (V);

K_e, K_m – electrical and mechanical constants of a motor; Φ – magnetic flux of excitation; i_a – load current in the armature (A); L_a – equivalent motor armature inductance (H); R_a – equivalent motor armature resistance (Ω); U_a – armature voltage (V); U_b – voltage drop on brushes (V); J – motor rotating inertia (kg m^2); K_f – damping coefficient in shaft bearings.

Usually, parameters U_b and K_f are neglected in electric drive simulations, but they should be accounted for in the multi-motor drive systems as the additional factors of asymmetry in parallel branches of the driveline. The machine control system is simulated separately to provide acceleration and deceleration of drives by programmable armature voltage U_a supply. For the electric drive simulation above the nominal rotation speed, torque is calculated depending on the rotation speed and applied load.

3.6. Models of gearboxes with bearings and bolted joints

In the most advanced studies of dynamical processes in rotating machines with gearboxes, the complex system of "rotor-bearing-housing" is commonly considered to reflect the existing internal clearances, coupling effects of natural modes and non-stationary loading. Radial clearance and waviness of bearings are investigated in a 4-DOF model [287]. A study of the effect of the radial internal clearance of a ball bearing on the dynamics of a rotor is given in [288]. Many studies are known on regular and chaotic dynamics and stability regimes under the action of imbalances, and external and parametric excitation. These studies of heavy rotor and bearings interaction dynamics are related to constant conditions of speed and loading, mainly found in power generation units. Transient resonances under gradually changing rotation speed are also investigated using parameters maps and Campbell diagrams.

Nonlinear vibration of a two-DOF rotor supported by rolling bearings with clearance is investigated in [289] where the inner and the outer race centres are assumed not to be collinear. As noted in [290], all mining machines are operated in dusty environments causing quick contamination of any lubricant by hard sharp particles and resulting in the wear of bearings and inner gearbox shaft and gear misalignment, which is difficult to account for in gearbox modelling under non-stationary loading conditions. Therefore, transient vibrations of shafts in bearing supports are less investigated, e.g., in pinion stands [291] and gearboxes [292]. An advanced 16-DOF dynamical model of a gearbox with radial clearances

in the bearings is developed and simulated in [293], where the authors noted that bearings contribute to natural modes of vibration.

To understand the importance of bolted joint loosening in dynamics, a simulation of a 3D finite-element model was conducted in [294] and the authors concluded that a creep slip phenomenon exists at the contact surface, which causes bolt self-loosening. Other different factors which influence the self-loosening of bolted joints have been investigated, e.g., the repetition of small slippages at the bearing surface [295] and the effect of hole clearance and thread fit [296]. Transverse displacements and shear stress are considered as the main factors of self-loosening, hence, friction forces created by pretension forces in a thread and joined contacts are the main remedy against it. Usually, bolts are prevented from loosening by different methods, e.g., Grover washers, split pins, and second nuts. However, reliable fixing does not eliminate the creep and plastic deformation of bolts and threaded studs under severe axial loading. Details of bolted joints simulation are presented in the book [297]. Dynamic shear stress represents the main contribution to the self-loosening of bolted joints [298]. The authors discovered that there is a critical shear load amplitude below which loosening would not happen and bolted joints made of quenched and tempered steel and stainless steel have a significant anti-loosening performance.

Based on the conducted analysis of gearbox modelling approaches, it was concluded that the constructed model has to account for the whole dynamical system, i.e., gears, shafts, bearings and bolted joints, which play a crucial role in machine dynamics. Even high-order MDOF models without one of these elements will not reflect exactly the behaviour of industrial plants, which is required for their condition monitoring based on dynamics simulations. On the other hand, if correctly composed, the low-order dynamical models may be practically useful for understanding the reasons for damages and failures in complicated industrial machines.

4. DYNAMICAL MODELS IN CONDITION MONITORING AND ANALYSIS OF INDUSTRIAL MACHINES

The implementation of a model-based approach in condition monitoring helps to determine the most influencing factors on machine dynamics. The detailed multibody dynamical models are represented for different mining and metal processing machines, which can greatly reduce the risks of failures.

4.1. Articulated underground mining vehicles

The haul trucks and load-haul-dump (LHD) vehicles are the main mobile machines engaged in blasted minerals transportation. Their condition monitoring is not a trivial task due to the harsh working environment. The developed virtual soft-sensors are based on low-sampled data and dynamical models for the identification of operational cycles and prediction of the remaining useful life of drivetrain elements.

4.1.1. Detection of working cycles

The problem of the operation of underground haul trucks is investigated, namely, the detection of unloading events when the additional sensor of hydraulic pressure is not available or damaged. In this case, other standard signals from the electronic control units (ECU) can be used to detect automatically these events for the analysis of blasted bulk material transportation [299]. Research aimed to develop a procedure that can reliably identify and count the cycles of a haul truck's unloading moments when the main signal of hydraulic pressure is not available for measurement due to either sensor or cable damage. This is a frequently occurring problem, which requires a solution. The typical

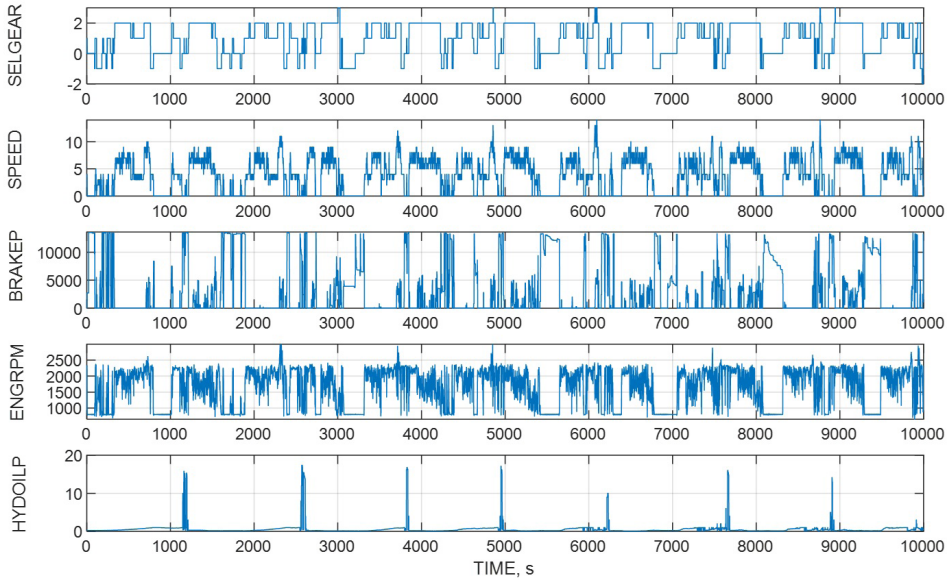

Fig. 4.1. Signals of haul truck: SELGEAR, SPEED, BRAKEP, ENGRPM and HYDOILP

time series of truck motion signals are shown in Figure 4.1 (see notations in Table 4.1).

Pre-processing of source data. The source data from monitoring systems of underground vehicles are stored in the database server of the ore mining company. A list of parameters available for the analysis of underground haul trucks is given in Table 4.1. The procedure of resampling is implemented to obtain the same lengths of data for all parameters with different sampling. Several parameters are linearly scaled for analysis by the coefficients of multiplication – A, and bias – B. The truck was operated by the same driver and at the same mining face, which resulted in approximately equidistant cycles. Depending on transportation routes, each vehicle can produce 8–12 cycles per shift.

Preliminary data analysis and signals selection. Data exported from the database are in the tables where parameters used in calculations can be in different columns. To implement the same procedure automatically over the different data sets, columns of the source data used in the calculations are assigned with indexes (Table 4.2), which means the order of the corresponding column in the tables of different data sets.

Table 4.1. List of parameters monitored in the underground haul truck

No.	Parameters	Description	Units	Sampling, s	Coef. A	Coef. B
1	DATE	Date	yyyymmdd	–	0	0
2	TIME	Time	hhmmss	1	0	0
3	BRAKEP	Brake pressure	KPa	1	0.001	0
4	ENGCOOLT	Engine cool. temp.	°C	90	0	0
5	ENGEXB	Manual brake	0/1	1	0	0
6	ENGHOURS	Hours of work	Hours	90	0	0
7	ENGOILP	Engine oil temp	KPa	30	0	0
8	ENGRPM	Engine rotations	RPM	1	0.001	0
9	ENGTPS	Engine acceleration	%	1	0.1	5
10	FUELUS	Fuel consumption	L/h	1	0.1	10
11	GROILP	Gear oil pressure	KPa	1	0.001	10
12	GROILT	Gear oil temp.	°C	15	0	0
13	HYDDRV	Hydraulic drive	0/1	5	0	0
14	HYDOILP	Hydraulic pressure	MPa	15	1	0
15	HYDOILT	Hydraulic temp.	°C	1	0	0
16	INTAKEP	Intake air pressure	KPa	5	0.1	0
17	INTAKET	Intake air temp.	°C	15	0	0
18	SELGEAR	Gear selection	–4…0…4	1	1	0
19	SPEED	Machine speed	km/h	1	1	0
20	SWITCHMOVE	Switch direction	0/1	1	0	0
21	TRNAUT	Gear automatic mode	0/1	1	0	0
22	ATRNBPS	Brake pedal position	0…100	1	0	0
23	TRNLUP	State of lock-up	0/1	1	0	0

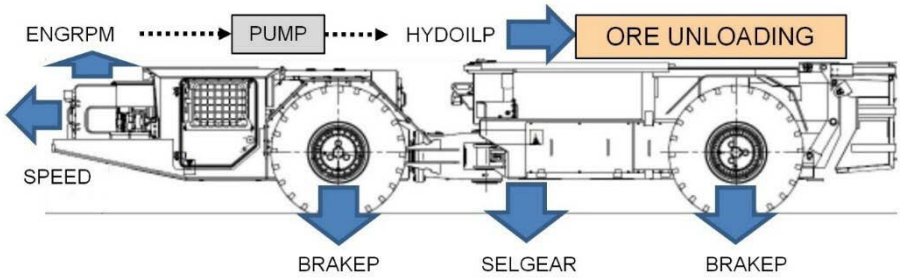

Fig. 4.2. Schematic representation of the haul truck unloading process

The selection of the informative signals among the monitored parameters is based on the dynamics of real machine operation. Therefore, when bulk material is unloaded by the axial force of the hydraulic cylinder, the driver should use the braking system to prevent machine motion in the opposite forward direction (Fig. 4.2). The four signals, which are used for the detection of unloading events, are represented in Table 4.2 with their indexes for three data sets #1, #2 and #3.

Table 4.2. List of parameters used in the calculation and their indexes in the 3 data sets

No.	Signals	Description	Set #1	Set #2	Set #3
1	SELGEAR	Gear selection by the operator	7	8	18
2	SPEED	Speed of machine motion	8	9	19
3	BRAKEP	The pressure of the braking system	1	1	3
4	ENGRPM	Engine rotations per minute	2	2	8

The typical behaviour of signals during the haul truck unloading is shown in Figure 4.3. Some other signals available for monitoring (Table 4.1) which could be used for the identification of operational cycles, e.g., TRNBPS – brake pedal position; ENGTPS – engine acceleration, appeared to be ambiguous and not robust, hence, they were rejected during preliminary analysis.

Deviations of specific patterns in signals from one operational cycle to another can be caused by the volume of material loaded by the LHD machine, a specific driver's manner of truck control, the vehicle's technical condition (engine, brakes, transmission, hydraulics), ECU tuning parameters, road surface and mined material watering. Nevertheless, the signals of haul truck operation

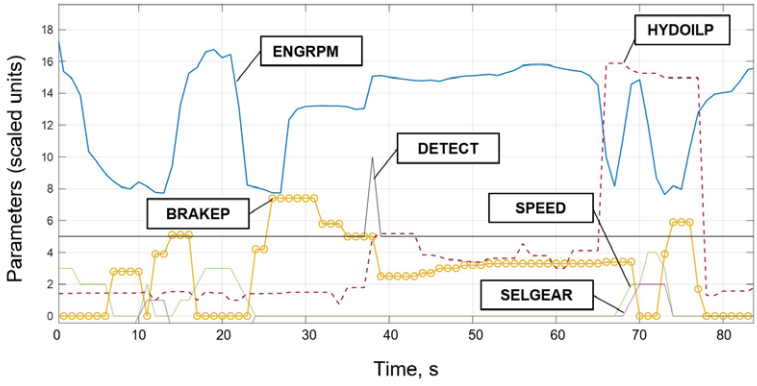

Fig. 4.3. Typical unloading cycle of the haul truck

exhibit some general repeatable regularities, which are not affected by all these factors, and the algorithm of signal processing enables them to provide robustness to any changes in operational conditions.

Signal processing algorithm. During truck unloading, the signal of brake pressure should be greater than a certain minimal value. At the same time, the signal of engine rotations should also be above a certain minimal level to provide a sufficient output flow of the hydraulic pump and the corresponding pressure in the unloading mechanism. Simultaneously, the driver selects a neutral gear and the machine does not move. Hence, logical conditions for the identification of an unloading event can be formulated as follows:

$$BRAKEP > BRAKE\_MIN; \tag{4.1}$$

$$ENGRPM > ENGRPM\_MIN; \tag{4.2}$$

$$SELGEAR = 0; \tag{4.3}$$

$$SPEED = 0, \tag{4.4}$$

where *BRAKE_MIN* – minimal braking pressure during truck unloading; *ENGRPM_MIN* – minimal engine rotations during unloading.

At the second step of data processing, false events are filtered. As it should be taken into account that a certain minimum time interval exists between cycles

and that short peaks in the detection signal are false events (the equivalent of noise), the following logical conditions are used for filtering:

$$COUNT > DELAY; \tag{4.5}$$

$$SUM < POINTS\_MAX, \tag{4.6}$$

where *COUNT* – number of time points since the previous event detection; *DELAY* – minimal time delay to the next subsequent event; *SUM* – number of time points in a detected event; *POINTS_MAX* – maximal number of points in the event. The initial values of the parameters used in the calculations are summarized in Table 4.3.

Table 4.3. Initial values of the parameters used in the calculations

No.	Signal index	Description	Value
1	SELGEAR	Gear selection by the operator	0
2	SPEED	Speed of machine motion	0
3	BRAKEP	The pressure of the braking system	1000
4	ENGRPM	Engine rotations per minute	1800 (1400)*
5	LOGIC0	Logical level “0” of detection	5
6	LOGIC1	Logical level “1” of detection	10
7	POINTS_MAX	Maximal points for filtering	4
8	DELAY	Time delay to the next event	100

*Note: Value 1800 is changed to 1400 at the stage of algorithm tuning.

Signals of BRAKEP and ENGRPM can be normalized either to 100% of the maximal level or to any other assigned value. Logical levels of event detection indicators DETECT1 and DETECT2 are assigned as LOGIC0 = 5 and LOGIC1 = 10, but can be changed to any arbitrary values suitable for further data processing. A schematic diagram of data processing is shown in Figure 4.4. The data processing procedure is organized in two subsequent loops: DETECT1 – detection of unloading cycles; DETECT2 – filtering of detected events.

The program code of the algorithm realization in MATLAB is represented below. Variable DATA_LENGTH contains the total number of samples in the data set, and variable UNLOADS contains the number of finally calculated cycles by

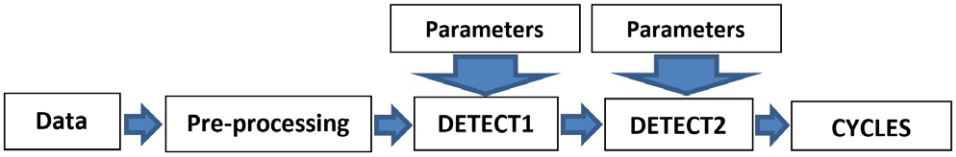

Fig. 4.4. Schematic diagram of data processing procedure

the algorithm. Variables *IND represent the indexes of signals in different data sets.

DETECT1 (detection)

```
DATA_LENGTH=size(data,1);
COUNT = 0;
UNLOADS = 0;
for i=1:DATA_LENGTH
if data(i,SELGEAR_IND)==0 &&
data(i,SPEED_IND)==0 &&
data(i,BRAKEP_IND) > BRAKEP_MIN &&
data(i,ENGRPM_IND) > ENGRPM_MIN &&
COUNT > DELAY
data(i,DETECT1_IND)=LOGIC1;
COUNT = 0;
UNLOADS = UNLOADS + 1;
else
data(i,DETECT1_IND)=LOGIC0;
COUNT = COUNT + 1;
end
end
```

DETECT2 (filtering)

```
for i=1:DATA_LENGTH
if i > POINTS_MAX
data(i,DETECT2_IND)=data(i,DETECT1_IND);
SUM=0;
for j=1:POINTS_MAX
```

```
SUM = SUM + data(i-j,DETECT1_IND);
end
if SUM < POINTS_MAX*LOGIC1
for j=1:POINTS_MAX
data(i-j,DETECT2_IND)=LOGIC0;
end
UNLOADS = UNLOADS - 1;
end
end
end
```

These procedures determine the beginning of every operational cycle as an impulse with the duration of one sampling interval (1 s).

Algorithm verification on real data. The robustness of the developed algorithm is checked on three data sets, as shown in Figures 4.5–4.7.

In the first stage of algorithm tuning, the output signal DETECT2 is compared with the real signal HYDOILP. In the second stage, the signal HYDOILP is not used and is only shown in the graphs below to understand where the algorithm is working properly.

In total, 97 cases of unloading events were processed. The reliability of the algorithm for cycle detection is about 90% and for false cycles, it is about 5%. It is interesting to note that in the last data set #3 (Fig. 4.7) the whole subgroup of events (third working shift) was not detected. The in-depth analysis showed that missing events occurred due to lower engine rotations ENGRPM when a truck is being unloaded, which could be caused by several reasons:

- The distance from the mining face to the conveyor is shorter (shorter cycle time) than in four other shifts, and therefore different working conditions are expected (not documented). More watering of ore material probably caused its easier unloading due to less friction and sliding resistance in the bucket, which in turn corresponds to the less required pressure and engine rotations.
- The average values of peak hydraulic pressure HYDOILP (shown by horizontal dashed lines in Figure 4.7) for the third shift are lower than for the other four shifts, which can be related to fewer volumes of material loaded into the truck by a certain LHD machine at the mining face, and consequently, less hydraulic pressure required for its unloading. This hy-

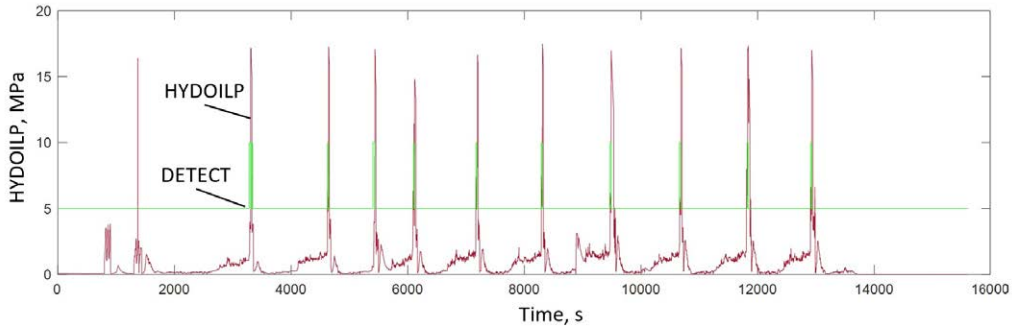

Fig. 4.5. Test data set #1 (10 cycles)

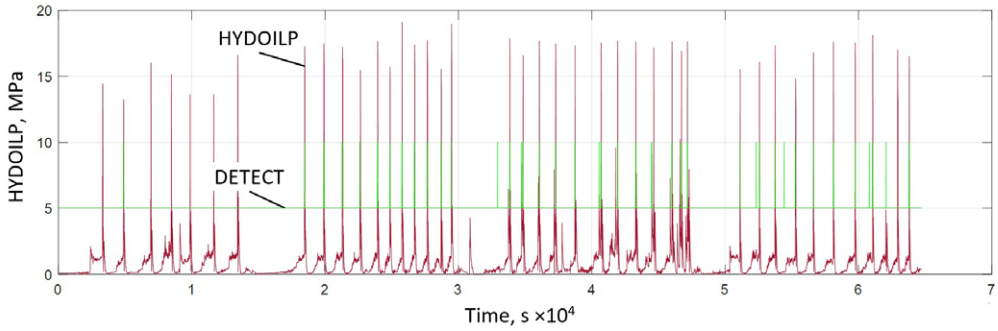

Fig. 4.6. Test data set #2 (40 events)

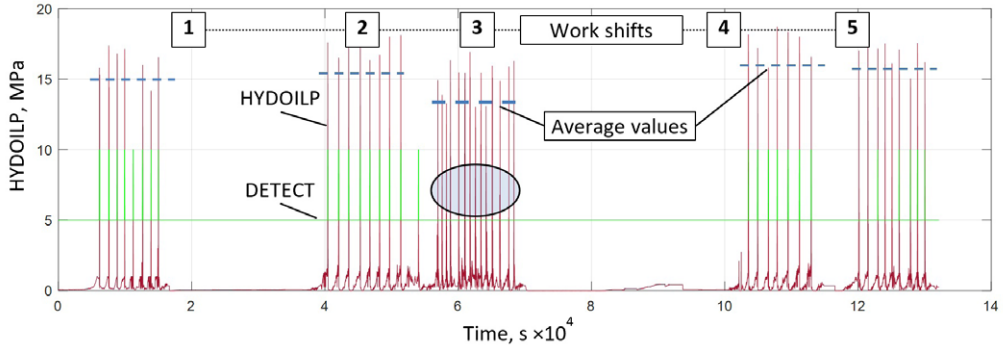

Fig. 4.7. Test data set #3 (47 events)

pothesis can be further interpreted as larger fractions of material (less compaction in the bucket) or, as a result, less density of the material.

- The operator's manner of machine driving, e.g., this person is more sensitive to the load in the bucket and provides precise control of the unloading mechanism with less required pressure and engine rotation.

Tuning of algorithm parameter ENGRPM_MIN from 1800 to 1400 helped solve this problem. This action does not restrict the generality of the algorithm, because it is undertaken only at the beginning of method implementation and therefore management staff do not interrupt calculations in the future. The automatic selection of thresholds should be done based on a statistical analysis of the historical data after the implementation of the developed algorithm.

The developed procedure of signal processing is a virtual sensor, which allows the fault-tolerant detection of operational cycles to be conducted. This is an important and not trivial task for the on-board monitoring systems of underground vehicles because the repair of a damaged sensor or its cable may require a few days or even a week. During this time, the monitoring system continues to collect data and some other failures may occur, which then need to be analysed in correlation to operational cycles. This is the case when the proposed method is especially useful.

The available data sets showed that information from the monitoring system is useful for better understanding and optimization of the operation of underground machines by comparing the manner of drivers working in the same vehicle, operation of different vehicles in the same working conditions, operation of one vehicle in different working conditions, etc. An in-depth detailed analysis is possible if additional tags are provided in the database describing the operational conditions of the particular underground truck and driver identification. Based on historical data processing, management staff can determine: the number of cycles for every driver during the working shift; the average speed of transportation in different routes; and specific fuel consumption for each cycle or per ton and kilometre.

The virtual sensor for detecting unloading cycles uses only standard signals, and the data comes from the ECU. The efficiency of the developed method is independent of external working conditions. It can be implemented as a software procedure that runs automatically once per shift over the historical data on mining enterprise servers. Further research is focused on increasing the accuracy and implementation of other event detection in mobile machines.

4.1.2. Torsional vibration monitoring and remaining useful life prediction

In the underground mines, the heavy load-haul-dumpers (LHD) and hauling trucks (HT) are operated in harsh conditions and subjected to severe dynamic loads due to hard regimes of powertrains loading and intensive steering by operators [300]. To prevent abrupt failures and optimise the maintenance process, monitoring systems are installed on board [301, 302]. The obtained data allow the determination of operational cycles of machines by different signals, however, the high-frequency quickly saturated transient torsional vibrations of large amplitudes are beyond observation [303]. The experimental investigation in the complicated transmissions with a split-path structure or switchable gears in heavy industrial machines requires the installation of strain gauges and special telemetry torque meters on the shafts with subsequent identification of natural oscillation modes and nonlinear behaviour [304]. The analysis of torsional vibrations helps improve machine control [305]. The experimental research of automotive drivetrain on the laboratory testing rig [306] showed a response up to 200 Hz, which is also predicted by the 5-degree-of-freedom lumped parameters model. The vibration properties of the powertrain system have a great influence on the cyclic fatigue damages due to possible resonances at different ranges of shaft rotations and gear meshing frequencies, while the mean engine torque is the main factor causing the fatigue damage of gear parts [307].

To estimate a residual (remaining) useful life (RUL), different prognosis models are under development to accurately predict the crack growth of powertrain components and internal combustion engines, e.g., cracked cylinder heads, and intake valves [308], based on both physics-based modelling and data-driven approaches [309].

Nevertheless, permanent torsional vibration monitoring systems are not characteristic of mining machines due to harsh conditions and issues of permanent power supply on the rotating shafts. Methods of electrical motor current monitoring for machine operation analysis will probably be available in the case of wide implementation of battery-powered underground vehicles. For a while, the mathematical modelling of vehicles has been the main method to study dynamic behaviour under different working conditions. However, some issues complicate the simulation. These are the nonlinear characteristics of drivetrain elements, e.g., angular clearances, which are difficult to measure by known methods, hy-

draulic torque converter [310] with a lock-up, or manual shifting of gears, which change the structure of the drivetrain. The lock-up, besides the influence on the torsional dynamics, can decrease fuel consumption at higher speeds [311] and affect some other operational parameters of heavy underground vehicles.

Since underground vehicles have no spring suspension because of height restrictions, one of the most important elements influencing their dynamics and performance is the tyres. The large-diameter wheels, having huge weight, with corresponding inertial moments, affect the natural modes of torsional vibrations in the powertrains. Besides, the tyres' protector configuration and its intensive wear directly influence torsional dynamics when the vehicle is accelerating and the wheels are subjected to stick-slip contact interaction with the uneven or watered road surface [312]. Since underground heavy vehicles have no spring suspension, tyre stiffness and damping properties determine the operator's comfort under the impacts of large pieces of bulk material and machine safety [313] in the case of tyre failure.

The design of powertrains in underground vehicles is similar for a variety of main producers (Fig. 4.8). Powertrains include a diesel engine combined with a hydraulic torque converter (TC) and manual gearbox, several Cardan shafts and differential-type axles. TC includes the lock-up function to increase power transfer efficiency at high speeds. On the other side, TC efficiently reduces impacts on transmission at the moments when the machine starts motion under load.

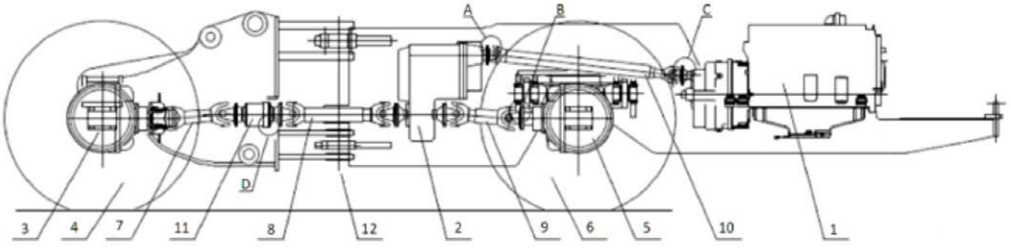

Fig. 4.8. Design of the underground mining vehicle:
1 – diesel engine with hydraulic TC; 2 – gearbox; 3, 4 – front axle with a limited-slip differential, brakes and wheels; 5, 6 – rear axle with brakes and wheels; 7, 8, 9, 10 – cardan shafts; 11 – intermediate support; 12 – articulation joints; A, B, C, D – couplings with potential angular clearances

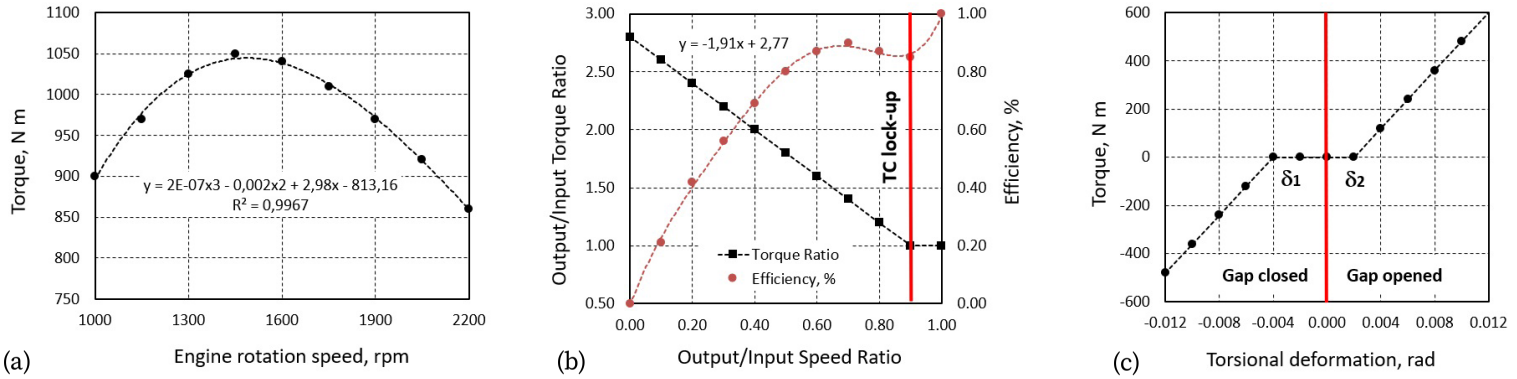

Fig. 4.9. Nonlinear characteristics of elements in transmission: (a) DEUTZ engine function of torque by rotation speed; (b) torque converter with lock-up; (c) cardan shafts with backlash

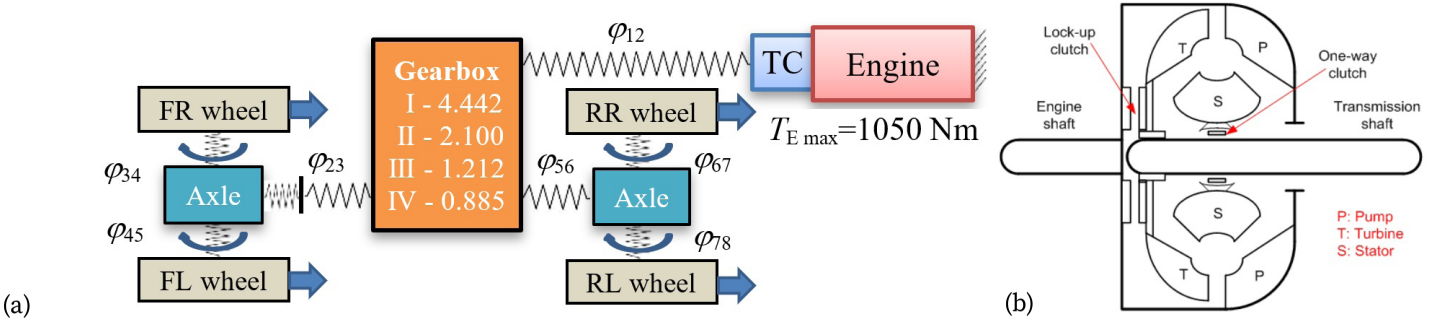

Fig. 4.10. Torsional vibrations model: (a) calculation scheme of transmission; (b) design of torque converter (TC)

When designing the dynamical model, certain issues encountered in the practice of underground vehicle operation should be taken into account, e.g. zero values in monitoring data, missing data due to failures of sensors and cables, different parameters of ECU tuning (engine, gearbox), variable road conditions (water, gradient, unevenness) and rocks properties, specific driving manner of each operator. Therefore, the dynamical model of an underground vehicle is based on certain assumptions:

- Inertial moments of the engine crankshaft, pistons, rods, and flywheel are constant.
- Engine torque is nonlinearly related to the speed of rotation (Fig. 4.9a).
- The speed of engine rotation is linearly proportional to the acceleration pedal position.
- The torsional stiffness of wheel tyres is constant and not dependent on deformation.
- Braking forces on all wheels are equal and linearly depend on the pedal position.
- Torque converter output is linearly related to the speed ratio of shafts (Fig. 4.9b).
- The stiffness of Cardan shafts is nonlinear (Fig. 4.9c) and independent of inclination.
- The interaction of torsional vibration and spatial motions is neglected.

The calculation scheme of the powertrain model with a scheme of a torque converter (TC) is shown in Figure 4.10.

The systems of differential equations of the dynamical model in absolute angles of rotation and relative angles of shafts' torsional deformation are as follows:

$$\begin{cases} J_1\ddot{\varphi}_1 = T_E\left(n_E, t\right) - T_{TC} \\ J_2\ddot{\varphi}_2 = T_{TC}\cdot i_G - T_{GF} - T_{GR} \\ J_3\ddot{\varphi}_3 = T_{GF} - T_{AFR}\cdot i_{DF} - T_{AFL}\cdot\left(1 - i_{DF}\right) \\ J_4\ddot{\varphi}_4 = T_{AFR}\cdot i_{DF} - T_{WFR} - T_B(t) \\ J_5\ddot{\varphi}_5 = T_{AFL}\cdot\left(1 - i_{DF}\right) - T_{WFL} - T_B(t) \\ J_6\ddot{\varphi}_6 = T_{GR} - T_{ARR}\cdot i_{DR} - T_{ARL}\cdot\left(1 - i_{DR}\right) \\ J_7\ddot{\varphi}_7 = T_{ARR}\cdot i_{DR} - T_{WRR} - T_B(t) \\ J_8\ddot{\varphi}_8 = T_{ARL}\cdot\left(1 - i_{DR}\right) - T_{WRL} - T_B(t) \end{cases} \tag{4.7}$$

$$\begin{cases} \ddot{\varphi}_{12} = \left(T_E\left(n_E,t\right)-T_{TC}\right)/J_1-\left(T_{TC}-T_{GF}-T_{GR}\right)/J_2 \\ \ddot{\varphi}_{23} = \left(T_{TC}i_G-T_{GF}-T_{GR}\right)/J_2-\left(T_{GF}-T_{AFR}i_{DF}-T_{AFL}\left(1-i_{DF}\right)\right)/J_3 \\ \ddot{\varphi}_{34} = \left(T_{GF}-T_{AFR}i_{DF}-T_{AFL}\left(1-i_{DF}\right)\right)/J_3-\left(T_{AFR}i_{DF}-T_{WFR}-T_B\left(t\right)\right)/J_4 \\ \ddot{\varphi}_{45} = \left(T_{GF}-T_{AFR}i_{DF}-T_{AFL}\left(1-i_{DF}\right)\right)/J_3-\left(T_{AFL}\left(1-i_{DF}\right)-T_{WFL}-T_B\left(t\right)\right)/J_5 \\ \ddot{\varphi}_{56} = \left(T_{TC}-T_{GF}-T_{GR}\right)/J_2-\left(T_{GF}-T_{ARR}i_{DR}-T_{ARL}\left(1-i_{DR}\right)\right)/J_6 \\ \ddot{\varphi}_{67} = \left(T_{GF}-T_{ARR}i_{DR}-T_{ARL}\left(1-i_{DR}\right)\right)/J_6-\left(T_{ARR}i_{DR}-T_{WRR}-T_B\left(t\right)\right)/J_7 \\ \ddot{\varphi}_{78} = \left(T_{GF}-T_{ARR}i_{DR}-T_{ARL}\left(1-i_{DR}\right)\right)/J_6-\left(T_{ARL}\left(1-i_{DR}\right)-T_{WRL}-T_B\left(t\right)\right)/J_8 \end{cases} \quad (4.8)$$

where, φ_i, φ_{ij} – angles of rotation and shafts deformation; J_i – moments of inertia; $T_E = f(n_E, t)$ – engine torque, depending on n_E – rotations; $T_{TC} = T_E(n_E, t) f_{TC}(n_E, n_G)$ – TC output torque, depending on input n_E and output n_G speed ratio; $T_B = f(n_B)$ – braking torque on a wheel, depending on pedal position n_B; T_{WFR}, T_{WFL}, T_{WRR}, T_{WRL} – rolling resistance torques on wheels, depending on road conditions and tyre wear; T_{GF}, T_{GR} – intermediate shafts torques; T_{AFR}, T_{AFL}, T_{ARR}, T_{ARL} – torques in front and rear axles; i_G – a current ratio of the manual gearbox; i_A – a constant ratio of the axle; i_{DF}, i_{DR} – variable ratios of front and rear axle differential, depending on vehicle steering and road conditions.

Viscous damping and angular clearances in the elastic joints are introduced via corresponding coefficients and functions. The resonance regimes from periodical excitation of a diesel engine are possible for simulation concerning output shaft speed of rotation, but not considered in this research. The overall torsional dynamics greatly depend on angular clearances in couplings under non-stationary loading conditions. This effect is accounted for with the estimated wear intensity of every shaft coupling by the service time. Additionally, methods of angular gap diagnostics can be applied in vehicle powertrains to estimate real values of clearances.

The examples of torsional vibrations simulation are represented in Figure 4.11, where gearbox shaft and front intermediate Cardan shaft torques are given with their endurance-limiting torques $T_{\max}$. These values are recalculated from the stress for corresponding steel grades taken from the powertrain components specification. The amplitude and composition of natural modes in transient signals depend on frequency response characteristics in every elastic shaft.

Further, the calculation procedure is implemented for fatigue cycle accumulation in the database for the powertrain elements depending on the working

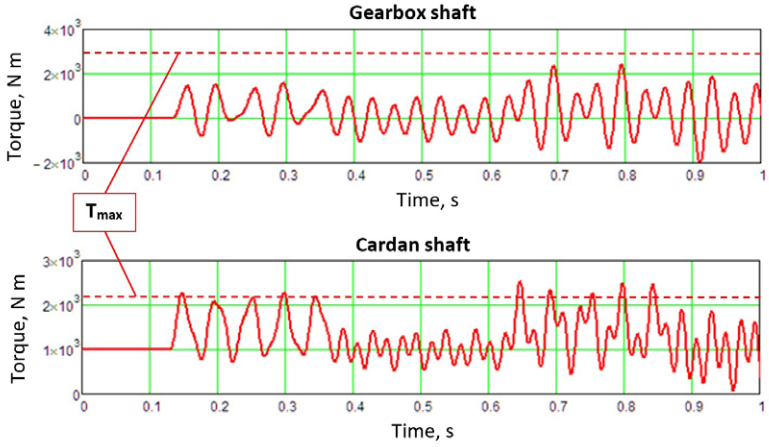

Fig. 4.11. Transient responses to impacts in powertrain: gearbox and cardan shafts

hours of vehicles. The example of RUL information of certain components (Cardan shaft No. 2) retrieved from the database is shown in Figure 4.12a. The S–N diagrams (Wöhler curve) are used to determine cyclic fatigue in elements. Goodman's law is used to process combined asymmetrical cycles of loading and transform them into equivalent reversal stress cycles. The prediction of the date for a predetermined level of RUL (5–10%) achievement is based on standard Miner's rule of damage accumulation.

The convenient representation of the RUL trend with appropriate working load in terms of transported tonnage of materials (Fig. 4.12b) can be used to schedule maintenance and production. Other useful information such as mean time between failures (MTBF), dates and reasons for replacement makes it possible to analyse the separate elements and the vehicle in general.

Nonlinear stiffness (gaps) in different elements of the powertrain resulted in more scattered torsional loads and in correspondingly wider range of accumulated fatigue cycles depending on regimes of vehicle operation (material loading, acceleration, quick stopping). The most dangerous regime for the powertrain of LHD vehicles is the intensive digging into a hill of blasted bulk material. Unavoidable slipping of wheels causes sharp rises and drops of torques in transmission. The torque converter can dampen some impacts to a certain extent. At the same time, the reverses of LHD with additional weight in the bucket also cause torsional vibrations of large amplitudes.

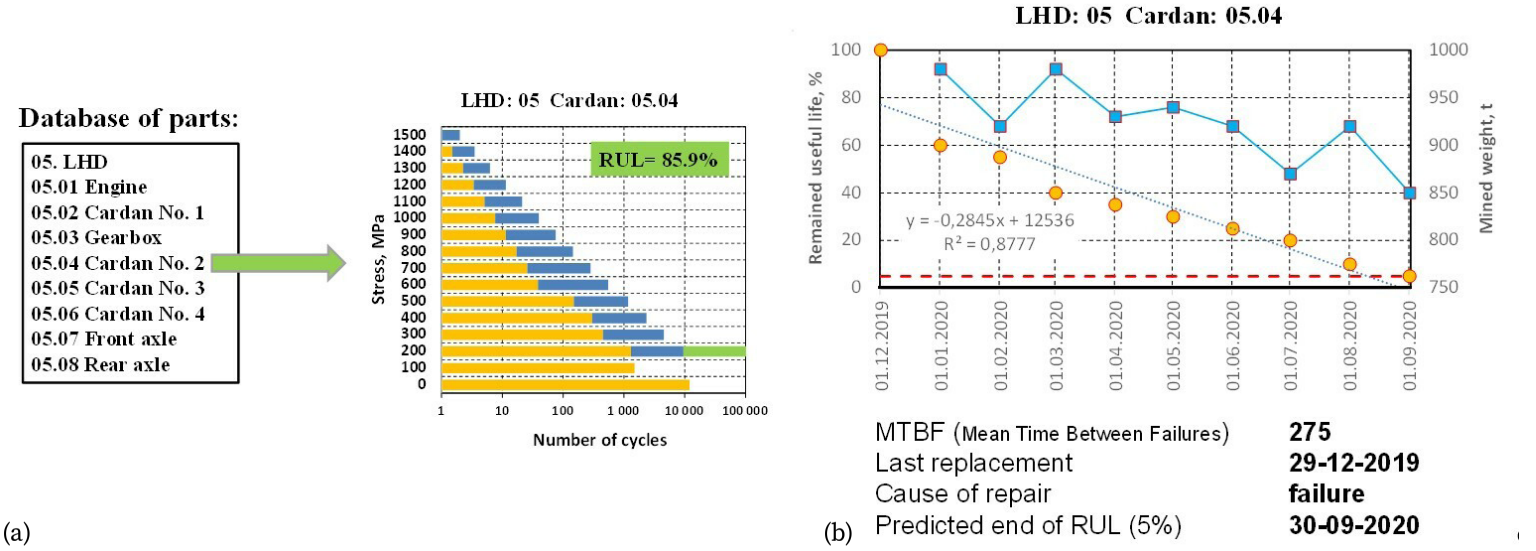

Fig. 4.12. Remaining useful life (RUL) calculations: (a) fatigue cycles; (b) trend of RUL reduction concerning the transported product based on data from the monitoring system

Full-scale vehicle simulation requires additional signals from the monitoring system – articulation angle steering (up to ±40°). Then, more real ratios i_{DF}, i_{DR} in front and rear axle differentials can be accounted for in torsional vibrations calculations.

The developed nonlinear dynamical model of the articulated underground vehicle makes it possible to determine the most severe working regimes from the viewpoint of peak torsional loads in elements of transmission. Including such dynamical models in on-board monitoring systems gives a possibility of calculating and accumulating in the database fast cycles of high amplitude by the slowly sampled data from the on-board monitoring systems that greatly increase the RUL prediction accuracy of elements and safe operation without abrupt failures. In the case of thorough registration of maintenance actions and working hours of vehicles, the developed approach of model-based fatigue monitoring can be applied for maintenance scheduling and parts replacement planning. In addition, using dynamical models helps assess each operator's manner of vehicle control and the improvement of working regimes from the reliability point of view.

4.2. Vibrating sieving screens with inertial exciters

A wide variety of vibrating screens is engaged in the raw materials processing industries. These vibrating machines are involved in the separation of the fractions of ore, coal and other bulk materials. Having a wide range of power, design and number of decks, sieving screens can process from 10 to over 1000 tons of material per hour. Cyclic excitation of the screen decks can be realised by the unbalanced rotating shafts, hydraulic cylinders or electromagnetic actuators. Using decks and particle motion criteria, screens are categorised into circular, elliptical or linear types. Some other types of trajectories or vibration fields can be provided. To increase overall productivity and final quality, several decks can be used.

The typical vibrating screen comprises the body and side panels connected by reinforcing beams, multiple sieving decks, and helical springs (Fig. 4.13a). All parts of the screen experience a significant level of wear. Therefore, huck-bolts are implemented instead of welded joints.

A model-based approach is developed for the diagnostics of spring stiffness reduction or crack initiation in vibrating screens [90]. The investigated sieving screen separates the incoming material (ore) into three grades: <40, 40110, and >110 mm. The maximum dimensions of the ore pieces falling into the sieve are 500×500 ×300 mm. Sieving material is fed to the screen by the belt conveyor having a certain

linear speed. The upper deck of the screen is usually designed as grizzly bars, which provide scalping of the input stream from the extremely oversized pieces to prevent damage. The upper and next levels of decks are subjected to blinding (Fig. 4.13b), which causes screen overloading and technological process interruption. Some methods are proposed for automatic cleaning but only for small-size meshes. Operators of large-scale screens have to clean up manually the accumulated material. The 4 screen supports consist of 3 springs in each corner with parameters ∅210/30 ×410 mm. The nominal stiffness of a full set of 12 springs and proper tuning of vibrators have to provide a designed orbit or trajectory of screen deck motion (Fig. 4.13c).

The screen is driven by two electric motors and individual belt transmissions with 0.582 ratios of pulley diameters. Special spherical roller bearings (FAG T41A series) are used on the shafts of unbalanced exciters.

Application of non-destructive testing (e.g. infrared imaging, magnetic, ultrasound) is a challenge for helical springs because of the complex geometry and non-stop operation mode of a processing plant. Therefore, it is preferable to use the signals of vibration sensors installed on the springs (Fig. 4.14a). Each of the four supporting units on the screen has several helical springs, whose geometry (Fig. 4.14b) and steel properties have gradually deteriorated. Consequently, the amplitude of forced vibration and natural frequencies of the screen are changing.

The unbalanced masses are placed on the shafts under safety covers and allow amplitudes of vibration to change by choosing the preinstalled different numbers of inserted pads. The default value of the producer for screen decks' vibration amplitude is 11 mm at a rotation speed of 850 min^{-1} and with 2 pads on the ends of every

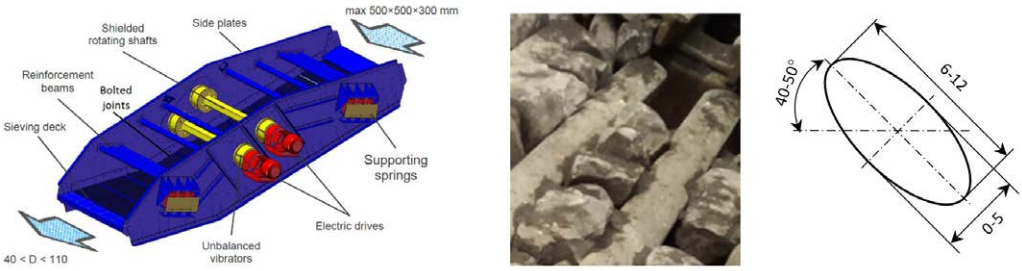

(a) (b) (c)

Fig. 4.13. Vibrating sieving screen (mifama.com.pl): (a) design and elements; (b) blinding with a near mesh size material; (c) the orbit of motion

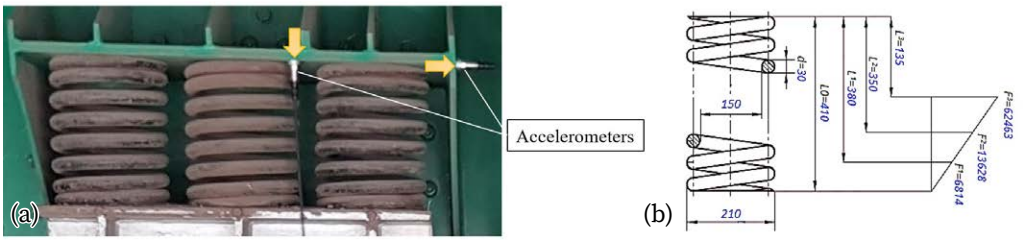

Fig. 4.14. Supporting unit with springs: (a) vibration sensors placement; (b) geometry and deformation limits of a single helical spring

shaft. Usually, vibrators are self-synchronized by either the kinematic gear couplings or dynamically. However, the investigated machine is designed without a kinematic coupling between drives. Hence, depending on the oscillations tuning (accuracy of unbalanced masses mounting, a bias of motors speed control) the screening process may be affected and additional stresses may appear in the elements.

The monitoring system of vibrating screen. The monitoring of sieved material at input and output is realised by the digital cameras. To prevent abrupt failures, a permanent monitoring system (Fig. 4.15) is installed on the investigated vibrating screen of the mining company. Falling pieces of material produce force impacts of large amplitude. Therefore, those stochastic nature disturbances should be accounted for in diagnostic procedures to prevent false alarms.

The conducted research aimed to scale up the functionality of the existing system and improve its performance in supporting spring diagnostics and process monitoring.

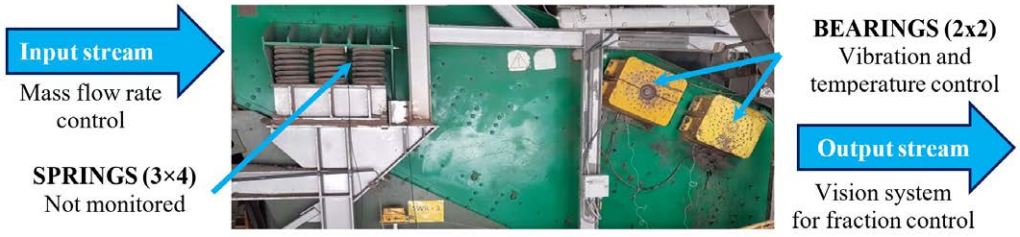

Fig. 4.15. Components of monitoring system on a vibrating screen (non-driven side) with two exciters

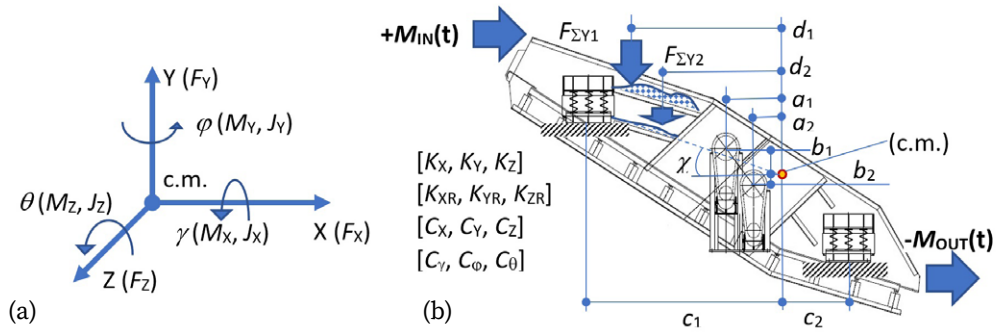

Fig. 4.16. Dynamical model of the vibrating screen:
(a) 6-DOF system of coordinates; (b) geometrical parameters

Dynamical model. The proposed dynamical model assumes that the screen is a rigid body vibrating on the four supporting units having bilinear stiffness characteristics in the case of cracks initiating. Hence, a six-degrees-of-freedom (6-DOF) model is developed, which includes three axes (X, Y, Z) of linear displacements and three angles (γ, φ, θ) of screen body rotation (Fig. 4.16a). The calculation scheme for the analysis of the vibrating screen is shown in Figure 4.16b.

Periodical excitation from two unbalanced vibrators (Fig. 4.17a) is considered a deterministic part of external forces:

$$F_U(t) = m^2 \sin(t + \psi), \tag{4.9}$$

where m – the masses of each unbalanced vibrator; ε – eccentricity; ω – speed of shaft rotation (rad s^{-1}); $\Delta\psi$ – the phase difference between two vibrators because of detuning.

The stochastic part of the equivalent external force $F_{\Sigma Y1}(t)$ applied to the screen consists of two components (Fig. 4.17b):

1) The first component $F_{\Sigma Y1}(t)$ having alpha-stable distribution S (α; β; γ; μ) includes impacts from the input flow. The median point of equivalent force application (p.f.a.) has relative displacements $L_X(t)$, $L_Z(t)$ from a nominal position with Gauss distribution $N(\mu; \sigma)$. Some technological parameters, namely, feed volume, fraction sizes and conveyor geometry affect the external force distribution.

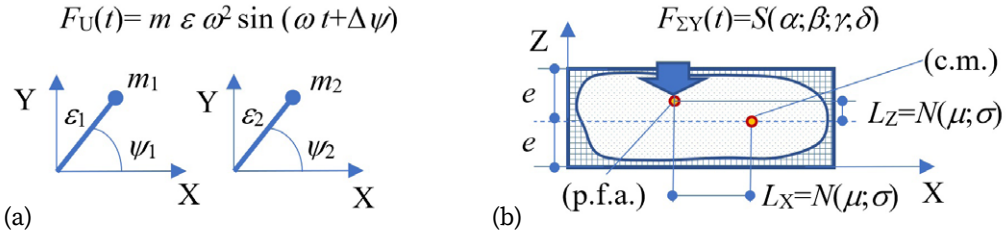

Fig. 4.17. External forces applied to the screen: (a) deterministic; (b) stochastic

2) The second component $F_{\Sigma Y2}(t)$ includes impacts which happen during periodical motions of particles over the decks. The input $+M_{in}(t)$ and output $-M_{out}(t)$ flow should satisfy the mass balance condition, which assumes that the dynamical system has a constant mass during oscillations.

The subsequent sections of the screen may have different inclination angles. Therefore, spring-mass model verification based on vibration measurement has to be based on trigonometric relations between the centre of mass coordinates in the model and the sensors' positions on the screen. The whole system of the differential equations governing the dynamical model is as follows:

$$\begin{cases} M\ddot{x}+C_x\dot{x}+K_x x = A\cdot F_U(t)-k_1\cdot F_{\Sigma Y}(t)\cdot\cos(\chi) \\ M\ddot{y}+C_y\dot{y}+K_y y = B\cdot F_U(t)-F_{\Sigma Y}(t) \\ M\ddot{z}+C_z\dot{z}+K_z z = C\cdot F_{\Sigma Z}(t) \\ J_x\ddot{\gamma}+C_\gamma\dot{\gamma}+K_{XR}\gamma = F_{\Sigma Y}(t)\cdot L_X(t) \\ J_y\ddot{\varphi}+C_\varphi\dot{\varphi}+K_{YR}\varphi = F_{\Sigma Y}(t)\cdot\cos(\chi)\cdot L_Z(t) \\ J_z\ddot{\theta}+C_\theta\dot{\theta}+K_{ZR}\theta = D\cdot F_U(t)+F_{Y\Sigma}(t)\cdot L_Z(t) \end{cases} \tag{4.10}$$

where $K_X = (K_{X1} + K_{X2} + K_{X3} + K_{X4})$ – stiffness of springs in horizontal directions x and z ($K_Z = K_X$); $K_Y = (K_{Y1} + K_{Y2} + K_{Y3} + K_{Y4})$ – stiffness of springs in vertical direction y; K_{XR}, K_{YR}, K_{ZR} – torsional stiffness of angular motion; C_X, C_Y, C_Z – damping of vibrations; C_γ, C_φ, C_θ – damping of rotations; k_1 – coefficient of contact interaction; χ – screen inclination angle; $F_{\Sigma X}(t)$, $F_{\Sigma Y}(t)$, $F_{\Sigma Z}(t)$ – stable distribution $S(\alpha; \beta; \gamma; \delta)$ of stochastic equivalent force from material impacts; L_X, L_Z – normally distributed $N(\mu; \sigma)$ a position of equivalent force $F_{\Sigma Y}(t)$ application, where μ – mean value; σ – standard deviation from nominal position (middle of the deck); A, B,

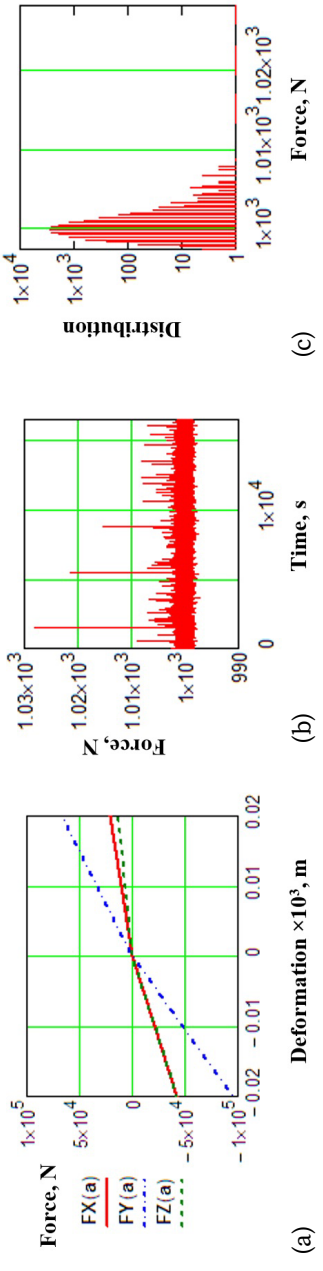

Fig. 4.18. (a) Bilinear stiffness of springs; (b) stochastic force in time; (c) force distribution

Fig. 4.19. (a) Transient vibration; (b) vibration spectra for new (c) and cracked spring

C, D – functions of χ, θ; angles and $\psi_{1,2}$ angles of two vibrators rotation; a_i, b_i, c_i, d_i – position of the centre of mass (c.m.) and (p.f.a.).

The system of differential equations is integrated by the Runge–Kutta method of 4th order with fixed time step. The external stochastic impacts are generated in advance as a vector of numbers and are introduced into the right part of corresponding equations at every time step.

Simulation of springs wear. The predictive maintenance of vibrating screens requires the detection of two main failure modes of springs: reduced stiffness and cracks. The usual approach of machine disassembling and visual inspection, e.g. retained deformation of every spring, is not possible.

After defect initiation and growing in any spring, its linear stress-strain characteristic transforms into the bilinear function, i.e., compression and stretching stiffness are different. The lateral spring stiffness depends on the defect location. Within the vertical plane of vibrator rotations, the vibration signal may have signs of spring damage, otherwise, these defects are undetectable.

To construct the diagnostics rules, the dynamical model, whose parameters are given in Table 4.4, is simulated. The elastic forces of supporting springs with bilinear stiffness are shown in Figure 4.18a. The simulated stochastic impacts from the input flow of material pieces in the time domain are represented in Figure 4.18b and its significantly skewed distribution in Figure 4.18c.

The time series and spectra of vibration for healthy and damaged springs are given in Figure 4.19. Under the action of external impacts, the dynamical system of the vibrating screen responds by transient vibration in the different coordinates of motion. The transient process is quickly attenuated (Fig. 4.19a). In theory, the shift of resonant frequency from its nominal value corresponding to a new spring may be a diagnostic parameter. However, maintenance staff replaces springs not simultaneously in every supporting unit, which has 3 or more springs on other types of screens. Therefore, a single spring stiffness variation is difficult to discriminate, especially due to their typically very small values (Fig. 4.19b). The nonlinear stiffness of springs results in harmonics of the main natural vibration mode (1–2 Hz) and modulation side-band at the excitation frequency (15 Hz) as shown in Figure 4.19c.

The orbit of screen motion reconstructed from the orthogonal vibration signals and phase space plots in coordinates of vertical displacement and velocity are shown in Figure 4.20. The orbit and phase space plots are changing with spring stiffness reduction and crack appearing.

Table 4.4. The parameters taken in simulations of the dynamical model

No.	Parameter	Notation	Value	Units
1	Vibrator 1 horizontal position	a_1	1.400	m
2	Vibrator 2 horizontal position	a_2	0.800	m
3	Vibrator 1 vertical position	b_1	0.900	m
4	Vibrator 2 vertical position	b_2	0.300	m
5	Position of upper springs	c_1	2.600	m
6	Position of lower springs	c_2	1.300	m
7	Point of force $F_{\Sigma Y1}$ application	d_1	2.200	m
8	Point of force $F_{\Sigma Y2}$ application	d_2	1.200	m
9	Width between the springs	$2e$	2.200	m
10	Mass of empty screen	M	15 230	kg
11	Inertial moment	J_X	2.08×10^5	kg m^2
12	Inertial moment	J_Y	4.25×10^5	kg m^2
13	Inertial moment	J_Z	6.13×10^5	kg m^2
14	Stiffness of linear motion	K_X	2.12×10^6	N/m
15	Stiffness of linear motion	K_Y	4.80×10^6	N/m
16	Stiffness of linear motion	K_Z	2.12×10^6	N/m
17	Stiffness of rotation	K_{XR}	3.25×10^6	Nm/rad
18	Stiffness of rotation	K_{YR}	2.60×10^6	Nm/rad
19	Stiffness of rotation	K_{ZR}	5.35×10^6	Nm/rad
20	Position of p.f.a.	L_X	0.200	m
21	Position of p.f.a.	L_Z	1.600	m
22	Angle of inclination	χ	22.5	grad
23	Unbalanced mass of vibrators	m	90	kg
24	Speed of vibrator rotation	ω	88	rad/s
25	Eccentricity of vibrators	ε	0.210	m
26	The phase difference of vibrators	ψ	5	grad
27	Damping of linear motion	C_X, C_Y, C_Z	1.97	s^{-1}
28	Damping of rotation	C_γ, C_φ, C_θ	4.29	rad s^{-1}
29	*S* distribution, exponent	α	1.2	–
30	*S* distribution, skewing	β	1	–

Continuation of the table 4.4

31	*S* distribution, scaling	γ	0.5	–
32	*S* distribution, localization	δ	1000	N
33	*N* distribution, the mean value	μ	0	m
34	*N* distribution, standard deviation	σ	0.1	m
35	Input-output flows of material	M_{in}, M_{out}	236	kg/s

The results of dynamical model simulations are represented in Figure 4.21 with different parameters of machine body vibration concerning the spring's bilinear stiffness change (decrease) from 100% to 50% of the upper positive branch of deformation characteristic. The step of change is 1% for the 90–100% range and 10% for the 90–50% range.

These graphs show that almost all parameters have a linear relation with vertical (*Y*-axis) stiffness change. Horizontal amplitude (*dx*) in Figure 4.21a has a specific bump above 90% and then goes linearly, while vertical amplitude (*dy*) is always

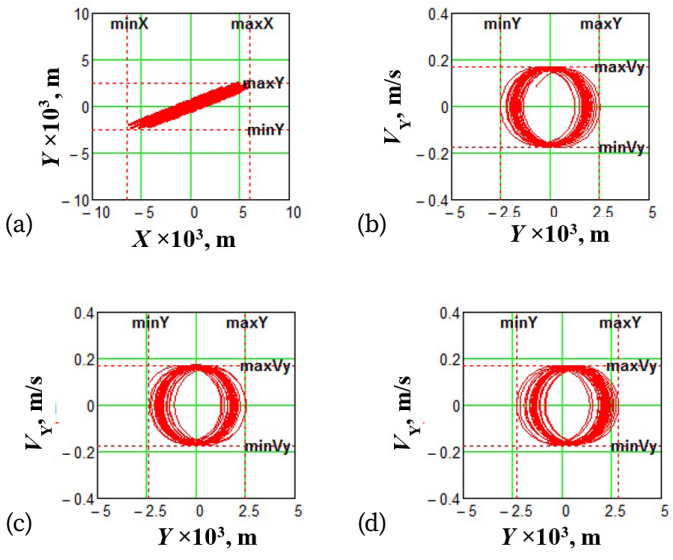

Fig. 4.20. (a) Motion orbit and PSP of vibrating screen: (b) with new springs; (c) with less by 20% stiffness K_Y; (d) with a crack in spring (nonlinear K_Y)

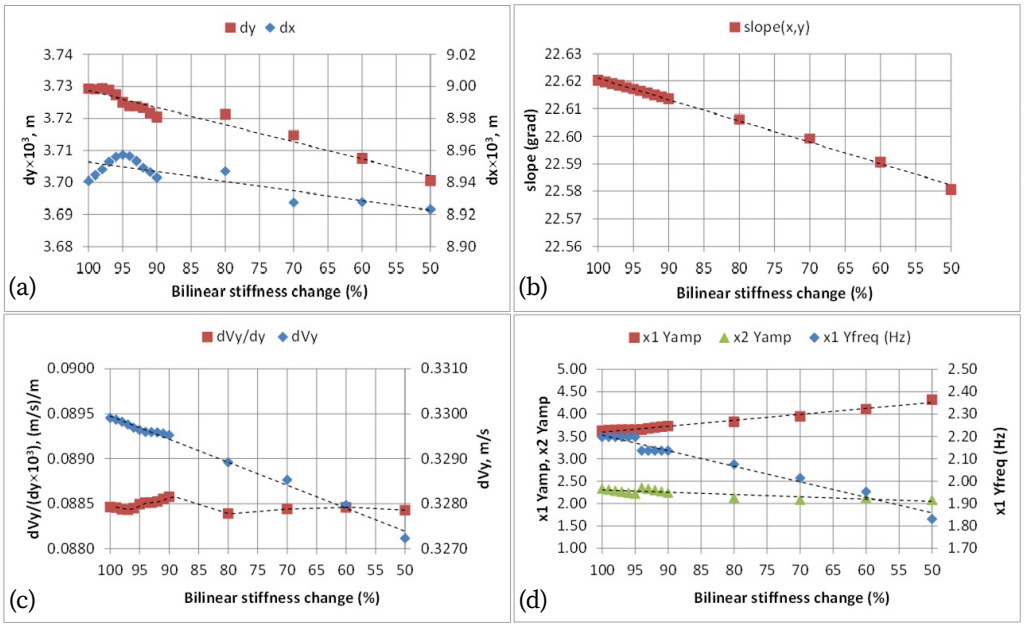

Fig. 4.21. Diagnostic parameters of vibrating screen springs investigated on the model: (a) orbit size (*dx*; *dy*); (b) orbit slope (*x*; *y*); (c) form of phase space plot (dY_y/d_y), (dV_y); (d) natural frequency (×1 Y_{freq}) and amplitudes of first (×1 Y_{amp}) and second (×2 Y_{amp}) harmonics

linear. The sensitivity of these parameters is very small ~0.03 mm/50%. Orbit slope (*x*; *y*) in Figure 4.21b is exactly linear but has weak sensitivity to stiffness change ~0.05°/50%. The form factor of the phase space plot (dV_y/d_y) in Figure 4.21c is almost linear within the whole range of stiffness change, while the amplitude of vibration velocity dV_y is always linear. The sensitivity of velocity is 0.03 (mm/s)/50%.

Natural frequency (×1 Y_{freq}) and amplitudes of its first (×1 Y_{amp}) and second (×2 Y_{amp}) harmonics in Figure 4.21d show linear behaviour but with opposite relation: frequency and first harmonic go down, while second harmonic amplitude increases. The sensitivity of natural frequency is 0.4 Hz/50% and the reaction of its harmonics amplitudes is ~0.2...1.0 mm^2/50%.

Industrial measurements. Vibration measurements are accomplished by the Kistler LabAmp 5165A 4-channel modules and accelerometers K-Shear 8702B500. The other instrumentation included National Instruments 9233 4-channel modules and accelerometers EC Systems VIS-311A and Endevco 751-10. All sen-

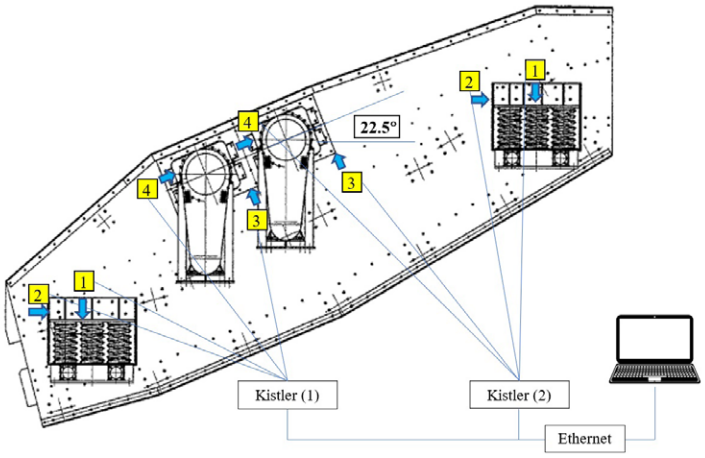

Fig. 4.22. Positions and measurement directions of accelerometers mounted on the vibrating screen

sors have an extended range of measurement (±50–500 g) and sensitivity (10–100 mV/g). Positions of accelerometers and measurement directions are shown in Figure 4.22.

Building orbits of screen motion. The spatial motion orbit stipulated by the screen designers (Fig. 4.13c) is estimated by the vertical and horizontal vibration signals measured on every supporting unit. Notations of signals correspond to

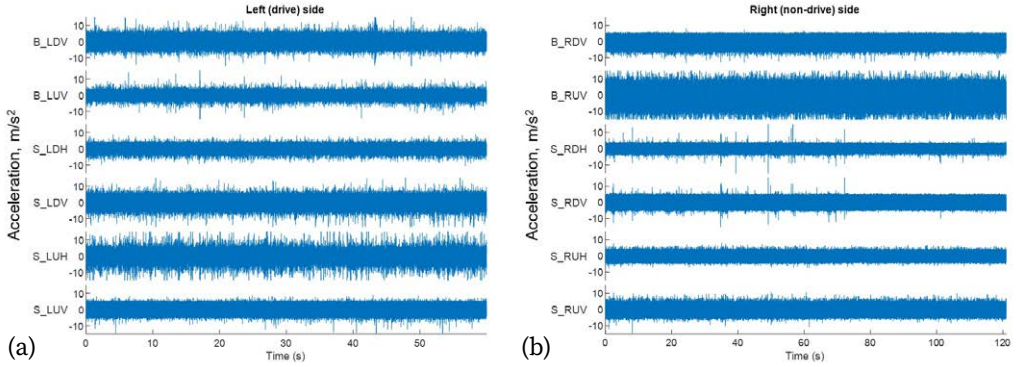

Fig. 4.23. Signals of screen acceleration on:
(a) the left (drive) side; (b) the right (non-drive) side

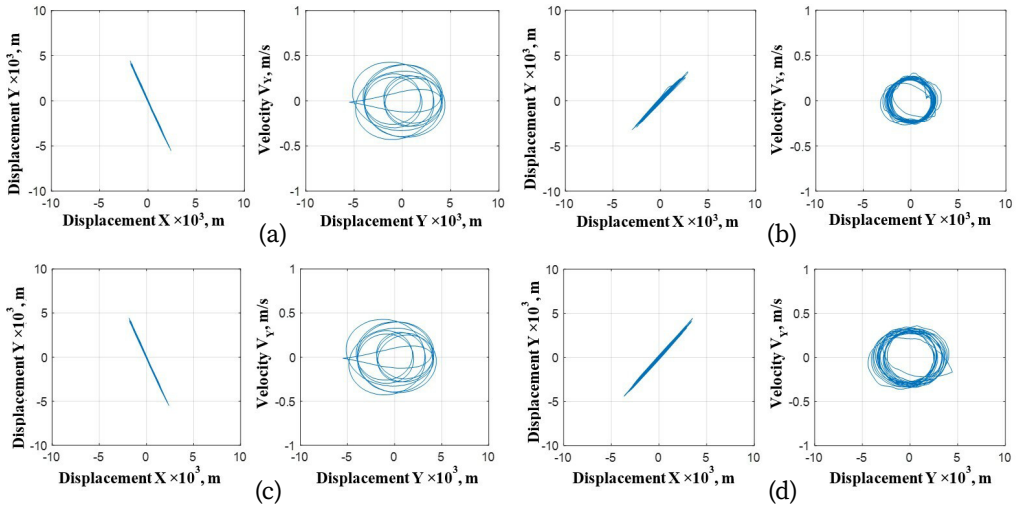

Fig. 4.24. Vibration orbits and phase space plots measured on the supporting springs: (a) up left; (b) up right; (c) down left; (d) down right

Table 4.5. The diagnostic parameters of measured vibration

Pos.	dy × 10^3, m	dx × 10^3, m	Slope, grad	dV_y, m/s	dV_y / (d_y × 10^3), (m/s) /m	×1 Y_{amp}, m/s²	×2 Y_{amp}, m/s²	×1 Y_{freq}, Hz
LU	9.92	4.22	66.9	0.86	0.086	3.50	0.66	1.7
LD	9.88	4.18	67.1	0.85	0.087	4.10	0.66	1.7
RU	6.40	5.87	47.5	0.58	0.090	3.16	0.41	1.8
RD	8.83	7.18	50.9	0.72	0.082	3.36	0.75	1.7

S – springs, B – bearings; L, R – left and right side; U, D – up and down; H, V – the horizontal and vertical direction of measurement. The time series on springs contain the main dominating frequency of excitation about 15 Hz, which corresponds to vibrator shaft rotations.

The orbits obtained by the double integration of the original acceleration signals and phase space plots are represented in Figure 4.23. Orbits on the left springs are inclined to the horizon by 66–67° and by 47–51° for the right side

(Fig. 4.24). Amplitudes of vertical vibrations are about ±5 mm and horizontal – about ±3–4 mm and lay within the design values range (values of projections on the *X* and *Y* axis in Fig. 4.13c). The phase space plots are quite different for the left and right sides even for the similar orbits graphs that give a piece of additional diagnostic information for further analysis. The numerical diagnostic parameters determined by the measured vibration are shown in Table 4.5.

The configuration of orbit greatly depends on the nonlinear trends in the initial signal of acceleration, which affects the final view of the displacement signal after double integration operations. This problem is resolved by the proper selection of a time slot for signal analysis without the remarkable transients from falling pieces of material. Also, the polynomial trend of the 8th order is removed from the initial signals at every stage of their integration.

Damping factors and resonant frequencies. The resonant frequencies and damping in the system are identified by the analysis of the transient response from the falling pieces of material (Fig. 4.25). The verified values of damping factors are given in Table 4.4. Since frequency-independent damping is admitted in the model, some discrepancies may appear in exponential decay values determined experimentally. It is necessary for the synchronous recording of vibration signals and video stream for joint processing to obtain qualitative estimations of stochastic impacts from the input flow of material. The frequencies of identified natural modes of the investigated screen are represented in Table 4.6 and low-frequency spectra are shown in Figure 4.26.

Because of response deviation in the used types of accelerometers in the low-frequency range (12 Hz), natural frequency identification and separation need

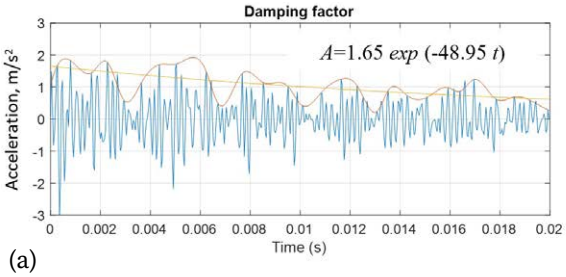

(a)

(b)

Fig. 4.25. (a) Transient vibration on the spring;
(b) image of the input pieces of material

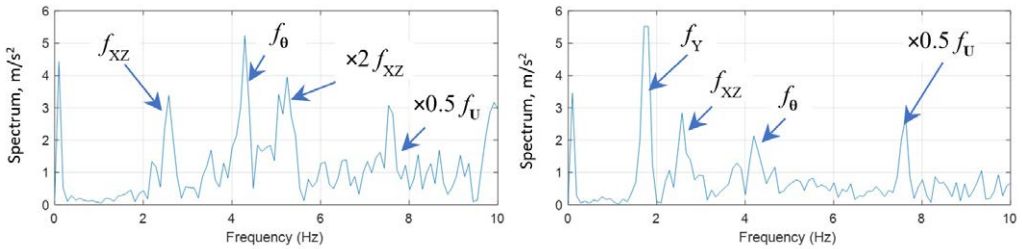

Fig. 4.26. Spectra of low-frequency vibration on the right side of:
(a) up spring; (b) down spring

Table 4.6. The natural frequencies of the vibrating screen

Units	Linear motion frequencies			Rotation motion frequencies		
	f_X	f_Y	f_Z	f_γ	f_γ	f_θ
Hz	1.8	2.6	1.8	3.8	2.9	4.1
rpm	108	156	108	228	174	246

another type of sensor. For comparison, the result of the bump test conducted by Metso Company with the ScreenCheck system on a similar type of vibrating screen is shown in Figure 4.27. Three peaks within the frequency range of 60...180 rpm (1–3 Hz) are the lowest modes of this screen and are quite similar

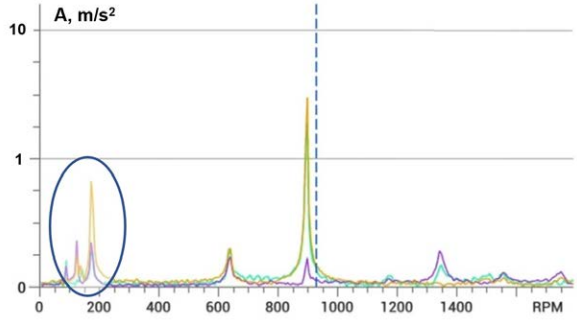

Fig. 4.27. Natural frequencies identified by the bump test
with the system ScreenCheck (Metso)

to values in the investigated screen (Table 4.6). Other peaks correspond to higher modes of vibration (the dotted line is a frequency of exciter rotation).

The screen body is supported by a set of springs. If a change of spring stiffness appears (for example, due to wear or crack), the vibration of the screen will be asymmetrical. It may lead to damage of sieving screen elements. Each suspension unit of the screen consists of 2–4 springs. In such a case, the detection of a single failed spring by the static deformation test under load is not possible. It could be concluded by disassembling and visual inspection of the suspension unit. The non-destructive testing techniques cannot be used here due to the complex geometrical configuration of springs.

The fundamental frequency of screen oscillation caused by unbalanced force (≈15 Hz) significantly exceeds the lowest natural frequency (<3 Hz). Thus, diagnostics of springs by the resonant frequencies shift and harmonics analysis is quite possible although at least 10 s sampling time is required to provide 0.1 Hz spectrum resolution. That is possible under non-stationary stochastic loads, which do not greatly affect natural frequencies. Instead, material impacts excite these frequencies and increase the signal-to-noise ratio at the natural frequency range. Beside, damping factors can be assessed by these impacts as diagnostic parameters.

The 50% of stiffness reduction (0.5 K_Y) will result in 0.4–0.6 Hz or 25–30% of frequency change from the nominal values of about 2 Hz. Taking into account the low natural frequencies 13 Hz, this method of diagnostics needs low-frequency displacement sensors.

An advantage of the proposed dynamical model is in accounting for the random disturbances occurring from the pieces of sieved ore, which modify the amplitude of the signal and point of the equivalent force application. The levels of impact from the falling pieces of material are much fewer than the amplitude from vibrators and quickly attenuated. Anyway, these impacts excite rotational components of motion, which can be as well used as diagnostic parameters.

A localisation of damaged springs among four supporting units might be determined by comparison of 4 signals from different bearings, or sensors installed directly on the supporting units to obtain the more significant difference in displacements between them. The block diagram of the developed diagnostics procedure implementation is shown in Figure 4.28. On-line and off-line steps are divided into separate data flows.

Modification of the stiffness of springs and nonlinear properties due to cracks are noticeable in the results of simulations as the harmonics of natural frequencies

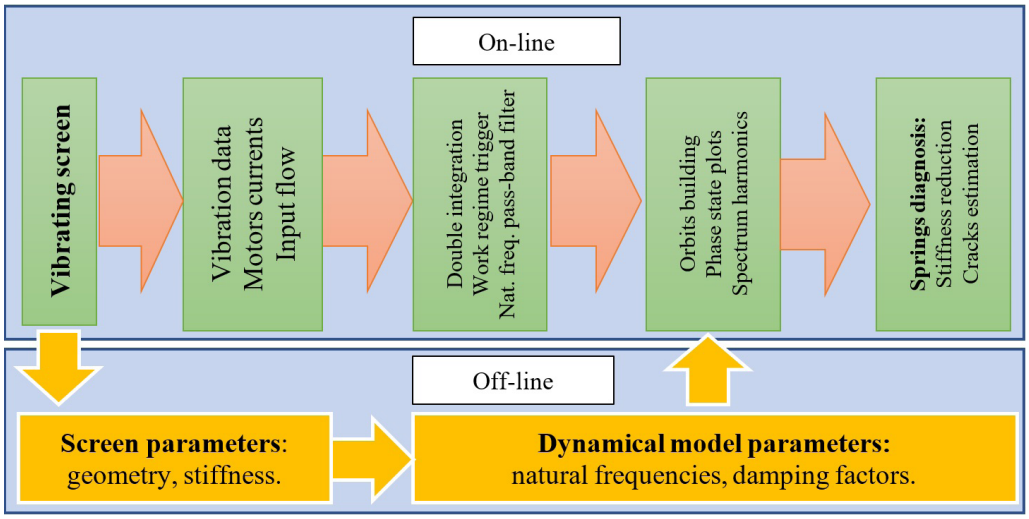

Fig. 4.28. The block diagram of diagnostics procedure implementation

and side-band modulation of the main forced vibration. Simulation experiments on the dynamical model undermined linear relations of orbit size parameters and natural frequency with its first and second harmonics amplitudes. However, the sensitivity of these parameters to bilinear stiffness change is not strong enough.

The proposed parameters of vibrating screen spring monitoring and diagnostics based on natural frequency, its harmonics and the form factor of phase space plot can be generalized for any of three linear coordinates of motion (x, y, z) and angles of rotational vibration (γ, φ, θ). This approach exhibits significant advantages as compared to the spectral methods because it does not require high sampling frequencies.

Using generalised coordinates of screen motion (x, y, z) and derivatives (dx/dt, dy/dt, dz/dt) enables comprehensive visualisation of the whole portrait of the dynamical system. In this research, the author does not address bifurcations of nonlinear systems, which makes the PSP technique strictly susceptible to minor changes in parameters associated with fault development. Application of the PSP technique in daily practise needs to develop qualitative measures of trajectories analysis.

Introducing into the model the external force from the falling pieces of material with the alpha-stable distribution allows a more correct description of a real sieving process for diagnostic purposes. The proposed methods of the vibrating screens monitoring and diagnostics allow the theoretical detection of even weak

(<10%) deterioration of supporting springs stiffness by the different parameters. Linear model response denotes a good condition of springs without damage.

The changes in frequency response functions at the higher natural modes out of the vibrators excitation frequency range can be associated with the structural elements failures or loosen bolted joints and can be considered potential diagnostic parameters.

4.3. Hydraulic mechanisms and machines

High-power hydraulic drives and actuators are an integral part of mining and metallurgical machines. They have certain advantages over mechanical transmissions. However, they have their own working characteristics and failure modes during operation, which require special methods of condition monitoring.

The dynamic properties of hydraulic drives and the mechanisms that contain them are in many ways similar to purely mechanical systems since the working fluid is assumed as incompressible and acts like a usual spring. However, in the process of operation, a frequent change in the volume of fluid in the working space of the cylinders requires the consideration of hydraulic machines and mechanisms as a system with variable elastic-mass parameters and dimensions. The additional problems in modelling create the hydraulic fluid flows in outer space, e.g., under conditions of accidents or safety valve opening. In this case, the constant stiffness of the hydraulic spring becomes nonlinear due to the reduction of compressed fluid volume.

4.3.1. High-pressure rig for drilling tubes testing

The abrupt failure is investigated in the industrial plant for hydrostatic pressure testing of tubes. Significant damages to the testing machine are observed after the moving tube impact when the tube cap has released due to a screw-thread defect. A detailed analysis is conducted of static and dynamic forces acting on elements of structure. Conditions are determined by the sharp cap penetration into the thrust plate and possible damage of the upper protection casing from the water jet and tube pieces impacts. The two options are proposed for plant modernization to reinforce structure for safe work under pressure from 70 MPa to 125 MPa. Simultaneously, the productivity of testing plants up to 14–20 tubes per hour is achieved depending on their sizes.

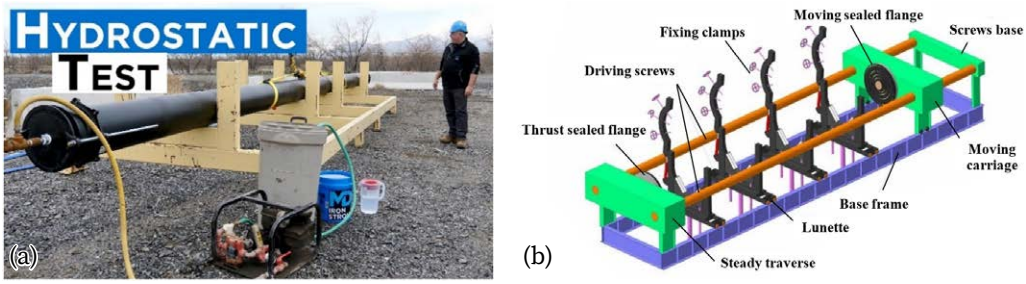

Fig. 4.29. (a) Design of a field test rig [314];
(b) mechanized industrial press for hydraulic testing of tubes [315]

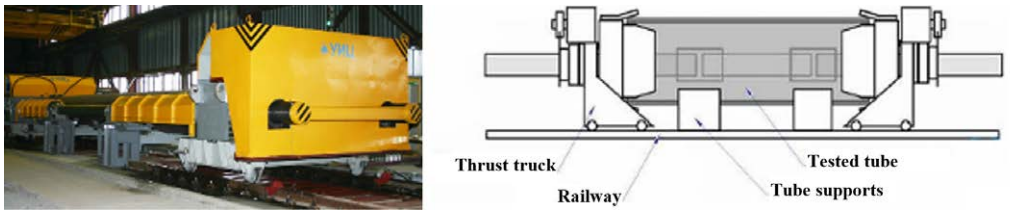

Fig. 4.30. Design of hydraulic press for large diameter tubes testing
with movable axial thrusts [316]

The hydrostatic pressure testing of tubes is an obligatory technological operation after their production in metallurgical plants or by field-tests before drilling operations on oil and gas sites. During the tests, the tube is closed by screw-threaded caps from both sides and filled with water by special pumps to a high pressure of up to 125 MPa. Tubes are kept at this pressure for about 5–10 s to check possible leaks and defects, then they release water and reinstall caps on the next tube. Such a sequential technological process is realized by the special mechanized hydrostatic presses, which may be damaged from the tube exploding due to a crack or a defect of the screw-thread of caps in the case of the machine and surrounding protective structure being improperly designed.

The examples of the design of the existing hydraulic presses for testing tubes with a diameter of up to 1420 mm and a pressure of 70 MPa are shown in Figures 4.29 and 4.30. In these designs for tubes of various lengths, the end thrusts are provided, adjustable by a screw electric drive, as well as locks fixing the tube

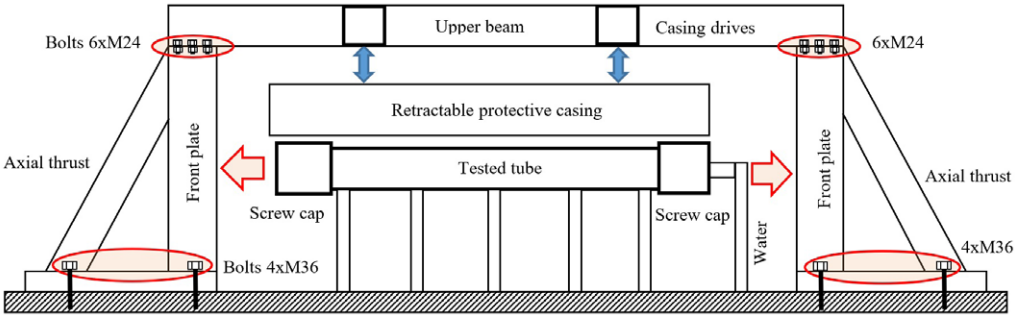

Fig. 4.31. The design of the hydraulic press for tubes testing
with the places of major damages

along the length with a hydraulic drive. However, such variants of hydraulic presses do not provide high productivity for a wide assortment of tubes. The safety issues arising during the operation of high-pressure machines in the restricted areas of workshops and satisfying controversial demands for productivity always need great efforts from the designers. Therefore, industrial customers install testing presses of their design. Such an example of the investigated hydraulic press is represented in Figure 4.31.

During one of the tube tests on this press, under the pressure of 20 MPa (even less than the maximum value by design), one of the end caps suddenly released due to the screw-thread defect and the tube being moved by a water jet hit the protective

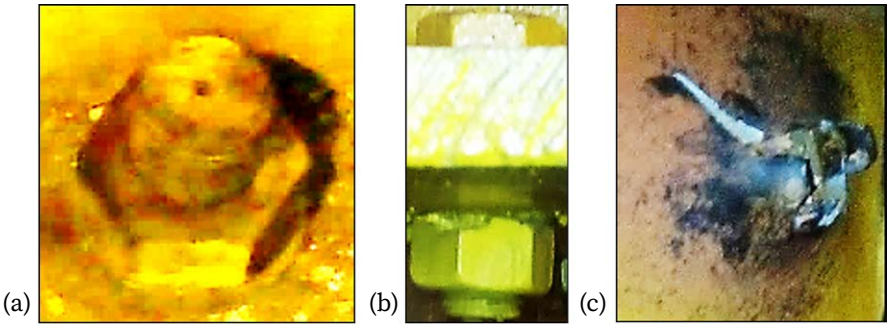

Fig. 4.32. Deformed parts of a hydraulic press: (a) anchor bolt M36;
(b) top beams fastening bolts M24; (c) hole in the front plate (h = 14 mm) of axial thrust

structure of the machine causing deformations and penetration damages. Inspection of the structure after hitting the cap on the left thrust showed visually noticeable signs of deformation of the foundation bolts M36 (Fig. 4.32a) and the bolts M24 of the upper beam joint (Fig. 4.32b). The front plate with a thickness of 14 mm on the right thrust was punched by the impact of the mass composed of the tube with water and the right cap with a sharp end of the pressure line tip (Fig. 4.32c).

Following this incident, it was necessary to conduct a detailed analysis of the strength capacity of the existing protective structure and to develop a modernization plan to restrain all possible static loads and dynamic impacts for safe operation under higher pressures, i.e., 69–125 MPa. Multi-disciplinary research was required (fluid dynamics, mechanical shock and vibration, materials penetration) to estimate diverse impacts on the structure and it was necessary to conduct the multi-variant calculations for a wide variety of testing tubes in terms of their sizes.

According to the API 5CT standard [317], the mechanical properties of the tube material are independent of the assortment of products. Their properties depend only on the tube strength group (class) given in this standard. Impact strength is not controlled on tubes, but only on blanks of caps. In the calculations of the tube fracture, the material reference information included in ISO/TR 10400:2007 is used [318]. The hydrostatic test pressure is limited by the standard [317] to a maximum value:

$$P_T = \frac{2f \cdot \sigma_{y\min} \cdot t}{D} \quad , \tag{4.11}$$

where P_T – the hydrostatic test pressure (rounded by 0.5 MPa), MPa; f – coefficient equal to 0.6 for strength classes H40, J55, and K55 at $D > 244.48$ mm, or 0.8 for all other classes and sizes; $\sigma_{y\min}$ – conditional minimum yield strength for tube body, MPa; D – nominal outer diameter, mm; t – nominal wall thickness, mm.

According to the standard [318], the calculation of the internal pressure at which the metal plastic deformation begins in thick-walled tubes with an end seal (Lame's formula taking into account radial and tangential stresses) is performed according to the formula:

$$P_Y = \frac{\sigma_{y\min}}{\left[\frac{3D^4 + d_{wall}^4}{D^2 - d_{wall}^2} + \frac{d^4}{\left(D^2 - d^2\right)^2} - \frac{2d^2 d_{wall}^2}{\left(D^2 - d^2\right)\left(D^2 - d_{wall}^2\right)}\right]^{1/2}}, \tag{4.12}$$

where $\sigma_{y\min}$ – the specified minimum tensile yield strength, MPa; D – the nominal outer diameter of the tube, mm; $d_{wall} = D - 2kw_{all}\,t$ – inner diameter of the tube, mm; $k_{wall} = 0.875$ – coefficient taking into account the deviation of 12.5% of the wall thickness; t – nominal tube wall thickness, mm; $d = D - 2t$ – the nominal internal diameter of the tube, mm.

As the yield strength of the tubes, it is taken the tensile stress required to obtain the elongation of the sample under the load specified in [317], which is determined using an extensometer. The minimum internal pressure of plastic fracture of a tube with mechanical seal according to the yield criteria of Tresca and von Mises, MPa:

$$P_R = \frac{2k_{dr}\sigma_{u\min}\left(k_{wall}t - k_a a_N\right)}{D - \left(k_{wall}t - k_a a_N\right)}, \tag{4.13}$$

where $k_{dr} = (0.5)^{k_h+1} + (1/\sqrt{3})^{k_h+1}$ – a correction factor taking into account tube deformation and metal hardening; k_h – the coefficient of hardening of the true stress–strain curve (0.06–0.14 for standard strength classes, 0.30 for strongly hardened two-phase steels); $\sigma_{u\min}$ – minimum tensile strength of samples, MPa; k_a – the fracture strength coefficient of samples; $a_N = t\,k_{ac}$ – defect (crack) depth, which can be accepted as permissible at a given acceptance level (0.635 mm with a wall thickness of 12.7 mm), mm; k_{ac} (0.05 or 5%) – predetermined acceptance level; k_a – the coefficient of the metal viscosity influence in the presence of a crack with a depth of a_N (≤1.0 for viscous steels, 2.0 for less viscous steels).

The yield and ultimate strength of the material depend on the group and class of tubes [317]. According to the source data: $a_N = k_{ac}\,t$ mm; $k_a = 1.0$, the calculations of the minimum internal pressures P_T, P_Y, P_R were performed at $H_{\max} = 16$ mm, $D_{\min} = 140$ mm when the maximum values are obtained. The smallest tube fracture pressure will occur with a minimum wall thickness ($H_{\min} = 6$ mm) and a maximum diameter ($D_{\max} = 340$ mm). As the depth of the crack increases relative to the wall thickness, the minimum pressure of tube fracture decreases linearly.

The calculation procedure is proposed for the dynamic impacts on the axial thrusts when the cap is failed, the high-pressure water jet flows out and the possible movement of the tube parts with subsequent penetration into the front plate of the thrust and protective casing.

Assumptions of the model. Mathematical representation of the real physical processes in the industrial hydro-mechanical machine requires certain assumptions.

- The tube moves over the supports without friction because of small contacts between the cylindrical body and the convex surfaces of perpendicular beams (rail profile). The acceleration of the cap and the remaining part of the tube lasts until the water pressure drops to atmospheric pressure, then the parts move by inertia.
- The impact of the caps on the axial thrusts is considered at the tube position on the supporting beams. The broken cap motion occurs without touching the upper protective casing; otherwise, its speed will be lower than the maximum due to the rebound. The whole amount of the kinetic energy of the impacting mass transforms into the potential strain energy of the target, i.e., without friction and heat losses (ideal inelastic shock). This is the worst case for penetration.
- The released water volume, whose mass is determined by the inner tube diameter and the compression ratio, moves as a free jet because of the long distance from the axial trusts (up to 5.0 m). Climatic changes in the temperature do not affect the density and the coefficient of linear expansion. The hydraulic shock inside the tube resulting from pressure relief is not taken into account because the tube becomes an open vessel.
- Only one cap failure is supposed, the second one moves together with the tube under the action of a water jet flowing out under pressure, hence, impacts on the axial thrusts do not occur simultaneously. The time difference of collisions on the left and right sides of the structure depends on the mass ratio of the tube parts and the distances from the thrusts. They are between front plates of thrusts – 15 m; from the right thrust to the tube end – 1 m; from the left thrust to the tube end – 1.5…5.0 m for the tubes of 12.5…9.0 m in length respectively.
- The calculation of the dynamic effect is carried out separately on the bolts and the front plates of the thrusts because penetration and structure response have different scales of time. The impact shear force acts on the bolts of only this support because even the standard elongation of 0.3% (45 mm) of the upper beams (the length of the deformable part is 15 m between the thrusts) already compensates the lateral displacement greater than the diameter of the bolts on the opposite side. Therefore, on the opposite support, the shear force in the bolts can be neglected.
- The degree of steel hardening and the dynamic yield stress are dependable on the strain rate and the static yield stress [319]. The ratio of the dynamic

and static yield stress for St3 steel, of which the protective casing and the front plates of the axial thrusts are made, is 4.1 at a strain rate of 10^5 s^{-1}. However, in our case, the strain rates do not exceed 10^2...10^4 s^{-1}, hence, the dynamic hardening can be ignored.

- The deformation of the front plate of thrust and protective casing occurs only by compression in the direction of impact force, while the shear and bending deformations are not involved. A worst-case scenario is when tube fragments hit the target with a sharp edge. The expansion range of tube fragments is limited by interaction with surrounding structure, i.e., damages beyond the structure and rebound of fragments are not estimated.

Calculation of water jet impact. The force exerted by the water jet depends on the distance between the barrier and the tube end where the cap was broken or the section where the tube was transversely broken (Fig. 4.33). In the compact part, the flow is a continuous stream; in the fragmented part – separate jets; in the sprayed part, single drops [320]. As this distance increases, the pressure force of the jet decreases, since the area of the dispersion circle increases and the pressure in the centre of this circle decreases.

The submerged high-pressure water jet (13–18 MPa) can produce a complicated dynamic structure including cavitation effects [321], different flow patterns and self-excited vibrations when injected close to the surface in the open channel [322]. According to experimental trials [323], the impact force of the high-pressure free jet for pressures up to 85 MPa remains unchanged up to a distance of 0.3 m from the nozzle. At a distance of 0.7 m, it decreases by only 14%. Outside the compact part, the effect of the jet on the barrier becomes insignificant from the viewpoint of the parts' strength capacity. Therefore, it is considered in the

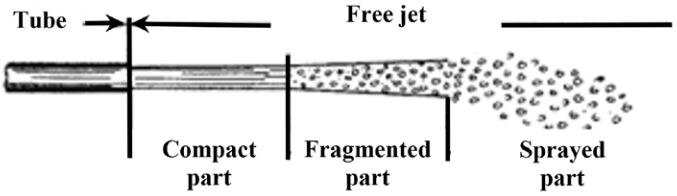

Fig. 4.33. Schematic separation of liquid stream parts when they flow out of a tube

calculations that the compact part of the jet acts on the structure due to the high pressure and small distances from the tube to the protective casing, and the axial pressure impact is not affected by the water flowing from the tube.

The impact of the liquid when it flows out of the vessel under pressure [324], [325]:

$$H = \frac{\Delta P}{\rho \cdot g}, \tag{4.14}$$

where ΔP – the difference between the internal and external pressure (almost equal to the internal pressure in the tube when it flows into the atmosphere).

The fluid flow rate through the hole:

$$v = \phi\sqrt{2gH}, \tag{4.15}$$

where ϕ is the velocity coefficient:

$$\phi = \frac{1}{\sqrt{\alpha + \zeta}}, \tag{4.16}$$

where α is the Coriolis coefficient; ζ is the pressure loss coefficient (resistance).

Volumetric water flow:

$$Q = \mu \cdot S_0 v, \tag{4.17}$$

where S_0 – the cross-sectional area of the hole (inner diameter of the tube); $\mu = \varepsilon\phi$ fluid flow rate; ε – jet compression ratio. If the stream diameter at the outlet of the tube is equal to the diameter of the hole, then the compression coefficient $\varepsilon = 1$ and, therefore, $\mu = \phi$, and the resistance coefficient $\zeta = 0.5$.

The behaviour of the fluid flow depends on the Reynolds number:

$$\mathrm{Re} = \frac{v_u \cdot d}{\upsilon}, \tag{4.18}$$

where $v_u = \sqrt{2gH}$ – the flow velocity under ideal flow conditions; d – the inner diameter of the tube; υ – kinematic viscosity coefficient of water.

For such low-viscosity liquids as water and high Reynolds numbers ($\mathrm{Re} > 10^5$), the coefficients of the outflow conditions vary within small limits and their average values are: $\varepsilon = 0.94$, $\zeta = 0.06$. $\phi = 0.97$, $\mu = 0.91$. When calculating the impact of

the jet on the structure, to obtain an upper estimate of the strength, they can be taken equal to unity.

In hydraulically smooth steel tubes of circular cross-section, when the thickness of the boundary layer is greater than the height of the irregularities, the value of Re ≤ 2200–2300 for laminar flow, the value of Re ≥ 2200–2300 is for turbulent flow. With laminar flow, the length of the compact, denser part of the jet (Fig. 4.33) increases.

The dependence of the kinematic viscosity coefficient of water on temperature:

$$\upsilon(t) = \frac{1.787 \cdot 10^{-6}}{1 + 0.0337 \cdot t + 0.000221 \cdot t^2} \tag{4.19}$$

The values of the kinematic viscosity coefficient of water at $t = 0°C$, $\upsilon = 1.787 \times 10^{-6}$ m^2/s at $t = 50°C$, $\upsilon = 0.658 \times 10^{-6}$ m^2/s, i.e., reduced by 2.7 times. Therefore, in winter, with an increase in water viscosity, the effect of the jet on the structure will be slightly greater than in summer. However, the water density change in the temperature range $t = 0…+50°C$ is only 1.2%.

Following the work [325], water jet impact at known flow rate:

$$H = \frac{v_0^2}{2g}, \tag{4.20}$$

where v_0 – the fluid velocity at the outlet; g – the acceleration of gravity.

The hydrostatic axial force on the tube surface (initial) when a break occurs with an equivalent diameter d_c:

$$F_0 = S_c p, \tag{4.21}$$

where $S_c = \frac{\pi \cdot d_c^2}{4}$ – gap area; p – the internal pressure of water.

The time during which the compressed water volume at pressure p flows out before its pressure equalises with atmospheric pressure:

$$T_c = \frac{\varepsilon \cdot V_w}{Q}, \tag{4.22}$$

where $\varepsilon = p/E_w$ – the relative compression of water (0.0616 at a pressure of 125 MPa); E_w – volumetric modulus of elasticity of water (2030 MPa); Q – the flow

rate of water through a gap with a section S_c at a given pressure (it is considered linearly decreasing and equal to the average value during the compressed volume of water flow). The time of 6.16% of the water volume flow until the test pressure (125 MPa) will equalise to atmospheric pressure (0.1 MPa) is 0.0011–0.0015 s for the entire tube assortment.

The forces of the jet action on the barriers under different conditions are determined following [325]. The formula for the fixed perpendicular barrier (Fig. 4.34a):

$$F_1 = 2\gamma \cdot S_0 H, \tag{4.23}$$

where $\gamma = \rho \cdot g$ – specific gravity of water (9810 N/m^3); S_0 – the cross-sectional area of the jet (the area of the barrier is greater than 4–6 diameters of the cross-section of the jet).

If a flat fixed barrier is located at an angle α to the jet direction (Fig. 4.34b), then the force of the jet is determined as:

$$F_2 = 2\gamma \cdot S_0 H \cos^2 \alpha. \tag{4.24}$$

The force of the jet action on a fixed surface deflecting the flow by 180° (Fig. 4.34c) is twice as high as in the case shown in Figure 4.34a:

$$F_3 = 4\gamma \cdot S_0 H. \tag{4.25}$$

If a flat obstacle moves in the direction of the jet axis with speed u, then the force of the jet action on it will be equal to:

$$F_4 = 2\gamma \cdot S_0 \frac{(v_0 - u)^2}{2g} = 2\gamma \cdot S_0 \frac{w_0^2}{2g}, \tag{4.26}$$

where $w = v_0 - u$ – relative velocity.

Axial hydrostatic force on the thrust:

$$F_5 = S_0 p. \tag{4.27}$$

Radial hydrostatic force to break a tube without taking into account the weight of water:

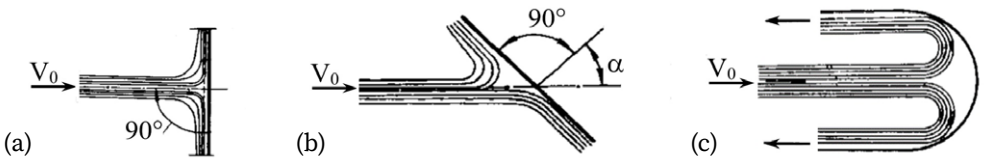

Fig. 4.34. Options for the water jet impact on barriers [325]:
(a) perpendicular barrier; (b) inclined surface; (c) inside the spherical surface

$$F_6 = p \cdot l\pi d\,, \tag{4.28}$$

where l – tube length; d – internal diameter.

Contact stresses at the point of impact:

$$\sigma_i = \frac{F_i}{S_i}, \tag{4.29}$$

where $i = 1, 2, 3$ – options of a water jet drop onto an obstacle (Fig. 4.34).

If the contact stress exceeds the tensile strength of the protective casing material St3 (380 MPa), then its plastic deformation will occur, and with sufficient kinetic energy of the jet, it will penetrate the sheet metal of the casing (5 mm thick).

A sharp increase in the speed of fluid movement in the tube when one of the caps is broken can cause the so-called "negative" hydraulic shock, which manifests itself in the propagation of a low-pressure wave along the entire length of the tube. However, the hydraulic processes in the pipeline connecting the tube to the high-pressure pump can be ignored, because the flexible pipeline has high damping properties against pressure shocks.

The velocity of a shock wave in an elastic steel tube is determined by the formula [325]:

$$a = \frac{\sqrt{\frac{E_w}{p}}}{\sqrt{1 + \frac{E_w}{E_{st}} \cdot \frac{d}{\delta}}} = \frac{a_s}{\sqrt{1 + \frac{E_w}{E_{st}} \cdot \frac{d}{\delta}}}\,, \tag{4.30}$$

where α_s – the speed of sound in water (1425–1435 m/s depending on density); E_w – volumetric modulus of elasticity of water (2030 MPa); E_{st} – the bulk modulus of

elasticity of the tube material (196 GPa); ρ – water density; d – the tube diameter; δ – tube wall thickness.

When the cap is broken, the low-pressure wave reaches the other end of the tube and, reflected of it, returns by time:

$$t_p = \frac{2l}{a}. \tag{4.31}$$

The pressure drop in the case of indirect ($t_{\text{open}} < t_{\text{p}}$) full hydraulic shock (fluid velocity varies from zero to v_0) is calculated by the modified Joukowsky equation:

$$\Delta p = \frac{\rho \cdot 2lv_0}{t_{open}}, \tag{4.32}$$

where t_{open} – the opening time of the tube, i.e., the time the cap moves along the screw-thread until it disconnects the tube.

The volumetric modulus of elasticity of water E_w determines what external pressure must be applied to reduce the volume by 2 times. To reduce the volume of water by 1%, an external pressure of about 20 MPa must be applied. In the range of tube test pressures up to 125 MPa, the compression of the water column along the tube length will be up to 6.16%. The length of the released liquid column will be 0.554–0.770 m, and the mass of this water – 4…65 kg.

Some correction of the additional volume of water will be made by an elastic increase in the diameter of the tubes:

$$\Delta r = \frac{p \cdot r^2}{E_{st} \cdot \delta}. \tag{4.33}$$

In the range of elastic deformation of the tube Δr = 0.116–0.945 mm, the volume of water will change by 0.6%, which will practically not affect the calculation results. The "hydraulic spring" will decrease stiffness as the pressure drops, but this effect can also be neglected with an error of about 10% in the pressure range of 10–70 MPa. In a given temperature range of tube tests 0…50°C, the error in the estimated water volume will be about 0.5%.

The main natural mode of structure oscillation. According to the classical theory of shock [326], when two bodies collide, their partial elastic or plastic deformation occurs at the contact point until the normal component of the relative velocity at the contact point vanishes at some time. In this case, the kinetic

energy of the impacting body undergoes a complete transition to the internal potential strain energy of both bodies. From Newton's second law in differential form:

$$F = m\frac{dv}{dt} \tag{4.34}$$

get the formula for the momentum of force:

$$F \cdot dt = m \cdot dv, \tag{4.35}$$

where dt – small time interval, m – mass (constant), and F – force proportional to dv.

There are three cases of the interaction of bodies upon impact:

1) the body bounced off the obstacle at a speed of v_1, then $dv = v_0 + v_1$;

2) the body joined with the barrier, then $dv = v_0$;

3) the body broke through the barrier and flowed further, then $dv = v_0 - v_2$.

The greater the speed and weight of the body, and the shorter the time it comes in contact with the barrier, the greater the impact on the barrier. If the shock is elastic, then the collision time does not depend on the speed of the collision because of the constancy of the period of oscillations with constant mass and coefficient of elasticity of the impact mass and obstacle.

In a collision without rebound of two bodies of masses m and M, the equation of motion without damping takes the form:

$$\frac{d^2x}{dt^2} + \omega^2 x = 0, \tag{4.36}$$

where $\omega = \sqrt{\left(\frac{1}{m} + \frac{1}{M}\right)K} = \sqrt{\frac{Mm \cdot K}{M+m}}$ – the natural frequency of free oscillations, rad.

Solution of this equation under initial conditions ($t = 0$, $dx/dt = v$):

$$x = \frac{v}{\omega} \cdot \sin(\omega \cdot t). \tag{4.37}$$

The maximum value of the impact force F will be:

$$F_{\max} = K \cdot x_{\max} = K\frac{v}{\omega}. \tag{4.38}$$

Impact time can be considered equal to the period of natural oscillations $T = 2\pi/\omega$. Substituting the value of the natural frequency, we obtain:

$$F_{\max} = v\sqrt{\frac{(M+m)\cdot K}{Mm}}; \tag{4.39}$$

$$T = 2\pi\sqrt{\frac{M+m}{M\cdot m\cdot K}}. \tag{4.40}$$

These formulas show that the impact force $F_{\max}$ depends on the speed of the impacting body, its mass, as well as on the mass and stiffness of the obstacle.

As we neglected the heat loss upon impact and assumed the complete transition of the kinetic energy of the impacted body to the potential energy of the obstacle deformation, then:

$$\frac{mv^2}{2} = \frac{Kx^2}{2}, \tag{4.41}$$

where x is the displacement during structural deformation, and the right part is the potential energy of an elastically deformed body with stiffness K.

The maximum displacement (at the end of the deformation):

$$x_{\max} = v\sqrt{\frac{m}{K}} = \frac{v}{\omega} \tag{4.42}$$

The expression for the maximum displacement and elastic force:

$$F_{\max} = K\cdot x_{\max} = K\frac{v}{\omega}. \tag{4.43}$$

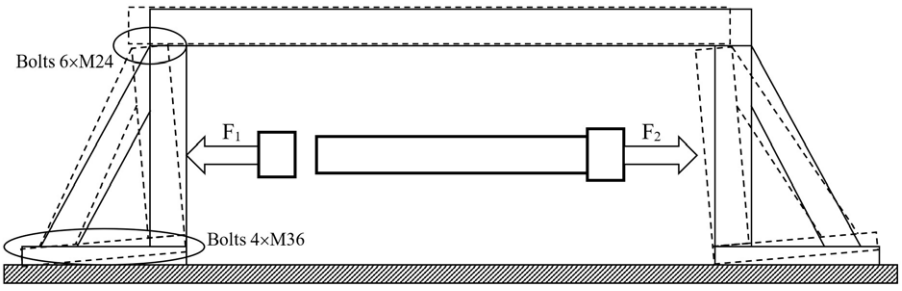

Fig. 4.35. The main mode of structural deformation upon impact

In the calculations of complex structures with distributed masses, deformations occur by the several forms (modes) of oscillations. The main mode of natural vibrations corresponds to the combination of the largest mass and element with the lowest stiffness in the structure. In the hydraulic press with a total mass of 4070 kg, the distribution of partial masses is as follows: 1) the left thrust – 875 kg (22%); 2) the right thrust – 875 kg (22%); 3) upper beam with mechanisms of the protective casing – 2320 kg (56%). Given the above masses, the design can be considered three lumped masses, where the main mode of deformation is the inclination of the axial thrusts (to either side) when foundation bolts (4×M36) and fastening bolts (6×M24) on the upper beams are stretched, as the softest elastic couplings (Fig. 4.35).

The natural frequency of the main vibration mode depends on the compliance of the bolts:

$$\lambda = \frac{l}{E_{st} A_b}, \tag{4.44}$$

where E_{st} – is the modulus of elasticity of the bolts; A_b – the total bolts section; l – the deformable part of the bolt.

During vibrations (tilts) of the structure, four M36 foundation bolts and four M24 bolts of the upper beam are tensioned. For the parallel elastic bolts, their stiffness is summed up [327].

The main natural frequency of free vibration:

$$F_s = \frac{1}{2\pi}\sqrt{\frac{K_s}{M_s}}, \tag{4.45}$$

where K_s – total stiffness of elastic bonds; M_s – the mass of structural parts oscillating in phase at a given frequency. The value of the fundamental frequency of the structure is F_s = 197 Hz. The period of natural vibrations of the structure is $1/F_s$ = 0.005 s.

On the front plates of the axial thrusts, there are 50 mm thick wooden linings. These pads reduce the likelihood of rebounding the caps upon impact, but they affect the structural strength only indirectly due to increasing time of impact. The impact force decreases due to less stiffness at a given location in the structure.

The results of calculating the impacts on axial thrust for the entire assortment of tubes under test are shown in Figure 4.36. It is assumed that the worst case of failure is when the left cap is broken on the longest tube of 12.5 m. The indices on the graphs have the following meaning: 1 – the left side (impact by

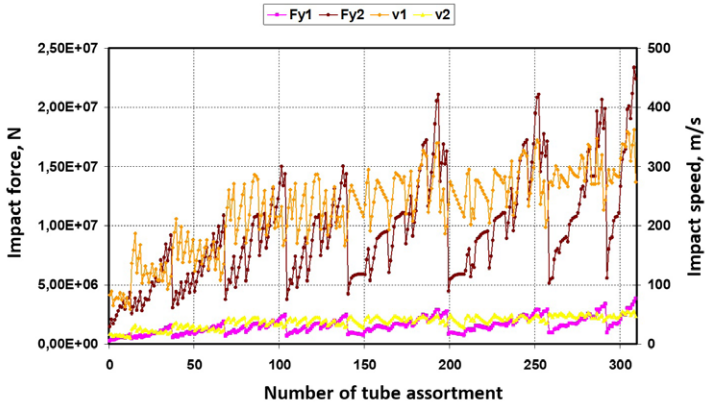

Fig. 4.36. Impact force and speed on axial thrusts by the assortment of tubes

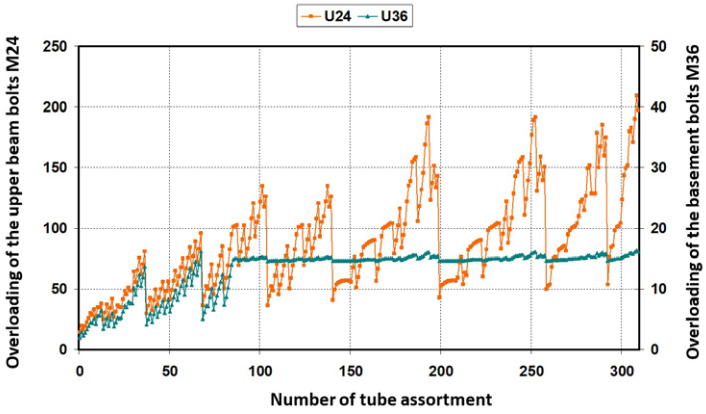

Fig. 4.37. Overloads on bolts M24 of upper beams fastening and basement bolts M36 of axial thrusts

a cap); 2 – the right side (impact by tube + water + cap). The greatest force of impact is produced by the right part (tube + water + cap), which has a larger mass than the left part (cap). The velocities are inversely proportional to the masses and depend on the distances from the thrusts. For example, disruption of the left cap from the tube D = 339.72 mm, h = 13.06 mm, L = 12.5 m, at a pressure P = 53.0 MPa causes a shock to the right support of the mass of the tube with water and cap m = 2420 kg at a speed of v_0 = 46.9 m/s and force $F_{y2} = 2.243 \times 10^7$ N.

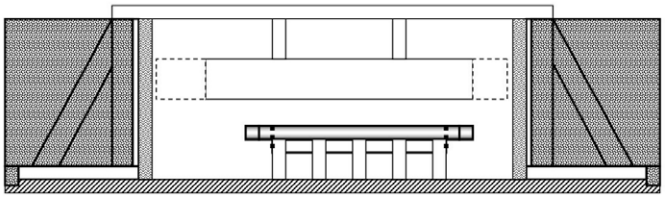

Fig. 4.38. Design option of the press for pressures up to 69 MPa

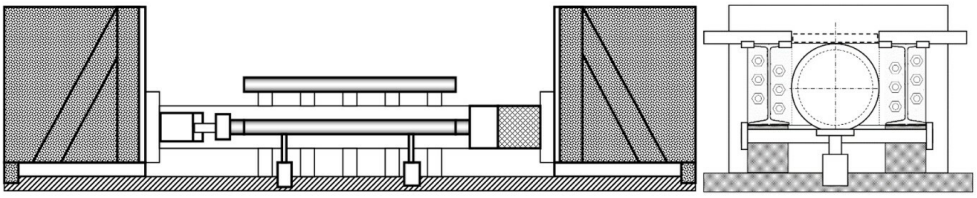

Fig. 4.39. Design option of the press for pressures up to 125 MPa

With such shock loads, the complete damping of the speed of the body requires a significant thickness of the sand layer (more than 1 m), although minimal implementation costs. More effective is the filling of the free volume of the axial thrusts behind the steel plate with reinforced concrete with a layer thickness of at least 500 mm in the direction of the tube axis. Besides, an increase in the mass (inertia) of the axial thrusts by 2–3 times proportionally reduces their displacements upon impact and, accordingly, the load on the bolted joints.

Overloading on the upper bolts M24 and basement bolts M36 are given in Figure 4.37.

A comparison of the maximum permissible bolt loads and the calculated tensile and shear loads acting upon a minimum impact force of $F_y = 1.5 \times 10^6$ N on the front plate of the thrusts shows that the bolts do not withstand the tensile and shear loads. At maximum loads up to $F_y = 5.0 \times 10^7$ N, the bolts will not withstand the loads, and the thrusts cannot be restored by minor repairs.

Based on the results of the modelling, two options for press modernisation are proposed for different levels of working pressure. The first option (Fig. 4.38) assumes only axial thrust reinforcement, while the second option (Fig. 4.39) assumes full modernisation and additionally increases the productivity of the

press due to the mechanisation of manual operations and provides more safety conditions for workers.

Multi-disciplinary research is conducted including fluid dynamics, mechanical shock and vibration, and materials penetration to estimate diverse impacts on the structure of high-pressure hydraulic press for tubes and screw thread caps quality testing [328]. The general recommendation for reducing dynamic loads on a structure is to keep the tube as close as possible to the protective casing and axial thrusts. On the other hand, some clearance is necessary to prevent excessive pressure between the casing and the tube during the tube burst, which increases the loads in the structure.

Despite existing uncertainty in the position of crack and fracture on the tube, the main deformation mode and the natural frequency (about 197 Hz) of the structure are determined making possible stress calculation without the finite-element model.

The proposed holistic approach to strength capacity assessment under the action of a variety of different loading factors (lumped masses, pieces of fractured metal, water jets) on the surrounding structure can be successfully applied to different industrial machines. For example, pipeline failure applications for the prediction of equipment and worker damage from high-pressure water and hydraulic oil impacts, as well as minerals bursts due to stress in the underground and open-pit mining areas.

4.3.2. Powered roof supports in underground longwall mining

The powered sections of hydraulic props are among the main mechanisms in the underground longwall mining complexes providing safe work of personnel and Longwall Top Coal Caving (LTCC) process efficiency (Fig. 4.40a). The design of hydraulic props requires two telescopic pistons for a wide range of serviced heights. The carrying capacity of everyone may reach 1000 t at a working pressure of 32–45 MPa (Fig. 4.40b). Modern automation systems provide overall supervision and vertical or horizontal position control over the section consisting of hundreds of double-cylinder props. Numerical analyses are known in this domain directed on mechanical design optimisation to restrain severe loading [329–339] and hydraulic system simulation [340–342] to reduce undesired dynamics.

Along with standard functions of pressure supply and redistribution for carrying capacity control in the whole section, every hydraulic cylinder is equipped

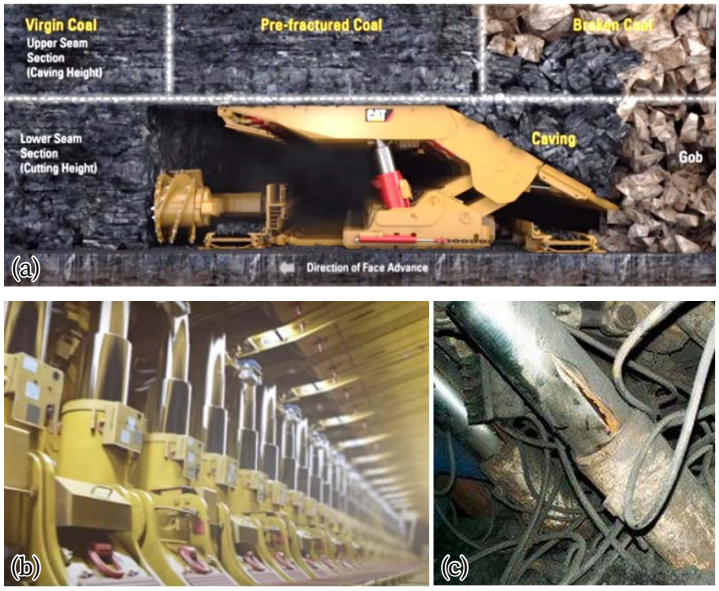

Fig. 4.40. (a) The principle of Longwall Top Coal Caving (LTCC) mining;
(b) automated section of powered roof supports; (c) damaged hydraulic cylinder

with a safety valve, which should prevent overloading by releasing pressure above the pre-installed level. Nevertheless, the props frequently failed due to dynamic loading from the released rock blocks with unrecoverable damages like sealing leakages, and cylinder and piston deformations. Therefore, safety valves are subjected to intensive testing on special facilities to optimise hydraulics control [343, 344].

The maintenance of hydraulic systems and full replacement of failed cylinders in underground mines require significant costs and cause long downtimes. The hidden damages of sealing in cylinders are difficult to detect but they lead to dangerous consequences due to load redistribution among neighbouring props and their overloading.

Testing of safety valves is conducted on the special rigs where a huge mass (about 20 t) falls from a certain height (up to 1.0 m) and imitates impact from the rock (Fig. 4.41a–c). The typical design of safety valves is represented in Figure 4.41d and its installation on the cylinder is shown in Figure 4.41e. Some approaches exist to reduce the dynamics of hydraulic systems: multi-plate valves [345], hydro-pneumatic accumulators [346], and two-stage valves [347]. For ex-

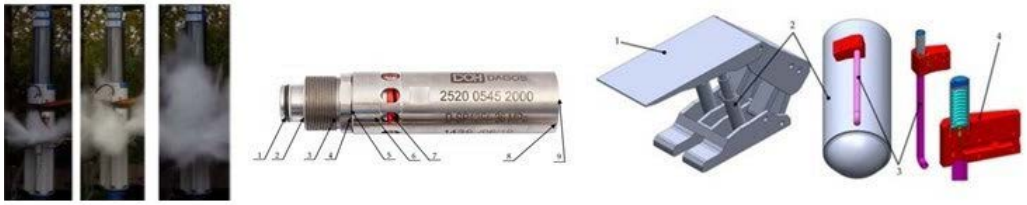

(a) (b) (c) (d) (e)

Fig. 4.41. Safety valve testing and fluid flow with different impact height: (a) – 0.3 m, (b) – 0.4 m, (c) – 0.5 m [343]; (d) design of a safety valve [40]: 1 – round seal, 2 – connection stub, 3 – round piston seal, 4 – piston, 5 – piston pressure plate, 6 – casing, 7 – spring, 8 – thrust plate, 9 – adjustment screw; (e) hydraulic roof support: 1 – canopy, 2 – cylinders, 3 – small section pipe, 4 – safety valve [342]

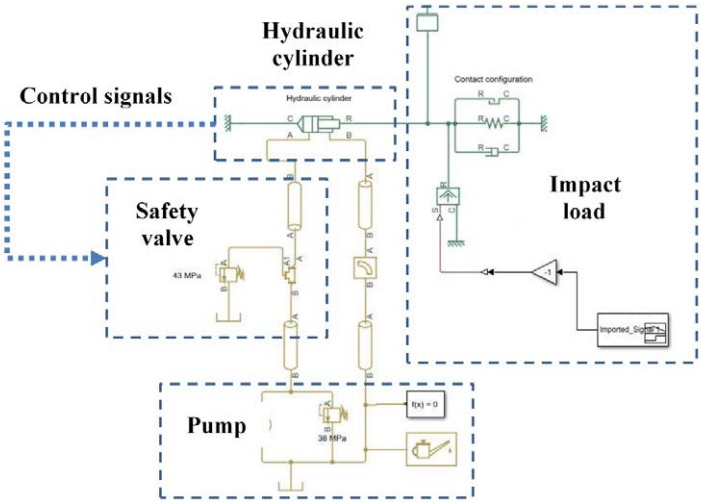

Fig. 4.42. Model of hydraulic roof support

ample, the flow rate of two-stage valves from OSTROJ Company (Czech Republic) may reach 7000 L/min [348]. Fast inertial valves are proposed in [349] with a general strategy of roof support adaptation to stochastic loading [350]. Summarising the aforementioned information, the following problems are encountered in the safety valves:

- Not equivalence (15–20%) of applied load and internal pressure due to friction losses.
- Time pressure delay to applied dynamic load due to the limited speed of a fluid wave.
- Harsh working conditions (dust, humidity, temperature) and explosive limitations.
- Deterioration of valve spring material due to fatigue over the operation period.

The dynamical model of a hydraulic prop with a safety valve is developed using MATLAB Simulink software [351]. The model includes the following blocks: hydraulic cylinder, pump for pressure supply, safety valve with regulated open-

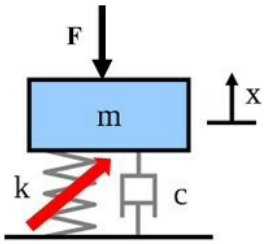

Fig. 4.43. Dynamical model of
a hydro-mechanical system of roof support

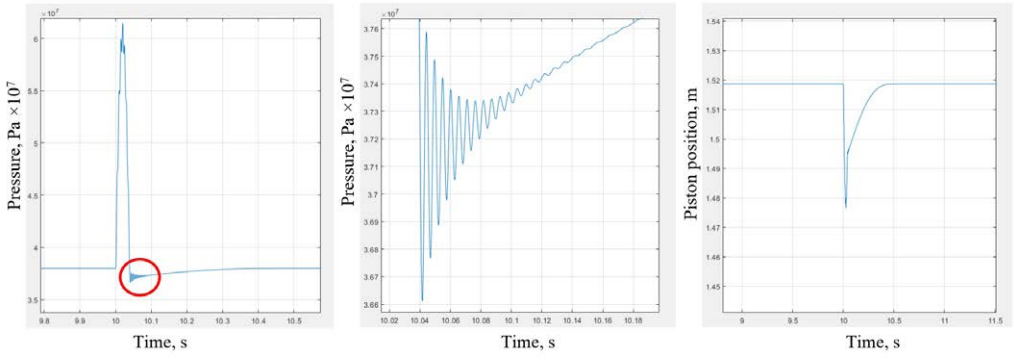

Fig. 4.44. Simulation of load application to the hydraulic cylinder
with the closed safety valve: (a) pressure; (b) zoomed pressure;
(c) piston displacement

ing time, impact load of falling mass, pipes for fluid delivery to a cylinder and exhaust pipe where the valve is installed (Fig. 4.42). Parameters of the safety valve and hydraulic cylinder are adjusted by data of the equipment supplier from work [343].

The test rig is simulated without the opening of the safety valve to determine the free oscillations frequency of the closed hydraulic system. For this case, the stiffness of the hydraulic spring in a cylinder is as:

$$K(t) = \frac{E_0 A}{h(t)}, \tag{4.46}$$

where E_0 – fluid bulk modulus under normal conditions (includes air content, temperature and fluid pressure); A – effective inner area of piston chamber; $h(t)$ – a fluid height in the cylinder.

For double-acting telescopic cylinders, this formula is applied to every section. The total stiffness of the cylinder includes deformations of the walls and piston rods [352]. A hydraulic spring with a certain test mass (20 t) constitutes a dynamical system with a variable stiffness (Fig. 4.43), and the frequency of the main vibration mode is about 200–300 Hz.

On the MATLAB Simulink model, the shock impact was applied without opening the safety valve to verify the model by the natural frequency of oscillations. The results of such simulation are represented in Figure 4.44. A further analysis of this system is given in the section on its dynamics control.

4.4. Steel rolling mills

The different types of rolling mills for the production of steel strips, rods and tubes belong to the most dynamical large-scale industrial plants. A wide variety of driveline designs are formed by multistage gearboxes, pinion stands, universal spindles, switchable couplings and the huge number of rolling stands having 2, 4, 6 and up to 20 rolls including compact rolling mills (blocks) with both vertical and horizontal rolls for wire and rod production.

Standard maintenance procedures usually implemented for the majority of rotating machines (balancing, shaft alignment) are not applicable for rolling mills due to frequent changes in rolls and technological schedules. Harsh operating conditions affect vibration parameters and diminish the implementation of standard diagnostics methods where loads and speeds are supposed to be stationary. That

makes it very important to understand the causes of different dynamic processes occurring under variable working conditions.

4.4.1. Drivelines of heavy hot rolling mills with gearboxes

The hot rolling mills constitute a wide class of industrial machines used for large-size metal ingot deformation with a final product formed in heavy coils. Historically, they were first subjected to torque measurements and analysis of dynamical processes [353, 354]. The general models of nonlinear dynamical systems with clearances are represented in [355]. There are several main drivetrains types, which are shown in Figure 4.45.

The first type is primarily used in roughing stands and includes two motors, intermediate shafts and spindles for every work roll driving. The second type is used in finishing stands and includes one motor and pinion stand to split torque between the two driven rolls. Lastly, the third type is used in particular for wide

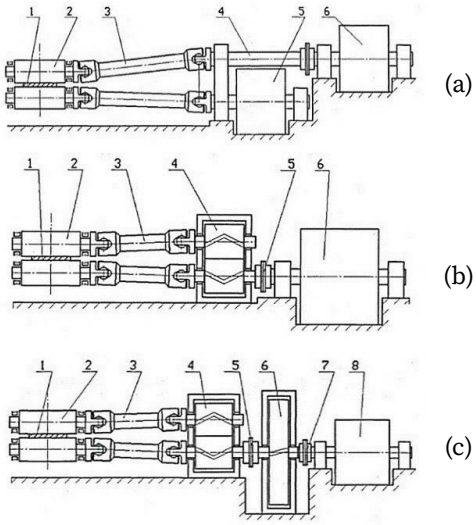

Fig. 4.45. Different drives arrangement of rolling mills: (a) separated drivetrains; (b) drivetrain with a pinion stand; (c) geared drivetrain: 1 – rolled metal; 2 – work roll; 3 – spindles; 4 – intermediate shaft (a) or pinion stand (b, c); 5 – motor (a), motor coupling (b) or intermediate coupling (c); 6 – motors (a, b) or gearbox (c); 7 – motor coupling; 8 – motor

Fig. 4.46. (a) Spindles with slipper pads; (b) wear of slipper pads; (c) weight balancing scheme: 1 – head of spindle; 2 – journal bearing; 3 – two balancing springs

strip heavy hot rolling mills and includes one or more gearboxes and pinion stands. The DC and AC speed-regulated electric drives are used.

Factors affecting gaps opening. Backlashes at both heads of spindles constitute up to 70–80% of summary drivetrain wear. Gaps opening depends on the following factors:

- spindle rotation speed and inertial forces of elements;
- speed matching of rolls and incoming pieces of metal;
- tuning of spindle weight balancing unit;
- spindle angular position before the transient process;
- static and dynamic loads ratio.

Some of the above-mentioned factors could be controlled theoretically but not in practice due to the stochastic nature of the steel rolling process. Many studies are devoted to gearbox vibrations and dynamics due to teeth meshing inaccuracy and related resonances. Universal joint kinematics is widely represented in the literature. However, the weight balancing units of rolling mill spindles have not been investigated concerning torsional vibration control.

The spindles with slipper pads (Fig. 4.46a), which always have certain wear of pads (Fig. 4.46b), are equipped with weight balancing units consisting of two springs fixed by screws at the bottom of supporting journal bearing (Fig. 4.46c). Since a compensation force depends on the work roll's vertical position, which varies with the roll's diameter and strip reduction, the controlled hydraulic type units are also used but in a much smaller number of plants.

The stiffness of the weight balancing springs varies in the range of 0.5–3.0 kN/mm (for both springs) and spindle weight is about 20–200 kN for

the different drivelines. Hence, to balance the spindle by 5% of its weight, the spring position has to be regulated by the screws with an accuracy of 1–2 mm. It is difficult to satisfy in the maintenance period and impossible during the operation, which leads to unavoidable gap opening twice per spindle rotation before every loading. The universal cardan joints are effective but seldom used. The gap depends on friction in the bearings of the pinion stand and gearbox. It opens if a dynamic load exceeds the static load. Besides angular backlashes, there are radial clearances due to wear in the bearings. When the gravity and tangent force have opposite directions in a gearbox, the radial clearances play the same role as the angular backlashes during transient torsional vibrations. The tangent forces lift gear shafts from its idle position. One stage gearbox will produce a higher response at the exit wheel bearings. The stages gearbox will show higher transient vibration at the middle gear block. An increased shock vibration causes fixing screws' plastic deformation and requires frequent maintenance to avoid cracks at the edges of the tooth. Therefore, methods of torsional vibration reduction are required to eliminate all gaps in the driveline before the load is applied.

Natural modes of torsional vibrations. Drivetrain layout and nominal torques determine shaft diameters, inertial moments of rotating bodies and gearbox ratios. Dynamics simulation has been fulfilled for TAF estimation in the drivetrains. Backlashes nonlinearity has been taken into account by the usual logical conditions during simulation.

Table 4.7. Natural modes frequencies (Hz) of torsional vibration and gearbox ratios

Mode No.	Stand 0	Stand 1	Stand 2	Stand 3	Stand 4
1	13	14	11	12	12
2	28	22	18	17	15
3	32	27	23	20	20
4	44	30	27	30	34
5	75	63	52	35	55
6	111	84	66	81	81
7	121	166	124	82	–
8	196	–	–	–	–
Gearbox ratio	**23.92**	**19.26**	**19.54**	**10.11**	**7.36**

The natural frequencies of the torsional vibrations are represented in Table 4.7 for the five different drivetrains of a continuous hot rolling mill. Stand 0 has two 1-stage gearboxes. Stands 1, 2, and 3 have a 2-stage gearbox and stand 4 has a 1-stage gearbox. Regardless of design, the lowest natural frequencies lay in the narrow range of 10–30 Hz.

The calculation scheme of the drivetrain with two gearboxes (Stand 0 in Table 4.7) is shown in Figure 4.47, which is investigated in detail.

The two lowest modes usually give the most contribution to TAF value, which is almost equal for all couplings without gearboxes. However, for geared drivetrains, TAF may be much higher for different elements along a drivetrain (Fig. 4.48), especially when backlashes exist.

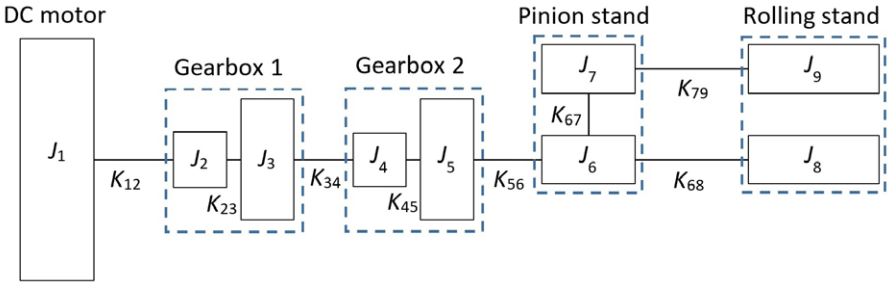

Fig. 4.47. Drivetrain calculation scheme (Stand 0)

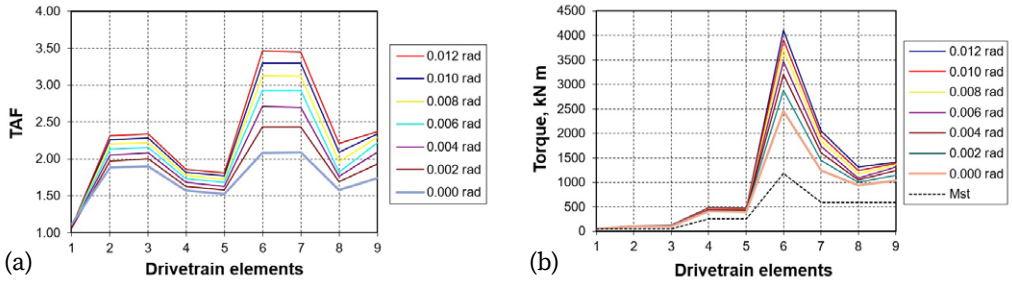

Fig. 4.48. (a) Variation of the TAF; (b) peak torque T_{max} along a drivetrain in Figure 4.47 under conditions of backlashes in both spindles ($\delta_{68} = \delta_{79} = 0.000 - 0.012$ rad): 1 – motor current, 2 – K_{12}, 3 – K_{23}, 4 – K_{34}, 5 – K_{45}, 6 – K_{56}, 7 – K_{67}, 8 – K_{68}, 9 – K_{79}

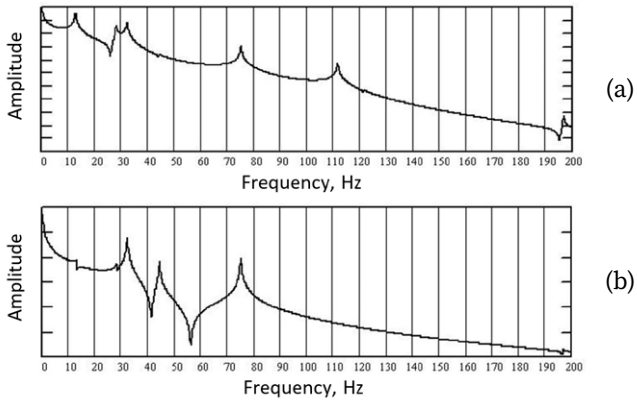

Fig. 4.49. Amplitude-frequency diagrams (FRF) for different points in the drivetrain: (a) shaft between gearboxes – K_{34}; (b) lower spindle – K_{68}

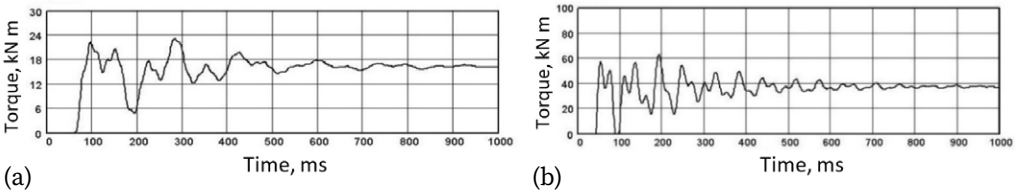

Fig. 4.50. Transient torques in the drivetrain: (a) M_{34} – intermediate shaft; (b) M_{68} – lower spindle

The lower and upper lines in the graphs correspond to both spindles' summary angular backlashes variation from zero to 0.012 rad with 0.002 rad step, respectively. Despite maximum angular backlash in the spindles (8, 9), their TAF and peak torque are less than in the intermediate shaft (6) and pinion stand (7). Torque amplitude transfer functions W_{34} (f) and W_{68} (f) from rolls (input) to corresponding couplings (output) are shown in Figure 4.49 and used for drivetrain modal analysis.

The transient torques M_{34} and M_{68} are simulated in a time domain and shown in Figure 4.50. It can be seen that the first torsional mode (13 Hz) is most important in K_{34} coupling (intermediate shaft between two gearboxes) but the third mode (32 Hz) plays a more important role in K_{68} coupling (lower spindle). Therefore, TAF distribution is so uneven in the drivetrains with gearboxes. It depends

on the distribution of modal nodes. Usually, the main modes have nodes close to motor and gearboxes with a large rotating inertia.

The transient process in the dynamic system depends on many factors: spring-mass parameters, time of load increasing, backlashes opened gaps, and motor speed control algorithm. As a rule, the spring-mass parameters are not available for modification in industrial machines. In some cases, elastic couplings are available for natural frequency tuning. The time of rolling torque rising may be controlled with less effect. Therefore, motor speed is the most suitable method to control torsional dynamics in practice. To reduce angular backlashes, different electromagnetic or other types of braking devices for end mass stopping before the loading are developed but are not always applicable in industrial machines.

4.4.2. Compact wire and rod rolling mill with a changeable structure

A comprehensive analysis of the design and dynamics of a high-speed Reducing Sizing Mill (RSM) is conducted. Modal analysis is implemented for multistage gearboxes with a changeable structure based on Frequency Response Functions (FRF). Natural modes of torsional vibration in the neighbouring stands are determined with the out-of-phase oscillations of rolls [356].

Design of driveline with changeable structure. The first two pairs of RSM rolls form the reducing mill; the last two pairs are the sizing mill (Fig. 4.51). The mill is designed for a speed of 120 m/s, while the working rolling speed is below 100 m/s. To provide a higher rolling speed, RSM has a compact design with a 150–250 mm distance between pairs of rolls (stands) and hydraulic units for adjusting the rolling line.

The RSM of Morgan type contains four cantilever pairs of rolls, inclined at the angle of 90° to each other (no-twist scheme). The standard groove system is used "oval-round-round-round" for high accuracy of products. The RSM is driven by an AC electric motor and multi-stage gearbox, which has 9 servo drives based clutches. When rolling different products, an operator can switch the clutches to satisfy technology requirements on roll gaps and to ensure minimum tensions in RSM that provide better geometry of the final product. On the other side, this useful feature adds more complications to the dynamic analysis of RSM.

According to the data of the RSM manufacturer, the design of switchable clutches has the view shown in Figure 4.52a. The outer yoke, moving along the shaft, closes one of the gears or disconnects both couplings from the shaft. Each

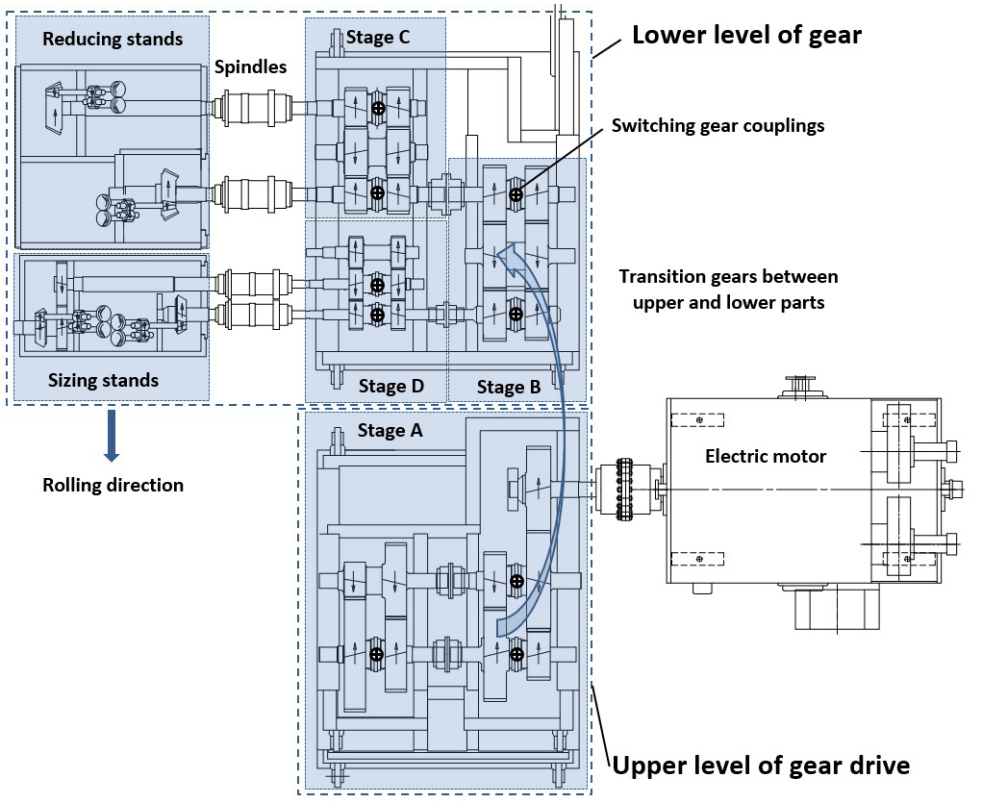

Fig. 4.51. Structure of the RSM drive and locations of gearbox ratio control clutches (⊕)

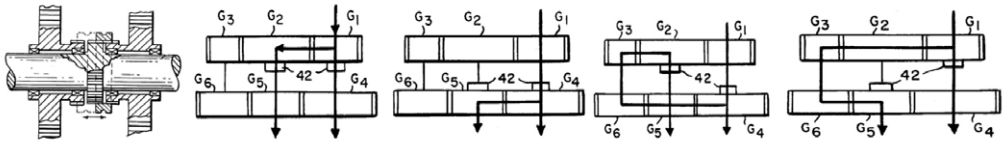

(a) (b)

Fig. 4.52. (a) Design of the switchable clutch; (b) power flows when switching clutches

state corresponds to certain power flows shown in Figure 4.52b as an example of stage D. In this stage, the intermediate shaft (gears G_3–G_6) is on the left and not between the drive shafts (gears G_1-G_4 and G_2–G_5) like in the other stages.

The correspondence of the RSM clutches positions and transmission ratios for each stage of gearbox is presented in Table 4.8. The positions of the clutches

Table 4.8. States of gearbox servo clutches and speed ratios in the stands

No.	State of stage A	Pos. of clutch #1	Pos. of clutch #2	Pos. of clutch #3	Ratio motor / output A
1	1	N	N	A	0.3655
2	2	A	N	N	0.7292
3	3	N	N	B	1.1981
4	4	N	A	N	2.3900
	State of stage B	**Pos. of clutch #4**	**Pos. of clutch #5**	**Ratio input B / input C**	**Ratio input B / input D**
5	1	B	A	1.2553	1.3095
6	2	B	B	1.2553	1.3721
7	3	A	A	1.1458	1.3095
8	4	A	B	1.1458	1.3721
	State of stage C	**Pos. of clutch #6**	**Pos. of clutch #7**	**Ratio inputC / stand 1**	**Ratio input C / stand 2**
9	1	B	A	0.9765	1.0
10	2	B	B	0.9355	1.0
11	3	A	A	0.9033	1.0
12	4	A	B	0.8654	1.0
	State of stage D	**Pos. of clutch #8**	**Pos. of clutch #9**	**Ratio input D / stand 3**	**Ratio input D / stand 4**
13	1	B	B	0.9333	1.0
14	2	A	A	0.9149	1.0
15	3	B	A	0.9556	1.0
16	4	A	B	0.8936	1.0

are indicated as follows: A – gear is activated to the side of the roll; B – gear is switched to the motor side; N – clutch is disconnected. In even stands 2 and 4, there is a direct transfer of the torque after stages C and D (ratio = 1), and in odd stands 1 and 3 the speed of the spindles decreases (ratio < 1). Stage B is up, C and D down, and stage A can be either down or up in the unbranched part of the transmission for all four stands.

Gear ratios of spindles/rolls remain constant: stand 1 – 2.1715; stand 2 – 2.4474; stand 3 – 3.9193; stand 4 – 3.9193. For example, for a final size of rod 4.5 mm A = 1,

B = 3, C = 4, D = 3 and the total gear ratio of the gearbox: i = (motor/in. B) × (in. B/in. C) × (in. C/spindle) = 0.3655 × 1.1458 × 0.8654 = 0.3624. Then i value is multiplied by the constant spindles/rolls ratio of stand 1 – i × 2.1715 = 0.7869. Having such an easily reconfigurable transmission, RSM provides technological flexibility for rolling passes designers of steel producers.

Dynamical model of gear driveline. In this research, an approach based on FRF is used to describe and study dynamic processes in RSM as a whole system of geared transmission and rolled material. The efficiency of methods in the frequency domain depends on the correctness of calculation schemes and their parameter verification. The frequency range, depending on the tasks being solved, is limited to the highest frequency of the disturbance or to the maximum considered natural frequency of the system. There are several criteria for assessing the optimal range of natural frequencies when modelling dynamics in mechanical systems. The errors of transition from a system with distributed parameters, as the most accurate, to a simplified model with discrete masses, are determined. For example, for five masses, the error (as the ratio of frequencies) is from 10% for the first mode to 60% for the fifth mode. The optimal range of natural frequencies of the torsional system can be estimated by the ratio of the amplitudes of the maximum and minimum components, which should be less than 10. The same rule is for the ratio of the highest and lowest natural frequencies. If this number is larger, the natural frequencies and modes need reconsidering. This criterion is also used for reducing the masses of the dynamic model. With a much smaller unit of the ratio of the maximum natural frequency to the partial frequency of a certain mass, it can be excluded.

The standard reasons for the vibration increase in the high-speed RSM that affect the accuracy of the rolled material are the following: eccentricities of work rolls; imbalance of parts of the driveline; misalignment of shafts due to wear of bearings and defects of installation; defects in couplings, gears and bearings. At the maximum operating speed, the frequency range of any disturbances in RSM is limited to 1000 Hz. Based on this range of vibration, to analyse the influence of factors, the RSM model should include electric motors and gears as the lumped masses and intermediate shafts and geared coupling as elastic links.

The calculation diagram of the RSM torsional system model is shown in Figure 4.53, where the following components are taken as the individual masses: motor gears A, B, C and D of the gearbox and roll assemblies of stands 1–3.

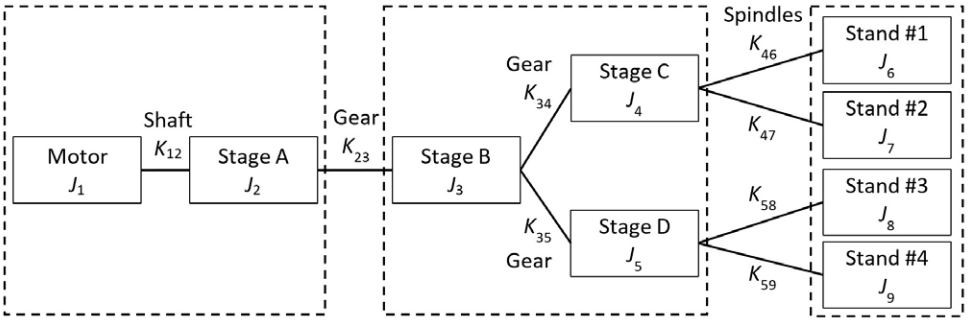

Fig. 4.53. Calculation scheme of RSM drive dynamical model

Table 4.9. Parameters of calculation scheme

Parameter	Description	Value	Units
J_1	Inertia of electric motor	3×10^3	kg m^2
J_2	Inertia of stage A	0.5×10^3	kg m^2
J_3	Inertia of stage B	0.5×10^3	kg m^2
J_4, J_5	Inertia of stages C, D	0.4×10^3	kg m^2
J_6, J_7	Inertia of stands 1, 2	0.2×10^3	kg m^2
J_8, J_9	Inertia of stands 3, 4	0.1×10^3	kg m^2
K_{12}	Stiffness of motor shaft	5.1×10^5	N m/rad
K_{23}	Stiffness between stages A-B	5.0×10^5	N m/rad
K_{34}, K_{35}	Stiffness between stages B-C, B-D	7.9×10^4	N m/rad
K_{46}, K_{47}	Stiffness of spindles in stands 1, 2	7.1×10^3	N m/rad
K_{58}, K_{59}	Stiffness of spindles in stands 3, 4	5.2×10^3	N m/rad

The following components are taken as elastic links: a motor shaft, transition gears of stages A, B, C and also spindles of rolls. As the external torques of the load, the moment of the drive M1 and four moments of rolling in the stands M6–M9 are taken. In the driveline model, the upper and lower rolls are considered together, closed on the rolled metal. The calculated values of the dynamic model parameters J_i, K_{ij} are given in Table 4.9.

The systems of differential equations of the RSM model are composed of absolute angles of lumped masses oscillation:

$$\begin{cases} \ddot{\varphi}_1 = \left(M_1 - M_{12}\right)/J_1 \\ \ddot{\varphi}_2 = \left(M_{12} - M_{23}\right)/J_2 \\ \ddot{\varphi}_3 = \left(M_{23} - M_{34} - M_{35}\right)/J_3 \\ \ddot{\varphi}_4 = \left(M_{34} - M_{46} - M_{47}\right)/J_4 \\ \ddot{\varphi}_5 = \left(M_{35} - M_{58} - M_{59}\right)/J_5 \\ \ddot{\varphi}_6 = \left(M_{46} - M_6\right)/J_6 \\ \ddot{\varphi}_7 = \left(M_{47} - M_7\right)/J_7 \\ \ddot{\varphi}_8 = \left(M_{58} - M_8\right)/J_8 \\ \ddot{\varphi}_9 = \left(M_{59} - M_9\right)/J_9 \end{cases} \tag{4.47}$$

and relative angles of deformation in the shafts and couplings:

$$\begin{cases} \ddot{\varphi}_{12} = \left(M_1 - M_{12}\right)/J_1 - \left(M_{12} - M_{23}\right)/J_2 \\ \ddot{\varphi}_{23} = \left(M_{12} - M_{23}\right)/J_2 - \left(M_{23} - M_{34} - M_{35}\right)/J_3 \\ \ddot{\varphi}_{34} = \left(M_{23} - M_{34} - M_{35}\right)/J_3 - \left(M_{34} - M_{46} - M_{47}\right)/J_4 \\ \ddot{\varphi}_{35} = \left(M_{23} - M_{34} - M_{35}\right)/J_3 - \left(M_{35} - M_{58} - M_{59}\right)/J_5 \\ \ddot{\varphi}_{46} = \left(M_{34} - M_{46} - M_{47}\right)/J_4 - \left(M_{46} - M_6\right)/J_6 \\ \ddot{\varphi}_{47} = \left(M_{34} - M_{46} - M_{47}\right)/J_4 - \left(M_{47} - M_7\right)/J_7 \\ \ddot{\varphi}_{58} = \left(M_{35} - M_{58} - M_{59}\right)/J_5 - \left(M_{58} - M_8\right)/J_8 \\ \ddot{\varphi}_{59} = \left(M_{35} - M_{58} - M_{59}\right)/J_5 - \left(M_{59} - M_9\right)/J_9 \end{cases}, \tag{4.48}$$

where J_i – moments of inertia of concentrated masses; φ_i – absolute angles of rotation of the masses; φ_{ij} – relative twisting angles of the elastic links (shafts); M_1 – electric motor torque; $M_6 \ldots M_9$ – moments of load on the rolls; $M_{ij} = K_{ij}(\varphi_i - \varphi_j)$ are the moments of elastic forces. Each equation in the first system (4.47) describes the angular motions of one mass, and the second system (4.48) corresponds to one elastic link of a partial system (two masses on intermediate stiffness). The system (4.47) is used to calculate the natural frequencies and modes, and the system (4.48) is for calculation the FRFs of the drivetrain. Amplitude and phase functions of frequency in the stands of RSM are shown in Figure 4.54 (stands 1–2, 3–4 are similar).

Modal analysis of torsional vibrations. The developer of RSM (Morgan) determined the frequency of the main natural mode of torsional vibration as 19.6 Hz. Its node (maximum torque) is located between the motor and gearbox, which is characteristic of many other rolling mills due to the large inertia of electric drive.

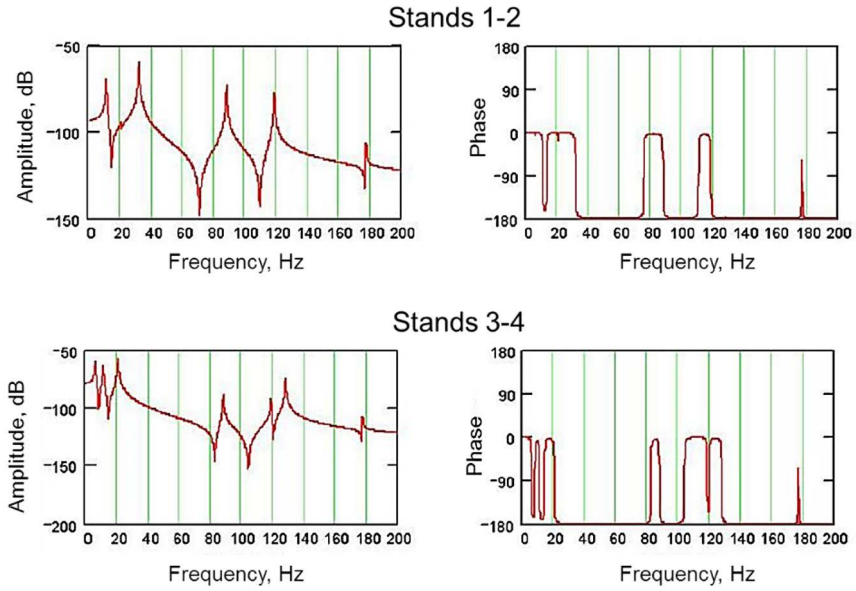

Fig. 4.54. Amplitude and phase FRF diagrams in the stands of RSM

The frequency of the main mode, although it is low enough for a highly efficient drive system, should not cause any problems, as this is taken into account in the design of the electric drive speed controller. A notch filter within the frequency range of 15–25 Hz is provided to attenuate at least 4 times (12 dB) and to avoid any tendency of the system to oscillate at the main mode frequency. Above the main frequency range, oscillations can occur at higher natural frequencies, which will not affect the speed controller, as they are beyond the cut-off frequency of the filter.

Due to the large scatter of the moments of inertia in the RSM gearbox, the drive speed regulator is set to the minimum of 4 different gear ratios ranging from minimum to maximum. The setup parameters of the speed regulator are stored and automatically assigned when a certain gear ratio is selected by the mill operator.

The values of the four lower frequencies given by the manufacturer of the RSM:

19.6 22.2 27.6 34.3 (Hz).

The average values of the natural frequencies calculated by the model:

19 20 30 36 93 116 141 279 (Hz).

Table 4.10. Modes of RSM drive torsional vibrations

	Natural frequencies (Hz)							
Masses	**19**	**20**	**30**	**36**	**93**	**116**	**141**	**279**
J_1 (motor)	–0.166	–0.006	0	0	–0.020	0.010	0.013	–0.006
J_2 (stage A)	0.056	–0.002	0	0	0.283	–0.233	–0.436	0.866
J_3 (stage B)	0.028	0.002	0	0	0.440	–0.324	–0.517	–0.498
J_4 (stage C)	0.243	0.327	0	0	0.797	0.718	0.295	0.038
J_5 (stage D)	0.333	–0.185	0	0	0.263	–0.560	0.671	0.040
J_6 (stand 1)	0.420	0.597	0.861	0	–0.092	–0.051	–0.014	0
J_7 (stand 2)	0.420	0.597	–0.508	0	–0.092	–0.051	–0.014	0
J_8 (stand 3)	0.472	–0.270	0	0.738	–0.046	0.058	–0.046	–0.001
J_9 (stand 4)	0.472	–0.270	0	–0.674	–0.046	0.058	–0.046	–0.001

Deviations of the calculated values of frequencies do not exceed 10%. The values of the first four natural frequencies of the torsion system, given by the manufacturer, appear to correspond to their average values since the specified frequency range of the notch filter for suppression in the control system of the lower frequency is 15–25 Hz.

According to the phase frequency functions of the drive, the modes of the rolls' oscillation in the RSM stands are determined. The calculated values are given in Table 4.10 for a gearbox setup for 4.5 mm of output product diameter rolling.

An increase in the amplitude of tension oscillations should be expected in those interstand gaps and at those frequencies where the out-of-phase torsional vibrations of the rolls are observed. Such combinations of the phases of oscillations of the rolls are outlined in the table, which corresponds to the vibration nodes, i.e. the places of transition amplitude through zero.

At frequencies of 20 and 116 Hz, we should expect an increase in tension oscillations in the pair of stands 2–3, at a frequency of 30 Hz – in a pair of stands 1–2, and at a frequency of 36 Hz – in pairs 3–4. Since the first four frequencies have similar values, the whole range of 20–35 Hz should be considered unfavourable from the viewpoint of interstand dynamical interaction. In addition, it covers the range of possible frequencies of the motor rotation 14.2–28.3 Hz. At the remaining natural frequencies, the oscillations of the rolls occur in all the stands in phase.

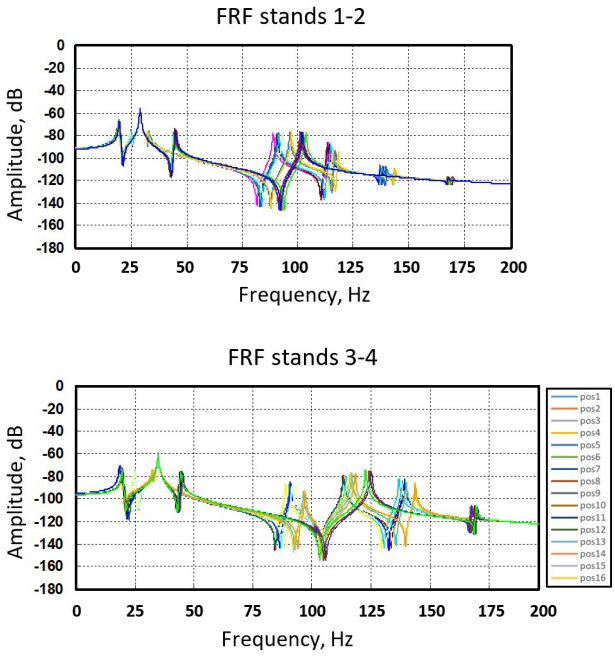

Fig. 4.55. Scattering of FRF in stands 1–2 and 3–4
for the different setups of RSM gearbox ratios

The same behaviour is throughout the entire range of gear ratios. Under transition from 13.5 to 14 mm of rod size, another out-of-phase waveform appears at frequencies of 92–103 Hz between the stands of No. 2 and 3 but it has an opposite sign with the mode at frequencies of 116–127 Hz. Therefore, it is compensated for in these stands.

The control of the entire range of total motor/rolls ratios in the ranges 0.1572–1.2173 (reducing stand) and 0.0778–0.5330 (sizing stand) causes changes in the moments of inertia, reduced to the motor shaft speed, within the 316–2195 kg/m^2 range. Correspondingly, the natural frequencies of the torsion system and the resonant speed ranges where the vibration amplification is possible and the reduction of the quality of rolled products in geometric dimensions will be decreased.

The influence evaluated of different stages ratios in the gearbox on the amplitudes of the torsional vibrations of the rolls in the RSM and the corresponding oscillations of interstand tensions. The gear ratios of the input and output stands and the states (1, 2, 3, 4) of each gear stage (A, B, C, D) are indicated in

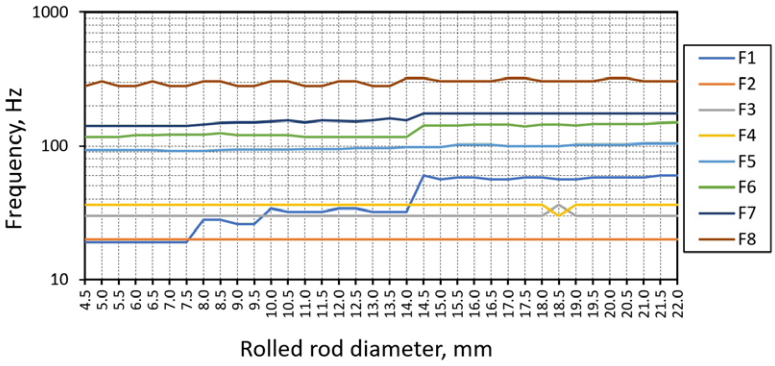

Fig. 4.56. Changing the natural frequencies (F_1–F_8) of the RSM drivetrain by the rolled rod diameter

Table 4.8. For the two reducing stands (1, 2), AB-C ratios play the role, and for the two sizing stands (3, 4) AB-D plays the role. The first four natural frequencies in the range 19...45 Hz almost do not change (Fig. 4.55) for different switching clutches setups (curves 1–16 in the graphs correspond to positions of clutches in Table 4.8).

Initially, the RSM drive has the structural heterogeneity of the first two reducing stands (1, 2) compared with the last two sizing stands (3, 4). Stage C of the gearbox of stands 1 and 2 has larger gears and spindle diameters in comparison with stage D of stands 3 and 4. However, these drive branches correspond to close natural frequencies that cause the beating of torsional vibrations in the drive.

With an increase in the output section of the rod, the lowest mode frequency (19 Hz) (Fig. 4.56) drifts at 7.5–8.1, 9.5–10, and 14–14.5 mm, as well as the third (30 Hz) and fourth (36 Hz) modes frequencies in the range of 18–19 mm. Higher frequencies are monotonous, and there is no phase change on a different assortment in these modes of oscillation.

Due to the change in the deformation parameters in the stands when rolling rods of various diameters, it is impossible to ensure the required zero level of tension for the entire size range of the mill. Therefore, some gear ratios in the RSM stands, ensuring rolling without longitudinal forces, are not the same for different diameters of the wire and rod.

A rational number of gear ratios for the entire dimensions can be selected for the diameter, the production volume of which is the largest, or for each stand are

selected as weighted averages, taking into account the design production volume of wire rod of each diameter. The operation of the RSM with such gear ratios will have significant technological advantages in comparison with the existing values. The most unfavourable, from a dynamic point of view, combinations of gear ratios in the RSM steps, at which the amplitudes of the torsional vibrations modes are out-of-phase on the rolls and, accordingly, the deviations of the tensions between adjacent stands, are maximal.

Elastic properties of thin rods between the stands have insignificant effects on the natural frequencies of torsional vibrations. Therefore, this component is not included in the modal analysis. However, dynamic processes in individual stands may have an effect on axial oscillations in the rod and maximum rolling speed, since perturbations lead to fluctuations in the interstand tensions.

Parametric oscillations of the rolled rod. The rising output speed of RSM up to 120–140 m/s is accompanied by increasing vibration amplitudes and frequent cases of "cobbling" when material loses axial stability and an uncontrolled growing loop is quickly accumulated inside the closed space of RSM housing. This phenomenon is observed in any RSM, i.e. steel producers have certain technological limits restricting overall plant productivity.

The modal analysis of the geared driveline of four stands showed that out-of-phase torsional oscillations of rolls exist for certain natural frequencies in the neighbouring stands of RSM and constitute the triggering mechanism of rolled material instability. Parametric oscillations of rolled metal are supposed to be the most probable mechanism of instability. Therefore, research is directed to the analysis of the torsional vibrations effect on the axial vibrations of the rod.

The parametric oscillations were previously considered concerning the axially moving strip [357,358], universal joints of spindles, gearbox meshing stiffness

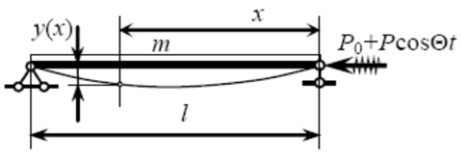

Fig. 4.57. Calculation scheme of rod vibrations between neighbouring stands under the action of a longitudinal periodic force

variation, and cold rolling mills chatter [359]. Vibrations of a rod in the interstand spaces were investigated and it was proposed to stabilize the rolling mill to use not only the deflection of the rod loop but also the frequency of transverse vibrations [360]. However, in modern solutions for high-speed wire and rod rolling [361, 362], this factor is not considered.

The calculation scheme of rod oscillations with linear mass m and hinged clamping of the ends on the fixed supports is presented in Figure 4.57. It is known that if under the action of a static longitudinal load, a loss of static stability happens, then under the action of a vibration load of the same kind, the loss of dynamic stability of rods is possible. Such a load is called parametric, and the result of its action may be parametric resonance. Periodic axial load excites transverse vibrations and deflection of the rod $y(x)$.

The condition for violation of the stability of high-speed rolling is the loss of longitudinal stability of the rod under the action of compressive stresses. Depending on the accepted conditions of embedding at the ends of the roll, as a rod in the interspace, the natural frequency depends on the ratio of the equivalent compressive stress and the critical Euler voltage, at which the rod loses stability.

Static critical stress and deflection by the first mode for rigid clamping of the rod ends:

$$\sigma_c = 4\frac{\pi^2 \cdot E \cdot J}{l^2 \cdot F}, h_0 = \frac{\rho \cdot F \cdot g \cdot l^4}{384 \cdot E \cdot J}. \tag{4.49}$$

The same for the hinged rod:

$$\sigma_c = \frac{\pi^2 \cdot E \cdot J}{l^2 \cdot F}, h_0 = 5\frac{\rho \cdot F \cdot g \cdot l^4}{384 \cdot E \cdot J}, \tag{4.50}$$

where E – Young's modulus; F – section; J – moment of inertia; ρ – material density; l – length of rod. It turns out that for the hypothesis of rigid embedding of the ends of the rod by rolls of adjacent stands, the critical stress before a loss of stability is 4 times more, and the allowed deflection is 5 times less than for a hinged rod. Considering the rolls' rotation in the adjacent stands, the hinged fixing of the rod ends looks more acceptable.

If the value of the critical stress exceeds the limit of proportionality of the material of the rod, then the loss of stability occurs in the zone of plastic deformations. In this case, instead of Young's modulus, the Engesser–Karman modu-

lus is used, which characterizes the relationship between the deformations and stresses beyond the elastic deformation limits. During the hot rolling with rod temperature of about 1000°C, metal modulus $E = 1.0 \times 10^9$ MPa.

The effect of tension forces in the rod on the dynamic stability of the rolling process was evaluated. In the existing design of the RSM, the roller shaft, although cantilevered, is rather rigid; therefore, they are considered stationary in the vertical direction. In such a formulation, only the axial component of the periodic tension or friction force in the rolls P_0 can create an external dynamic effect. Periodically varying axial force can influence transverse oscillations due to parametric oscillations and loss of rod stability.

When determining the parameters of the calculation scheme in Figure 4.57, it is assumed that the rod has a constant cross-section for a certain rolling schedule, and therefore a constant linear mass m and its bending stiffness K relative to the central axis of the cross-section is constant and is determined as:

$$K = E \cdot J = \frac{2 \cdot E \cdot J_y \cdot J_z}{\left(J_y + J_y\right)}, \tag{4.51}$$

where E is the modulus of elasticity of the rod (taking into account the temperature); J_y and J_z are the main moments of the rod along two axes (for an oval section). In the rolling process, due to external disturbances, the axial component of the tension force P_0 receives a periodic increment: $P(t) = P_0 \cos\Theta t$, where Θ is the oscillation frequency. Then, taking into account the inertial forces arising from the oscillations of a weighty rod with mass m, the differential equation of transverse vibrations of a rod has the form:

$$K\frac{\partial^4 y}{\partial x^4} + \left(P_0 + P \cdot \cos\Theta t\right)\frac{\partial^2 y}{\partial x^2} + m\frac{\partial^2 y}{\partial t^2} = 0\ . \tag{4.52}$$

The partial derivatives in the previous equation are denoted as:

$$\frac{\partial^2 y}{\partial x^2} = y^{II}, \frac{\partial^2 y}{\partial t^2} = \ddot{y}, \frac{\partial^4 y}{\partial x^4} = y^{IV}. \tag{4.53}$$

Then the expression (4.52) takes the form:

$$Ky^{\mathrm{IV}} + \left(P_0 + P \cdot \cos\Theta t\right) y^{\mathrm{II}} + m\ddot{y} = 0\ . \tag{4.54}$$

The solution of a partial differential equation of the form (4.54) is in the form:

$$y(x,t)=f_k(x)\sin\frac{k\pi x}{l}. \tag{4.55}$$

After substituting the solution (4.55), equation (4.54) can be represented as:

$$f_k^{\mathrm{II}}+\omega_k^2\left(1-\frac{P_0+P\cdot\cos\Theta t}{P_k}\right)f_k=0\ , \tag{4.56}$$

where $\omega_k=\frac{k^2\pi^2}{l^2}\sqrt{\frac{C}{m}}$ – natural frequency of order k; $P_k=\frac{k^2\pi^2K}{l^2}$ – the critical force of order k for a hinge rod.

Introduce the notations:

$$\bar{\omega}_k=\omega_k\sqrt{1-\frac{P_0}{P_k}}; \tag{4.57}$$

$$\mu_k=\frac{P}{2\cdot(P_k-P_0)}. \tag{4.58}$$

Then, taking into account (4.57) and (4.58), equation (4.56), for the first mode of dynamic instability, is reduced to the form:

$$f^{\mathrm{II}}+\bar{\omega}^2\cdot(1-2\mu\cdot\cos\Theta t)\cdot f=0. \tag{4.59}$$

An equation of this type is known as the Mathieu equation. In a more general form for a function $F(t)$ of any kind of periodic change in the load, it is known as the Hill equation:

$$f^{\mathrm{II}}+\bar{\omega}^2\cdot(1-2\mu\cdot F(t))\cdot f=0\ . \tag{4.60}$$

One of the main properties of these equations is the presence of dynamic instability regions, which arise at certain ratios between the parameters of the system $\bar{\omega}_k$ and μ when the equation has unlimitedly increasing solutions, that is, concerning elastic systems, parametric resonance can occur. The boundaries of the first domain for the equation are determined by the expression:

$$\Theta_1=2\bar{\omega}\sqrt{1\pm\left(\mu+\frac{\mu^2}{8\pm9\mu}\right)}. \tag{4.61}$$

The upper and lower bounds of the second region are determined by dependencies.

$$\Theta_2 = \bar{\omega}\sqrt{1+\frac{1}{3}\mu^2}\,,\ \Theta_2 = \bar{\omega}\sqrt{1-2\mu^2}\,. \tag{4.62}$$

The boundaries of the third region are determined by the expression:

$$\Theta_3 = \frac{2}{3}\bar{\omega}\sqrt{1-\frac{9\mu^2}{8\pm 9\mu}}\,. \tag{4.63}$$

The diagram of the first three regions of dynamic instability is shown in Figure 4.58. The first (main) region of instability is the most dangerous. The regions of dynamic instability for lower frequencies usually degenerate into "skeletal" lines. At unfavourable ratios between the parameters $\Theta/2\bar{\omega}$ and μ, when the operating point of the system falls into the shaded areas, a resonant increase in the transverse displacements of the rod occurs and the tension forces in the inter-stand spacing of the RSM begin to increase. In this case, the value Θ is the frequency (rad^{-1}), and 2μ is relative amplitude, one of the modes of natural torsional vibrations of the drive and rolls in the adjacent stands of the RSM. The value $\bar{\omega}$ is the natural frequency of the transverse oscillations of the roll, as a weighty rod.

The rod length between the rolls of RSM: stands 1–2 – 820 (mm); stands 2–3 – 852 (mm); stands 3–4 – 290 (mm). For certain rod dimensions, the two stands of the RSM are out of work, and then the distances between the corresponding stands are summed. At the maximum values of the longitudinal stresses in the rod of 8 MPa (N/mm^2), the frequencies of transverse oscillations are as follows: stands 1–2 – 19.5...13.8 (Hz); stands 2–3 – 18.9...13.4 (Hz); stands 3–4 – 55.4...39.2 (Hz).

The calculated frequencies of transverse oscillations of the metal appear within the range of natural frequencies of torsional vibrations of the RSM drive. Actual frequencies will decrease in the relative range of 1...0.707 $(1/\sqrt{2})$ depending on the heating temperature of the metal (up to 950...1000°C), since reduced modulus of elasticity of the metal. The obtained dependences between the geometry of the rod (J_y and J_z), the frequencies and amplitudes of the torsional vibrations of the drive, as well as the heating temperature, make it possible to calculate in advance possible areas of instability using RSM stands depending on its setting for rolling each type of range. The influence of damping due to elastic-plastic deformation of the rod between the stands on the stability of oscillations during rolling was neglected. In theory, damping narrows the areas of instability, and

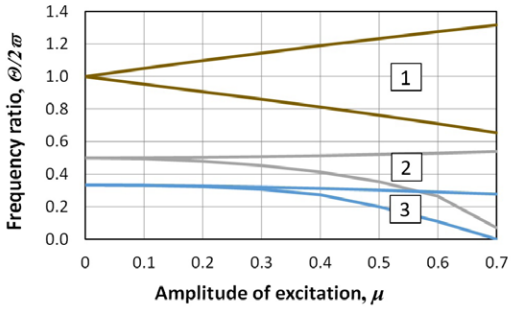

Fig. 4.58. Areas (1–3) of the dynamic instability of rod vibrations with hinged clamping of the ends in the rolls of neighbouring stands

resonance occurs at greater values of the amplitude of the external action. In general, linear damping cannot eliminate parametric resonance.

Simulation of impulsive disturbances. Impacts at the entrance of the RSM are represented by the step-up torque on the rolls in stand 1. The pulse durations vary in the range of 0.001–0.010 s, which corresponds to the defect on the rod at a speed of 110 m/s. The delays of rod transportation between the stands are 0.003–0.01 s. The synchronous and out-of-phase oscillations in the drivelines of neighbouring stands are shown in Figure 4.59.

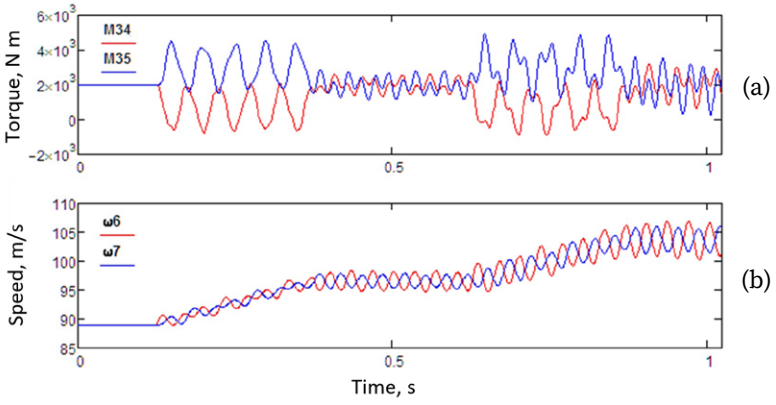

Fig. 4.59. Oscillations of: (a) torques; (b) roll speed in the neighbouring stands

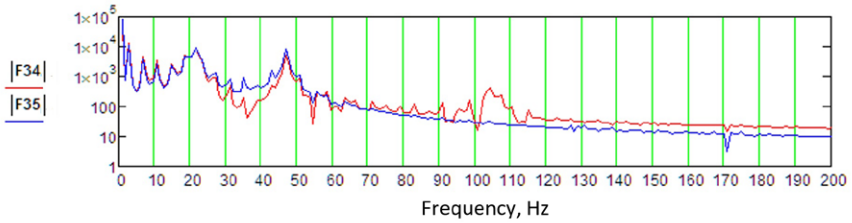

Fig. 4.60. Spectra of torques oscillations

At long duration (low frequency) of disturbances, the higher natural frequencies about 100 and 150 Hz practically do not manifest themselves (Fig. 4.60). As the frequency of a pulsed disturbance increases (duration decreases), the vibration modes associated with these natural frequencies and localized in gear stages C and D become noticeable in transients even at a disturbance amplitude of only 1% of the static rolling moment.

Oscillations of interstand tensions. The calculation of the tensions during the mismatch of the frequency and phase of roll oscillations in the adjacent stands is calculated as:

$$\frac{dT_{ij}}{dt} = \frac{E_{ij} \cdot S_{ij}}{L_{ij}} \cdot \left(v_i^0 - v_j^1 \right), \tag{4.64}$$

where E – modulus of elasticity; S – rod section; L – interstand distance; v_i^0, v_j^0 – entry and exit speed of rod in the neighbouring stands i and j.

Under combinations of vibration parameters (amplitude, frequency, phase) in two stands (i is the next, j is the previous one), the rod speed is specified as:

$$v_i^0 = v_0 + R_i \cdot A_\omega \cdot \sin\left[\left(1-\alpha\right) \cdot \omega \cdot t + \left(1-\beta\right) \cdot \pi \right], \tag{4.65}$$

$$v_j^1 = v_0 + R_j \cdot A_\omega \cdot \sin\left(\omega \cdot t\right), \tag{4.66}$$

where α, β (0...1) is the mismatch in frequency and phase in adjacent stands; R_i, R_j – rolls radii; A_ω, ω is the amplitude and frequency (rad^{-1}) of torsional vibrations of the rolls.

The calculations are made for a 5.5 mm rod size, with appropriate RSM drive settings with the nominal diameters of the rolls in stands 1 and 2 – 228 mm, stands

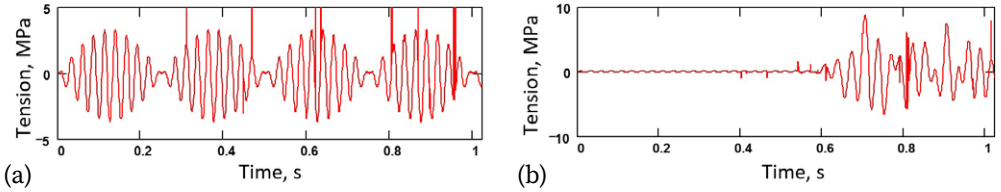

Fig. 4.61. Tension fluctuations between stands 1–2 with the frequency mismatch: (a) $\alpha = 0.1$, (b) $\alpha = 0.01$

3 and 4 – 156 mm. Calculations with a nominal linear rolling speed of $v = 110$ m/s, the amplitude of rolls torsional oscillations $A_\omega = 0.03$ rad^{-1} and identical phases ($\beta = 1$) showed that with a frequency deviation of $\alpha = 0.1$ in adjacent stands, the resulting tension is in the form of an amplitude-modulated signal (Fig. 4.61).

The alternating tension fluctuations can lead to the formation of a loop. A smaller mismatch (closer frequencies) leads to a longer beating period $T_{\text{beat}} = 1 / (F_2 - F_1)$, which in the case of long duration can look like a random variation of technological factors. During high-speed rolling, the integration of the difference in rolls' instantaneous speeds and the increase in tension forces between the stands occur very quickly, until the rolls completely slip or the rod breaks in the stands. Given the dense spectrum of the natural frequencies of the RSM drive in the range of up to 60 Hz, we can expect an increased effect of torsional vibrations through tensions with amplitude modulation periods of 3–5 Hz.

The average tension between the last stands 3–4 remained unchanged because rolls fluctuated synchronously (Fig. 4.62). In these stands the disturbance

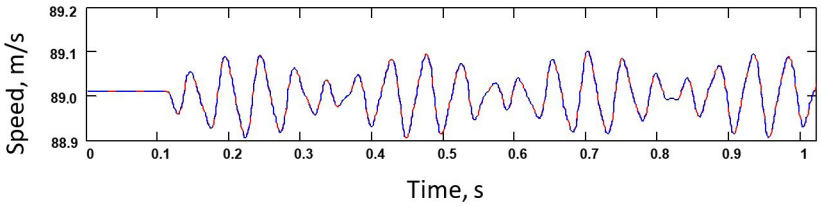

Fig. 4.62. The synchronous rolls' vibration with a constant average speed in stands 3 and 4

was no longer from the rolls, but from the unbranched part of the drive (stages A, D), as a delayed reaction to the disturbance from the rolls in stand 1.

In this case, the beats were caused by the difference in the parameters of the drive branches in stage D. This is confirmed by the presence of a certain delay of the reaction from the moment of time $t = 0.1$ (s) of the application of a load impulse in stand 1 and another beat frequency (4 Hz instead of 3 Hz). Fluctuations of moments of elasticity between the engine and stage A, between stages A and D occur in the same phase.

All branched parts of the gearbox exhibit nonsynchronous (out-of-phase) oscillations with amplitudes proportional to the magnitude of the disturbance, which at small load moments and large amplitudes of torsional vibrations can lead to the opening of gaps and subsequent amplification of vibration in the gears of the RSM stages. Simulation of disturbances from the engine, for example, by applying a step change in the rotational speed reference causes oscillations in the entire gearbox only at the fundamental natural mode frequency of 20 Hz.

The RSM drive was modelled in absolute angles of rotation of the lumped masses. When even a minimum attenuation coefficient of about 0.001–0.0001 is introduced into the model for all the masses of the drive, the transient processes decayed.

The influence of tensions on friction. Tensions influence the friction in the deformation zone of the adjacent stands. To determine the friction coefficient in the deformation zone, taking into account the obtained on the model amplitudes of the torsional vibrations of the rolls and the tension oscillations, the earlier introduced "effective friction coefficient" is used. A common limitation of this earlier introduced term is the absence of the formulas of frequency and phase of oscillations.

The deviations of the friction coefficient, calculated with the rolling force $N = 50$ kN, the corresponding cross-sectional areas and the deviations of the ten-

Table 4.11. Parameters of tension fluctuations and friction in the stands of RSM

Stands	Interstand distance, mm	Rod stiffness, N m	Speed, m/s	Specific tension, MPa	Friction coefficient deviation
1–2	820	3.86×10^6	85.216	±3.3	±0.0013
2–3	852	3.22×10^6	98.850	±2.1	±0.0018
3–4	290	8.83×10^6	105.769	±6.5	±0.0033

sion forces in the stands are presented in Table 4.11. With an average value of the friction coefficient $f = 0.20$, its deviations are about 0.5%.

In practice, the influence of tension fluctuations on friction conditions during high-speed rolling can occur due to inertial forces, which at a cross-section of 5.5 mm and a speed of 100 m/s will reach values of the order of 350 N (acceleration 120×10^3 m/s^2 and mass 2.917×10^{-3} kg in the deformation zone). Alternating

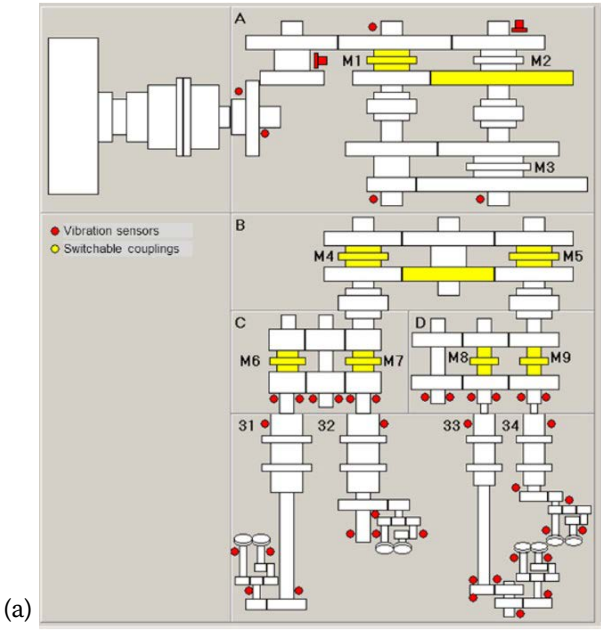

(a)

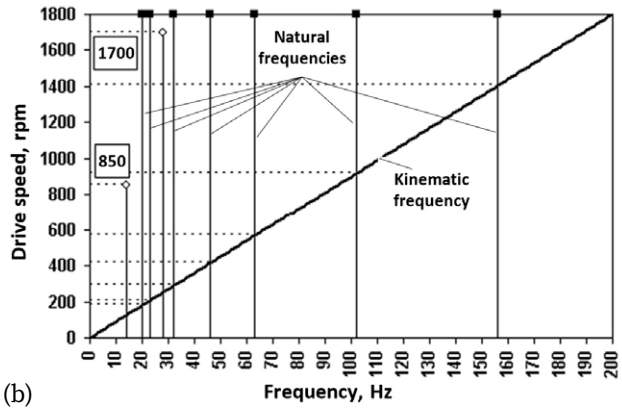

(b)

Fig. 4.63. (a) Interface of RSM modelling system;
(b) diagram of potential resonances

forces will also depend on the section of the strip, and change in proportion to the fundamental mode frequency of vibration.

Since $A = dv/dt = (v_0\omega)\sin(\omega t)$, where v_0 is the amplitude of the vibration velocity obtained in the model calculations (±0.05 rad^{-1}), ω is the natural frequency (up to 400 rad^{-1}), which gives the amplitude of rod acceleration ±20 m/s^2. For a metal mass of 0.2 kg and length of 0.852 m, the variable inertial force will be about ±4 N, which is 2.5% of the total force in the range of 0–100 N from the steady-state value in the first stand of the RSM.

The tension signal is an informative parameter for diagnosing the stability of high-speed wire and rod rolling. It can be determined by the vibration sensors on the bearings of rolls, unlike torsional vibrations by the sensors on the shafts, which are not suitable for RSM. The developed dynamic model of the RSM can be efficiently used for determining the influence of the technical state of gearing (total wear, local defects) on a dynamic process and simplifies fault detection under the variable structure of the gearbox.

The RSM drive structure is constantly changing during operation. The software has been developed for multivariate calculations for each rolled dimension of metal. The program interface is presented in Figure 4.63a. One of the software functions – the frequency diagram, which is shown in Figure 4.63b, where the vertical lines correspond to the natural frequencies, the horizontal lines represent the speeds in each stand, and the inclined lines correspond to some chosen kinematic frequencies of disturbances. The coincidence of the kinematic and natural frequencies determines the allowable ranges of the drive speed, which are indicated on the vertical scale. The user of the program (mill operator) selects the final size of the rod and the algorithm sets the necessary clutches (in yellow colour) to the active state, thereby changing the structure of the dynamic model. Then, the mill operator sets the operating speed of the mill and gets a complete picture of what is happening inside the block in the form of a kinematic diagram. Calculations of torsional vibrations are carried out in advance.

This software module can be integrated into the RSM control system as an advisor to mill operators, or for work in automatic mode to control the speed of the electric drive to reduce resonant vibrations during the rolling process.

Detection of instability in the RSM. In various places of the RSM drive a sufficient number of vibration sensors are installed (Fig. 4.63a): stage A – 7, stage C – 6, stage D – 6, stand 1 – 5, stand 2 – 5, stand 3 – 8, stand 4 – 5, in total – 42 sensors. Due to the presence of sensors it is possible not only to diagnose the equipment but also

to perform mill control by predicting the onset of unstable conditions at elevated rolling speeds.

The amplitude of the vibration signal depends on the ratio of the support stiffness, the sensitivity of the sensors (100 mV/g) and the amplitude of the tension fluctuations. With constant support stiffness and sensor parameters, the vibration signal in a given frequency range (20–40 Hz) will be proportional to the standard deviation of the tension force. The noise immunity of this tension diagnostics method is ensured by the fact that all other kinematic sources of noise are far beyond the specified frequency range at speeds up to 110 m/s.

4.4.3. Tandem cold rolling mills

A detailed analysis of the specific phenomenon of chatter vibrations is represented, which occurs in all types of single-stand and multi-stand (tandem) cold rolling mills as well as in other industrial machines under certain conditions. These vibrations cause severe failures of mechanical parts or final product quality deterioration. Factors affecting the excitation and amplification of chatter vibrations as well as approaches to their modelling are considered and possible methods for their damping and control are discussed.

Factors of chatter vibrations excitation. The friction forces between the treating tools and material (including rolled strip) have a nonlinear relation with many factors: machine design, lubrication conditions, rotating speed and others. Such kind of instability is considered either as kinematically excited from the torsional system [363], self-excited [364–367] or parametrically excited by friction in the contact of rolls and strip.

Some of the authors pointed out that the chatter excitation is caused beyond the strip and work roll contact zone. Their investigations concern rolls, gears and other parts vibrations. They matched kinematic sources with the main frequency of chatter. It was stated that chatter marks on the rolls and strip are the result of resonance in the mill due to an integer number of defect wavelengths along the rolls' circumference [368–371]. Other authors investigated frequencies of the elastic rolls and strip displacement as a possible source of chatter. They matched different system mode frequencies with the chatter frequency.

The electric drives and control system parameters are considered in [372] where the author builds a stable rolling area in the domain of the stand electrical drive parameters. The friction and slipping velocity relation linearization was ad-

mitted. The electrical drive stability is discussed in [373]. Linear models and the transfer function method are frequently used for the complete mill dynamic description including drives and mill automatic control system, roll stack and strip in the tandem mill. However, these models do not allow chatter investigation for the real plant conditions as the friction in the contact zone is a nonlinear force.

The next group of studies concern the contact friction and emulsion instability as a source of vibrations [374, 375]. The authors in [376, 377] investigated the effect of the roll grinding process on the strip chatter marks and mill vibration. They showed the exact relation between usually invisible roll surface defects after grinding and chatter vibrations in the rolling mills. Dampers and speed range control for grinding machines are proposed to avoid those causes of chatter. The authors in [378] and others describe the positive feedback in the linear system of the mill and tried to find a condition of the mill vibration self-excitation due to contact friction linearization.

For the mechanical systems dynamics description, the Lagrange method and equation is the most widely known approach. As considered, the relative slipping appears during chatter between strip and rolls and it is necessary to assign the Raleigh dissipation function following the Lagrange method. This function should describe friction forces' dependence on relative slipping velocity and allow the integration of the Lagrange equation. Usually, nonlinear formulas are used, which contain the drop zone incorrectly called "negative friction" by some authors. The well-known Van-der-Pole and Raleigh dissipation polynomial functions describe non-damped self-excited vibrations.

The theoretical approach, which helps avoid the Raleigh function by using the movable system of coordinates, is described in [379, 380]. The energy balance method for the moving strip kinetic energy and distributed friction forces was used instead of the Lagrange equation. Strip tensions are taken into account. The nonlinear positive feedback as the cause of chatter was described and a method for model-based rolling mill control was proposed.

In the publications [381–388], authors have developed the models of chatter. However, sophisticated nonlinear models need more accurate parameters. Firstly, there are no practical methods for online accurate determination of the analytical dissipation function in the rolling mills, especially for the different frequency ranges. Secondly, nonlinear models may give in reality unexpected results due to system bifurcations at the bound of stability as it concerns high-speed rolling mills. The mentioned difficulties for deterministic models initiated

statistical approaches to chatter research. The chaotic oscillations models were proposed for chatter investigation because the rolling mills are the non-conservative systems.

The early chatter detection is more developed in the metal treating machines control than in the rolling mills. There are some methods for chatter vibration prediction in drilling and cutting. The authors of work [389] used the ARMA (Auto Regression Moving Average) model and controller. The described real-time monitoring system determines the system damping factor and main mode frequency. The designed method was tested in the rig and showed well enough results in chatter forecasting (about 2 s before chatter onset). The neural networks were used to control driveline chatter vibrations. Some of the methods for avoiding chatter vibrations focus on clearances between mill housing and roll chocks and chatter detection based on monitoring of interstand tension have been patented [390, 391]. Since the 1970s, some theoretical and experimental studies of the coupled dynamic processes in the drivelines and stands of the tandem cold rolling mills have been conducted and the main factors affecting chatter vibration were determined [392–396], which are reviewed further herein.

Torsional vibrations and load balance regulator. It was experimentally discovered in every rolling mill that the roll's eccentricity (preferably backup rolls) causes large (50–70%) torque variation and much less (35%) electrical drive current oscillations when the speed was kept in the resonant ranges. The strip product and rolls in some cases were affected by chatter marks. Conditions for chatter appearance occur depending on average torque and speed, gear wear and drive load balance regulator settings. When the drive load for one roll is much less (by 20–30%) than for another roll, then gear couplings exhibit such shocks that the system becomes parametrically excited by the periodic changing of stiffness. The rubber spindle coupling was proposed to eliminate such vibration. Also, the load balance unit was corrected by feeding impact not only to the upper but to the lower drive, too. Such measures have effect only in transient periods of mill speed changing.

Rolls eccentricity compensation. Almost all modern systems of roll eccentricity compensation do not take into account phase conditions in the neighbouring stands of tandem mills in the low-frequency range of backup rolls beating. They act independently in every stand taking as input the back tension signal in every stand and using Hydraulic Automatic Gauge Control (HAGC) cylinders for changing the rolling force. Chatter research in the 5-stand tandem mill showed that the

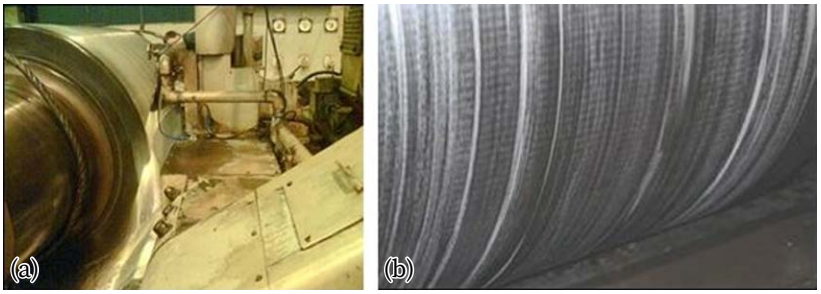

Fig. 4.64. (a) Vibration measurements in two axes with accelerometers installed on the grinding wheel support; (b) diagnostics of hidden periodic defects on the backup roll

three middle stands 2, 3 and 4 demonstrate the same phase in the low-frequency range (2–4 Hz) of backup rolls beating. However, stand 5 shows out-of-phase oscillations in this range because of the stiffness compensation mode. Therefore, roll eccentricity compensation systems may affect 3rd octave chatter.

Rolls grinding operations. Periodic oscillations were discovered during the work rolls gritting operation. The unbalanced rotating drum caused periodic surface hardness and then chatter marks appeared on the work rolls. Gritting machine design (belt coupling and drum) was improved and chatter marks were eliminated.

The conducted measurements of vibration and technological parameters on the roll grinding machines (Fig. 4.64a) explained the causes of periodic defects (Fig. 4.64b).

Defects are induced in the contact between the grinding wheel and the treated backup roll when the machine is not equipped with the special control function, which provides compensation for the wheel diameter decreasing because of its wear in every pass. The research resulted in building regions of process stability on the diagram of wheel feed and grinding depth that allowed avoidance of additional excitation of chatter in the tandem mill due to hidden defects on the rolls.

Winding reel vibrations. In single-stand reversing mills, the coil beating compensation systems are installed. Unfortunately, the majority of other mills often demonstrate the interaction between the coils on the reels and the first or last stands. It mostly appears when the backup roll diameters in the last stand are equal to the coil diameter. When tension begins to oscillate with the backup

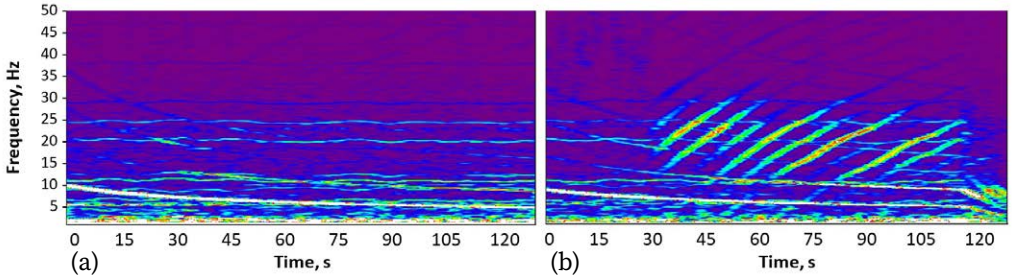

Fig. 4.65. Time-frequency diagrams of the exit tension signal in stand No. 5 of the tandem mill: (a) reel No. 1 in good condition; (b) reel No. 2 with defected rollers

roll rotating frequency while the coil diameter gradually changes, the resonance appears. Another type of resonance in the temper mills involves reel driveline torsion oscillations with the natural frequencies or coil rotating frequency harmonics. Time-frequency diagrams are the most suitable tools for long-term process spectrum analysis in such cases. The two coils compared which were rolled in the tandem mill to the different winding reels (Fig. 4.65). One reel (No. 2) had problems with the coil supporting rollers. It was diagnosed successfully by the exit tension analysis in the last stand No. 5. Besides, approximately 1520% of the cases of chatter occurred under the constant mill speed at the end of coils when the coil and stand No. 5 backup rolls diameters became equal (about 1600 mm). Such cases were identified and tension oscillations were avoided due to mill speed control.

Cooling emulsion concentration and temperature. Lubricant degradation as a vibration source under high-duty conditions has been investigated by many authors. Narrow contacts (10–15) × (1000–2000) mm between strip and work rolls are the only places where the biggest part of power (up to 10 MW) from electric motors is being transferred by the friction to rolled metal for its elastic-plastic deformation. Therefore, even the smallest disturbance in contact friction conditions under the high loads in stands (10–15 MN) may produce impulsive impacts with the wide band spectrum. Consequently, it excites the natural frequencies of the mill. The obvious methods for emulsion concentration control by the vibration signals in the stands were reported. Besides the very high cost of emulsion, the roll cooling system could not be able to vary concentration quickly (time of response is 20 min), so it cannot be used for fast chatter control. It has been

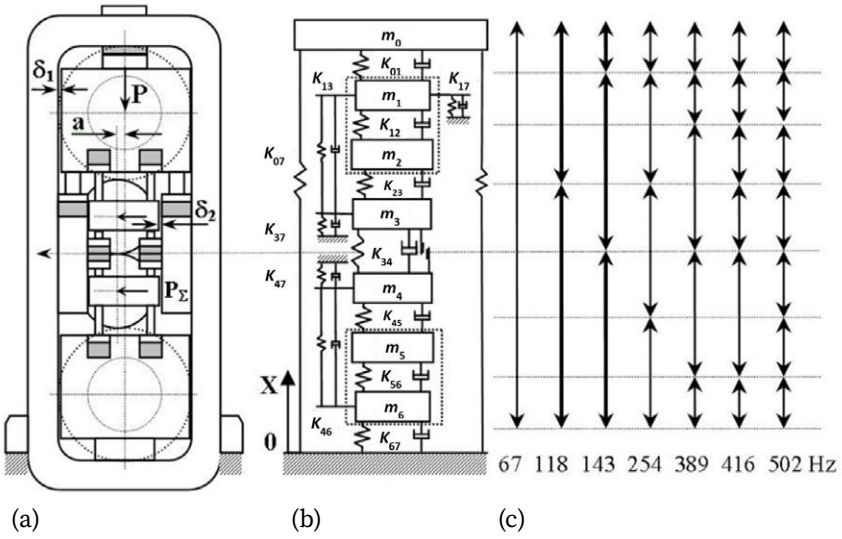

Fig. 4.66. (a) Design of the 4-high rolling stand with hydraulic systems; (b) spring-mass model; (c) vibration modes

shown by simulation and experiment that in tandem mill for two neighbouring stands there is an optimal friction factor for minimal susceptibility to chatter.

It was known that there is a possibility of self-excited vibrations initiation by periodical temperature changes in the contact zone during rolling. Emulsion temperature may reach the upper limit of its destruction. Following the results of our analysis of emulsion, there is no evident relation between the emulsion type, its concentration and chatter occurrence in the tandem mill. Chatter is rather dependent on backup roll defects, which greatly increase the vibration.

The dynamical model of the rolling stands. A 4-high stand (Fig. 4.66a) of tandem cold rolling mill is considered in [397], which consists of massive cast housing, the top and bottom set of work rolls (WR) and backup rolls (BUR), placed with its necks into chocks with the roller bearings and hydrostatic sliding bearings, accordingly. The chocks are placed into the housing where side backlashes appear (designated as δ_1 and δ_2) because of removable flat liners deterioration. Therefore, stands are designed in such a way that WR chocks are shifted forward (last stands) or backward (first stands) from the BUR axis by a = 10–15 mm. There are four hydraulic blocks fitted to each rack of housing which contain 4 big cylinders for upper BUR balancing during stand maintenance (WR changing) and 8 or 16 (depending

on stand design) smaller cylinders, which are involved in strip flatness regulation by the positive or negative WR bending. Bending cylinders are regulated automatically in the last stand or manually in the previous stands depending on the WR wear and strip flatness. In general, WR bending causes random contact stiffness deviations between the top and bottom WR and BUR. It is described further herein that either stochastic or controllable stiffness change can occur during mill operation.

Besides, the two main cylinders of the HAGC system for rolling load creation and strip thickness regulation are placed between the upper crossbeam and BUR chocks (some mills have HAGC cylinders at the bottom). The small deviation of stiffness occurs due to HAGC oil column and roll diameter changes after their scheduled replacement. The deformation of every element influences the stand summary modulus of elasticity (46 MN/mm).

To obtain vibration response specific for different measuring points a detailed spring-mass model has been designed (Fig. 4.66b). Unlike in all known models, the WR bending and BUR balancing forces are included as stiffness instead of external

Table 4.12. Parameters of calculation scheme of the 4-high rolling stand

Parameter	Description	Value	Units
m_0	Mass of upper cross-beam with HAGC cylinders	80.0	10^3 kg
m_1	Mass of upper BUR chocks	26.7	10^3 kg
m_2	Mass of upper BUR	45.0	10^3 kg
m_3	Mass of upper WR with chocks	8.7	10^3 kg
m_4	Mass of lower WR with chocks	9.1	10^3 kg
m_5	Mass of bottom BUR	45.0	10^3 kg
m_6	Mass of bottom BUR chocks.	24.3	10^3 kg
K_{07}	Stiffness of housing racks and top cross-beam	29.01	10^3 kg
K_{01}	Stiffness of HAGC cylinders and upper BUR chocks	22.02	MN/mm
K_{12}, K_{56}	Stiffness of sliding bearings and BUR bending	87.99	MN/mm
K_{23}, K_{45}	Stiffness of WR and BUR contact	19.89	MN/mm
K_{34}	Stiffness of WR bending, contact and strip deformation	20.00	MN/mm
K_{17}	Stiffness of upper BUR weight balancing cylinders	25.00	MN/mm
K_{67}	Stiffness of lower BUR chock and level tuning jack	38.95	MN/mm
K_{37}, K_{47}	Stiffness of WR negative bending cylinders	15.00	MN/mm
K_{13}, K_{46}	Stiffness of WR positive bending cylinders.	15.00	MN/mm

forces. Such an approach allows a statistical analysis of the stand vibration under the variable operating schedules and helps find methods for chatter active control. Stand vibration is assumed to be symmetrical for both the operator and drive side (without skewness) because that is proved by measurements. Positive movement is assumed upward. Experimental modal analysis of the rolling stand and the detailed FEM analysis showed that the 4-high rolling stand cumulative mass fraction is about 0.80–0.85 for the first 4–9 modes. The natural frequencies range for the average values of stand parameters covers a band of 50–600 Hz (Fig. 4.66c). The parameters of a typical 4-high rolling stand are given in Table 4.12.

It is commonly admitted that the feedback loop, which is created in the rolling stands by the interdependence of rolling force, strip thickness, tensions and speed, is the main cause of instability. Chatter in the tandem mill excited by this mechanism can occur only due to symmetrical modes around the strip plane with the opposite phases of the upper and lower pairs of WR and BUR motion. Chatter excitation through the strip thickness variation (δh = 20–50 microns) can only be initiated by the modes with the several masses movement near the strip plane. The out-of-phase WR movement causes only periodic roughness defects on the strip or BUR (Ra = 2–3 microns).

The modes of vertical vibrations are represented in Figure 4.66c and Table 4.13. In practice, the first mode of about 67 Hz does not appear. The conducted measurements of vibration on the four roll chocks have shown that for the thick strips (h_1 > 0.8 mm) chatter is not excited because the main mode of 118 Hz has a node beyond the WR gap.

Table 4.13. Natural frequencies and vibration modes in the rolling stand

f_n, Hz / Mass	67	118	143	254	389	416	502
	1	2	3	4	5	6	7
m_0	0.302	–0.302	0.584	0.022	–0.043	–0.003	–0.001
m_1	0.509	–0.098	–0.364	–0.149	0.840	0.064	0.028
m_2	0.533	–0.031	–0.512	–0.077	–0.458	–0.052	–0.050
m_3	0.432	0.305	–0.228	0.684	–0.018	0.234	0.725
m_4	0.352	0.461	–0.013	0.685	0.270	–0.010	–0.684
m_5	0.190	0.609	0.356	–0.109	0.020	–0.391	0.050
m_6	0.136	0.471	0.292	–0.147	–0.097	0.886	–0.038

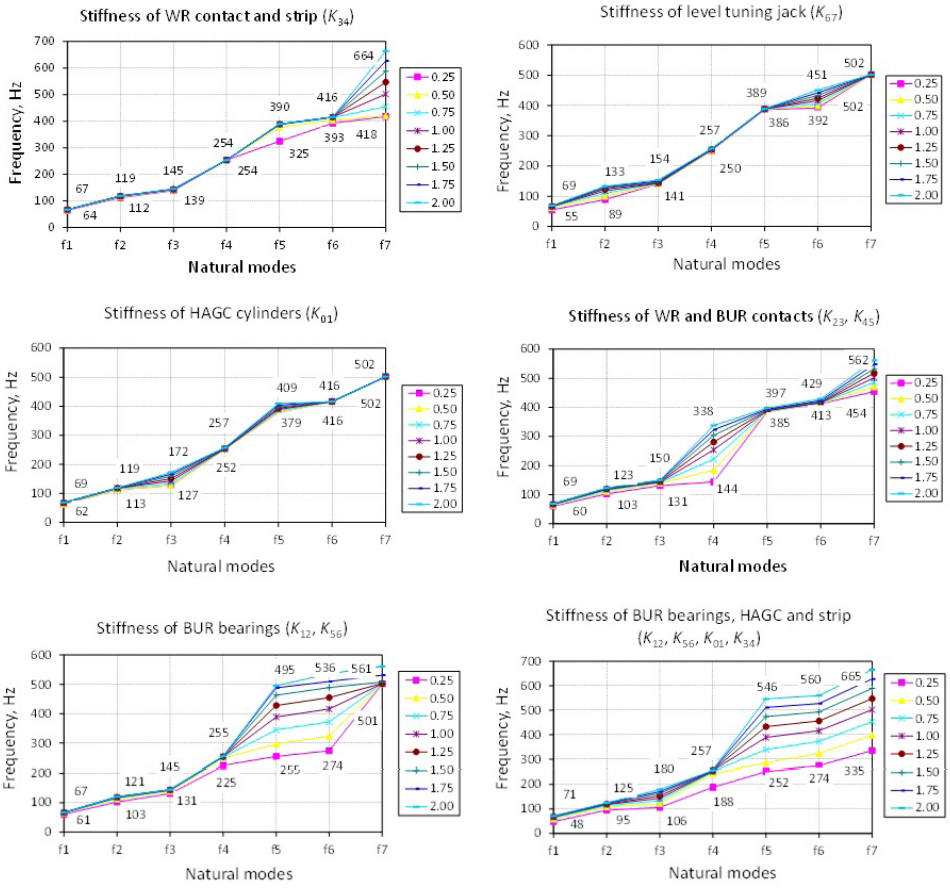

Fig. 4.67. Changes of natural frequencies by the stiffness of stand elements

Dependences of natural frequencies (numbered 1–7 as in Table 4.13) on the stiffness of different elements of the rolling stand are shown in Figure 4.67. The nominal stiffness values (1.0) vary in the range of 0.25...2.0.

The results of the statistical calculations show that the stiffness of hydraulic elements (K_{13}, K_{46}, K_{37}, K_{47}), which are newly introduced in the model, can change natural frequencies and modes (Fig. 4.68). Node displacement of the principal vibration mode (~118 Hz) can be achieved due to the HAGC stiffness (K_{01}) decreasing by 25% from the nominal value or the stiffness of the rolling level tuning unit (K_{67}) increasing by 50% at the bottom of the stand. Both actions can be done only before the rolling process starts, i.e., during the mill set-up procedure.

Calculations by the developed model showed that work roll bending does not affect significantly the principal mode frequency (f_2 in Fig. 4.68a). However,

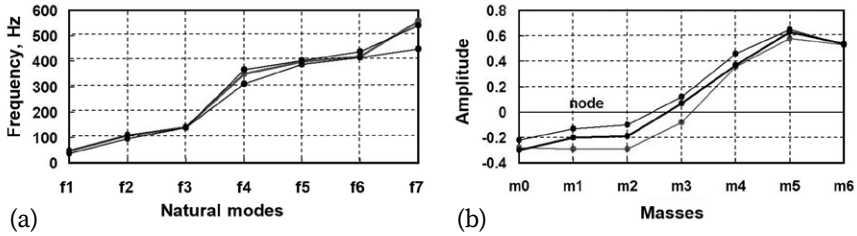

Fig. 4.68. (a) Scattering of natural frequencies; (b) principal mode (f_2 ~ 118 Hz) deviation by the work rolls bending stiffness (K_{13}, K_{46})

variation of WR bending stiffness can move the node from the position between masses 2 and 3 (upper WR and BUR) into the gap between masses 3 and 4 (upper and lower WR) (Fig. 4.68b). Therefore, it can be used for chatter active control not only by the high-frequency periodical impacts but also due to comparatively slow stiffness control in the stands. This method of chatter vibration control does not require an oil pumping station with a high flow rate and fast switching valves to produce quick control impacts of large amplitude.

BUR balancing cylinders usually have constant stiffness and less influence on node movement even with the greater force (1600 kN) in comparison with the WR bending force (960 kN negative and 460 kN positive). The only problem, which has to be solved, is a WR initial profile design to fulfil high demands on strip flatness. Hence, the complex of chatter control channels is required.

Strip damping due to elastic-plastic deformation. By the process observation, chatter occurs rather for thin and hard strips. It is related to the strip dissipation properties. The larger strip section size and its plastic deformation in comparison with the elastic deformation increases energy dissipation of the roll stack during the vertical oscillations. The hysteresis loop width of the spring-mass system depends on rolling parameters. In the tandem mills, the last stands always have a narrower hysteresis loop than the previous ones and more sensibility to chatter as the rolling speed increases to the mill exit.

The elastic-plastic properties of the rolled strip play a main role in the mill vibration. By the various estimations, the rigid-plastic theory can serve until the fraction of external energy to the whole energy of elastic deformation of a material is, at least, not less than three. It becomes important in cold rolling of thin strips where elastic restoring of strip thickness (h_1–h_e) is comparable with an ab-

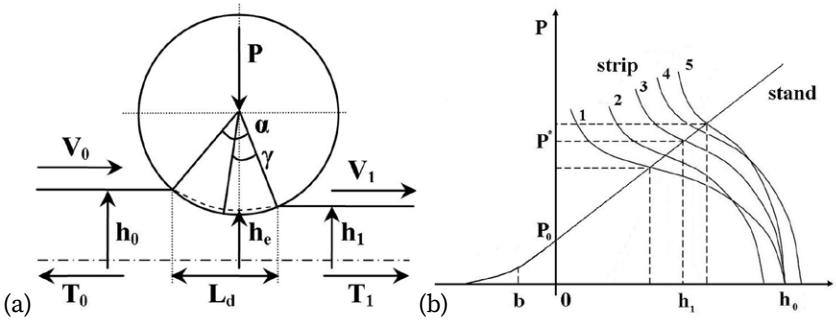

Fig. 4.69. (a) Strip and WR contact scheme; (b) stand and strip deformation diagram

solute reduction (h_1–h_0), especially in the last stands of the tandem mills. The strip deformation scheme is represented in Figure 4.69a. In a modern rolling theory, the strip properties are described by the nonlinear formulae including initial yield stress, tensions, strain and strain rate with other rolling parameters. Statistical deviations of the strip properties and rolling parameters as a rule are not taken into account. It does not allow reliable prediction of the dynamic phenomena of chatter vibrations in the rolling mills.

The strip stiffness K_s and its viscous damping C_s are described with the fraction derivatives of a rolling load deviation by the strip thickness reduction and its deformation rate. Also, the dynamics sensitivity factor λ is introduced by the following formulas:

$$K_S = -\frac{\partial P}{\partial h_1}; \tag{4.67}$$

$$C_S = -\frac{\partial P}{\partial \dot{h}_1}; \tag{4.68}$$

$$\lambda = \frac{\partial \sigma}{\partial \lg(d\varepsilon / dt)} \tag{4.69}$$

Stand and strip stiffness graphs are represented in Figure 4.69b. An initial nonlinear stand deformation b due to backlashes is eliminated by the stand preloading P_0. There is a variety of operation points around a mill set-up load value P^* and thickness h_1 because of rolling parameters variation.

Curve (1) corresponds to back and/or front tensions increasing; curve (2) – to a lower input thickness; curve (3) – to the working point of mill set-up; curve (4)

Table 4.14. Strip rolling parameters in the 5-stand tandem cold rolling mill

Rolling parameters	Stand 1	Stand 2	Stand 3	Stand 4	Stand 5
Strip exit thickness h_1, mm	1.400	0.840	0.546	0.382	0.363
Strip absolute deform. $\Delta h = h_0 - h_1$, mm	0.600	0.560	0.294	0.164	0.019
Rolls and strip contact length L_d, mm	15	16	12	10	10
Strip linear velocity V_1, m/s	6.5	10.8	16.6	23.8	25.0
Time (freq.) of deform. L_d/V_1, ms (Hz)	2.30(435)	1.48(676)	0.72(1389)	0.42(2381)	0.40(2500)
Strip relative deform. $\varepsilon = \Delta h / h_0$, %	30	40	35	30	5
Strip stiffness K_s, MN/mm	20	21	41	73	628
Strip damping C_s, MN s	0.092	0.044	0.025	0.017	0.096
Deformation velocity $d\varepsilon/dt$, s^{-1}	130	270	486	714	125

Notes: 1) Length of deformation zone L_d accounts WR contact indentation.
2) Initial thickness is $h_0 = 2$ mm. 3) Stands loads are assigned equal to $P_{1-5} = 12$ MN.

– to an increment in the output thickness and curve (5) – to a possible increment in the friction coefficient and the average yield stress or a decrement in the back and/or in the front tensions. It can be seen in Figure 4.69 that random rolling parameters can change strip stiffness significantly (tangent of inclination angle at a working point) and, hence, natural frequencies and modes.

It is known that a quick jump up of λ factor appears when $d\varepsilon/dt > 10^3$ s^{-1}. It is particular for the material hardening properties. Strip deformation conditions in the 5-stand tandem mill are given in Table 4.14.

The parameters combination gives minimal strip damping value in stands 3 and 4, which are most susceptible to chatter vibrations in practice. Deformation velocity increases with stand number and for stand 4 is close to critical value 10^3 s^{-1}. The commonly used method in the mill automatic monitoring systems or by mill operators for chatter cancelling is the slowdown of rolling speed, which is addressed to the strip deformation rate and its damping ability, respectively.

Besides, the strip reduction schedule changing in the last stands can be used for chatter control due to more damping in the strip material. It was tested in stands No. 3 and No. 4, and approximately every step down by 1% of relative reduction e gave 20 m/min of additional mill speed. Also, specific tension reduction by 5 N/mm^2 gives a mill speed increase by 40–50 m/min.

The wear of chocks and stand housing give WR an additional degree of freedom in the backlash gap and enables the interaction of vertical and horizontal

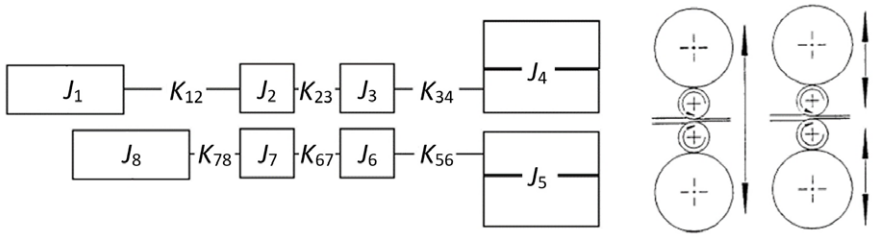

Fig. 4.70. Spring-mass models: (a) individual drivelines of work rolls; (b) 4-high rolling stand with 3rd and 5th octave symmetrical modes of chatter vibration

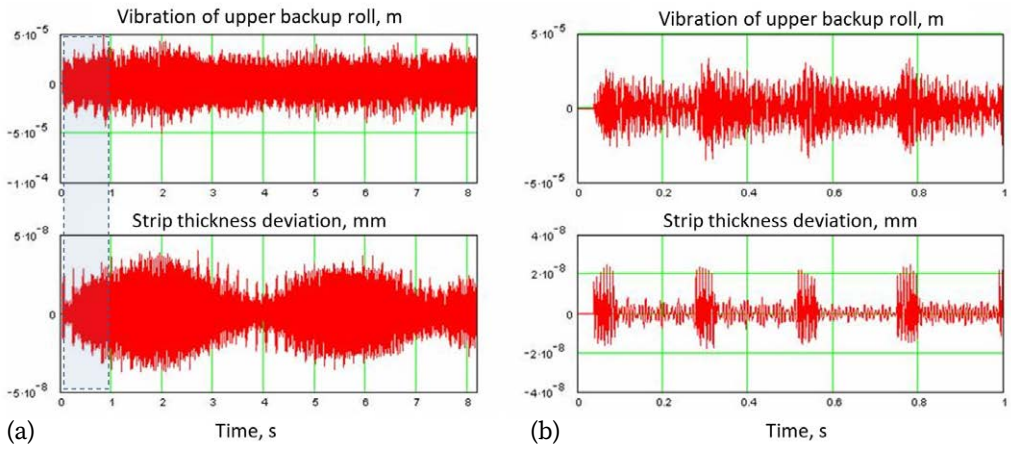

Fig. 4.71. Modelled vibration signals at the mill speed 1200 m/min: (a) low-frequency vibration amplitude modulation; (b) high-frequency strip thickness deviation

vibration modes. WR and its chocks may start to vibrate within the stand housing gap under the random variation of the strip tensions difference ΔT (tension rollers misbalance), rolling load P (rolls eccentricities, strip yield stress) and M (drive torque fluctuations under torsional vibrations).

Tandem mill dynamics simulation. The spring-mass mathematic models of the twin DC motors drivelines (Fig. 4.70a) and 4-high stands (Fig. 4.70b) are developed and analysed with the proper parameters of the investigated tandem mill.

Modelled vibration signal and strip exit thickness variation are shown in Figure 4.71 for different time scales but for the same mill speed of 1200 m/min. The distance between the stands for this mill is 4 750 mm. When the frequent pulse series are superposing, the stand is late to dissipate disturbances and chatter amplitude comes up. During this process, low-frequency vibration beating also appears (Fig. 4.71a).

The stand dissipation coefficient is calculated during the strip breaks when the roll stack oscillates for some time without the strip. In such way, a decrement time of about 0.3 s is obtained. For the mill rolling speed of 1200 m/min (20 m/s), the distance of 4.75 m between stands will be covered in 4.75/20 = 0.2375 s, which is less than 0.3 s. Hence, after a certain speed limit (4.75/0.3 = 15.83 m/s), the last stands rolling hardened metal with low damping ability will not be able to dissipate energy after previous impacts and vibration amplitude will rise. The abnormal roll eccentricity and phase matching of thickness variation impacts (Fig. 4.71b) will increase mill sensitivity to chatter.

The frequency spectrum and envelop line for the strip periodical thickness pulse sequence are shown in Figure 4.72. The parameters of the thickness variation series are as follows:

T_d – pulse series period (backup rolls diameter and stand speed dependent) (4.2 Hz);

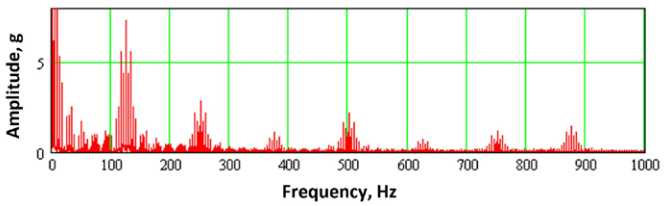

Fig. 4.72. The model spectrum of the upper backup roll vibration

T – period of pulses (main chatter frequency) (125 Hz);

τ – duration of pulse (defects width) (200 Hz);

Δt – sampling rate (spectrum width) (1000 Hz).

Measured chatter vibration spectra for stands 2–5 showed that such a picture is characteristic of every chatter case. There are always 3–5 harmonics during the roll stack resonance at the main frequency (about 120 Hz), which looks similar the one in Figure 4.72.

There are two ways to produce such a spectrum of dynamical system response: linear systems output for pulse sequence input; and nonlinear system response to periodical input. Both situations may have a place in the mill. The first factor already exists in the form of strip thickness variation and depends on previous stand vibrations. To tackle it, the function of high-frequency thickness measurement is designed in the developed vibration monitoring system. The other cause may appear in two cases: rolls slipping in the contact zone and backlashes opening in the stand between the housing and roll chocks. These factors are more available for elimination by the appropriated amount of cooling emulsion supplied and the horizontal position of roll stabilisation by the tension forces.

Horizontal stability of the rolls. The probabilistic approach to chatter vibrations based on WR horizontal instability in the tandem mills has been applied in [391]. A simplified empirical criterion was derived for chatter probability estimation (original notations):

$$\Pi_i = \frac{E \cdot U_{Ci} \cdot e_{\Sigma i}}{h_i \cdot \sigma_{0i} \cdot f_i \cdot F_i}; \tag{4.70}$$

$$\Pi_i / \sum_{i=1}^{n} \Pi_i \geq \frac{1}{n}, \tag{4.71}$$

where Π_i – dimensionless chatter probability factor; i – stand number; E – strip modulus (MPa); $Uc_i = V_1 \alpha / h_0$ – mean deformation rate (s^{-1}); $e_{\Sigma i}$ – summary WR and *BUR* eccentricity (mm); $\sigma_{0i} = \sigma_{\text{init}} + m\,(100(H - h_{i-1})/H)^K$ – yield stress at ith stand entry (MPa); σ_{init}, m and K – initial yield stress before rolling and material hardening constants; H, h_0 and h_i – initial, entry and exit strip thickness (mm); f_i – contact friction factor; F_i – chatter vibration main frequency (Hz, s^{-1}); n – number of stands. Condition (4.71) means chatter increased probability in i^{th} stand if it is more than $1/n$ value (equal for all stands probability). However, *WR* bending force and drive torque have not been used for horizontal forces balance

composition. Therefore, new formula is proposed for steady state condition (for one *WR*):

$$0 < \frac{a \cdot P}{R_{BUR} + R_{WR}} + F \cdot K_f - \frac{\Delta T}{2} - \frac{M \cdot i \cdot \eta}{R_{WR}}, \tag{4.72}$$

where P – rolling load; a – *WR* chocks displacement; R_{BUR} and R_{WR} – *BUR* and *WR* radiuses; F and K_f – summary bending force and friction factor in the *WR* chocks and piston contacts; $\Delta T = T_0 - T_1$ – strip entry and exit tensions difference ($T_0 > T_1$ is assumed); M – drive torque; i and η – drivetrain gears ratio and efficiency (0.8–0.9). *WR* bending forces and reactions from drive torque at the *WR* chocks were taken into account. Every component in equation (4.72) may be used for comparison with the others. In practice, a half-difference of the strip tensions is used as a most scattering parameter:

$$\frac{\Delta T}{2} \cdot k < \frac{a \cdot P}{R_{BUR} + R_{WR}} + F \cdot K_f - \frac{M \cdot i \cdot \eta}{R_{WR}}, \tag{4.73}$$

where $k = 1 + S_{dev}$, S_{dev} – standard deviation obtained from measurements.

Simulation of chatter regeneration effect in the tandem mill. The resonance related to the coincidence of phases of material waviness in the subsequent rotations in the cutting machine is a well-known effect, called "regenerative chatter". A similar phenomenon occurs in the tandem cold rolling mills when the waviness of the moving strip is induced by the vertical vibration in the previous stand and then transported to the next stands (Fig. 4.73a).

Synchronization phenomenon is the basic physical phenomenon, which happens in several mechanical oscillators (stands) interacting by the elastic connecting link (strip). It has been less investigated so far in comparison to other factors of chatter such as strip thickness, width, chatter marks on the rolls after their grinding, and roll bending.

The main mode frequency may vary from 90 to 150 Hz for different mills. However, for the considered tandem mill, all stands have very close frequencies of the main mode of vertical vibrations (118–120 Hz). Simulations showed that the three last stands (Nos. 3–5) are always synchronised (Fig. 4.73b) when chatter is amplified. Due to the results obtained on the developed dynamical model, it was possible to formulate ideas about possible remedies against the chatter vibrations, which subsequently were realised in the mill monitoring system [398].

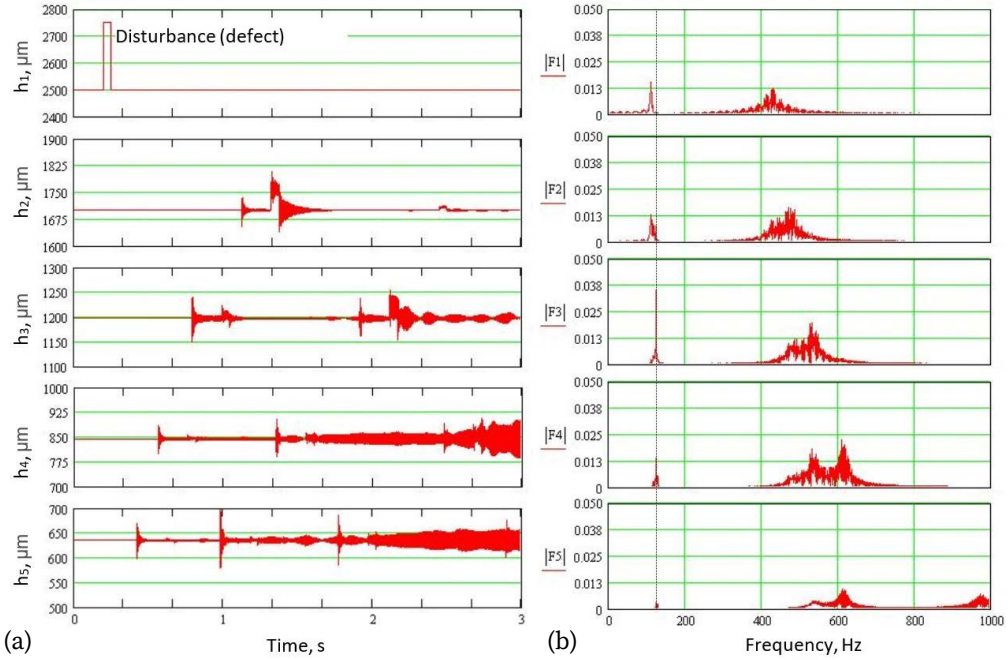

Fig. 4.73. Regenerative chatter by strip thickness
and subsequent stands synchronisation in the tandem mill:
(a) time-series of strip thickness; (b) spectra of vibration

4.4.4. Multi-motor gear drive of slabbing mill

A real case study of abrupt failures in a new multi-motor gear drive of vertical rolls is investigated in the heavy slabbing mill. Modal analysis is conducted and the lowest torsional vibration modes are verified by the data from an industrial plant. Conditions of parametric resonances due to variable stiffness of teeth are determined within the range of working speed. The branched gear drive is investigated by the nonlinear dynamical model with backlashes. It is shown that instantaneous dynamic loads in the driveline are strongly dependent on the difference in gap sizes and phase shifts between two intermediate gears in the output gear wheel coupling. Deviation in electrical parameters is considered the additional cause of not equal load sharing of parallel motors. The conducted research allowed the prevention of further gearbox failures and optimization of mill control [399].

The multi-motor, split path power or so-called summation drives are used in large-scale machines and rotating aggregates when the technological capabilities of equipment manufacturers limit the dimensions of gearboxes of traditional design. The use of a multi-motor drive allows, depending on the specific circuit, the reduction in the power of individual electric drives and the total cost of the unit several times. Deep separation of power flows is considered rational, i.e., their summation at the last stage, where the loads are maximal. An additional advantage of multi-motor drives is a reduction in the inertia of every drive, which is important for precise control of industrial machines.

In addition to the positive features of multi-motor gear drives, there are some design and operational problems. They concern the need to eliminate static uncertainty, ensure equal angular gaps, optimal selection of the number of flows and joint control schemes for electric drives, which not only equalize static loads but also suppress out-of-phase oscillations of branches due to the inaccurate gears (run-out, eccentricity, transmission errors).

The presence of opened gaps in the kinematic pairs of any rotating machines significantly affects the overall response to external loads, e.g., in mining excavators with multi-motor drives. The increased dynamics in the gear drives of heavy hot rolling mills occur due to specific technological loads when a pair of driven rolls capture metal in harsh operating conditions with increased wear and backlashes in split path drivelines. Especially significant is the effect of backlashes opening when asymmetry exists in parameters of parallel working electric drives of the machine, which is operated under reversing regimes with stepwise or impulsive loads. In rolling mills, the high torsional loads do not allow the use of planetary gears for roll driving. To increase the power of some steel processing aggregates, e.g., strip coilers in cold rolling mills, 2–3 motors are axially connected with short intermediate shafts and no problems have been reported on their synchronous working.

In addition to the abovementioned reasons, there are internal factors of dynamics that are often not accounted for when gearboxes are designed as a partial subsystem of a whole driveline. One of these factors is a periodic change in teeth stiffness, which plays its role even under constant speed and load. This disturbance may cause parametric resonances, which are not possible to suppress by linear damping and lead to severe torsional vibrations comparable by amplitude to the static technological torques within certain ranges of speed.

The described further research is initiated by the accident with critical failures of gears in a modernized gear drive of the heavy slabbing mill. The single-motor

drive system that worked for many years (Fig. 4.74a) was replaced with the new multi-motor drive system (MMDS) to add power and increase overall plant productivity. Vertical rolls are driven by two-stage spur gear MMDS, which consists of branched first stages with direct current (DC) and four motors (Fig. 4.74b). These electric motors have an independent excitation scheme with pairwise parallel speed control for each vertical roll. Horizontal rolls of the second stand of the slabbing mill are directly driven by two DC motors via spindles without a gearbox.

Right after the new gearbox commissioning, an increased level of vibrations was observed, which finally resulted in dramatic failure and long-time downtime of the slabbing mill. After gearbox repair and replacement of main gears, vibration continued to be at a high level and the customer decided to investigate the cause of such unexpected behaviour. Internal dynamical processes were suspected as a reason for early failures because static load limits for this gearbox were not exceeded during several months of mill operation.

Following these approaches, in-depth analysis and mathematical simulation of dynamical processes in the multi-motor gear drive of the heavy slabbing mill are represented. Special emphasis is placed on the investigation of parametric excitation in spur gears and the influence of gears' phasing on out-of-phase torsional oscillations in the MMDS. Interactions between vertical and horizontal stands and deviation of electric motor parameters are emulated in the developed nonlinear dynamical model.

Dynamical model of the gear driveline. According to traditional approaches and methods of dynamic processes simulation in rolling mills, the driveline system of the stand is usually represented by the calculation scheme with a small number of lumped masses (from 2 to 4) and constant stiffness of elastic connections between them, taking into account backlashes as bilinear nonlinearities. This approach is quite correct, since peak values of load torques usually appear during the first period of oscillations (10–20 Hz) in the range of lowest modes of torsional oscillations, and the highest modes are decaying during this time. However, with parametric perturbation, higher modes can be sustained and amplified when natural frequency matches with the periodic parameter changes or their harmonics. Therefore, the mathematical model of a slabbing mill includes the inertia of two motors, all gears and roll with the added mass of the ingot. The backlashes and variable stiffness of the gears are taken into account in numerical simulation. Two independent symmetrical parts of each roll gear drives are combined into the whole gearbox housing, hence, only one part of the gearbox

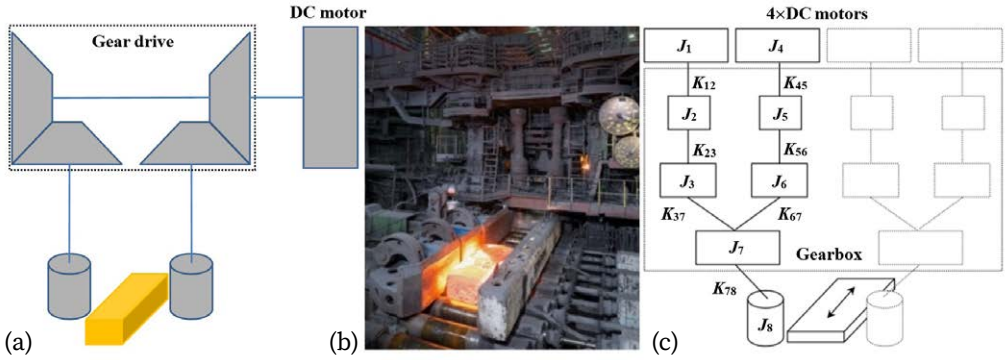

Fig. 4.74. Gear drive of vertical rolls in a slabbing mill:
(a) previous single motor drive; (b) new multi-motor gear drive;
(c) calculation scheme of one half of gearbox

Table 4.15. Parameters of calculation scheme

Parameter	Description	Value	Units
J_1, J_4	Inertia of one electric motor	7000	kg m^2
J_2, J_5	Inertia of one input gear	2100	kg m^2
J_3, J_6	Inertia of one intermediate gear	1700	kg m^2
J_7	Inertia of one output wheel	5200	kg m^2
J_8	Inertia of one roll	1830	kg m^2
K_{12}, K_{45}	Stiffness of one motor shaft	15.7×10^8	N m/rad
K_{23}, K_{56}	Stiffness of one gear at stage I	32.7×10^8	N m/rad
K_{37}, K_{67}	Stiffness of one gear at stage II	13.8×10^8	N m/rad
K_{78}	Stiffness of one spindle	0.61×10^8	N m/rad

is considered (Fig. 4.74c). The designations and numerical values of the model parameters are shown in Table 4.15.

All parameters are reduced to the roll rotation speed. The spindle has the lowest stiffness and the first stage of the gearbox has the highest stiffness. The inertia of the roll is 3 times lower than the one of the gear wheel and 3.5 times lower than the moment of inertia of the motor. In such systems when an instantaneous load is applied to the terminal mass (roll) with low inertia, significant oscillations of

torques may occur. Based on the calculation scheme, the system of differential equations is as follows:

$$\begin{cases} J_1\ddot{\varphi}_1 + C_1\dot{\varphi}_1 + M_{12} = M_1 \\ J_2\ddot{\varphi}_2 + C_2\dot{\varphi}_2 - M_{12} + M_{23} = 0 \\ J_3\ddot{\varphi}_3 + C_3\dot{\varphi}_3 - M_{23} + M_{37} = 0 \\ J_4\ddot{\varphi}_4 + C_4\dot{\varphi}_4 + M_{45} = M_4 \\ J_5\ddot{\varphi}_5 + C_5\dot{\varphi}_5 - M_{45} + M_{56} = 0 \\ J_6\ddot{\varphi}_6 + C_6\dot{\varphi}_6 - M_{56} + M_{67} = 0 \\ J_7\ddot{\varphi}_7 + C_7\dot{\varphi}_7 - M_{37} - M_{67} + M_{78} = 0 \\ J_8\ddot{\varphi}_8 + C_8\dot{\varphi}_8 - M_{78} = - M_8 \end{cases} \quad (4.74)$$

where φ_i – angle of inertial masses rotation (rad); J_i – rotating inertia (kg m^2); C_i – equivalent damping coefficients (N m s/rad); $M_{ij} = K_{ij}(\varphi_j - \varphi_i)$ – elastic torques (N m); M_1, M_4 – driving torques of two motors (N m); M_8 – technological load applied to one roll, equal to half of total rolling torque (N m).

Modal analysis of the driveline. Modal analysis is conducted to understand drive dynamics. The natural frequencies of one roll driveline are represented in Table 4.16. The dynamical model is verified by the recordings of electric motors' currents. The lowest natural modes are identified, the first is near the frequency ≈ 29 Hz and the second ≈ 41 Hz (Fig. 4.75).

This coincidence is accurate enough, taking into account some decrease in damped oscillations frequency. It is not possible to identify the highest natural modes using the electric drives' signals because of 100 Hz sampling frequency

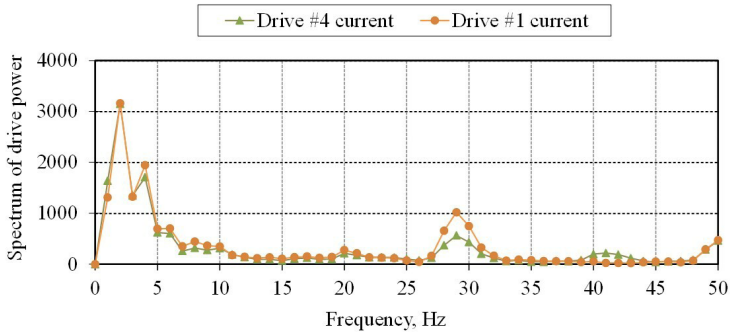

Fig. 4.75. The spectrum of electric motors power

Table 4.16. Natural modes of torsional oscillations

Natural frequencies	ω_1	ω_2	ω_3	ω_4	ω_5	ω_6	ω_7
[rad/s]	**186**	**270**	**545**	**954**	**1078**	**2069**	**2085**
[Hz]	**30**	**43**	**87**	**152**	**172**	**329**	**332**
J_1	–0.079	–0.543	0.363	–0.156	–0.118	0.024	–0.024
J_2	–0.067	–0.367	–0.118	0.475	0.495	–0.443	0.433
J_3	–0.060	–0.265	–0.326	0.500	0.420	0.551	–0.556
J_4	–0.079	0.543	0.363	0.156	–0.118	–0.024	–0.024
J_5	–0.067	0.367	–0.118	–0.475	0.495	0.443	0.433
J_6	–0.060	0.265	–0.326	–0.500	0.420	–0.551	–0.556
J_7	–0.040	0.001	–0.700	0.001	–0.360	–0.001	0.078
J_8	0.985	0.001	0.088	0.001	0.011	0.001	–0.001

limit in mill control. Some deviation of real frequencies can be as well due to a joined mass of rolled ingot coupled by contact friction with roll inertia J_8 in the deformation zone.

Three even natural modes ω_2, ω_4, ω_6 (43, 152, 329 Hz) correspond to torsional vibrations of separated branches, while four odd modes ω_1, ω_3, ω_5, ω_7 (30, 87, 172, 332 Hz) correspond to symmetrical oscillations of parallel branches in the gear drive (Fig. 4.74, Table 4.16).

The first mode (30 Hz) has a node, i.e. the point around which neighbouring inertias oscillate, in the spindle shaft. In this case, the masses J_1–J_7 oscillate out-of-phase with the roll's mass J_8 and gaps opening in the spindle may produce higher input loads on gears in the case of non-equal load sharing between vertical drives or non-synchronous speed with horizontal stand. In the wide strip hot rolling mills, this node is located, as a rule, on the shaft between the motor and the gearbox.

The second mode (43 Hz) corresponds to out-of-phase oscillations of one branch J_1–J_3 against other parts of drive J_4–J_6 together with output gear wheel J_7 and roll J_8. This mode may cause gaps opening in stage II of the gearbox and additional cyclic loading on the gear couplings.

The third mode (87 Hz) corresponds to out-of-phase oscillations of motors J_1, J_4, against gears in the first branch J_2, J_3, second branch with output wheel J_5, J_6, J_7 and roll J_8.

The highest modes (152, 172, 329, 332 Hz) show different combinations of phases with the opposite motion of separate pairs of gears as a whole body or output gear wheel against them. These modes are dangerous from the viewpoint of gear gap opening and teeth shock loading, but their influence depends on damping factors in the torsional system.

The most generalized natural modes of this drive system are possible when two separate parts of the gearbox with two motors oscillate against each other (7.6 Hz) or in-phase (24.6 Hz) against the inertia of rolls with ingot. These modes coincide by phase with the first mode for separate parts of the gearbox (30 Hz) and therefore only one part of gearbox is considered in the calculation scheme.

The opened angular gaps in the spindles have a significant impact on the dynamic loads in all sections of the driveline – from the spindle up to the motor shaft. However, when the operator reverses the mill and rolls capture the slab, drives usually are accelerated, gaps are kept closed by the inertial torque of the roll, and the dynamics in the driveline are not as high as could be when the mill is decelerated. Nevertheless, the proximity of several pairs of natural frequencies (ratio $\omega_2/\omega_1 = 1.43$, $\omega_5/\omega_4 = 1.13$, $\omega_7/\omega_6 = 1.01$) indicates that this driveline is prone to beat of elastic torques resulting in torque amplification not only when metal is being captured by rolls, but also in the steady rolling mode.

Parametric excitation in the gear meshing. To keep the gear ratio constant at each moment, the next pair of teeth must contact each other by the time the previous pair of teeth leave the contact. The duration of the contact, depending on the teeth number of the meshing gears, is characterized by the overlap contact ratio:

$$\varepsilon_\alpha = \frac{\sqrt{r_{a1}^2 - r_{b1}^2} + \sqrt{r_{a2}^2 - r_{b2}^2} - a\sin\alpha}{\pi m \cos\alpha} \tag{4.75}$$

where α – pressure angle; a – centre distance; m – gear module; r_a, r_b – outside and base radiuses of a pinion (1) and wheel (2) gears. Usually in large-scale gearboxes $1 < \varepsilon_\alpha < 2$. Values of $\varepsilon_\alpha < 1$ are not desirable as there is no two-pair engagement. With ε_α increasing from 1 to 2, the duration of one-pair engagement is shortened, and with $\varepsilon_\alpha = 2$, three-pair contact overlap appears in gears. For spur gears with $1 < \varepsilon_\alpha < 2$, the stiffness change is significant for dynamic simulations. With the number of teeth of the slabbing mill gear drive: $z_1/z_2 = 53/81$ – stage I and $z_3/z_4 = 51/125$ – stage II, the contact ratios are $\varepsilon_\alpha = 1.78–1.79$, therefore, one-pair and two-pair engagements are possible.

At a maximal rolling speed of 3 m/s, the peripheral speeds in the gears: stage I – 13 m/s, stage II – 10 m/s. For the 7th class of gearbox manufacturing precision, taking into account the hardness of the teeth about 4252 HRC, the coefficient of gears meshing dynamics is 1.17–1.22 by the recommendations of ISO 6336 that corresponds to values of excitation $\mu \approx 0.17–0.22$. This coefficient accounts for non-load and under-load transmission errors.

According to experimental data from similar heavy rolling mills and other machines with gear transmissions, the damping of the system is about $\zeta = 0.02…0.15$ (assumed as an average for natural modes). Hence, in the gearbox of the slabbing mill, the stiffness pulsation $\mu = 0.17–0.22$ can exceed the critical value, at least for the first-order resonance ($n_\omega = 1$), i.e., when the natural frequency is equal to half of the excitation frequency ($\omega_0 = \omega_1/2$).

Intermediate gears phasing. The analysis of the geometry of the gearbox helped identify its features concerning the use of a multi-motor scheme. The source of periodic disturbances is not the synchronization of the teeth of each pair of intermediate gears with the gear wheel because the angle between the axes of their centres is 60.2° (Fig. 4.76).

In this sector, there is no integer number of gear teeth $n_z = 60.2°/2.88° = 20.903$, where 2.88 is the angular pitch of the teeth of the output wheel of the gearbox. Therefore, in the process of rotation, periodic perturbations occur with teeth meshing frequency from one branch intermediate gear (K_{37}), then from the other (K_{67}) with a constant phase shift between them: $\varphi_z = 0.903 \times 2.88° \times \pi/180° = 0.0454$ rad.

Given the phase shift, the formula for the variable stiffness of the gear coupling is:

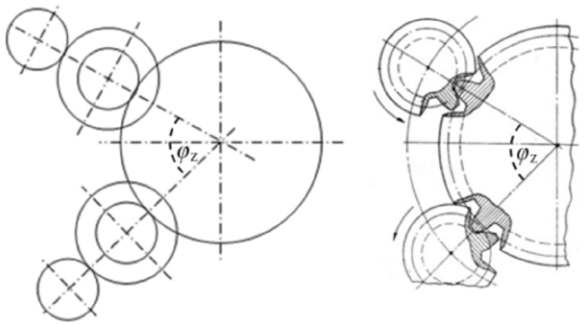

Fig. 4.76. Schematic angular phasing of intermediate gears on the output gear wheel

$$K_{ij}\left(t,\omega_z\right)=K_0\left[1+\Delta K\cdot\text{sign}\left(\sin(\omega_z t+\varphi_z)\right)\right] \tag{4.76}$$

where K_0 – nominal gear stiffness; $\Delta K = 0.17–0.22$ – change in teeth stiffness without regard to wear; $\omega_z = z_w\,\omega_w$ – gear meshing frequency; z_w – number of teeth; ω_w – the variable angular speed of the corresponding shaft.

Transitional parametric resonances. After mill reversing and during acceleration to the maximal rolling speed of 3 m/s, the driveline passes through five ranges V_1–V_5 of parametric excitation shown in Figure 4.77.

For the first-order resonances ($\omega_0 = \omega_1/2$), gear meshing frequencies are given as half values: gear (I)/2 and gear (II)/2. Mean values of resonant ranges of rolling speed are as follows (m/s):

$$\begin{aligned}
V_1 &= 2r_1\Big/\left(i_{12}z_p\right)=0.66\\
V_2 &= 2r_1/z_w=1.04\\
V_3 &= 2r_2\Big/\left(i_{12}z_p\right)=0.95\\
V_4 &= 2r_2/z_w=1.51\\
V_5 &= 2r_3\Big/\left(i_{12}z_p\right)=1.92\\
V_6 &= 2r_3/z_w=3.05
\end{aligned} \tag{4.77}$$

where ω_1, ω_2, ω_3 – natural frequencies; r – rolls radius; z_p, z_w – input pinion and output wheel gear teeth number; i_{12} – total gearbox ratio (1.528 × 2.451 = 3.746). Values V_2 and V_3 are very close and a higher level of excitation is expected in the range 0.95...1.04 m/s of mill speed.

Under the terms of the electric drive manufacturer, the difference in motor parameters is allowed within 5%. After the repair or change of any motor, the mill maintenance staff has to adjust the magnetic flux of each of the four motors in idle mode. They change shunt resistances and currents in the excitation windings to reduce the effect of variation in the magnetic and electrical parameters. They aim to equalize the idle armature current of each of the four motors. The developed computer model allows the investigation of the influence of deviation in parameters (K_e, K_m – electrical and mechanical constants of the motor) on the dynamics of the mechanical system of the driveline.

Steel ingots are processed within 10–13 reversal passes. After the first pass, due to ingot elongation, two stands of the slabbing mill (horizontal and vertical) begin to work in the continuous regime when they are connected via the

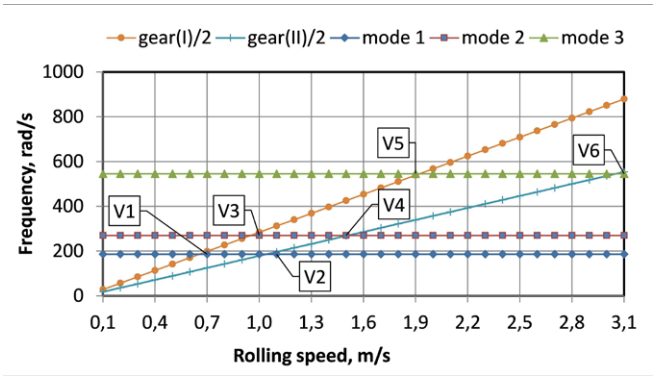

Fig. 4.77. Resonance ranges of rolling speed

rolled ingot with high axial stiffness. In this case, rolling torque M_8 in the vertical stand will also greatly depend on the roll's linear speed synchronization with the horizontal stand. To reduce this component of loading, the mill control system provides, individually for every pass, a limit on the speed and its synchronization in neighbouring stands. Limiting drive speed restrains the stick-slip slab motion in the rolls, which is the most dangerous regime of the load causing severe damage.

Model simulations. In each series of passes of ingot processing, average rolling torque changes due to different ingot sizes, metal temperature and reduc-

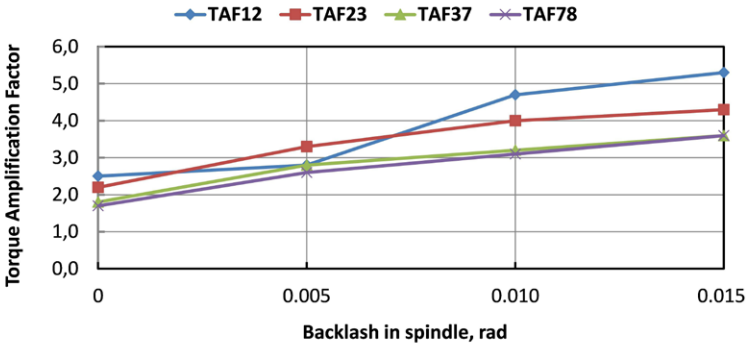

Fig. 4.78. Torque Amplification Factors (TAF) in different sections of the driveline: TAF_{12} – motor shaft; TAF_{23} – stage I of the gearbox; TAF_{37} – stage II of the gearbox; TAF_{78} – spindle

Table 4.17. TAF for different backlashes Δ [rad] and gaps opening states $K_\Delta = 0...1$

No.	Conditions of loading and backlashes gaps opening	Motor shafts K_{12}, K_{45}	Stage I K_{23}, K_{56}	Stage II K_{37}, K_{67}	Spindle K_{78}
1	Gearbox no gaps for both parts $\Delta_{12} = \Delta_{23} = \Delta_{37} = 0$; $K_{\Delta 12} = K_{\Delta 23} = K_{\Delta 37} = 1$; $\Delta_{45} = \Delta_{56} = \Delta_{67} = 0$; $K_{\Delta 45} = K_{\Delta 56} = K_{\Delta 67} = 1$; Spindle no gap: $K_{\Delta 78} = 1$; $\Delta_{78} = 0$; $\nu = 3$	2.30	1.70	1.47	1.30
2	Spindle gap opened $K_{\Delta 78} = 0$; $\Delta_{78} = 0.015$; $\nu = 3$	5.33	4.33	3.62	3.57
3	$K_{\Delta 78} = 0$; $\Delta_{78} = 0.010$; $\nu = 3$	4.67	4.00	3.19	3.13
4	$K_{\Delta 78} = 0$; $\Delta_{78} = 0.005$; $\nu = 3$	3.83	3.33	2.77	2.61
5	$K_{\Delta 78} = 0$; $\Delta_{78} = 0.005$; $\nu = 2$	4.04	3.39	2.88	2.64
6	$K_{\Delta 78} = 0$; $\Delta_{78} = 0.005$; $\nu = 1$	4.04	3.39	2.88	2.67
7	Spindle gap half-opened: $K_{\Delta 78} = 0.5$; $\Delta_{78} = 0.005$; ν=3	3.40	2.83	2.43	2.24
8	Spindle gap closed: $K_{\Delta 78} = 1.0$; $\Delta_{78} = 0.005$; $\nu = 3$	2.50	2.20	1.85	1.70
9	Gearbox gaps are half-opened for both parts $\Delta_{12} = \Delta_{23} = \Delta_{37} = 0.001$; $K_{\Delta 12} = K_{\Delta 23} = K_{\Delta 37} = 0.5$; $\Delta_{45} = \Delta_{56} = \Delta_{67} = 0.001$; $K_{\Delta 45} = K_{\Delta 56} = K_{\Delta 67} = 0.5$; Spindle gap half-opened: $K_{\Delta 78} = 0.5$; $\Delta_{78} = 0.005$; $\nu = 3$	4.17	6.00	5.32	2.13
10	Gearbox gaps are all half-opened for both parts $\Delta_{12} = \Delta_{23} = \Delta_{37} = 0.0001$; $K_{\Delta 12} = K_{\Delta 23} = K_{\Delta 37} = 0.5$; $\Delta_{45} = \Delta_{56} = \Delta_{67} = 0.0001$; $K_{\Delta 45} = K_{\Delta 56} = K_{\Delta 67} = 0.5$; Spindle gap half-opened: $K_{\Delta 78} = 0.5$; $\Delta_{78} = 0.005$; $\nu = 3$	3.67	3.67	2.98	2.22
11	Gearbox gaps in stage I equal for both parts $\Delta_{12} = \Delta_{37} = 0$; $\Delta_{23} = 0.001$; $K_{\Delta 12} = K_{\Delta 37} = 1$; $K_{\Delta 23} = 0.5$; $\Delta_{45} = \Delta_{67} = 0$; $\Delta_{56} = 0.001$; $K_{\Delta 45} = K_{\Delta 67} = 1$; $K_{\Delta 56} = 0.5$; Spindle gap closed: $K_{\Delta 78} = 1$; $\Delta_{78} = 0$; $\nu = 3$	3.00	4.00	2.98	1.65
12	Gearbox gaps in stage II equal for both parts $\Delta_{12} = \Delta_{23} = 0$; $\Delta_{37} = 0.001$; $K_{\Delta 12} = K_{\Delta 23} = 1$; $K_{\Delta 37} = 0.5$; $\Delta_{45} = \Delta_{56} = 0$; $\Delta_{67} = 0.001$; $K_{\Delta 45} = K_{\Delta 56} = 1$; $K_{\Delta 67} = 0.5$; Spindle gap closed: $K_{\Delta 78} = 1$; $\Delta_{78} = 0$; $\nu = 3$	3.10	3.67	4.26	1.65
13	Gearbox gaps different for both parts $\Delta_{12} = \Delta_{23} = \Delta_{37} = 0.001$; $K_{\Delta 12} = K_{\Delta 23} = K_{\Delta 37} = 0.5$; $\Delta_{45} = \Delta_{56} = \Delta_{67} = 0.002$; $K_{\Delta 45} = K_{\Delta 56} = K_{\Delta 67} = 0.5$; Spindle gap closed: $K_{\Delta 78} = 1$; $\Delta_{78} = 0$; $\nu = 3$	3.33 3.33	5.67 2.67	5.32 5.11	1.60 1.65

tions assigned by an operator following a technological schedule. The time of load ramp rising is changing from the first to the last passes due to slab section reduction and its front edge elongation. In simulations, the worst case of the load is assumed with instantaneous stepwise torque rising.

The peak values of torsional loads are characterized by the Torque Amplification Factors (*TAF*) for different sections in the driveline (motor shafts, gears in two stages and spindle), which are calculated $TAF_{ij} = M_{\max ij} / M_8$, where $M_{\max ij}$ – peak elastic toque in couplings; M_8 – static technological torque, applied to roll. Maximum rolling speed $v = 3$ m/s is assumed. The dependence of TAFs on spindle backlash, which constitutes 70% of the total gap is represented in Figure 4.78.

Technological torque on the roll is calculated depending on the metal section and reduction in stands for every pass. The dynamical component of loads, because of the two stands' interaction with a mismatch of their speeds, is emulated by the additional torque applied to the roll. The results of the simulation are represented in Table 4.17.

Under frequent technological reversals of the slabbing mill, the difference in dynamical loads is greater when the wear of gears in the branches of the gearbox is more uneven. In this regard, it is necessary during the repairs to choose a pair of gears with the smallest difference in the wear of the teeth or replace them both. Rolling speed has an insignificant effect on dynamics. The indexes (*i*, *j*) of the backlashes Δ, opening states K_Δ and parameters of dynamics *TAF*, *M*, *F* correspond to the notations given in Figure 4.74c.

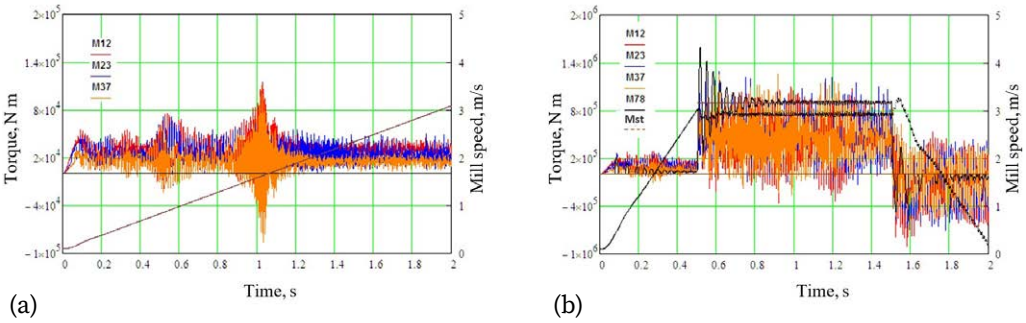

Fig. 4.79. Transient torques in the driveline under different conditions:
(a) idle mode ($v = 0...3$ m/s, $\mu = 0.2$, $\Delta_{ij} = 0$);
(b) under load ($v = 0...3$ m/s, $\mu = 0.2$, $\Delta_{78} = 0.015$)

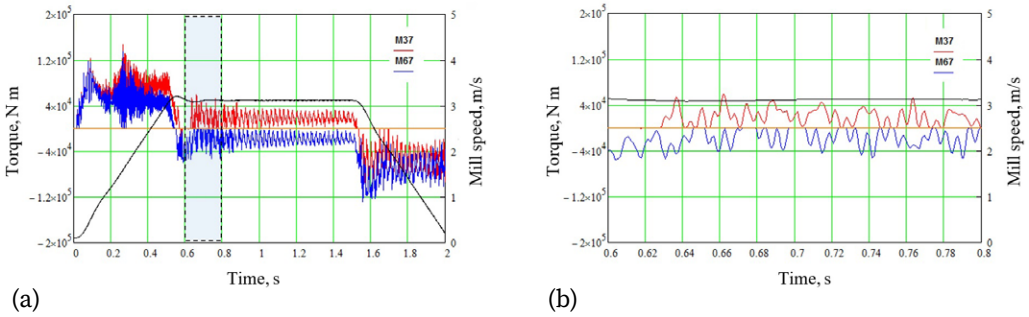

Fig. 4.80. Dynamical torques in parallel branches of the driveline under deviation of electrical constant of one motor: $v = 0...3$ m/s, $\mu = 0.1$, $\Delta_{37} = \Delta_{67} = 0.0001$ rad, $\Delta K_e = 0.5\%$

In the time domain, the results of the model simulation are shown in Figure 4.79, there are elastic torques in the gearbox during mill speed changing in idle mode and under stepwise load 900 kN m. Backlash in the spindle is assigned to its maximal value of 0.015 rad.

In idle mode, the passage through the resonant zones is accompanied by an increase in the amplitude of out-of-phase oscillations in the gears of the parallel branches of the gearbox. Torque crossing through the zero level causes gaps opening in the gears and back shocks of teeth. There are practically no fluctuations of torques in the spindle from gear meshing.

Under the load, torque amplification factors during the transient process are not very high ($TAF_{ij} = 2.0...2.1$), which corresponds to other studies of this mill. This is due to gaps closing during mill acceleration. Unlike this, *TAF* values in Table 4.17 are much greater because gaps are intentionally assigned opened ($K_{\Delta ij} < 1$) to show potentially maximum dynamic loads that can occur if the slab enters at stable speed or during mill deceleration.

The largest amplitudes of parametrically excited oscillations are observed in the couplings of the output wheel of stage II at a mill speed of about V_2–V_3 = 0.9–1.0 m/s and $V_4 = 1.5$ m/s. Other ranges V_1, V_5, V_6 do not show significant excitation.

Simulation of the meshing phase shift $\varphi_z = 0.0454$ rad between two intermediate gears showed that this factor alone plays a minor role if no backlashes are introduced in the model. However, non-synchronous meshing starts to play its role

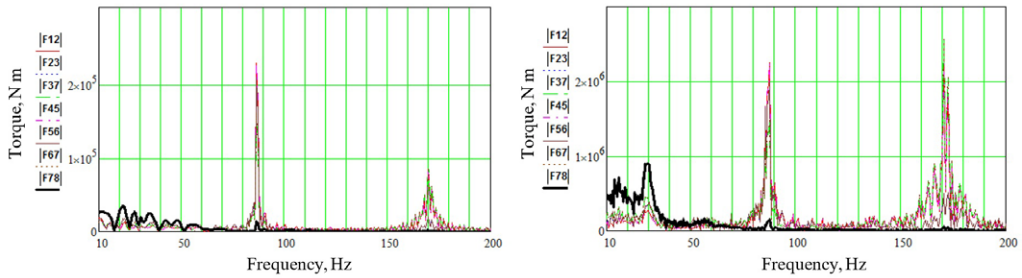

Fig. 4.81. Spectra of dynamical torques in the different sections of the driveline:
(a) idle mode ($v = 0...3$ m/s, $\mu = 0.1$, $\Delta_{ij} = 0$);
(b) under load ($v = 0...3$ m/s, $\mu = 0.2$, $\Delta_{78} = 0.015$)

when gaps are opened similar to the case when the motors' electrical parameters are different. Simulation of small ($\Delta K_e = 0.5\%$) electrical constant difference in one of the motors is represented in Figure 4.80. This leads to static load deviation and gaps opening with subsequent out-of-phase oscillations in both branches of the gearbox. Therefore, the MMDS requires quite accurate parameter tuning to equalize static loads. With a serial connection of two motors, the static load is better shared, but the dynamic load is not damped. In the frequency domain, parallel branches have similar responses.

Spectra of dynamical torques are shown in Figure 4.81. In idle regimes, electric motors demonstrate insignificant response at natural frequencies. The spindle shaft (F_{78}) shows mainly low frequency (30 Hz) as predicted by modal analysis. All other sections: motor shafts (F_{12}, F_{45}), stage I (F_{23}, F_{56}) and stage II (F_{37}, F_{67}) of the gearbox responded at higher modes of vibration (87, 172 Hz). The two highest modes of vibration (329, 332 Hz) are very close in terms of frequency, however, they are not excited in the driveline. Natural modes at 43 and 152 Hz are also not visible in the spectra.

The results obtained on a slabbing mill are consistent with the effects reported on the MMDS of open-pit mines excavators and tilting mechanism in steel converters having spur gear couplings, i.e., the possibility of parametric oscillations. The difference in gaps of the parallel gearbox branches increases their influence on torsional dynamics compared with symmetrical distribution even for smaller values. The non-synchronous meshing of intermediate gears causes

out-of-phase oscillations in branches. The same effect has electrical parameters deviation in the two DC drives. The results of this study clarified the reasons for early gearbox failures but also made it possible to improve the operation of industrial machines.

5. DEVELOPMENT OF INSTRUMENTATION FOR CONDITION MONITORING

The instrumentation has been developed for torsional load monitoring and backlashes diagnostics in the drivelines of heavy machinery. The given devices were tested in real harsh conditions of industrial plants and showed their reliability and acceptable metrological parameters.

5.1. Digital wireless torque meter

Condition monitoring and diagnostics of minerals mining machines is a challenging task for operating companies and their maintenance staff. Conventional approaches based on measurements of vibration, temperature and other parameters are still not widely implemented in the mining industry due to non-stationary loading conditions. Registration of overloading and resonance modes by the electrical motor current is not sufficient in the case of heavy mobile vehicles or stationary mining machines having multibody structures. Telemetric torque measurement tools installed in the drivetrains of mining machines can account for the variation of loads and give valuable information on damages in geared transmissions.

In work [400], the developed digital telemetry torque meter based on strain gauges is represented. The focus is on the functionality required for industrial applicability and issues in the course of machines' operation and maintenance. The additional features the torque meters can use in mining machines diagnostics are considered. The design solutions of the developed torque meter account for all operational issues and requirements for its use in the harsh conditions of the mining and metallurgical industry: high electro-magnetic noise; high temperature and humidity; mechanical damages; oil, water and metallic dust; power supply on the shaft; wide range of rotation speed for different machines. A block diagram of the digital torque meter is shown in Figure 5.1.

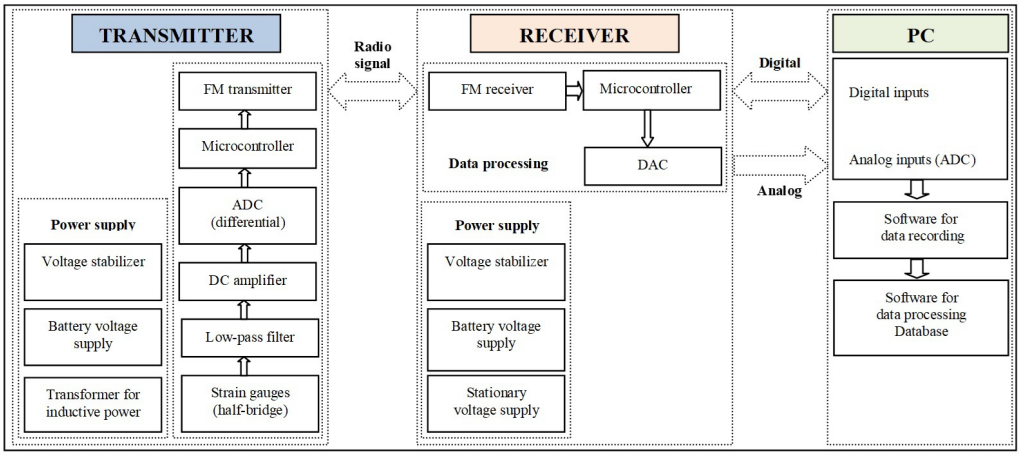

Fig. 5.1. Block diagram of a digital wireless torque meter

The telemetric channel includes strain gauges (half-bridge), a low-pass filter, a DC amplifier, a 12-bit ADC and DAC, an 8-bit microcontroller, two digital FM transceivers, a computer with an ADC board and input ports for recording digital measurement data. The carrier frequency of data transmission via the radio channel is 433.92 MHz and is fulfilled in a digital code by frequency-modulated signals, which offers a sufficient range of data transferring up to 20 m. This favourably distinguishes the developed scheme from similar systems with a carrier frequency of 100–600 kHz, which requires the installation of receivers at a distance of 10–30 mm from the shaft. The data exchange protocol between the circuit elements is performed in the Manchester code, which has a high noise immunity.

The sensor circuits (Fig. 5.2) use components from reliable producers (transceivers, microcontrollers, ADC and DAC, amplifiers, stabilised voltage sources), which are widely available in the electronic market for convenient replacement in the case of sensor damages.

Data transmission from the receiver to the recording unit (PC) can be performed both as an analogue signal after a digital-analogue conversion and in a digital code. The ADC board used in the PC incorporates 8 digital inputs and outputs and enables the generation of control signals or the change of the torque meter settings remotely. In a stationary monitoring system, for data transmission over a long line, the standard RS485 protocol should be implemented.

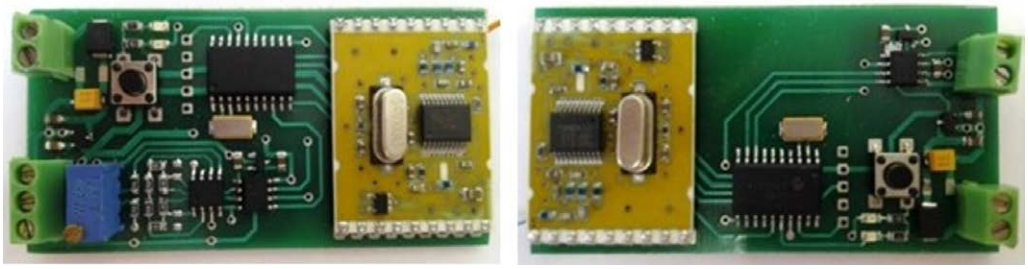

(a) (b)

Fig. 5.2. Telemetry torsional loads monitoring system: (a) transmitter; (b) receiver

The permissible temperature range of the system circuits operation is an important factor in the reliability and accuracy of the measuring since it causes a signal drift and, at sufficiently high temperatures, a failure of electronic components. The temperature range of most of the used circuit components is +85°C and the permissible temperature range of the transceiver chip is +70°C. That is why the torque meter can be used in hot conditions. It should be noted that when the shaft rotates, the transmitter is cooled by the airflow. To isolate the transmitter from heating, a sealed polymeric case and a heat-insulating gasket between the shaft and the mount are used. In addition, algorithmic temperature compensation can be provided depending on working conditions.

The structural design of the torque meter concerns the following units:

- transmitter housing and the location of the transmitting antenna;
- shaft mounting of the transmitter housing with a power supply;
- housing of the receiver and its location close to the receiver.

The design of the system and fastening clamps should protect against mechanical damage during machine operation and repairs, as well as oil, water and metallized dust. The design determines the reliability of the torque meter, and the cost of its operation, taking into account the time spent on equipment downtime and the cost of the failed modules.

The high carrier frequency (short wavelength) of the transceiver allows antennas to be placed inside a sealed plastic housing, which greatly simplifies the operation of the meter. In some systems with a lower carrier frequency, antenna winding is required around the perimeter of the shaft.

Primary sensors (strain gauges) of different vendors can be used with a resistance of 100–700 Ohms. Increasing the resistance of the sensors reduces the

power consumption of the transmitter circuit, which is desirable for continuously operating plants but long data transmitting distances or noisy working conditions require higher power consumption. In this system, the transmitter uses a DC amplifier with a stabilizer having a low voltage drop, which reduces the power consumption on the shaft.

The installation of a transmitter on a rotating shaft can be performed in two ways: by gluing on the thoroughly polished surface and by welding on the rough surface of the plate with previously glued strain gauges. The second method is preferable and easier for implementation but is excluded in underground coal mines with methane explosion threats.

The proposed torsional load monitoring system was tested on the laboratory rolling mill (Fig. 5.3a). In Figure 5.3b, the signals from the 12-bit ADC converter are presented. The load on the shaft has been changed 8 times and is shown in the line graph.

More details on torque meter parameters are given in Table 5.1. This version is planned for improvements based on gained experience and new capabilities in the field of electronics components development. The following functions are intended for inclusion in the next version of the torque meter: energy harvesting on the shaft; automatic zero calibration from the receiver side; signal scaling from the receiver side; measurement of shaft revolutions; diagnostics of clearances and high-resolution ADC (24 bits).

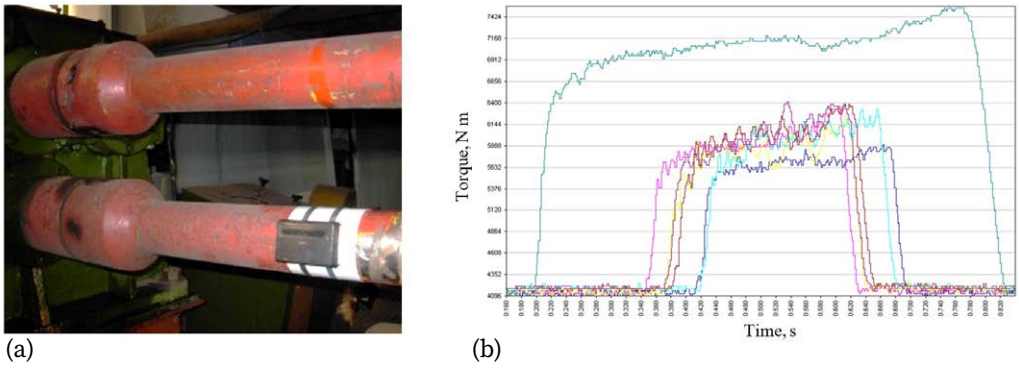

(a) (b)

Fig. 5.3. Testing of telemetry torque meter:
(a) transmitter mounted on the laboratory rolling mill shaft;
(b) signals obtained from receiver in several subsequent tests

Table 5.1. Parameters of the torsional vibrations measurement system

Parameter	Value
Measurement range factor	2, 4, 8
The primary sensor type strain gauge	200–700 Ohm
Current consumption up to	30 mA
Sensor power supply on the shaft battery or inductive	3...4 V
Type of signal frequency modulation	FM
Frequency deviation	15 kHz
Sampling frequency of the transmitter	600–750 Hz
Data sampling	8 bits
Frequency range of the measured signal	300 Hz
Data transfer rate via the radio channel	19–38 Kbps
Distance to the receiving antenna	10–20 m
Allowable shaft rotation speed	3000 rpm
Allowable vibration on the shaft in all directions	100g
Operating temperature in the measurement zone	–10... +85 C
Measurement accuracy	0.3...0.4%
Carrier frequency (two frequencies allowed)	433.92 MHz
Output signal (digital/analogue)	0...10 V
Protection	IP67

Testing of the torsional measurement system determined such metrological characteristics as sensitivity to transverse and axial impacts on the shaft and frequency response functions of the whole channel. Other factors requiring further investigation include temperature influence on the sensor, especially creep of the adhesive compositions, and the effectiveness of sealing materials against moisture and dust in the underground conditions. Further work is focused on the application of the improved system for mobile vehicles and multi-motor drives of belt conveyors. One more application of torque meters is the realisation of feedback control loops for active torsional vibration damping in multibody drivelines.

Torque sensors on the rotating shafts can be categorized as a new class of “on-shaft” measurements or “moving sensors”, which can inspect industrial machines. The torque sensor signal allows simultaneous recognition of numerous

defects like cylinder phasing and fuel injection in the vehicle engine, transmission errors, friction forces in clutches, damping of hydraulic couplings, inhomogeneity of gear meshing, and angular gaps in kinematic pairs. The installation of such a torque measurement system in industrial machines makes it possible to optimize technological regimes to reduce overloads and to calculate the remaining useful life of components.

5.2. Electronic device for backlash measurement

The developed electronic device for backlash measurement in the drivelines of industrial machines is represented in [401]. The measurement method consists in sequential reversion of the DC electric drive and rotation in both directions for 10–20 revolutions to stabilise the rotation speed. For reliable closure of the gaps, a small load moment (up to 5–10% of the load) on the work roll is required. Sensors are mounted on both sides of the diagnosed coupling.

Simulation of backlashes measurement on a model. The mathematical modelling of the proposed method is performed, bringing it as close as possible to real conditions. For this purpose, a design diagram of drivetrain was developed, containing the main elements and couplings with potential backlashes (Fig. 5.4). The scheme consists of an electric motor rotor (eng), a pinion shaft (gw1) and a gear wheel (gw2) (z1 = 26, z2 = 188), a lower (pw1) and upper (pw2) rolls of a gear stand and a lower (wr1) and upper (wr2) work rolls. Angular clearances in the joints: motor coupling (Δ1), gearing of the reducer (Δ2), main coupling (Δ3), gearing of the gear stand (Δ4), lower (Δ5) and upper (Δ6) universal spindles. It was assumed that the driveline stopped at an arbitrary position. All angular clear-

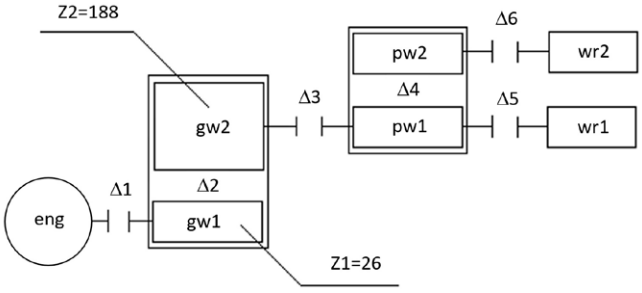

Fig. 5.4. The layout of the gear driveline and backlashes positions

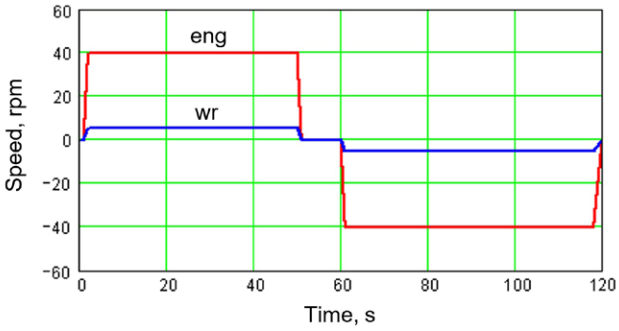

Fig. 5.5. Electrical motor speed diagram for one measurement test

ances are closed in the main direction of rotation of the rolling stand. Speed sensors should be placed at the uppermost point of rotation of the main elements. According to the scheme, there are 7 sensors and measured signals. The values of all 6 gaps in the given diagram are arbitrarily set.

A hypothetical algorithm for the rotation of the motor rotor is assumed. First, its speed is zero, then in a couple of seconds it accelerates to the set speed (40 rpm), rotates at this speed for 50 seconds, slows down, stands still for a few seconds, accelerates in the opposite direction, rotates at this speed for 57 seconds, slows down and stops (Fig. 5.5).

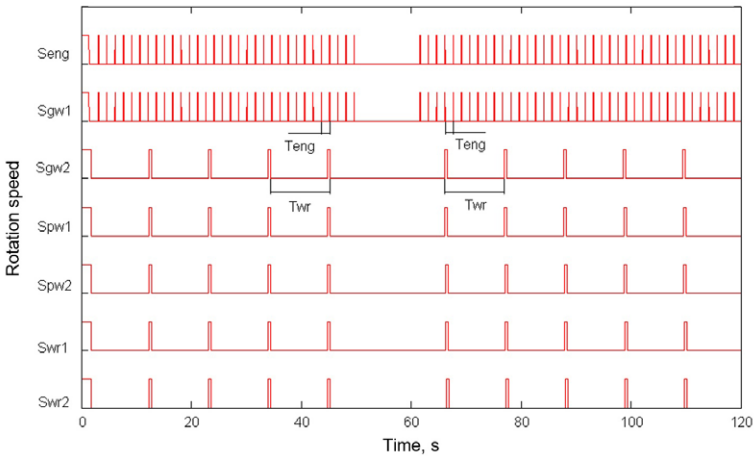

Fig. 5.6. The simulated signals of rotation speed sensors of the driveline

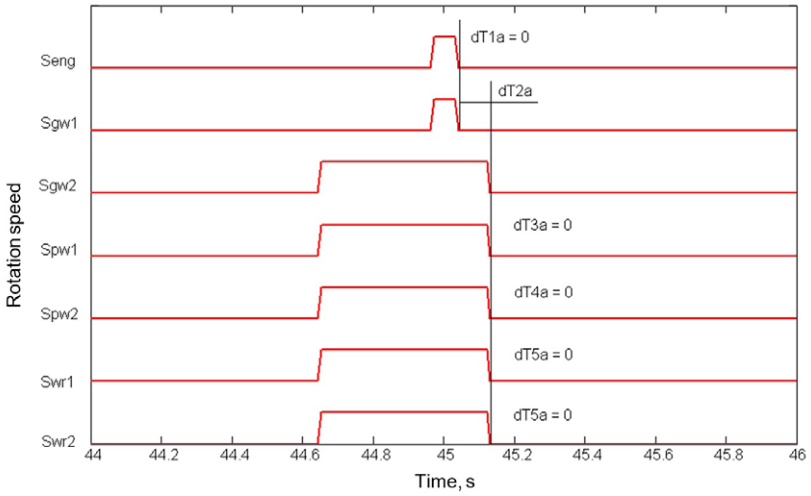

Fig. 5.7. Fragment of signals measurements at the forward drive rotation

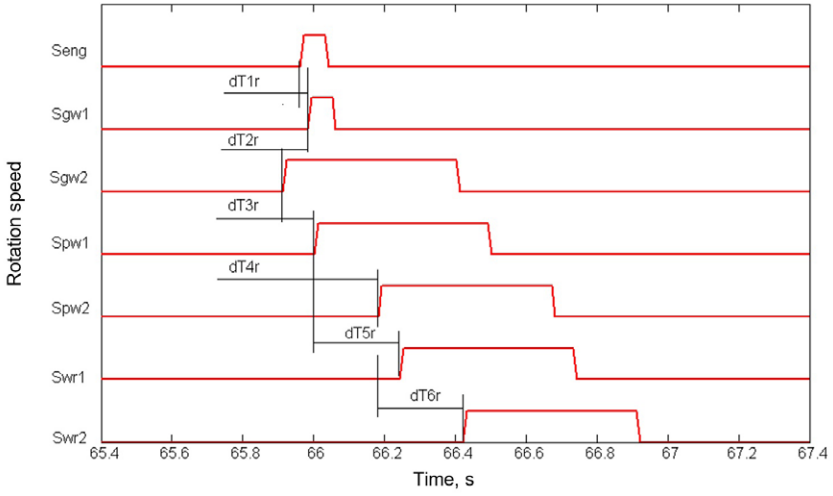

Fig. 5.8. Fragment of signals measurements at the backward drive rotation

When all of the above-mentioned conditions are met, such signals are obtained (Fig. 5.6).

To determine the angular backlash in the joint, it is necessary to select the recording fragments in phase with each other, i.e., symmetric, where the axis of symmetry will be the moment of stopping. Such fragments are shown in Figures 5.7 and 5.8.

For the forward drive rotation in Figure 5.7, the clearance in couplings is closed to one side of contact surfaces and the pulse offset is zero. The exception is coupling 2, where the speed is reduced and the signal offset (dT2a) inevitably occurs. The fragment at 65–67 seconds is in phase with this fragment. In this case, the backlashes in all joints are completely open and we see a shift in impulses along the entire driveline (Fig. 5.8).

To calculate the backlash in all joints, such dependences are used (rad):

$$\Delta 1 = \frac{dT1r}{Teng}; \Delta 2 = \frac{\left(dT2r - dT2a\right)}{Teng}; \Delta 3 = \frac{dT3r}{Twr};$$
$$\Delta 4 = \frac{dT4r}{Twr}; \Delta 5 = \frac{dT5r}{Twr}; \Delta 6 = \frac{dT6r}{Twr} \quad (5.1)$$

Thus, we have tested on a mathematical model a method to measure angular clearances, which can be applied to the drivelines of industrial machines.

Hand-held device for the angular gaps measurement. The proposed method of diagnosing gaps is based on the use of two standard speed sensors installed on the side surfaces of the shafts, and recording the time interval between successive pulses of the sensors at different points in the driveline. By comparing the difference in time intervals between pulses from the speed sensors during drive rotation in the forward and reverse directions, the total value of the gaps is determined. The open value of the angular gaps affecting the dynamics of the driveline is determined from the time intervals during idling and under load.

To implement this method of diagnosing angular gaps in the drivelines, an electronic device has been developed (Fig. 5.9) using contactless shaft rotation sensors as the primary transducers: two optical (Fig. 5.9a) or Hall-type sensors (Fig. 5.9b) with cables; two optical marks or two magnets mounted on the shaft; electronic device (Fig. 5.9c). Sensors are connected to the device via cables (see inputs 1 and 2 in Fig. 5.9d). There is also a communication port for recording output digital signals from sensors to a computer (see connector with LED indicator in Fig. 5.9d).

The following elements are located on the front panel of the device (Fig. 5.9b):

- 5-digit indicator (upper) difference in the number of pulses of sensors;
- 5-digit indicator (lower) of the number of pulses per shaft rotation;
- switch (“1 → 2”, “2 → 1”) for selecting the master channel for the pulse generator;
- clock output switch (“TI”) to a computer;

(a) (b) (c) (d)

Fig. 5.9. Backlashes measurement device:
(a) optical sensors; (b) Hall sensors; (c) design of front panel; (d) back panel view

- instrument power switch ("On");
- clock count start button ("Start");
- clock frequency switch ("2…32 kHz").

The functional scheme of the device is shown in Figure 5.10. The signals from the sensors come into the device, where after the channels' switcher go to the clock pulse generator.

The frequency of clock pulses is selected in advance in the range of 2…32 kHz so as not to overflow the 5-digit pulse counter per shaft revolution. The generator clock switch also sets the sensitivity of the device depending on the size of the gaps. Button "Start" initiates the generation and counting of pulses when the shaft rotates in the forward and reverse direction. Switch "Ch" is used to output clock pulses as a test for checking the line of communication with the computer. Angular gaps are determined by calculating the ratio of the value on the upper indicator to the value on the lower indicator. Linear clearance is determined by the initial diameter of the shaft or gear wheel.

With a minimum sampling rate of 0.0005 s (2 kHz), and shaft rotation speed of 1 rot/s, the detectable angular clearance is $0.0005 \times 2\pi = 0.00314$ rad (0.18 grad). For a shaft of 400 mm diameter (200 mm radius), linear (tangential) backlash is about $\Delta = 200 \times 0.00314 = 0.628$ mm. The largest gaps (up to 5–8 mm) are formed in the spindles with bronze slipping pads, while gearbox teeth wear is 0.2–0.5 mm. To diagnose such gaps at a shaft speed of 10 rot/s, the accuracy of determining the time intervals between pulses of two sensors should be about 0.1–0.5 ms, which corresponds to input signals sampling frequency 10–20 kHz. The maxi-

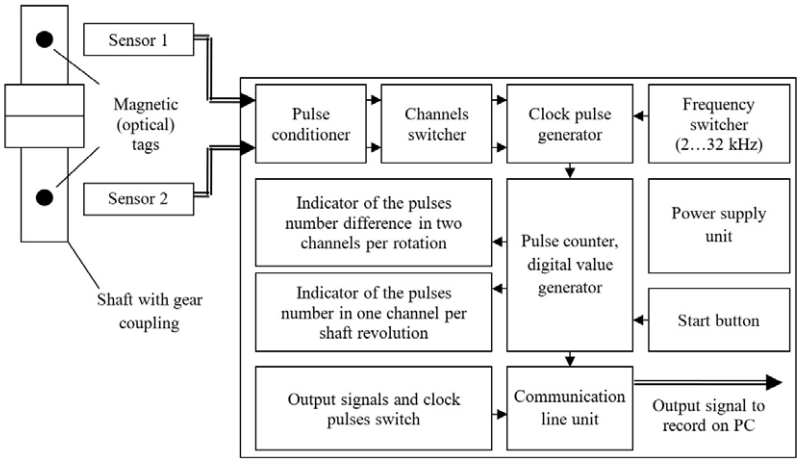

Fig. 5.10. Functional scheme of the device for measuring angular backlashes in the drivelines

mum sampling rate of the device is 32 kHz, hence, it covers the full range of industrial machines.

This device can work as a separate tool with battery power and as part of a measuring and computing complex based on a computer. To input signals from the device and save to the hard drive of the computer, the cable and connector on the back panel of the instrument are designed. In this case, signals can be input even without a special ADC board, and through the line-in input of a computer sound card. At the same time, in connection with the well-known property of sound cards to differentiate input signals, instead of each rectangular pulse, two pulses of different polarity are obtained, a positive pulse at the leading edge and a negative pulse at the falling edge of the original signal, which is then taken into account when processing in software. The ability to input signals from the device through a sound card greatly simplifies and reduces the cost of system configuration, since the cost of ADC boards is quite high and can be comparable to the cost of a simple computer.

The portable diagnostic device is realized with non-programmable logical elements. Further implementation is supposed to be based on a microcontroller with an LCD, which allows a better visualization and calculation of gaps directly in the device from an assigned user diameter, as well as considerable reduction in the size and power consumption of the device.

(a) (b)

Fig. 5.11. Measurement of gaps in the driveline: (a) gear coupling; (b) screw reducer

The developed device is tested on several drivelines of industrial rolling mills, as well as on auxiliary machines (strip coiler), where it showed good performance. Shaft rotation sensors are installed on the equipment using conventional magnetic tripod mounts at a distance of 10–20 mm from the shaft, on which two magnetic tags were installed with a diameter of 10 mm on both sides of the diagnosed unit, e.g. gear coupling (Fig. 5.11a) or a pressure screw gearbox (Fig. 5.11b).

Special mounting magnets on the shafts are not required, because drives are low-speed (up to 3–5 rot/s). The shaft in the place of installation of the magnets is only wiped with a grease cloth. The dimensions of the sensors on the shafts allow them to be installed on the short sections (up to 30–50 mm), for example, between the gear coupling and the gearbox housing, on the roll neck and the heads of the spindles.

With the help of the developed method and device, the inspections of drivelines in several rolling mills were performed. An example of backlash measurement is shown in Figure 5.12. The average value of angular backlash is determined as 5.15 mm with an acceptable standard deviation ±0.31 mm (6%). Systematic and random errors are considered following the Performance Test Standard PTC 19.1-2005 “Test Uncertainty” by the American Society of Mechanical Engineers (ASME). The main deviation creates drive rotation speed. Therefore, the minimal available by the electric drive idle speed should be used. The laboratory testing showed a potential accuracy of up to 0.1 mm. The results are less dependable on absolute rotational speed and applicable for a wide range of drive speeds.

The designed device and method of backlash measurement can be implemented in the monitoring systems of torsional loads. An important function of the

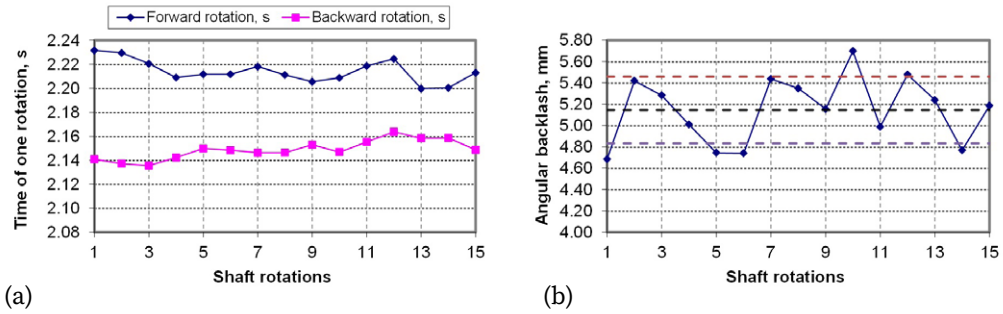

Fig. 5.12. Diagrams of backlashes measurement in the driveline:
(a) time of rotations (angular speed); (b) measured angular backlash
(mean value 5.15 mm, standard deviation ±0.31 mm)

proposed method and device is the ability to evaluate (continuous adaptation) the stiffness (compliance) of the driveline sections. Since the inertial parameters of the equipment practically do not change during operation, the obtained value of stiffness allows online identification of the dynamic model and performs peak torque calculations in those elements where torque meters are not possible to install.

By the same rotation sensors, the influence of spindle slot angular position (Fig. 5.13a) is measured and its influence on torsional dynamics is determined. Torque measurement is performed by the telemetry devices installed on the intermediate shaft in one driveline and on the motor shaft in the other. Statistical distributions of TAF concerning spindle angular position are shown in Figure 5.13b, c.

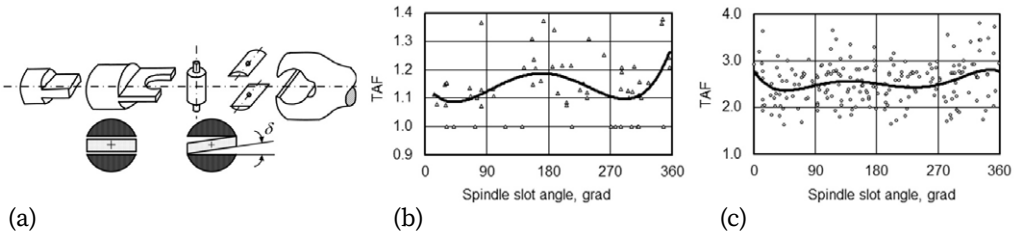

Fig. 5.13. (a) Design of spindle with slip pads; TAF measured by the spindle slot angular position in two different drivelines: (b) with two gearboxes;
(c) with one gearbox

Each point corresponds to one cycle of loading (slab rolling). Polynomial regression is used to approximate statistical data. The 0°, 180°, 360° angles correspond to the vertical slot position when TAF is the highest due to the unstable state of the head, and 90°, 270° – to the horizontal head position when TAF is the lowest due to gap (δ) closing by the laying head weight.

TAF deviation reaches 30–50% from the mean value. Such measurements and data representation allow the separation of other influencing factors and numerically estimate the statistical dependence of dynamics on angular slot position, which is caused by improper balancing and could be used for maintenance purposes.

6. MODEL-BASED METHODS OF DYNAMIC ANALYSIS AND WEAR DIAGNOSTICS

Higher dynamical loads resulting from intensive loading regimes cause transient torsional vibrations in the drivelines of industrial machines. Backlashes are considered the main parameters of the technical condition of heavy-duty machines. Some maintenance practices can help to reduce them but cannot avoid them completely. To overcome problems with the non-stationarity of diagnostic signals, new methods are developed, which use nonlinear effects for diagnostics purposes. In the analysis of electromechanical systems of machines, the multi-degree-of-freedom (MDOF) models are used for their diagnostics.

6.1. Angular backlashes diagnostics by the transient torque signal

The analytical research of nonlinear multibody systems usually assumes reducing the initial system to less DOF. That is inefficient when it is required to solve tasks of wear diagnostics. The higher natural modes may give a small contribution to the overall energy of torsional vibration but contain information about changes in nonlinear stiffness characteristics.

The possibility of measurements in the industrial machines helped to understand and estimate the influence of angular and radial backlashes on the vibration and torque signals. Torque measurements were performed using the telemetry system. The vibration was measured with the 4-channel signal conditioner (PCB model 48A22) and IMI Sensors accelerometers (model 603C01). The special software was used for signal recording and FFT transformation in conjunction with low-pass filtering and other signal-processing procedures.

The dynamical models of drivelines with enough detailed springs and masses were developed for diagnostic purposes [402, 403]. Model identification has been performed in a time domain and a frequency domain. The calculated natural frequencies of the investigated drivetrain were as follows 12, 15, 20, 34, 55 and 81 Hz.

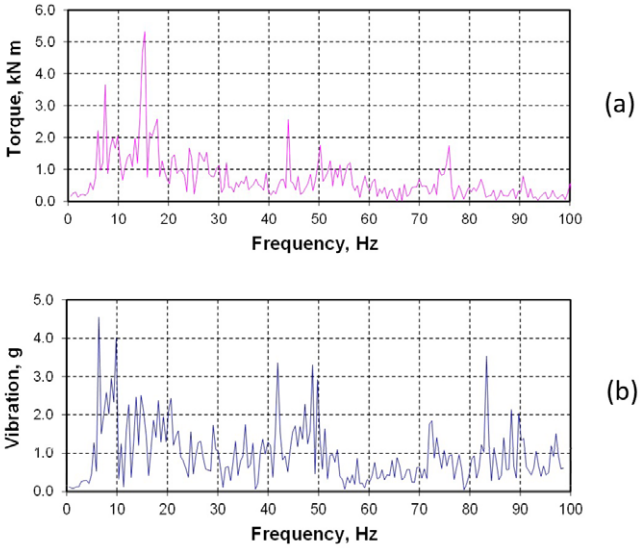

Fig. 6.1. Spectra (averaged) of measured signals: (a) torque; (b) vibration

The torque signal has peaks at the lower frequencies, while the vibration has them at the higher range (Fig. 6.1).

None of the frequencies of teeth couplings or bearings is observed in this frequency range. A little peak was observed in the torque signal at 67 Hz near the frequency of motor shaft rotation. The difference between the calculated and measured natural frequencies does not exceed 2%. The accuracy is good enough, taking into account the low frequency range and short time of the transient process.

The well-known fact that the opening of backlashes causes high-frequency vibrations was confirmed by simulation. It cleared up what frequencies exactly appear in the signals of torque and bearings vibration and how they could be used for backlash diagnostics. The comparison of model simulation and experiment (Fig. 6.2) has shown that higher natural frequencies associated with, but not equal to, partial frequencies of torsional vibrations appear in the torque signal. Also, the 2^{nd} and 3^{rd} harmonics of the main natural frequency will appear. The torque curve exhibits non-isochronism, which appears when the first period and the next periods of torque oscillations are not equal. The length of the period depends on wear in couplings and may be determined for diagnostics purposes. Such regularities have been adopted for wear diagnostics. The vibration signal requires additional low-pass filtering in analysis.

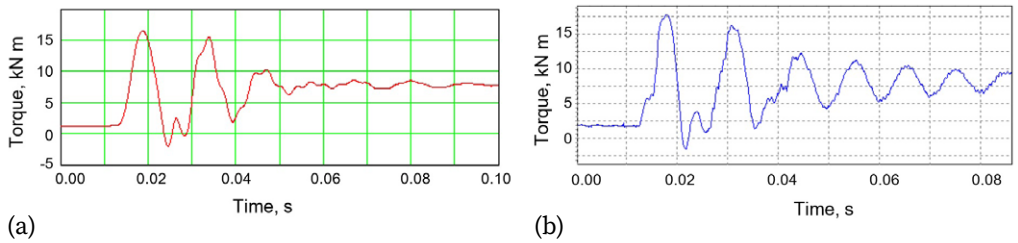

Fig. 6.2. Nonlinear torsional vibration: (a) calculation; (b) measurement

The spectrum amplitudes and phases (A12…A81 Hz) of corresponding natural frequencies (Fig. 6.3) were obtained for different wear (angular backlashes) of the gearbox and spindles. The algorithm of diagnostics is based on a combination of the amplitudes and phases at the different natural frequencies. In this case, variable A20 Hz and its phase are the most sensitive to wear by torque signal. For example, after the 2.5 mm wear in spindles, A55 Hz amplitude becomes less than A20 Hz. In this manner, other variables can be analysed to build different diagnostic rules, which vary for other points of torque and vibration measurement.

The proposed approach can diagnose opened part of backlashes, which has effects on driveline dynamics. In vibration measurements, radial gaps in the bearings have the same influence on the TAF as the angular gaps. The highest TAF corresponds to the opposite direction of shaft weight and gear coupling reaction force. The response of the linear dynamic model is taken as reference values for wear diagnostics.

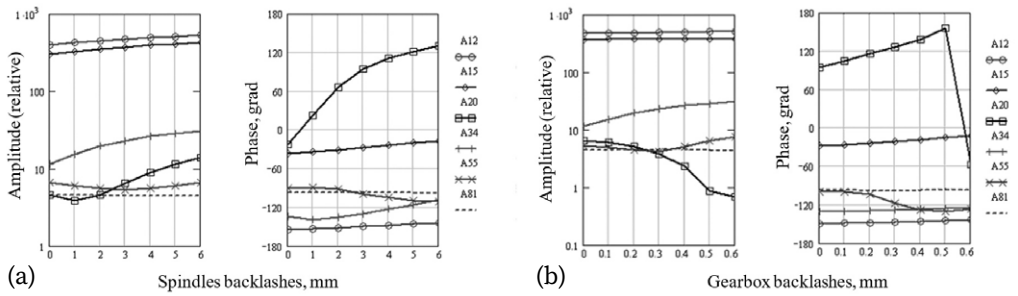

Fig. 6.3. Amplitudes and phases at natural frequencies (A12…A81 Hz) by the backlash in: (a) spindles; (b) gearbox

6.1.1. Diagnostics by the static and dynamic torque relation

The torque amplification factor (TAF) is one of the parameters for the estimation of system dynamics. For nonlinear systems, the dynamic response depends on static load (rolling torque). It was shown (Fig. 6.4) that the less static input torque M_{st} causes higher TAF, which nonlinearly depends on angular wear (0.000–0.012 rad). Such nonlinearity is almost invisible for $M_{\max}$ curves and is usually not taken into account in the strength capacity and durability calculations of the drivelines. However, such dependence can be used for diagnosing angular backlashes by the torque signal measurement [404].

The nonlinear functions $M_{\max} = F(M_{st})$ and $TAF = F(M_{st})$ obtained by torque measurements in the real hot rolling mill are given in Figure 6.5, where discrete values correspond to certain M_{st} levels during mill operation. The diagnostic method is based on a simple mathematical operation of measured data approximation by the polynomial function of 2nd order and comparison with modelled data for the same section of the driveline.

6.1.2. Statistical analysis and spectral representation of the input loads

The huge data sets stored in the databases of process automation systems and condition monitoring systems make it possible to improve continuous hot rolling mills' performance and reliability from the viewpoint of dynamics. The standard representation of input loads based on probability statistical distribution pro-

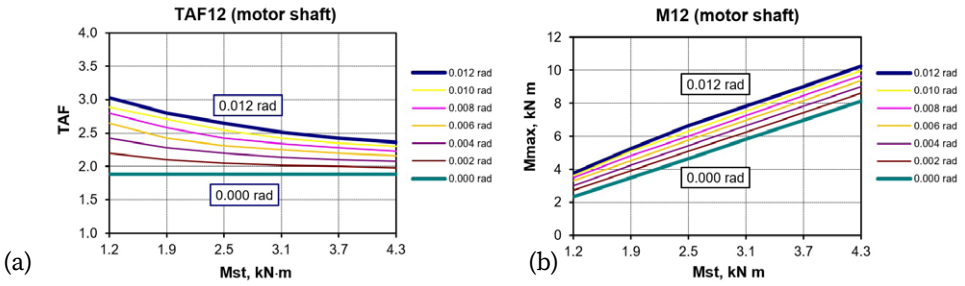

Fig. 6.4. Modelled nonlinear dependence of (a) TAF and (b) $M_{\max}$ on static torque M_{st} for different angular backlashes in the spindles (0.000–0.012 rad)

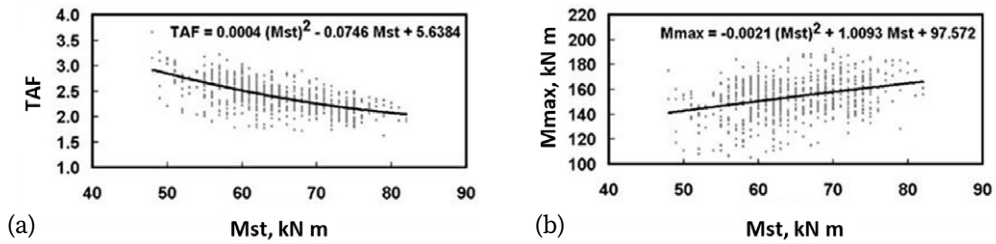

Fig. 6.5. Measured nonlinear statistical relations of M_{st} with: (a) TAF; (b) torque $M_{\max}$

vides the upper limits of stresses and strength capacity for machine designers, however, does not allow them to estimate the effect of input loads on machines' dynamic response. In this regard, the combination of statistical fields of input load scattering with the frequency response functions (FRF) is more informative. Conversion of step-like input loads into the frequency domain is carried out provided that the time of load rising is equivalent to the half-period of input load oscillation.

An analysis of the experimental data of the gaps in the spindles and drivelines showed that the magnitude of their open part has a complicated distribution. If the gaps in the spindles change according to a sinusoidal law (at different speeds

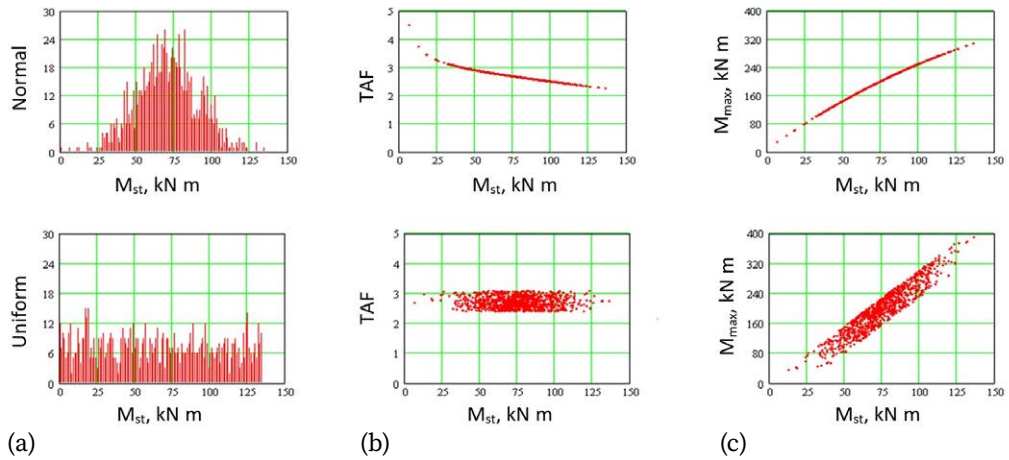

Fig. 6.6. Normal (upper) and uniform (lower) distributions of torques in the driveline: (a) input static loads M_{st}; (b) TAF; (c) output dynamical load $M_{\max}$

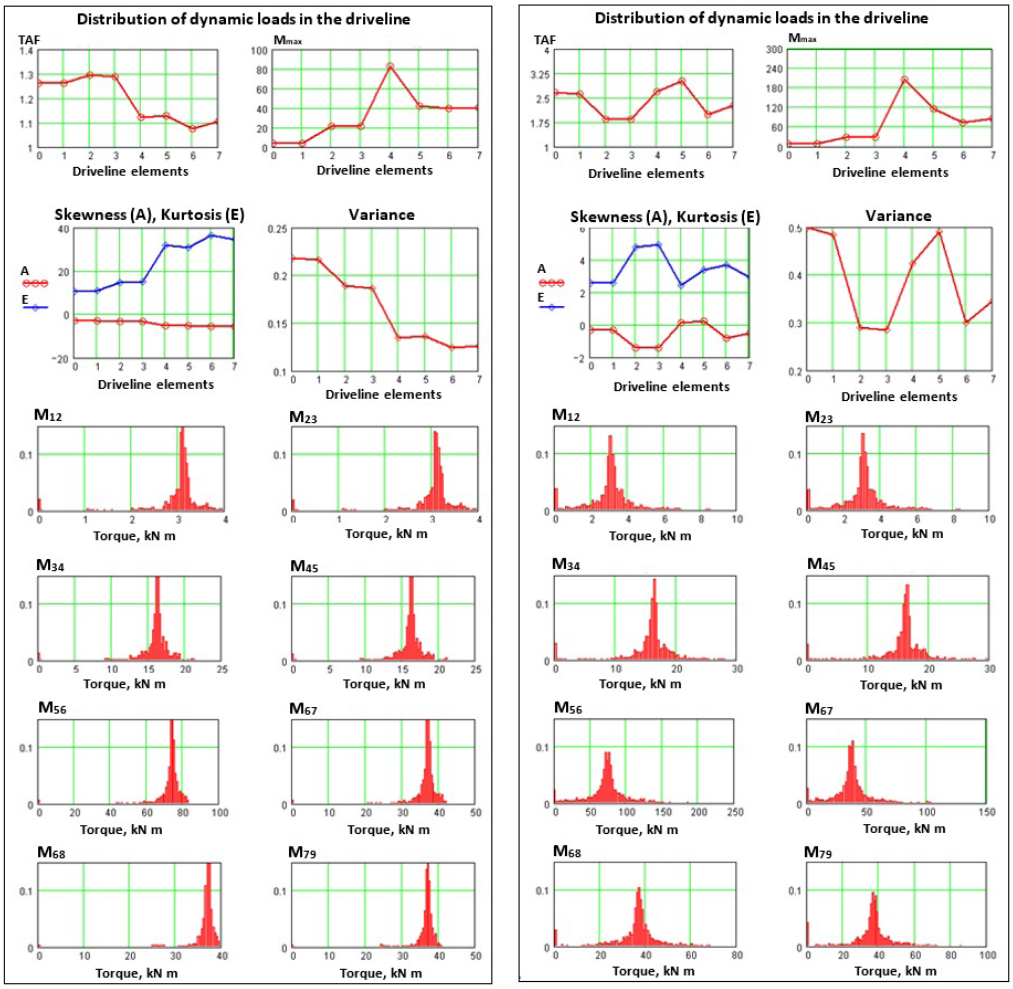

Fig. 6.7. Distribution of torques and their statistical parameters (skewness, variance) for the driveline elements (0–7): (a) in the linear system without backlashes; (b) with backlashes in both spindles 0.012 rad (6 mm)

and weight balancing force of the spindles), the open gaps along the driveline has a rather uniform distribution.

The calculations are made for the normal (Gaussian) and uniform distribution of the input load (rolling torque) on the work rolls (Fig. 6.6). In statistical simulations, several data sets were applied with the same distribution parameters (mean and deviation).

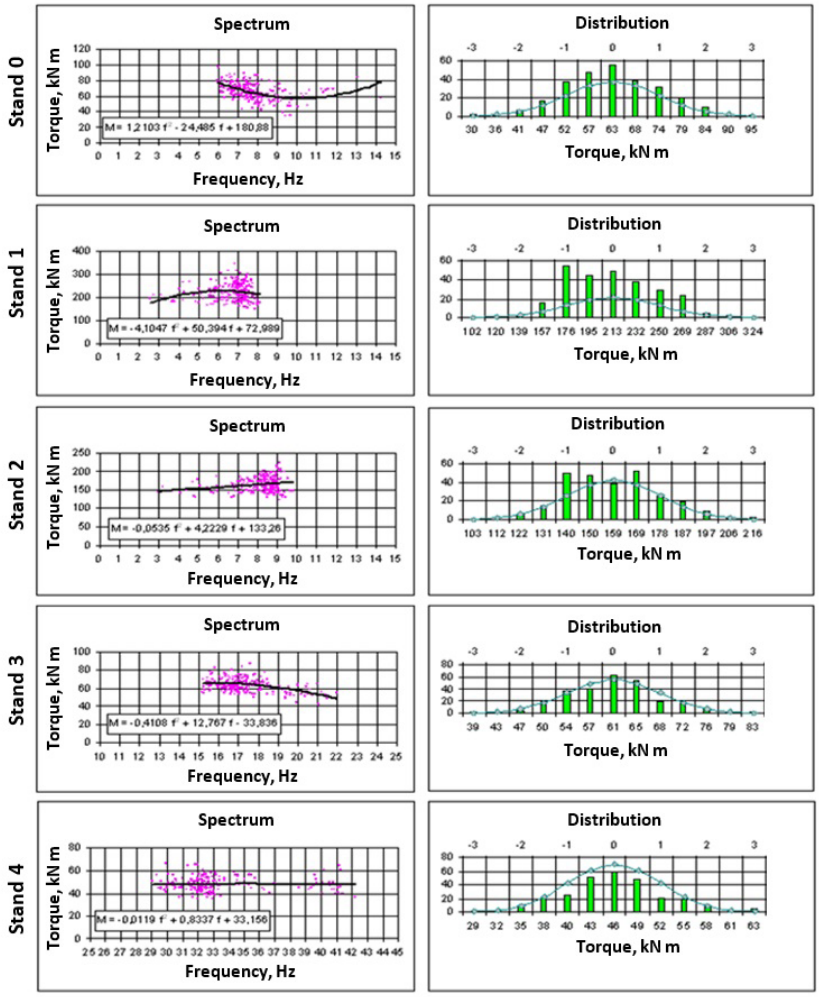

Fig. 6.8. Representation of input loads in the drivelines of continuous hot rolling mill (stands 0–4) by (a) spectra; (b) statistical distributions

The distributions of dynamic loads and distribution parameters in the linear system of the driveline without the wear and in the presence of clearances in both spindles are shown in Figure 6.7.

Those differences in the parameters of distributions constitute diagnostic methods based on statistical data analysis. Calculations showed that in a linear dynamic system of a driveline without gaps, regardless of the number

and structure of elastic links, the distribution parameters of the system response at each point do not change (rounding error bounds), which confirms the theory.

The results of dynamic loads analysis by the FRF method are shown in Figure 6.8 for the rolling mill stands. The spectra of the input loads, i.e., the dependence of the amplitude on the time of input torque rising as the half period of oscillation. This representation of the input load corresponds to the real term of "load spectrum", which often means only the distribution of load amplitudes over the levels. For statistical calculations, the initial load spectra are approximated by second-order polynomial dependences on frequency.

The use of spectral representation of input loads combined with FRF makes it possible to determine the spectra of dynamical loads along the drivelines with different layouts. The example of spectral representation of the measured input loads M_{st} and dynamic responses $M_{\max}$ in the five consecutive stands of a continuous hot rolling mill is shown in Figure 6.9. Also, the FRF at the motor shaft is given there. The fields of scattering look like discrete lines due to the different series of rolled strips' thicknesses. Frequencies of input loads are calculated as a double time of load torque rising. Since the rolling speed increases due to strip elongation, the input load frequencies shift to a higher frequency band with a stand number.

The neighbouring stands of the continuous mill have almost equal lowest natural frequencies of the drivetrains. As could be seen in Figure 6.9, the input load frequencies lay in the resonance bands of stands 4 and 5. Therefore, drivetrain dynamics can be reduced by the speed control in the stands to avoid loads scattering fields coinciding with the resonance bands in every stand.

The measurements have shown that input load M_{st} has usually a Gaussian (normal) distribution. The mean value M_{st}^{*} and standard deviation σ_{Mst} of the input static load can be determined by the electrical motor current. The problem of dynamic loads statistical calculations in the nonlinear mechanical systems of drivelines can be solved analytically based on the previously introduced polynomial relation of M_{st} and $M_{\max}$. Then, a mean value of the output dynamic load $M_{\max}^{*}$ can be described as:

$$M_{max}^{*} = \int_{-\infty}^{\infty} M_{max} \cdot P\left(M_{st}\right) \cdot dM_{st}, \tag{6.1}$$

where $P(M_{st})$ – normal density distribution function of M_{st} (for simplicity, variable M_{st} is taken with a zero mean, which does not influence the generality of the

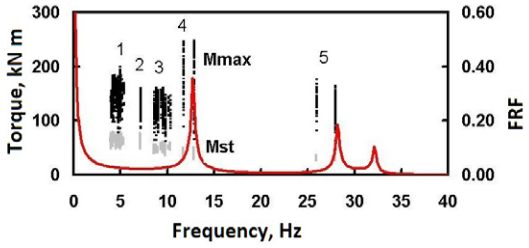

Fig. 6.9. Input loads spectra and the FRF of motor shaft for the five stands

result). Substituting the polynomial function $M_{\max}(M_{st})$ (3.25) and $P(M_{st})$ in (6.1) and integrating by M_{st} gives:

$$M^*_{\max} = \int_0^{\infty} \left(a_0 + a_1 M_{st} + a_2 M_{st}^2\right) \frac{1}{\sigma_{M_{st}} \sqrt{2\pi}} e^{-\frac{M_{st}^2}{2 \cdot \sigma^2_{M_{st}}}} dM_{st} = a_0 + a_2 \cdot \sigma^2_{M_{st}} . \quad (6.2)$$

It means that in such kind of nonlinear system, the maximum output torque $M_{\max}$ linearly depends on the dispersion $\sigma^2_{M_{st}}$ of input load M_{st}. By the similar transformations, it can be shown that a dispersion of output load $\sigma_{M_{\max}}$ depends on a dispersion of the input load $\sigma_{M_{st}}$:

$$\sigma_{M_{\max}} = a_1 \cdot \sigma^2_{M_{st}} + 2 \cdot a_2^2 \cdot \sigma^4_{M_{st}} . \quad (6.3)$$

Based on the above-derived relations, the statistical parameters of output loads can be estimated for every section along the drivetrains. Every driveline coupling will have its specific polynomial coefficients a_i varying during mill operation. Such an approach improves the reliability of strength capacity calculations at the design stage.

6.2. Torsional vibration monitoring by using electric motor current

Exceeding the dynamic load of the permissible limits in the transmission elements such as clutches, spindles, and gears causes their failure. The disadvantages of the known methods of mechanical load determination for a long-time operation of industrial machines are high requirements for gauge sensor durability, stability of power supply on the transmission shaft, and the reliability of

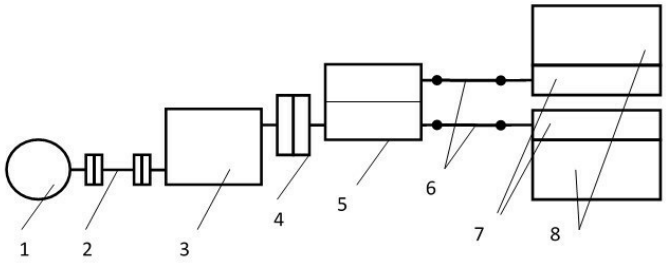

Fig. 6.10. A typical drivetrain of the rolling mill: 1 – DC electric motor; 2 – shaft; 3 – gearbox; 4 –gear coupling; 5 – pinion stand; 6 – slipper pads spindles; 7 – work rolls; 8 – backup rolls

signal transmission from the rotating shaft by the radio channel. Another drawback of the known methods when installing sensors in transmissions is the need to calibrate them with static torque in the test rigs, which have to provide large torque values (up to 2–3 MN·m). The technical difficulties of calibration increase even more because the dynamic moment of the load in real conditions exceeds the static 3–5 times. Besides, there are elevated temperatures, significant electrical interference, metal dust and vapours of lubricants, and imbalance of shafts

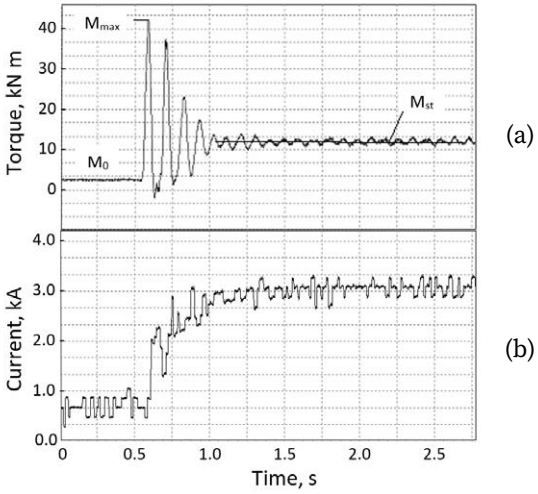

Fig. 6.11. Measurements of mechanical load by the (a) torque sensor; (b) electric motor current

(especially spindles), which require re-calibration of sensors, e.g., by the electric drive current signal. The accuracy of mechanical torque measurement by the known methods is about 5%. Another disadvantage is that torque sensors have a high complexity of installation and maintenance, which create delays during the operation of machines.

The method of dynamic load monitoring in the driveline described in [405] involves the measurement of the difference signal of counter-EMF in two serially connected DC electric motors. The disadvantage of this method is that it does not determine the amplitude of torque oscillations in transmissions with a single DC drive. The value of the difference counter–EMF depends on the variance of the values of the electrical parameters of the two electric drives, each of which may be up to 5%. Therefore, the maximum error in determining the amplitude of mechanical oscillations is about 10%.

The task is solved by dynamic torque monitoring in the transmission of industrial machines by the signals of the DC electric drive [406]. A new method of torque monitoring is based on a signal of electric current, which is measured during load increase. Then, the difference is determined between the dynamic signal and output signal after a low-pass filter with a cut-off frequency of less than a half of the fundamental frequency of the natural oscillations in the trans-

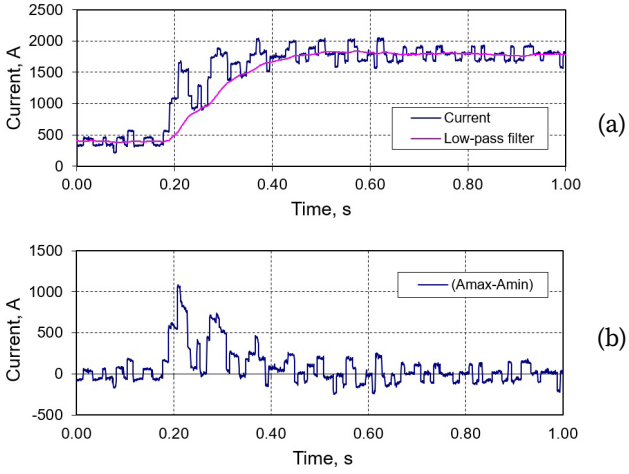

Fig. 6.12. Transient signals processing: (a) original and low-pass filtered signal; (b) amplitude of load oscillations by the difference signal of electric current

mission. The value of the maximum mechanical torque is determined by the amplitude of a differential signal. The essence of the method is illustrated with diagrams. Figure 6.10 shows a typical layout of the drivetrain, e.g., in the hot rolling mill.

Figure 6.11 shows an example of simultaneous measurements of mechanical torque oscillations and the electric drive current. Signal processing is shown in Figure 6.12 where the differential signal is calculated of the original electric motor current and low-pass filtered signal. Figure 6.13, a line graph, shows the coefficients of dynamics $K_{d(m)}$ measured by a torque sensor, the coefficients of dynamics $K_{d(e)}$ determined by the proposed method and the difference signal ($A_{\max} - A_{\min}$) of the motor current.

The method was tested on the driveline, consisting of a DC motor powered by a thyristor converter. Simultaneous measurements are performed by the strain gages with the telemetric system on an intermediate shaft during the transient loading. For each measurement, the following parameters were consistently determined.

The coefficient of dynamics by the amplitude of oscillations of mechanical load:

$$K_{d(m)} = \left(M_{\max} - M_0\right) \Big/ \left(M_{st} - M_0\right), \tag{6.4}$$

where M_0 is the moment of idling, M_{st} is the moment of static load, and $M_{\max}$ is the maximum moment of mechanical loading.

The difference signal of the electric current and signal after the low-pass filter with a cut-off frequency of 5 Hz, which is less than a half of the basic natural frequency (15 Hz) in this driveline:

$$\Delta A = \left(A_{\max} - A_{\min}\right), \tag{6.5}$$

The functional relation $K_{d(e)} = f(\Delta A)$ is determined by the measured data.

The maximum moment of mechanical loading:

$$M_{\max} = \left(M_{st} - M_0\right) \cdot K_{d(e)} + M_0 . \tag{6.6}$$

The dependence $K_{d(e)} = f(\Delta A)$ obtained at the training stage is used further without the use of the mechanical load measurements. When calculating $M_{\max}$,

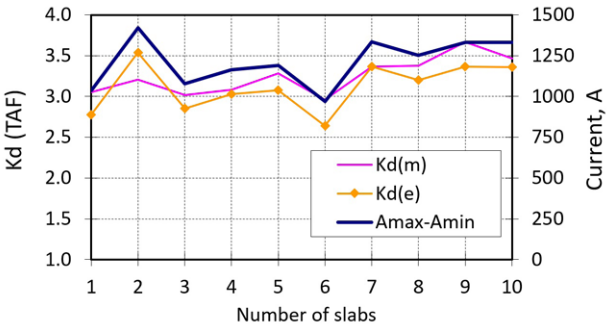

Fig. 6.13. Coefficients of dynamics (TAF):
$K_{d(m)}$ – mechanical load measured by a torque sensor;
$K_{d(e)}$ – determined by the new method;
$(A_{max} - A_{min})$ – difference of electric currents signals;
every point corresponds to one slab rolling cycle

parameters M_{st} and M_0 are determined by the current load signal, taking into account the driveline efficiency (90%).

Then, the values of $K_{d(m)}$ obtained by the measured mechanical load at the stage of training, and the values of $K_{d(e)}$ obtained by calculation are compared. The average relative error in determining the amplitude of oscillations of the mechanical load by the proposed method is about 10%. Hence, this is the method that provides a relatively simple solution, with acceptable accuracy but without the use of torque sensors, that determines the amplitude of torsional oscillations in the transmission of machines by using the electric motor current signal.

The parameters of the monitoring method depend on the design of each specific transmission, namely its main natural frequency, which is usually 10–20 Hz. To extract the informative component from the difference current signal, it is necessary to set the cut-off frequency of the low-pass filter to less than a half of the main natural frequency in transmission, which can be determined by known calculation methods according to the drawings of the transmission units and specified experimentally.

Since the basic natural frequency of the torsional system does not change after repair and replacement of machine parts (stiffness and moments of inertia of rotating masses are constant), the cut-off frequency of the low-pass filter

is determined once when setting the monitoring system. The proposed method does not require the installation of additional sensors and devices on rotating shafts.

6.3. Diagnostics of bolts loosening and radial backlashes in the gearboxes

The measurement of radial clearances in bearing supports and detection of bolts loosening due to their plastic elongation (creep) or weak tightening is an important issue for the maintenance of the heavy-duty gearboxes of powerful industrial machines. The solution to this problem is based on a nonlinear dynamical model of bearing supports. Diagnostic rules are developed and validated by the vibration signals measured on real gearboxes during several series of industrial trials. It has been discovered that radial clearances are the top factors affecting failures in heavy-duty gearboxes of industrial machines working under impulsive and step-like loading.

6.3.1. Nonlinear dynamical model of a shaft with bearings supports

Peripheral wear of the bearings on the transmission shafts and contacting surfaces of housing in heavy-duty gearboxes cause the appearance of radial gaps, which are open during the idling of the machine and closed after loading when the shaft moves to its steady working position. At the initial stage of wear, the open radial gaps cause nonlinearity (such as a dead zone) of the stiffness characteristics in the transmission supports, which leads to a significant increase in the amplitude of shock loads. Under gradual wear, contact opening of the fastening bolted joints occurs under more severe impacts. This leads to a fracture in the stiffness characteristics of the bearing. Wear of bolts (creep and plastic elongation) may cause failures of even newly installed gears, which have not yet been subjected to cyclic fatigue; therefore, clearance diagnostics is an important task in machine maintenance.

A nonlinear dynamical model with a circular clearance is developed to investigate transient vibrations in bearing supports [407, 408]. The disturbance for the shaft comes from the torque applied to the gearbox. The calculating scheme of the dynamical model is shown in Figure 6.14a, which describes the gearbox shaft oscillations in the bearing support with the initial gap and bolted joint opening in

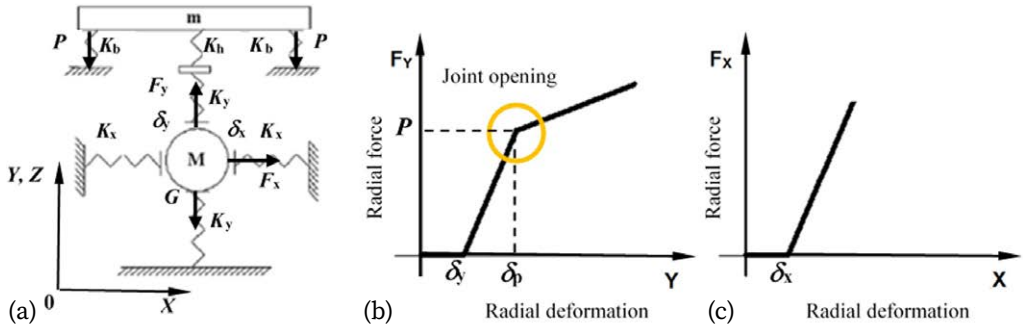

Fig. 6.14. Dynamical model of gearbox shaft in the bearing:
(a) calculating scheme; (b) nonlinear stiffness characteristics of the bearing with a clearance in (b) vertical and (c) horizontal directions

a vertical direction. Notations are as follows: P – bolt pre-load (tightening force); F_x, F_y – horizontal and vertical forces; $G = Mg$ – gravity force of shaft; m – mass of the bearing cover; M – mass of the gearbox shaft; K_b – stiffness of fastening bolts; K_h – stiffness of the gearbox housing; K_y – stiffness of the bearing in the vertical direction; K_x – stiffness of the bearing in the horizontal direction; δ_y, δ_x – total clearance along the vertical axis Y and horizontal axis X; δ_p – deformation at the fracture point.

The nonlinear (piecewise) stiffness characteristics of the bearing support in the Y and X directions are given in Figures 6.14b and 6.14c. The F_y line has an additional fracture point (δ_p, P) and less stiffness beyond it, which corresponds to the bolt loosening effect and contact opening above a certain level of loading. The F_x line has no such point because of gearbox housing has no changes in stiffness characteristics after gaps close up in this direction.

The following assumptions are considered in the dynamical model simulations:

- the effect of friction is accounted for in the damping factor;
- the stiffness of bolts and bearings without clearances is independent of load;
- shaft impacts do not produce plastic deformations of bearings and bolts;
- shaft motion is synchronous for both bearing supports.
- in the case of joint opening, vertical shaft motion is without shear stress on bolts.

The system of nonlinear differential equations of the model is as follows:

$$\begin{cases} M\ddot{x} + K_x x + C_x \dot{x} = \left|F_t\right| \dfrac{\tan \alpha_n}{\cos \beta} & (6.7) \\ M\ddot{y} + K_y y + C_y \dot{y} = F_t - G - K_m z & (6.8) \\ m\ddot{z} + K_m z + C_b \dot{z} = K_y y - nP - mg & (6.9) \end{cases}$$

where x, y, z – coordinates of motion; C_x, C_y, C_b – damping factors; K_m – total stiffness of bolts (K_b) and housing (K_h). The right part in formula (6.7) is a radial force in helical gearing; F_t – tangential force in the gearing; α_n – normal pressure angle of gear; β – helix angle of gear; n – number of bolts; P – bolt pre-load (tightening force).

Nonlinear stiffness with radial clearance is described as follows:

$$K_x = \begin{cases} K_x, \text{ if } \delta_x < \sqrt{x^2 + y^2} \\ 0, \text{ otherwise} \end{cases} \quad (6.10)$$

$$K_y = \begin{cases} K_y + K_m, \text{ if } \delta_y < \sqrt{x^2 + y^2} \le \delta_p \\ K_y + K_b, \text{ if } x\sqrt{+ y^2} > \delta_p \\ 0, \text{ otherwise} \end{cases} \quad (6.11)$$

The components of deformations projected on axes X and Y:

$$\Delta_x = \frac{x}{\sqrt{x^2 + y^2}} \left(\sqrt{x^2 + y^2} - \delta_x \right), \quad (6.12)$$

$$\Delta_y = \frac{y}{\sqrt{x^2 + y^2}} \left(\sqrt{x^2 + y^2} - \delta_y \right), \quad (6.13)$$

where δ_x, δ_y – initial clearances in the bearing; $\sqrt{x^2 + y^2}$ – shaft displacement from the initial position; $\left(\sqrt{x^2 + y^2} - \delta_x \right)$ – bearing deformation.

The absolute value of the reaction force in the gearbox support is:

$$R = \sqrt{F_x^2 + F_y^2}, \quad (6.14)$$

where F_x, F_y – horizontal and vertical forces acting on the shaft.

The main mode frequency of shaft natural vibrations in the bearings supports:

$$f_n = \begin{cases} \frac{1}{2\pi}\sqrt{\frac{K_y + K_m}{M}}, & if\ y < \delta_p \\ \frac{1}{2\pi}\sqrt{\frac{K_y + K_b}{M}}, & if\ y \geq \delta_p \end{cases} \tag{6.15}$$

During the period of rising load on the working tool (digging phase of a mining machine, slab biting in rolling mills), the reaction on the bearing of each transmission element depends on the radial gaps (including installation clearances and wear) and bolt loosening (weak tightening). In this case, the greater the radial clearance, the greater the amplitude of the vibration and phase shift at the natural frequency of radial oscillations of the shaft. These features are common for piecewise linear systems and can be used for the diagnostics of bearings and bolted joints.

6.3.2. Calculations by a dynamical model

The parameters for dynamical model simulations are taken from the investigated gearbox specification. Gears meshing angles $\alpha_n = 20°$, $\beta = 33°$, the input shaft mass $M = 1570$ kg; four (2 per side) double row tapered roller bearings 2097960 SPZ (300 × 420 × 160 mm); six bolted studs $M48 \times 800$ mm per every support, housing cover mass is $m = 940$ kg. The stiffness of housing $K_h = 1.480 \times 10^9$ N/m; bearing $K_y = K_x = 1.544 \times 105$ N/m; bolts $K_b = 7.509 \times 10^8$ N/m. Pre-loading of bolted studs varied from 20% and up to 70% of the proof stress in the range of elastic deformation of steel.

The solutions for the system of differential equations were obtained by the 4th-order Runge–Kutta method of numerical integration with a constant time step. Results of the dynamical model simulations are shown in Figure 6.15. The time series of torque and vibration show similar behaviour (Fig. 6.15a) because the increase of torque corresponds to the vertical motion of the input shaft and shocks into the upper cover. The trajectory of the shaft centre of mass motion in the case of the radial clearances ±1 mm in the bearing is represented in Figure 6.15b. The trajectory parts beyond the solid line circle correspond to elastic deformation, while shocks with amplitudes beyond the dotted line cause the unrecoverable plastic deformation of the bearing elements (rings, rollers). The trajectory of shaft motion may be irregular and depends on many parameters,

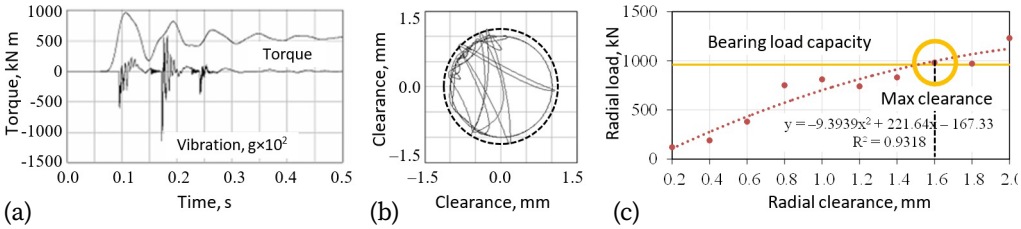

Fig. 6.15. Results of simulations in the time domain:
(a) torque and vibration; (b) trajectory (orbit) of shaft centre of mass motion;
(c) dependence of maximum radial load in the bearing on radial clearance

but the main factor is the radial clearance. Applied forces cause dynamic inclination of the shafts during the transient oscillations within the radial gaps, uneven distribution of instantaneous contact loads on the gears' contacts and their failure. The reasonable value of total clearance (about 1.6 mm) for undertaking maintenance actions can be determined from Figure 6.15c. It corresponds to the recommended bearing specification dynamic load capacity.

The same representations of radial clearance effect on the dynamic loading can be built for the bolt studs following their cross-section and yield stress of material to determine a reasonable moment of their replacement taking into account the accumulated plastic deformation (number of tightening).

Maintenance staff, performing online vibration monitoring or scheduled manual measurements of the shaft supports in the gearboxes, establish the tendency of the main natural frequency, amplitude and phase changes. On this basis, they predict the wear of bearings and decide on the maintenance actions, namely, bolts' tightening and bearing replacement, i.e., to serve the equipment by its real technical condition. The successful implementation of the proposed method of diagnostics into the maintenance practice involves the following steps:

1) Determine the approximate range of natural shaft oscillation frequency in the supports by the model (in our case, the natural frequency changes within the range 71–123 Hz).
2) Determine the initial clearance in the bearing during its installation on the shaft with calibrated probes or take the value from the bearing specification.
3) Perform vibration measurements on the bearing supports of transmission shafts and build the amplitude-frequency and phase-frequency diagrams.

4) Determine the natural frequency f_n of the shaft oscillations and its higher harmonics ($2 \times f_n$, $3 \times f_n$) by using the measured vibration signal in the pre-calculated range.
5) Determine the change of natural frequency, amplitude and phase at its higher harmonics by comparing the values in the previous measurement and the trend graphs.
6) Determine the wear (radial gap) in the bearing by the small change of natural frequency, the amplitude and phase at the natural frequency and its higher harmonics (<10%).
7) Determine the opening of the bolted joint by the significant decrease of natural frequency, amplitude and phase at the natural frequency and its higher harmonics (>10%).
8) Carry out the tightening of the bolts in the bearing supports and continue vibration measurements.
9) If the natural frequency, amplitude and phase at the natural frequency and its higher harmonics have not returned to the previous measurement values, replace the bolts and continue vibration measurements.

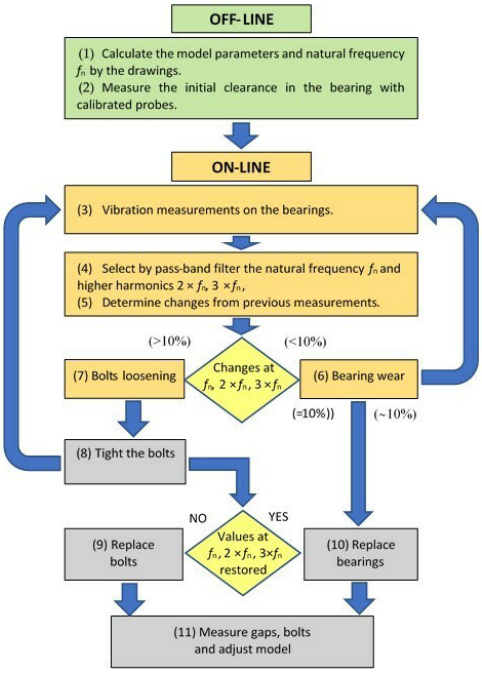

Fig. 6.16. Algorithm of radial clearances and bolts loosening diagnostics

10) If the natural frequency, amplitude and phase at the natural frequency and its higher harmonics have not returned to the previous measurement values, replace the bearing.
11) Determine the final radial clearance of the bearing after its replacement and adjust; if necessary, the previously obtained relations of the natural frequency, amplitude and phase at the natural frequency and its higher harmonics by the measured gap size to increase the accuracy of diagnosis.

The schematic representation of the diagnostics algorithm is given in Figure 6.16 along with the corresponding numbers of the steps from the description. Unlike the ISO 10816 standard, which is based on absolute values of vibration velocity to estimate condition, in heavy-duty gearboxes, comparing changes from the previous measurement is a more suitable approach.

The difference of 10% for recognition between bearing clearance and bolt loosening is derived experimentally by signal observation. It is valid for the investigated class of heavy-duty gearboxes and recommended to maintenance staff who inspect drivelines and measure vibrations every 3–4 days because of a high risk of failures. In the case of a permanent vibration monitoring system, this value can change by about 1.0–1.2% per day which corresponds to quick bolts loosening. After bolt tightening, vibration amplitudes are usually reduced by 8–10%. The wear of bearings and radial clearances contribute to gradual changes in the vibration amplitudes. For example, a change in natural frequency by 10% corresponds to a 20% stiffness change in the bearings, which can develop over several months.

This algorithm can be modified or adapted depending on maintenance practice in a given industrial plant or machine type, e.g., when bolts and bearings are replaced separately. In this case, the algorithm is applied individually for every shaft support.

To implement the model-based diagnostics, it is enough to have standard vibration sensors installed on the bearing supports of transmission shafts. Then, systematic measurements of vibration signals are conducted during the rising input load on the working tools of the machine and values of radial clearances with wear in bearings and bolted joints opening are determined. This is a principal distinction of the proposed method from the known approaches where a non-stationary (cyclically stationary) signal is interpreted as having a comparatively small deviation of average and dispersion in rotor velocity or loading. Instead, here the transient signal is used for diagnostic purposes and its spectral analysis is conducted in the range of natural frequencies but not the kinematic frequencies.

Since the natural frequencies of free oscillations do not change during the repairs and replacement of shafts, the proposed method has a higher noise immunity compared to the known methods of diagnostics at kinematic bearing frequencies. For the recording and analysis of the transient vibration signals, triggering signals of mechanical torque in the transmission or electrical motor current (taking into account the time delay of its response) can be used in condition monitoring systems.

6.3.3. Industrial trials

The method is tested in production conditions on a continuous hot rolling mill with the work rolls driven through the gearbox and the pinion stand. Experiments are conducted using Industrial ICP® accelerometers for permanent installation PCB 603CX1 (sensitivity 100 mV/g, amplitude range ±50 g) and line-powered signal conditioner PCB 482A22. Data is acquired by a National Instruments 16-ch 14-bit PCI-6071E ADC card and our software with a sampling frequency of 2 kHz. The sensors were vertically mounted by a screw stud on a magnetic base for curve surfaces PCB 080A133 (force 378 N) on the bearing supports of the input shaft of the gearbox. In parallel to vibration, the torsional load was measured on the motor shaft with the telemetry torque meter. Angular clearances in the driveline were also measured by the developed method and device.

The investigated 1-stage gearbox is shown in Figure 6.17a. The bearings loading of gearbox shafts depends on gearbox design (helical or spur gears, power

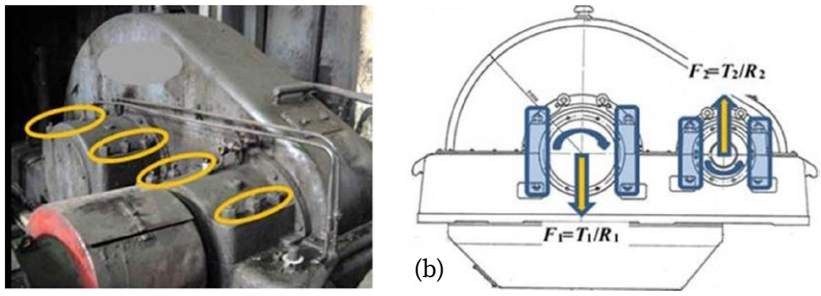

Fig. 6.17. Industrial heavy-duty gearbox: (a) bolt studs joints; (b) bearing supports with applied torques and forces provoking shafts transient motions

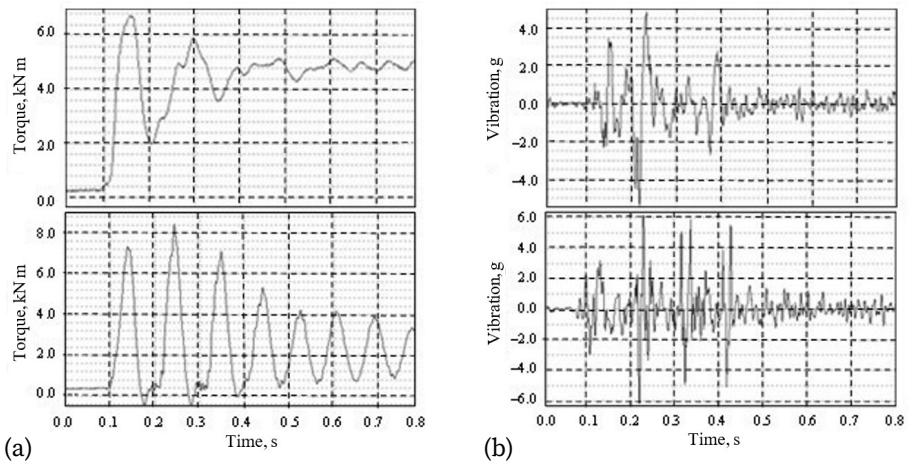

Fig. 6.18. Measurements on two different gearboxes:
(a) torque in the motor shafts and (b) vertical vibration on the bearing supports

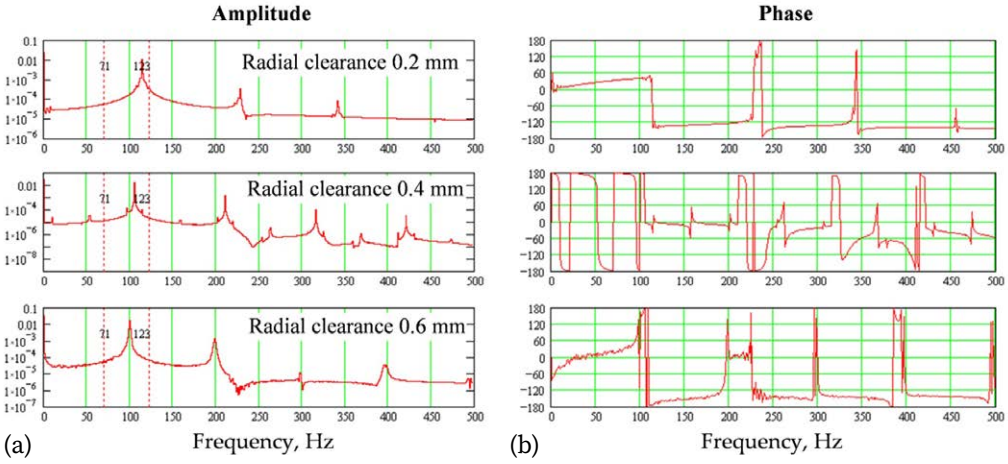

Fig. 6.19. Shaft vibrations depending on the radial clearance in the bearings
(without opening the bolted joints): (a) amplitude; (b) phase

paths), shaft position over stages, and the direction of shaft rotation concerning applied torques (Fig. 6.17b).

The extremely high dynamic regimes of this gearbox working in the transmission of the industrial plant require frequent (once every several days) main-

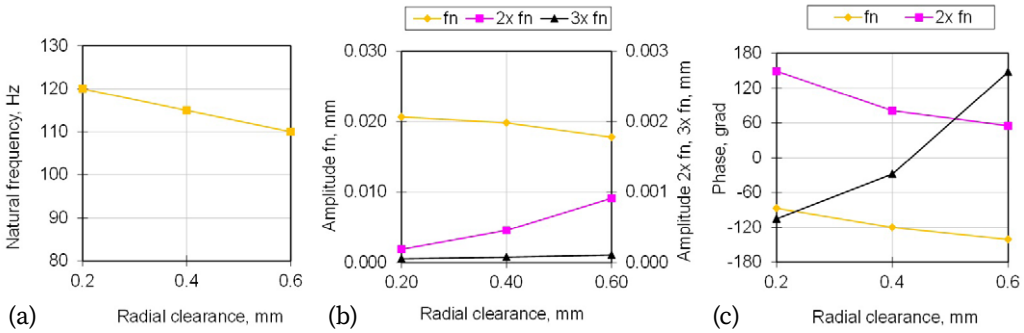

Fig. 6.20. Parameters of transient vibrations of gearbox shaft (without the bolted joint opening): (a) natural frequency; (b) amplitudes; (c) phases of harmonics

Table 6.1. Results of vibration measurements (Fig. 6.20)

Trial No.	Clearance, mm	Natural frequency harmonics, Hz	Amplitude, mm	Phase, grad
1	0.2 (measured)	$1 \times f_n$ – 120	0.020684	−87
		$2 \times f_n$ – 240	0.000189	149
		$3 \times f_n$ – 360	0.000054	−105
2	0.4 (predicted)	$1 \times f_n$ – 115	0.019850	−120
		$2 \times f_n$ – 230	0.000457	81
		$3 \times f_n$ – 345	0.000078	−28
3	0.6 (predicted)	$1 \times f_n$ – 110	0.017818	−141
		$2 \times f_n$ – 220	0.000913	55
		$3 \times f_n$ – 330	0.000108	148

tenance actions for bolt stud tightening, especially on those bearing supports where shafts move from the bottom idle position to the upper position (the input shaft in our case).

Bolt stud joints of shafts are subjected to creep and elongation although their nuts are fixed by the second nuts on the top and with split pins on the bottom. Sometimes, fixing nuts are welded to each other by rods. Bearings quickly deteriorate due to the brinelling of rings and rollers under shock impacts from the gear shaft. Another problem is the contact load redistribution in gearbox cou-

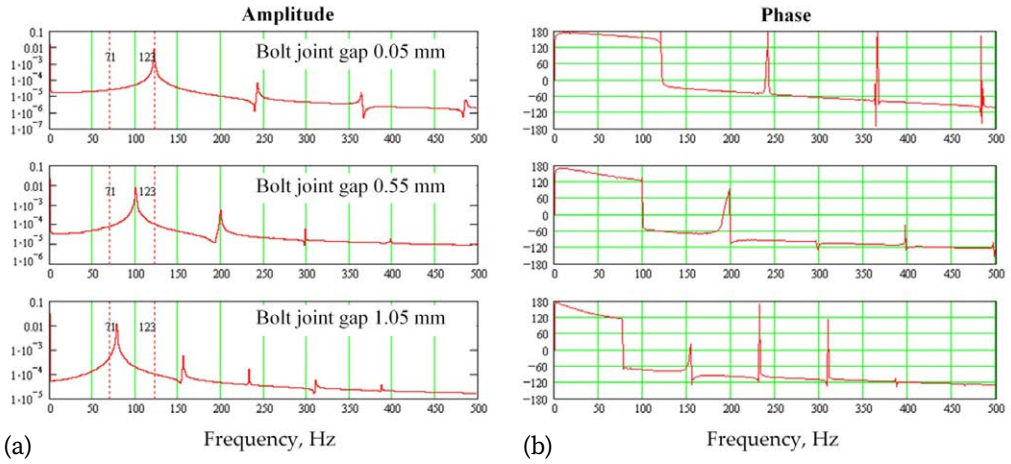

Fig. 6.21. Shaft vibrations depending on the radial clearance in the bearings (with opening the bolted joints): (a) amplitude; (b) phase

plings over the teeth length with subsequent cracks appearing at the end edges of teeth.

Several series of measurements were performed at intervals of one month at the same levels of technological load. Exemplary results of torque and vibration measurements conducted on the motor shafts of two gearboxes are shown in Figure 6.18. When analysing the transient processes in the gearboxes, it was found that the dynamic response of the shafts depends on the direction of their rotation. The maximum vibration is observed where the shaft gravity force and the total force applied from gear coupling are acting in opposite directions. The torsional load pulse causes the shafts to move within the radial clearance during the transient mode of motion to the steady position.

Usually, the calculated natural frequencies of the shaft lateral vibration are higher (100–400 Hz) than the natural frequencies range of the torsional system (10–30 Hz). Therefore, the radial gaps in the bearings distort the torsional vibration signal by the high-frequency components near or slightly above the idle torque level. In the case of minimal radial clearances, or when the shaft stays down in the bearing under load, the radial reaction to the torsional load repeats the patterns of the torque signal on the corresponding shaft.

After each series of measurements, the amplitude-frequency and phase-frequency diagrams of the vibration signal were plotted in the low-frequency range

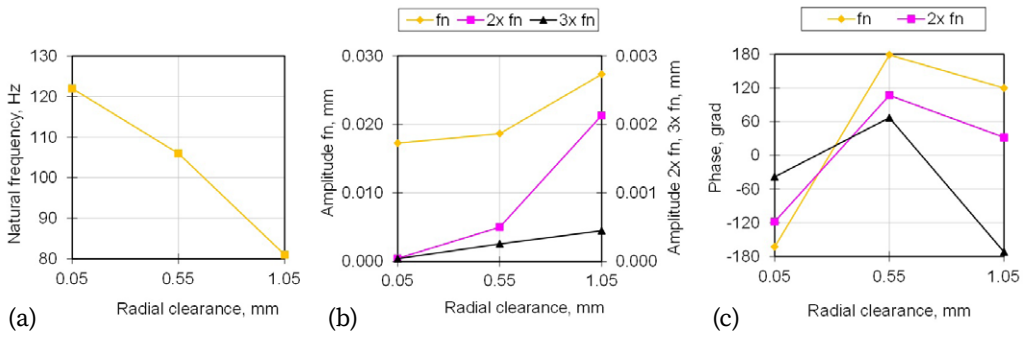

Fig. 6.22. Parameters of transient vibrations of gearbox shaft (with the bolted joint opening due to plastic elongation): (a) natural frequency; (b) amplitudes; (c) phases of harmonics

Table 6.2. Results of vibration measurements (Fig. 6.22)

Trial No	Clearance, mm	Natural frequency harmonics, Hz	Amplitude, mm	Phase, grad
1	0.05 (predicted)	$1 \times f_n$ – 122	0.017270	−163
		$2 \times f_n$ – 244	0.000045	−118
		$3 \times f_n$ – 366	0.000041	−38
2	0.55 (predicted)	$1 \times f_n$ – 106	0.018658	179
		$2 \times f_n$ – 212	0.000500	107
		$3 \times f_n$ – 321	0.000258	67
3	1.05 (predicted)	$1 \times f_n$ – 81	0.027319	120
		$2 \times f_n$ – 162	0.002131	32
		$3 \times f_n$ – 243	0.000450	−172

of 500 Hz. Results of the measurement series No. 1 are shown in Figures 6.19 and 6.20, and Table 6.1. The increase in the bearing wear (radial gaps) occurred from the minimum installation value (0.2 mm) to the maximum (0.6 mm). Graphs of the amplitude and phase diagrams of vibration with different wear (radial clearance) in the bearing without opening the bolted joint are shown in Figure 6.19.

The natural frequency in Figure 6.20 has a linear dependence on the gaps in the bearing support. The amplitude and phase of oscillations at the natural fre-

quency and its higher harmonics are close enough to the linear dependence but have a different (proportional or inversely proportional) character on individual harmonics, which is used to increase the reliability of the method.

In the course of gearbox operation, the amplitude of the shaft oscillations gradually changed and the bolted joint opening increased from the minimum value (about 0.05 mm) to the maximum (1.05 mm) when bolts may break due to plastic elongation and loosening. Results of the measurement series No. 2 are shown in Figure 6.21 and 6.22, and Table 6.2. Figure 6.21 shows graphs of the amplitudes and phases of vibration dependence on the wear (plastic elongation) of the bolts with the opening of the bearing bolted joint.

In the measurement series No. 1, the gap in the bearing was quite small (natural frequency about 123 Hz), but during the subsequent period of operation, there were large changes in natural frequency, amplitude and phase of oscillations (greater than 10%) that indicated the deterioration of fastening bolts.

The required tightening was performed, but in the next measurement No. 3 the natural frequency, amplitude and phase did not change relative to the values in the previous measurement No. 2, therefore the fastening bolts were completely replaced. The only available measurement parameter after the replacement of bolts is their elongation, which was about 5%, i.e., beyond the elastic limit, hence, plastic deformation is accumulated as a result of their multiple previous tightening.

Based on the experimental trials, the developed mathematical model is calibrated by the frequency of shaft natural vibrations. For this gearbox with a new gear shaft including new bearings and bolted studs, the natural frequency of shaft vibrations is about 123–125 Hz.

To calibrate the dynamical model, the manual adjustment of parameters is used without reverse estimation procedures. This approach is justified by several factors:

- Only the main mode of shaft free vibrations is used for diagnostic purposes and, since the masses of components are exactly known from gearbox specifications, the stiffness is a single parameter for calibration.
- Frequencies of torsional and radial free vibrations are quite different and do not interfere in the spectrum, hence, simple pass-band filtering is enough for their separation during the vibration signals analysis.
- The bearing stiffness changes slowly over months, but the bolted joint stiffness can change in a few days or a week, as in our case; therefore, these parameters can be distinguished.

The opening of the bolted joints causes greater changes in natural frequency than the wear of the bearing, as well as the amplitude and phase at the natural frequency and its higher harmonics. In the period when the bearing support has a large gap, but the opening of the joint is not yet developed, the accuracy of its definition is not high. However, for up to one week (or earlier) from the start of the joint opening, the gap in the joint continues to increase faster than the wear in the bearing, and it can already be accurately diagnosed by the proposed method.

Diagnostics of bearings clearances is most important for industrial plants and machines where the radial load or dynamic imbalance of shafts is comparable to their weight, i.e., shafts can move up and down inside the gaps from the initial idle position. The issue of diagnostics is that the gaps (opened part of clearances) of rolling bearings become closed when loading torque is applied to the driveline and they do not expose themselves in any way, although, they can increase torque amplification factor (TAF) up to 3–5 and cause bearing overloading.

In contrast to kinematic frequencies, natural frequencies are not changed with the speed of the drive (except high-speed turbines with journal sliding bearings). High amplitudes at these frequencies appear only during the torque increase on the machines and reflect the wear of bearings. Therefore, the diagnostics of clearances can only be efficient during transient periods of loading.

The main natural frequency of shaft radial oscillation can be determined by the standard vibration sensors. Preliminary band-pass filtering can be applied in the range of shaft natural frequency pre-calculated by the dynamical model. There is a fairly stable and narrow range of natural frequencies; therefore, the automatic realization of this method may not be difficult in the data processing software.

In the case where one or more kinematic frequencies match the natural frequency range, the proposed method is difficult to implement, but it has an additional positive effect–plant personnel can determine potentially dangerous resonant oscillations in the gearboxes. This is the reason to change the operational speed of the machine or the design of the bearing support.

Angular clearances in the driveline always result in an increase in torsional dynamics and the appearance of high-frequency components in the signals of torque and vibration that can mask local defects in bearings or gear meshing. Therefore, signal recording for local defect detection (spalling, cracks) by means of the traditional methods should be carried out by using logic triggering beyond the transient periods.

Radial clearances in the supports have a great effect on the driveline system dynamics and change parameters of torsional vibrations (frequency, amplitude, and phase) even if the angular clearances are sufficiently small or the gaps are closed under load. Therefore, in heavy-duty gearboxes, when analysing vibration signals, it is necessary to account for the ratio of the shafts' gravity forces, shaft position in the gearbox stages, direction of rotation and torque magnitude when certain shafts may lose contact with the support during input load fluctuations.

A complex criterion of heavy-duty machine strength capacity and reliability should include teeth bending stress increasing under the action of torsional and lateral shaft oscillations in the bearing supports with radial clearances and potential bolt joint opening.

6.4. Diagnostics of bolts loosening in the sieving vibrating screens

The diagnostics of any elements in vibrating machines, e.g., bearings and springs, is associated with significant issues related to cyclo-stationary signals processing with additional impulsive non-Gaussian noise from the falling pieces of material. One of the important elements of vibrating machines, e.g., sieving screens, are the bolts joining the decks to the machine housing. The tightening or replacement of cracked bolted joints requires machine stoppage that interrupts the whole technological chain of bulk material transportation with the engagement of a large workforce and time spent on repair.

According to the vibrating screen maintenance recommendations of equipment producers (Table 6.3), the bearings of vibrators and sieves mounting joints are the most frequently inspected units, which means they are highly susceptible to failures and malfunctions. This is confirmed by the real repairs data analysis (Fig. 6.23). Bolts, drives, bearings and sieves constitute 72% of all the issues that happened during the vibrating screen operation.

At the design stage, by using the discrete element method (DEM) and the finite element method (FEM), the natural modes of the screen can be analysed to confirm minimal structural stresses and required trajectories of bulk material motion. However, these approaches need significant computing resources. Also, a statistical distribution of material fractions in the input flow, particle configuration, and a detailed 3D model of the screen are required.

What is more important, the parameters of bolted joints change in the course of machine operation and maintenance (structural steel deformation and tight-

Table 6.3. Maintenance periods for vibrating screen elements

No.	Action	Maintenance period				
		50 h	week	month	year	2 years
1	Lubrication of vibrator bearings	■				
2	Control of sieves mounting joints		■			
3	Control of sieves and vibrators			■		
4	Control of springs			■		
5	Control of belt drives			■		
6	Inspection of sieves wear				■	
7	Inspection of drives				■	
8	Inspection of vibrators					■

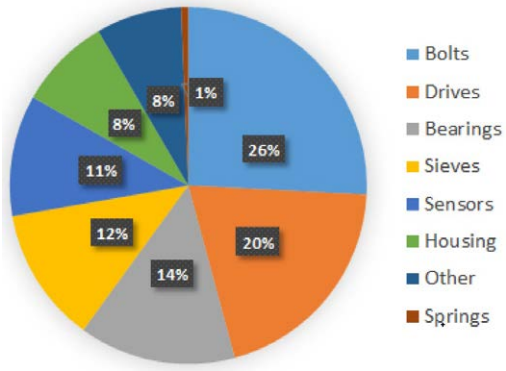

Fig. 6.23. Statistics of elements' failures in vibrating screen

ening torques are unknown). The appearance of clearances between the massive parts of vibrating machines may be thought to be the most critical but hidden for measurement operational parameters due to their significant impact on the lifetime and reliability of the vibrating screens.

6.4.1. Dynamical model of vibrating screen with bolted joints

For the analysis of bolted joints loosening in a vibrating screen, the 2-DOF dynamical model is developed [409], whose calculation scheme is represented in

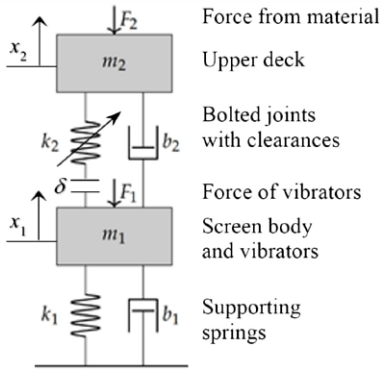

Fig. 6.24. The calculation scheme of the vibrating screen with the upper deck as a separate mass

Table 6.4. Parameters of the 2-DOF dynamical model of the sieving screen

Parameter	Value	Units
Mass of screen body, m_1	15 000	kg
Mass of upper deck, m_2	5 450	kg
Stiffness of supporting springs, k_1	0.56×10^7	N/m
Stiffness of bolted joints, k_2	1.46×10^8	N/m
Damping in supporting springs, b_1	10	s^{-1}
Damping in bolted joints, b_2	10	s^{-1}
Clearance in bolted joints, δ	$0.0...1.2 \times 10^{-3}$	m

Figure 6.24 and its parameters are in Table 6.4. The separation of the second mass corresponding to the upper deck is quite justified because its weight is usually about 3–5 t or 20–30% of the total weight of the screen.

The severe abrasive wear of beams will reduce the mass of the deck, while upper deck blinding with a near mesh size material can increase the weight of vibrating mass (Fig. 6.25). The mass of the deck depends on the mass of the sieved material at every moment. The further calculations concern only those bolts that fasten the upper heavy deck to the screen structure to restrain its vertical displacement, The other bolts loosening in side panels is related to other natural modes of the screen structure.

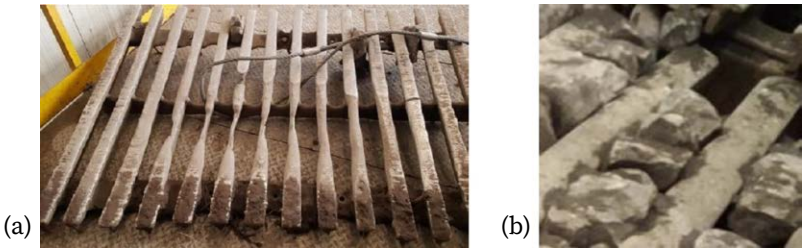

Fig. 6.25. The upper deck of vibrating screen:
(a) abrasive wear of beams; (b) blinding with a near mesh size material

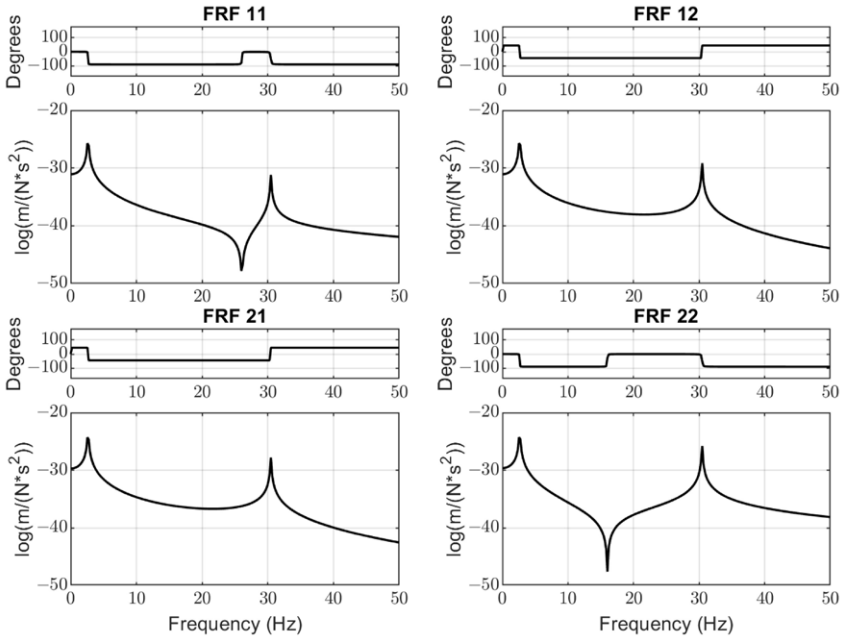

Fig. 6.26. Frequency Response Functions (FRF)
of the vibrating screen by the four channels

The modal analysis of the vibrating screen included the building of Frequency Response Functions (FRF). Taking into account that the total exciting force from both unbalanced vibrators acts on mass m_1 and impacts forces from the falling pieces of the material act on the mass m_2, the following four channels are analysed (Fig. 6.26):

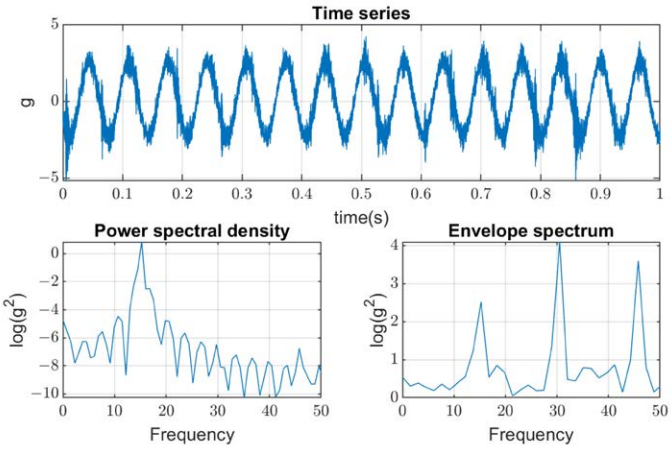

Fig. 6.27. Spectrum with higher harmonics of main frequency (15 Hz) of vibration measured on the bearings of inertial vibrators

- FRF_{11}: from vibrators' force F_1 to the displacement of mass m_1;
- FRF_{12}: from vibrators' force F_1 to the displacement of mass m_2;
- FRF_{21}: from material impacts force F_2 to the displacement of mass m_1;
- FRF_{22}: from material impacts force F_2 to the displacement of mass m_2.

The exact values of natural mode frequencies of vertical vibration are as follows: 1st mode – 2.6 Hz; 2nd mode – 30.5 Hz. Functions FRF_{11} and FRF_{22} have anti-resonance frequencies of about 26.2 Hz and 16.1 Hz, respectively. This means that the working frequency of vibrators should be at least ±5 Hz from the minimum point of FRF_{11} to avoid inefficient energy consumption by the electrical motors of vibrators.

While the first mode of vibration is mainly determined by the design parameters of the screen (total mass and stiffness of springs in the supporting units), the second mode of the screen's natural vibration depends on several factors. The most important factor is the gradually changing stiffness between mass m_1 and mass m_2, which greatly depends on bolted joints' condition (tightening and axial plastic deformations). The mass of sieved material on the screen decks has less influence on the second vibration mode.

The data obtained from the permanent vibration monitoring system show that the spectrum of excitation force measured on the bearings of the vibrator shaft contains higher harmonics (30 Hz, 45 Hz) at certain periods of screen op-

eration. This feature corresponds to the bad condition of one or several bearings or supporting springs (Fig. 6.27). After maintenance actions were undertaken on the screen, those higher harmonics disappeared, which proves their origin. Measurements of vibration in the four corners of the main screen housing on supporting springs showed that it vibrates as a rigid body. Hence, even one bearing with damaged rings or having excessive clearance can generate not only 15 Hz but also 30 Hz and 45 Hz harmonics and excite the second natural mode with increased tension in the bolted joints. Since the maintenance of bearings and bolted joints have different periods, this process can occur at any time of operation that requires new methods of damage detection in the condition monitoring system.

6.4.2. Simulation of the bolts degradation process

The vibrating screen simulations are conducted in several aspects. Firstly, the periodical excitation is applied to mass m_1 by the real forces acting in the industrial screen. Three cases are considered: (1) when bolts are tightened (linear stiffness k_2); (2) when the amplitude of vertical forces is beyond the yield stress of bolts material; and (3) when the clearances appeared with joints opening, which produces additional impacts on the bolted joints (nonlinear stiffness k_2) and their further quick degradation until the breaking. Results of simulations are repre-

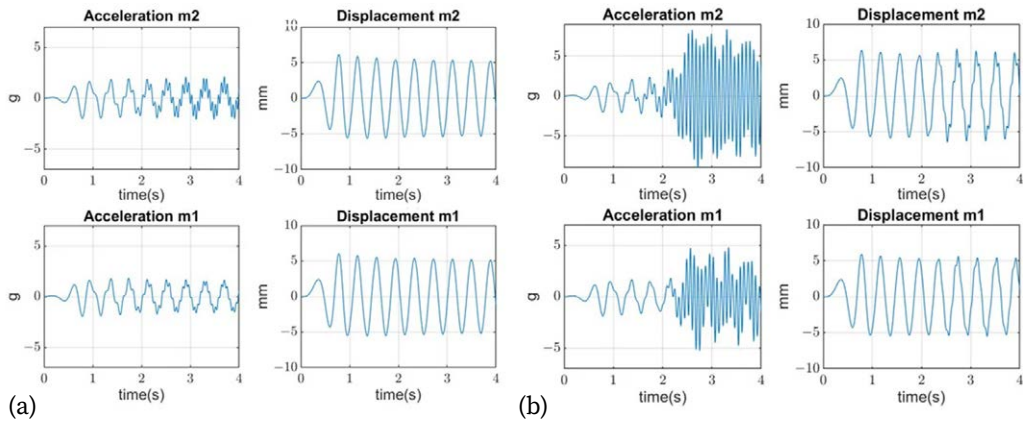

Fig. 6.28. Simulation of 2-DOF screen vibrations: (a) with bolted joints tightened in a good condition; (b) with bolted joints opening at high amplitudes of forces

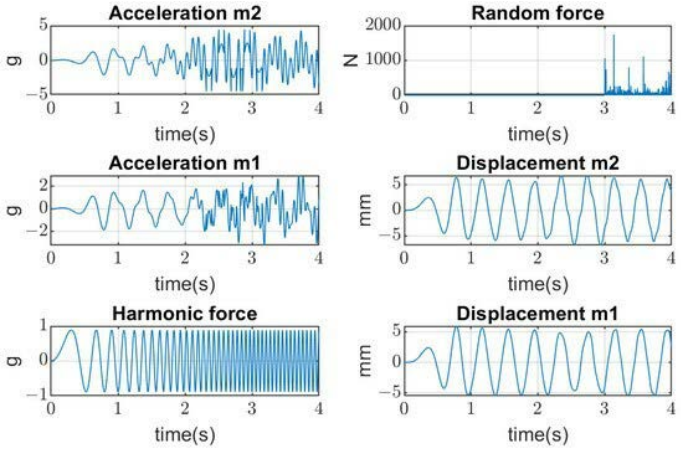

Fig. 6.29. Vibrations of the screen with application of random force resulted from stochastic non-Gaussian impacts of sieved bulk material falling on the upper deck

sented in Figure 6.28 where amplitudes of both masses in the time domain are represented. The values of the mass m_1 displacement are verified by the real data of measurement (about 5–8 mm).

At the second stage of simulations, the stochastic impacts are applied to the mass m_2 generated by the falling pieces of material, which have non-Gaussian distribution. The transient processes of the mass m_2 vibration (not measured) and mass m_1 (measured) are represented in Figure 6.29.

The mechanism of bolted joints loosening can be explained as developed in several steps and influenced by several factors. Since the nuts on the bolts are fixed by welding, we do not consider the trivial case of their loosening by rotation.

Firstly, bolts work within the linear deformation range. Later, during the initial period of deterioration (1–2 days), bolts experience periodic forces from the vibrators and in the case of additional impacts from materials the natural modes are excited and the amplitude of force reaches the yield stress of bolts material.

Then, residual plastic deformation increases and the amplitude of the second mode increases, too (out-of-phase upper deck motion). In the case of simultaneous defects or excessive clearances in the bearings of vibrators, the higher harmonics appear in the spectrum of excitation force, which greatly increases amplitudes of the second mode, hence, loading on the bolts. Finally, bolted joints provoke contact disintegration of the upper deck with the places of mounting on

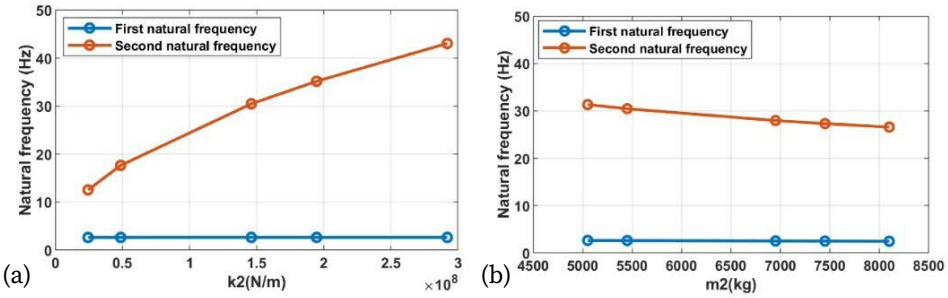

Fig. 6.30. Dependence of the natural modes frequencies on the:
(a) stiffness of bolted joints k_2; (b) mass m_2 of upper sieving deck

the screen. The next stage is bolts cracking beyond the ultimate stress of the steel material they are made of.

The upper deck of the screen consists of three sections with similar masses. Every section has different angles of inclination (banana screen) and different amplitudes of vertical components of forces. Therefore, the above-mentioned stages of bolt condition worsening will develop asynchronously requiring even more frequent maintenance actions. The bolts loosened in one section will have an impact on the other two sections. Hence, scheduled maintenance is better when conducted for the whole set of bolts on all the sections of the upper deck together.

A possible remedy against the frequent maintenance stoppages due to failures of bolted joints may be an implementation of the special damping pads made of polyamide or other elastic durable material. Their size should be calculated to achieve the stiffness required to tune out the second mode frequency from the main frequency of excitation (15 Hz) and its higher harmonics. The dependence of the natural frequencies on the k_2 stiffness is given in Figure 6.30. By our preliminary assessment, the stiffness of bolted joints should be reduced by 1.5 factor (on both sides of a joint) to solve this problem.

Based on the results of simulations, the modal parameters of the system should have high sensitivity to clearance in the bolted joints between two masses of the screen – the main body and the upper sieving deck. The dependencies of the first and second natural modes frequencies on the clearance in the bolted joints are shown in Figure 6.31a. In the range of small values of clearances (up to 0.5 mm), sensitivity is estimated at 25.6 Hz/mm. The sensitivity decreases for the larger values of clearances but remains high enough (about 7.3 Hz/mm) for prac-

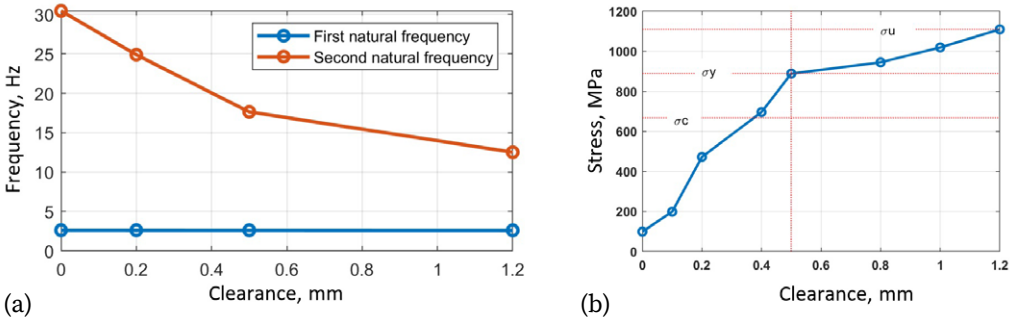

Fig. 6.31. The dependence of the (a) natural modes frequencies and (b) tensile stress of the bolts on the clearance in the joints

tical application. Since the excitation force is determined by the pre-installed eccentricity of the constant unbalanced masses of vibrators, the sensitivity will not be affected for a certain screen design and settings.

The results of dynamical model simulations are shown in Figure 6.31b, where the tensile stress of bolts is given concerning different clearance sizes. During the period of gradual deterioration, bolts are subjected to periodic forces from

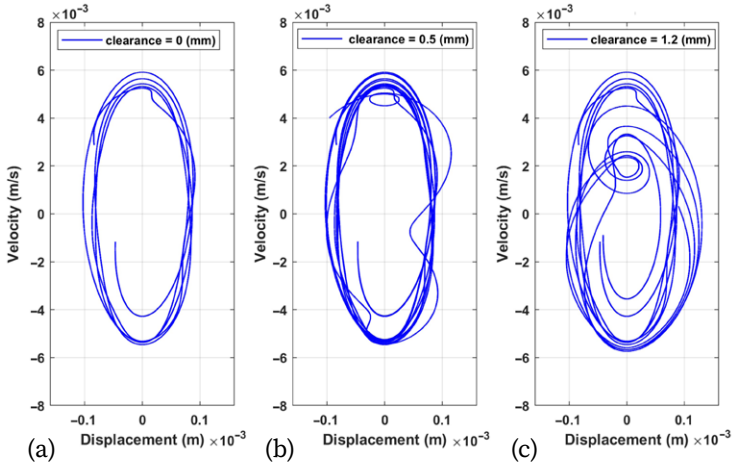

Fig. 6.32. Phase space plots of screen upper sieve (mass m_2) vibration for three cases of clearances: (a) normal state (0 mm); (b) moderated bolt looseness (0.5 mm); (c) critical bolt looseness (1.2 mm)

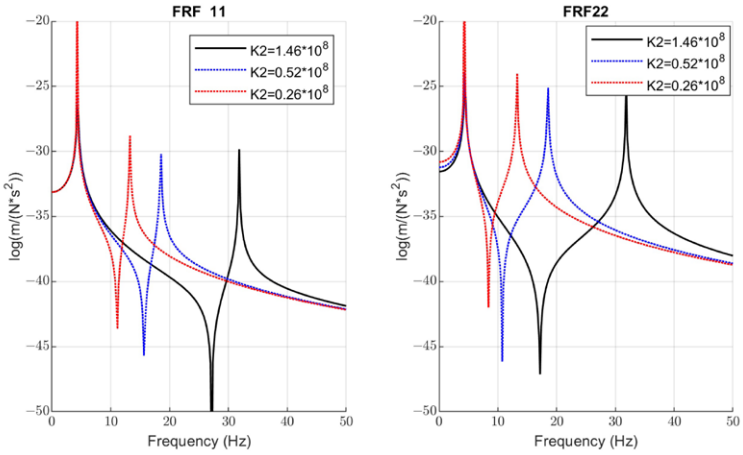

Fig. 6.33. The dependence of FRF_{11} and FRF_{22} on the bolts' stiffness k_2 (grades of loosening)

the vibrators, but the upper deck and the whole screen body still move in phase. At the next stage of degradation, the amplitude of the bolts' tensile forces reaches the yield stress σ_Y of the bolts' material, and plastic deformation appears, which creates gaps in the joints. With increasing clearances, the upper deck and screen body start to move out of phase, the ultimate stress σ_U is reached in some bolts, and failures occur.

The critical value of clearance is about 0.5 mm, above which the failure is unavoidable. In practice, with two accelerometers installed on the screen body and on the sieving deck, tensile forces (stress) can be easily calculated with relative displacements (deformation), which are then applied to the diagram. Such interpretation and visualization of the bolts' degradation process help the maintenance staff to undertake repair actions in time to prevent an abrupt failure and unplanned machine downtime.

For bolt looseness detection, the phase space plots (PSPs) are built (Fig. 6.32). Three cases are shown there–normal state (0 mm), moderated bolt looseness (0.5 mm), and critical bolt looseness (1.2 mm). The explicit changes in PSP are observable in the graphs, which are caused by the nonlinear characteristics of the bolted joints' stiffness when clearance appears.

The relations of FRF_{11} and FRF_{22} with the bolts' stiffness k_2 (grades of looseness) are represented in Figure 6.33. The anti-resonances observed on these

graphs are the distinctive features of a 2-DOF dynamical system. Their frequencies do not coincide with the vibrator rotations in the investigated screens; however, they allow a better understanding of how to avoid energy leaks. The greater stiffness (better tightening of bolts and their condition) corresponds to a deeper drop in amplitudes at these frequencies and greater energy leaks may occur. For the intermediate value of stiffness $k_2 = 0.52 \times 10^8$ (blue line on the FRF_{11} graph), the anti-resonance frequency (15.62 Hz) is very close to the vibrators' rotation frequency (15 Hz).

6.4.3. Laboratory trials

Since the measurements of bolt loosening and their regulation are almost impossible in industrial sieving screens, the experimental part of this research was conducted on the fully functional laboratory vibrating screen to demonstrate the possibility of bolted joint loosening detection by the vibration signals with the developed methods. Locations of the mounted sensors can be seen in Figure 6.34.

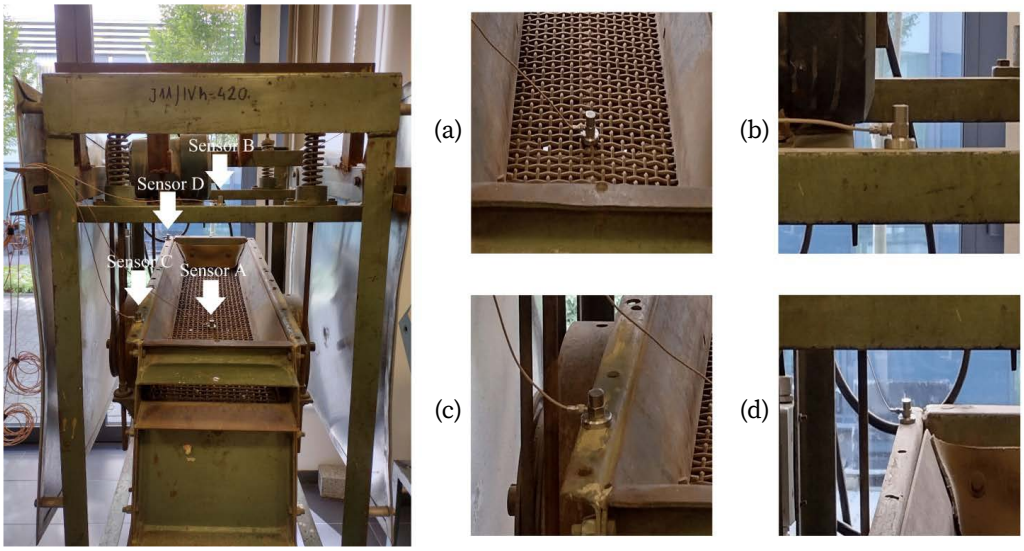

Fig. 6.34. The laboratory vibrating sieving screen with one inertial vibrator and bolted joints on the upper sieving deck; the sensors' positions: (a) sensor A – upper sieving deck; (b) sensor B – screen arm; (c) sensor C – bottom part of the screen; (d) sensor D – upper part of the screen

Three cases are investigated: normal state of bolted joints; one upper left screw is loosened; and two bottom screws are loosened. Parameters of signal processing are as follows: sampling frequency – 25 kHz; data length – 4 s (100 000 samples); frequency resolution – 0.25 Hz. The frequency of the first mode is about 4.2 Hz and the second mode is 16.7 Hz. In addition to the second mode frequency, the damping ratio was used in the same series of experiments as a diagnostic parameter of bolts loosening (Fig. 6.35).

Based on experimental data obtained on the laboratory screen, graphs of PSP are built for three cases and are shown in Figure 6.36. In the normal state, the

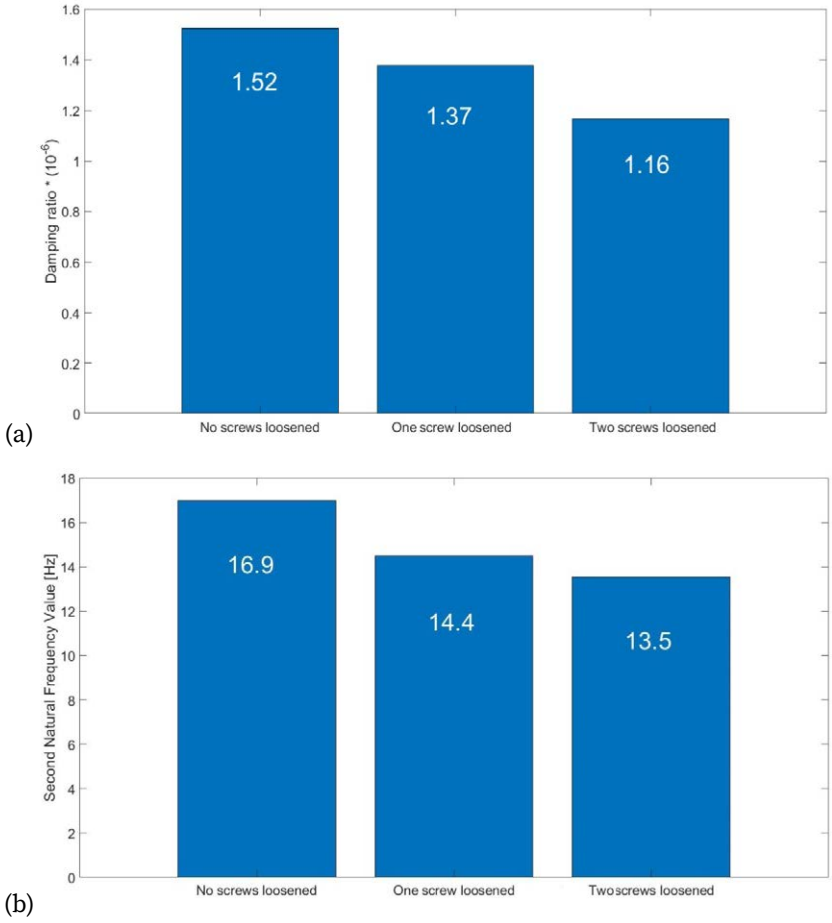

Fig. 6.35. The calculated values of diagnostic parameters in three investigated cases: (a) the 1st natural mode damping; (b) the 2nd natural mode frequency

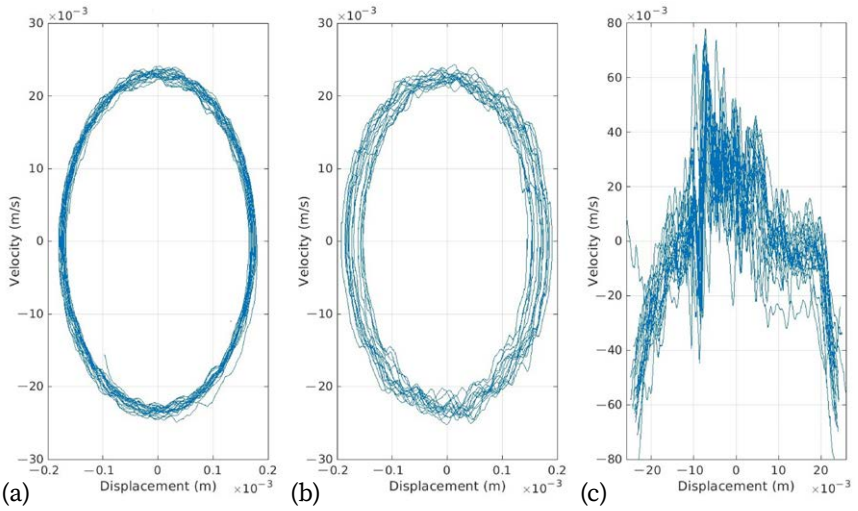

Fig. 6.36. Phase space plots generated on the data from three investigated cases: (a) normal state; (b) one bolt loosened; (c) two bolts loosened (critical state)

trajectory is characterized by minimal deviations. The second case with a weak looseness of only one bolt produces visible distortions in the trajectory of the upper sieving deck. The third case demonstrates the critical state (maximal looseness) of two bolted joints when the trajectory is fully irregular and transformed into unpredictable oscillations of high amplitude.

The numerical parameters of PSP graphs are given in Table 6.5. Any of them can be used as the diagnostic parameters of looseness or "health indicators" of bolted joints not only in the sieving screens but in other vibrating machines, too. Alarm levels can be clearly interpreted since the clearances always increase the amplitudes of vibrations

The gradual deterioration of bolts and appearing of clearances in the joints greatly increase the shock impacts produced by upper deck mass and further quick elongation of bolts. Therefore, their diagnostics and timely maintenance (tightening or replacement) are important for plant staff. Using higher classes of bolts' strength cannot solve the problem.

During the screen operation, maintenance personnel should periodically check the clearance of bearings in vibrators either manually (with dial micrometres or calibrated gauges) or by the signals of condition monitoring systems where it is reflected in the amplitudes of higher harmonics of rotation frequency.

Table 6.5. Parameters ($\times 10^{-3}$) of PSP shape based on the vibration signals

Parameters	Case (a)	Case (b)	Case (c)
D_{min}	−0.18	−0.19	−25.68
D_{max}	0.18	0.19	24.44
V_{min}	−24.60	−25.14	−79.57
V_{max}	24.10	23.97	77.99
$\Delta D = D_{max} - D_{min}$	0.36	0.38	50.12
$\Delta V = V_{max} - V_{min}$	48.70	49.11	157.56
$\Delta D \times \Delta V$	17.51	18.82	7897.11

A possible way to increase the maintenance interval on the existing screen is to introduce elastic pads on both sides of bolted joints. In this case, the stiffness tuning between masses allows the frequency of the second natural mode to shift from the frequency of the main excitation force and its higher harmonics.

In this research, only the bolts that fasten the upper deck to the screen structure are considered. The other bolts loosening, i.e., of the ones connecting side panels and reinforcement bars, is related to higher natural modes of the screen structure.

7. DYNAMICAL MODELS IN VIBRATION CONTROL OF INDUSTRIAL MACHINES

This chapter presents methods for dynamics control in different mining and metallurgical machines, which use specific features of their operation and available tools for measurement and control of drive speed and vibrations. Implementation of the developed methods showed a reduction of vibration amplitudes and overall dynamics for the achievement of higher performance and reliability of industrial machines.

7.1. Chatter vibration control in the tandem cold rolling mills

Chatter vibrations occurring in the high-speed cold rolling and tempering mills are currently intensively investigated because of a significant (by 25–30%) reduction in annual plant productivity and strip quality. The most advanced tendencies in this research area were discussed in [410, 411].

As previously noted, some approaches to chatter vibration research came from other metal treating operations (grinding, milling cutting, etc.) studies [412]. However, some aspects – namely regenerative chatter and its control – are still less reported. Stands interaction by the strip tension was analysed but not from the viewpoint of mill control. In addition, stands' synchronization due to roughness and thickness variation in the tandem mills was not investigated as an explicit cause of chatter amplification.

In practice, the only effective way to control chatter is a fast slowdown of mill by the vibration signals being monitored in special systems. However, the frequent speed drops reduce mill productivity and strip quality. Therefore, the main tasks for chatter control are as follows:

- Detecting chatter earlier, at least by 5 s before it comes to large amplitudes.
- Control stands interaction to prevent strip breaks due to tension in the tandem mill.

(a) (b) (c)

Fig. 7.1. (a) Hydraulic system of the rolling stand; (b) polyamide damping pads on the piston of backup rolls weight balancing cylinder; (c) on the work rolls chocks

- Damping chatter by the impacts of small amplitude (1–2%) to avoid disturbances.

Taking into account the above-mentioned tasks, the scope of research included:

- Passive vibration damping.
- Monitoring the speed-related kinematic disturbances.
- Natural frequencies and modes deviation in a multibody roll stack.
- Nonlinear relation of friction factor and rolling speed.
- Bearings vibration under roll bending conditions.
- Feedback loops and stands synchronization in the tandem mill.
- Chatter regeneration due to thickness variation.
- Monitoring of high-frequency thickness variation.
- Active chatter vibration control.

Passive vibration damping. It is widely used in different machines. The rolling stand hydraulics and rolls stack are represented in Figure 7.1a. Passive damping polyamide pads installed on the pistons of cylinders of backup rolls weight balancing system (Fig. 7.1b) and polymer liners on the work rolls chock (Fig. 7.1c) were proposed and tested to prevent horizontal shocks due to tension variation. However, such devices showed only about 10% efficiency in vibration amplitude reduction.

Monitoring the speed-related kinematical sources. It is a usual approach to vibration problem solving in any rotating machine. Methods of such vibration control consists in avoiding resonance ranges during plant operation including parametric excitation (gear couplings, cardan shafts and bearings). However, in

tandem mills, the number of possible sources of vibration is very big and different elements may have more or less importance in a short period (work rolls are changed every 3–4 hours). Besides, variation of natural frequencies and modes exists under the working conditions. Nevertheless, many cases of chatter elimination were reported based on mill maintenance improvement. For example, if an element vibration creates an integer number of periodic marks on a roll circumference, it becomes the source of vibration.

Deviation of natural modes due to strip properties. The different degrees-of-freedom models exist for chatter simulation in 4-high, 6-high, and 20-high mills. The chatter in the 3rd octave (about 120 Hz) appears only when the upper and lower pairs of rolls move symmetrically about the strip plane as shown by many authors. However, the influence of strip properties on mode deviation has not been studied enough. Vibration measurements in the tandem mill have been carried out with the accelerometers being mounted on every WR and BUR chock. Thin (0.6 mm) and thick (1.0 mm) strips have different modes of stack movement. Thin strip rolling corresponds to the main node in the roll bite, but the stiffness of the thick strip shifts the node out of rolls and strip contact that prevents chatter. A hardened strip corresponds to less damping in the roll bite. Experiments with the mill rotation under the working load and speed (rolls are pressed without the strip) have shown that vibration signals exhibit another pattern.

Nonlinear relation of friction factor and rolling speed. The dynamic model of friction-induced chatter vibrations includes parameters of technology and lubricant:

$$t_{oil}\left(v_R\right)=\frac{30+K_t v_R+t_R}{2}, \tag{7.1}$$

$$v\left(v_R\right)=v_{50}\left(1-1.3\sqrt{\frac{t_{oil}\left(v_R\right)-50}{t_{\max}-50}}+0.42\frac{t_{oil}\left(v_R\right)-50}{t_{\max}-50}\right), \tag{7.2}$$

$$f\left(v_R\right)=\frac{k_s\cdot\left(1+\left(0.4+0.01\varepsilon\right)\cdot Rz\right)}{1+0.25\cdot\sqrt{v\left(v_R\right)}-0.005v\left(v_R\right)}\left(0.07-\frac{0.1\cdot v_R^2}{2\cdot\left(1+v_R\right)+3\cdot v_R^2}\right), \tag{7.3}$$

where $t_{\max}$ – ultimate temperature of oil flash, K_t – roll surface temperature by speed relation factor, v_{50} – initial viscosity (at 50°C), Rz – WR surface roughness, ε – strip relative reduction, k_s – type of oil factor (synthetic or natural), t_R – cur-

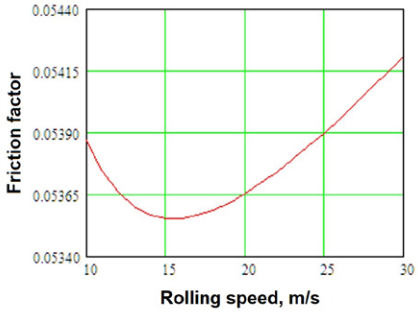

Fig. 7.2. Nonlinear dependence of friction factor
in the contact of *WR* and strip on the rolling speed

rent temperature of roll surface, v_R – linear speed of work roll. The calculation results obtained from the use of these formulas have shown (Fig. 7.2) that only roll surface temperature (t_R) may shift the minimum friction factor toward the higher speeds (15 m/s), while other parameters cause only vertical displacement of minimum value.

Chatter mostly occurs during the long coils rolling time (45 min) of thin strips (0.3–0.8 mm) when the roll temperature may exceed the limit of cooling emul-

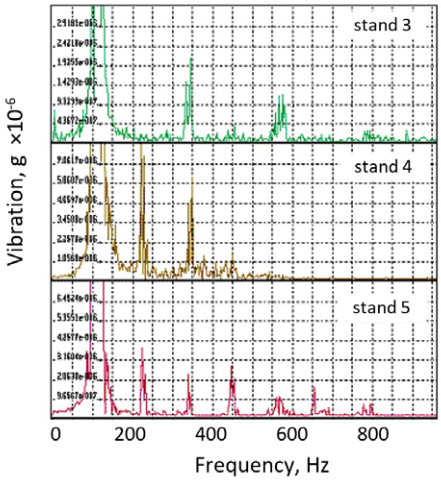

Fig. 7.3. Spectra of chatter vibrations in stands Nos: 3–5

sion degradation (150–200°C depending on its type) and cause instability in the mill. Therefore, it can be considered a bifurcation parameter of chatter.

The online control of WR temperature by pyrometers or based on observations is not reliable for chatter prevention. To identify contact friction instability and strip stiffness (hardening), the vibration spectra can be used, which are shown in Figure 7.3 for three different stands.

The observed spectrum patterns reflect the nonlinear features in the contact zone. The properties of the strip as an elastic-plastic element may be assessed by the harmonics of the main frequency. It is known that cubic nonlinearity gives odd harmonics (stand No. 3) and quadratic relation causes even harmonics (stands Nos. 4–5). Hence, odd harmonics (cubic curve) are rather related to the strip hardening, while even harmonics (curve with a minimum) characterise friction instability in the last stands.

Bearings vibration under roll bending conditions. It is a well-known fact that roll bearings in stands without a bending system (in the roughing stands of hot rolling mills) last twice longer than in stands with roll bending. It is due to work roll chock deformations under the maximum 900 kN of positive (up) and 450 kN of negative (down) bending forces. Deformation of chocks leads to bearing defects and vibration levels increasing. The periodic wear marks are observed on the roll necks and sliding bearings of BUR (Morgoil), which are caused by vibrations.

Calculations on the mathematical model (Fig. 7.4a) give sufficiently wide ranges of natural frequency deviation for the positive forces in the range of

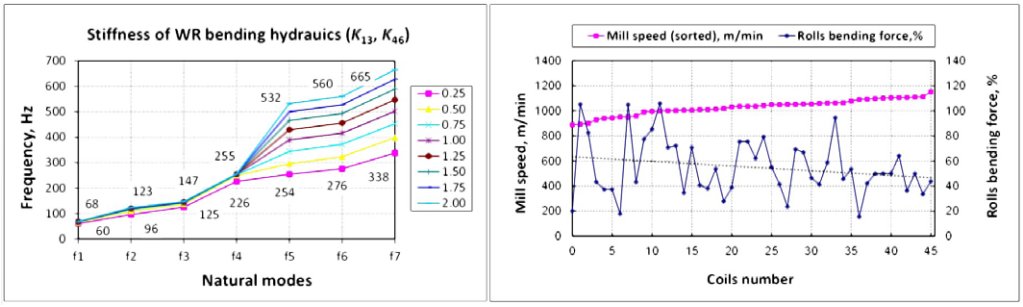

(a) (b)

Fig. 7.4. Influence of work rolls bending on:
(a) natural frequencies; (b) maximum rolling speed

+10...+100% (value 1.0 means +50% relative force level). That helps to understand difficulties with chatter identification during mill working as the natural frequencies shift remarkably. Statistical data processing showed that the available maximum mill speed is dependent on work rolls bending forces in the last three stands (Fig. 7.4b).

The experiments have been conducted without the strip in the mill and with the work rolls bending force changing in stand No. 3 (only positive bending) and stand No. 4 (with both bending directions) at the 600 m/min speed. Vibrations measured have shown that amplitudes (RMS) begin to increase after +50% bending force level with some deviations in the stands. So it is preferable for the thin strips rolling at the high mill speeds to have such roll profiles that there is no need to keep more than 50% bending forces in the last stands.

Feedback and stands synchronization in the tandem mill. The feedback loop mechanism in the tandem mills appears because the rolling load interacts with strip tension. Tension forces in elastic strips are determined as:

$$T_i = \frac{E \cdot S}{L} \int \left(v_i / \xi_i - v_{i-1} \right) dt, \tag{7.4}$$

where T – strip tension, N; E – modulus of elasticity, MPa; v – strip speed, m/s; ξ – strip elongation factor; L – strip length (distance between the stands), m; S – strip section, m^2; i – stand number; t – time, s.

Tension is proportional to the integral of the speed difference and may be explained as a low-pass filter. Hence, 90° phase shift between the input and output should appear, which does not depend on frequency. Roll stack movements give an additional 90° of phase shift, so entry and exit tension always oscillate with the 180° of phase shift.

It can be shown based on the continuity of mass flow through the mill during continuous rolling that a change in exit thickness will produce a change in strip speed, assuming that the entry gauge and exit speed remain constant. Feedback loop gain depends on rolling speed. Thus beyond the speed threshold, chatter will appear.

In [413], using Routh's stability criterion for the mill stack linear model, the critical strip speeds at which 3rd octave chatter occurs were obtained. Stability depends on tension response time constant and partial derivative of load by tension. In addition, mill internal damping is present in the criterion. Some authors suggested other stability criteria based on linear models. Testing of different known

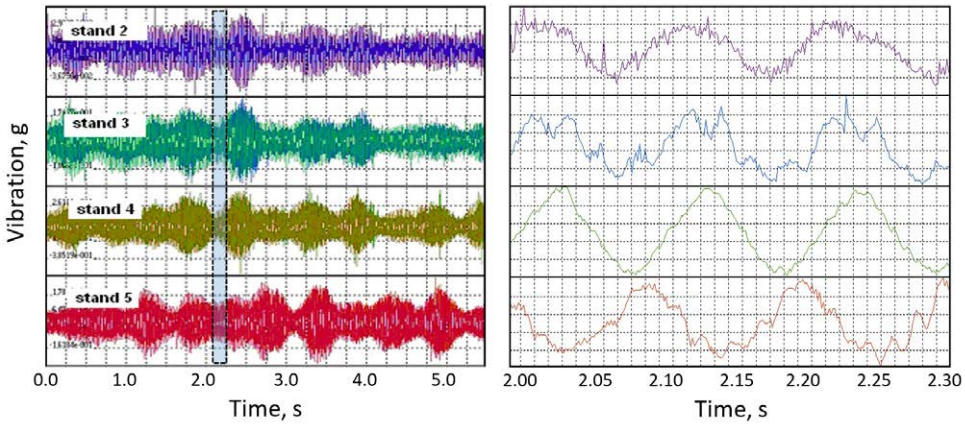

Fig. 7.5. Chatter vibrations – synchronous in stands 2, 3, 4 and non-synchronous in stand 5

criteria of stability has shown that it can be used rather for theoretical analysis than for real-time mill control.

Tandem mill chatter should be described in terms of the chain of coupled oscillators and synchronization conditions. Chatter vibration in stands No. 2–5 of a tandem mill is shown in Figure 7.5a. Figure 7.5b shows main chatter period (about 120 Hz). Stands No. 2–4 are synchronous within both low and high frequency, but stand No. 5 is always out of phase with the other stands because it works in a stiffness compensation mode of rolling force control. Nonlinear friction and strip stiffness in the contact make it difficult to conduct the analytical analysis of the whole system, which can be described by the parametric differential equations with a varying time delay [414].

Chatter regeneration by the strip waviness. The modern isotopic gauge meters are too slow (response time about 0.1 s) and are not able to measure high-frequency strip thickness variation (waviness periods 20–140 mm) in the tandem mill at high rolling speeds. In works [160, 161], regenerative effects due to strip thickness and roughness variation in the tandem mills have been studied in the dynamical models.

In cutting and other operations, the method of spindle speed variation is used for chatter avoidance due to regeneration from the previous passes' waviness. A tandem rolling mill cannot be controlled in such a way due to big transient oscillations (in 2–3 s) of drive torque. Slow mill speed variation will make the

dynamic situation even worse because of torsional vibration at the low natural frequencies (9–12 Hz) which lay in the HAGC system pass band.

One of the remarkable chatter features is noted in every research. During rolling under normal conditions, vibration signals in every stand are always accompanied by the modulation of low (2–3 Hz) frequency (Fig. 7.5a). Some authors explained this feature as frequency beating between neighbouring stands that have the same design. Other authors explain it as a BUR eccentricity influence, and others consider it a tension frequency.

Another explanation may be given for the modulation effect. Calculation with the dynamic model has shown that if a stand is disturbed by a series of periodic impulses (chatter marks on the incoming strip), it exhibits signal modulation and after a certain speed threshold becomes unstable. Despite the twice less speed in stand No. 2 than in No. 5, the same phases of low-frequency modulation are observed. It is impossible to explain this fact if we consider the BUR eccentricities as a kinematic source of modulation. However, it appears possible to explain this effect, if it is assumed that modulation is a result of thickness periodic defects accumulation, which is not directly speed-related and depends on phases of previous and current stands vibration. This fact proves that resonance vibration is a "regenerative chatter". Therefore, even under very high levels of vibration (rolls defects) in the last stand No. 5 of the tandem mill, chatter is never excited because there is no back effect of strip waviness.

During the occasional strip breaks, the real internal damping is determined by the decrement of transient oscillations (the time of attenuation is about 0.3 s). For the distance between stands equal to 4.75 m, above the speed limit of 4.75/0.3 = 15.83 m/s (where 0.3 s is a time of vibration damping), the previous stand is stable and the next stand is unstable because it is not able to dissipate periodical impacts.

Monitoring of high-frequency thickness variation. In continuous cold strip mills, where the longitudinal speed of the metal is 20–25 m/s, standard X-ray thickness gauges can only register low-frequency changes corresponding to the eccentricity or ovality of the backup or work rolls. High-frequency deviations in strip thickness that appear in the mill during vertical roll oscillations cannot be detected by existing isotopic thickness meters. With resonant vibrations, the amplitude of the thickness wave can exceed the permissible deviation according to the standard and cause the rejection of products by customers, especially on an auto sheet. It is assumed that the vertical vibrations of the last stand have a major

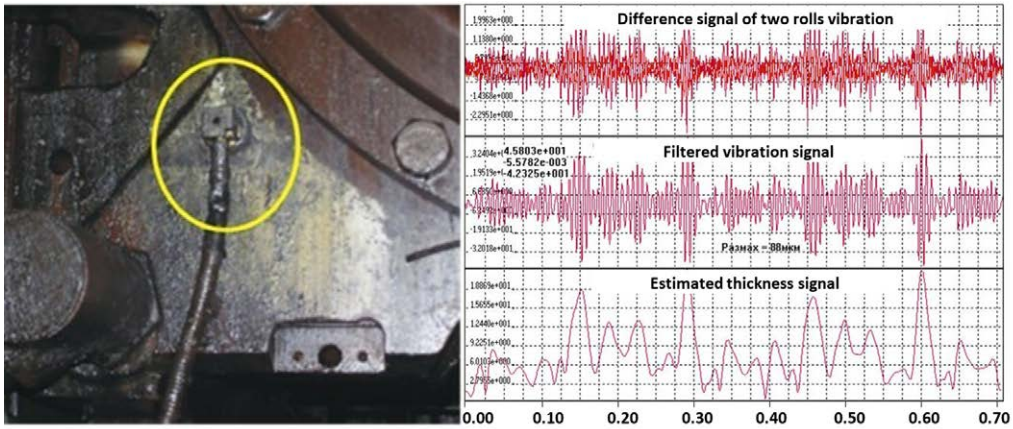

Fig. 7.6. Estimation of high-frequency strip thickness variation:
(a) accelerometer mounted on the backup roll chock;
(b) vibration signals processing

influence on the changes in strip thickness. Therefore, a method based on the vibration signals in the last stand of a tandem mill has been developed to measure such fast periodic defects.

To calculate the thickness difference from vibration signals, it is necessary to determine the phase values of the relative vertical displacements of the backup and work rolls. During continuous operation of the system, accelerometers on the mill are usually installed only on the chocks of the backup rolls (due to frequent changes of the work rolls). In the studies, four sensors were used for simultaneous measurements on the chocks of each roll in the quarto stands (support and working stands) and analytical dependencies were obtained that allow calculating the thickness changes only by vibration signals on the chocks of the support rolls. For most cases, the vibration of the stands occurs at frequencies of 100–130 Hz according to the fundamental mode of vibration in the 3rd octave, when the upper and lower pairs of rolls move out of phase. The developed method of high-frequency strip thickness variation measurement includes:

- vibration measurement on upper and lower rolls (Fig. 7.6a);
- filtering of accelerometer signals;
- double integration;
- scaling operation.

The results of vibration signals processing are shown in Figure 7.6b.

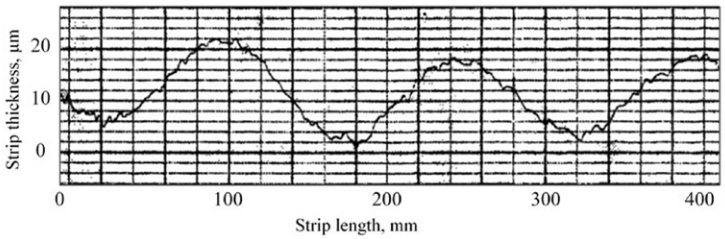

Fig. 7.7. Measurement of strip thickness by X-ray meter in the slow inspection line for coil section rolled under normal conditions without chatter

The proposed method has been verified by the direct measurements of the samples taken from the corresponding sections of the coil along the strip length and comparing it with the envelope of the vibration signal. The amplitude of strip thickness variation, which is measured in an X-ray thickness meter when the strip was recoiled under the slow linear speed (300 m/min) in the inspection workshop, is shown in Figure 7.7.

Depending on the low-pass filter parameters, more and more detailed patterns of strip thickness can be observed by the vibration signals in the rolling stand. However, additional tuning of the scaling factor is required in this case. Therefore, for practical needs, and the comparability with the signal of an X-ray thickness meter, too high cutting frequency is not advisable in signal processing procedure. The accuracy of the proposed method is estimated at 5–7% of the X-ray thickness meter but allows the detection of high-frequency defects on the strip, which cause resonance vibrations in the tandem cold rolling mills.

Active chatter vibrations control. Active chatter suppression methods are reported in the research papers and patents. This method of damping includes an additional source of energy (preferably hydraulics) and some devices, which produce regulated periodic force in the rolling mill stands.

As the mill speed drop during chatter control reduces productivity, there are two ways to solve a problem: to control rolling parameters (tensions, reductions) or minimize speed drop value. Tension decreased by 5 N/mm^2 between stands 4–5 leads to a 0.7–0.8 m/s speed increase. Relative strip reduction increasing in stands 12 (and decreasing in stands 3–4) causes a speed increase of 0.3 m/s for every 1% of relative reduction. These effects are not very significant in practice and their implementation is limited by technology.

The second way to improve mill performance is to recognize chatter before it comes to large amplitudes and thus to minimize speed drops because less vibration levels require less control efforts. There is a method for determining critical vibrations in strip rolling mills [415] where recognition of critical vibrations is carried out by strip tension fluctuations according to the expression:

$$CV = \mathrm{abs}\left[\mathrm{dif}\left(\Delta T_i / T_i\right)\right] \Big/ \mathrm{abs}\left[\mathrm{dif}\left(\Delta T_{i-1} / T_{i-1}\right)\right], \tag{7.5}$$

where CV is the vibration intensity factor, ABS – absolute value, DIF – first derivative, T_{i-1} – strip tension before the i-th stand, T_i – strip tension after the i-th stand, ΔT_i – current value of strip tension between stands, while the vibration intensity coefficient CV is no more than 20.

As a result of checking with this method, the following disadvantages were revealed:

- low noise immunity as a result of the use of the differentiation operation, which amplifies high-frequency noise (always present in the tension signals), and the use of filtering that introduces a delay in the response of the system;
- low reliability due to constant adjustment of the limiting level of the vibration intensity factor when changing the current values of the strip tension between the stands;
- low accuracy in determining critical vibrations from tension signals, which always have some delay concerning the signals of accelerometers installed in the stands.

Some other methods of chatter detection are known, e.g., based on electric motor current [416], having similar shortcomings related to later event detection than by vibration. Cross-correlation matrices of all available parameters (loads, tensions, torques, drive speeds) were estimated for chatter prediction and mill control. Also, several additional indicators were tested to improve the reliability of automatic mill speed control. The coefficient of harmonics (nonlinear distortion), modulation factor and some other indexes were tested online in the monitoring system. Band-pass filtering is used to improve signals in the desired frequency ranges. Data analysis has shown that vibration signals are more sensible than loads, tensions, etc., and are the most suitable signal for chatter control.

When developing a new method [417] for diagnostics of resonant vibration and control of a multi-stand cold rolling mill, we used the properties of a well-known physical phenomenon – synchronization of mechanical oscillatory sys-

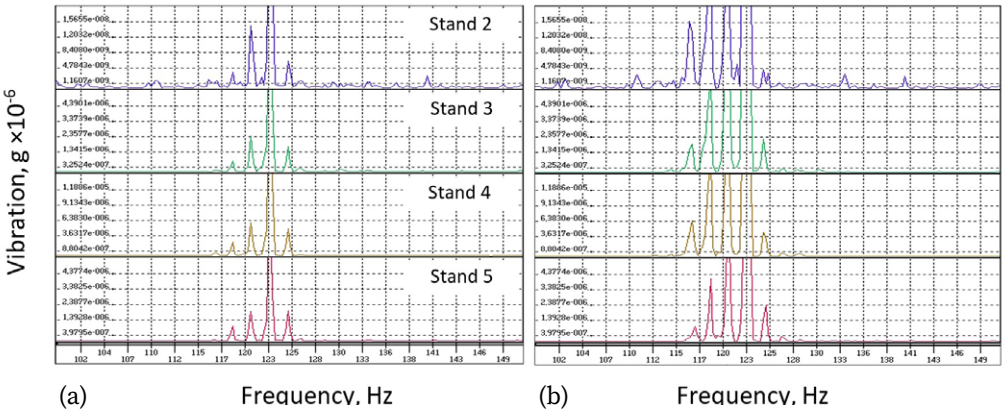

Fig. 7.8. Chatter main peak and side band peaks in the vibration spectra (stands 2–5): (a) under the normal vibration levels; (b) during chatter excitation

tems in the presence of elastic connections between them. In a multi-stand mill, the rolling stands are synchronized through an elastic rolled strip with vertical vibrations of the roll units.

The property of synchronization of vibrating mechanical systems with elastic links is the process of close natural frequencies "capturing" of adjacent oscillators (stands) F_i and their tendency to a mean value of the frequency F_{mean}. This leads to the convergence of frequencies at which the maximum values of the spectra of each stand become equal to the main natural mode of the vertical oscillation. Another feature of synchronization in the pre-resonance period of a multi-stand rolling mill is the ordering of the vibration phases, which is accompanied by an increase in the correlation coefficients of signals in each pair of adjacent stands (Fig. 7.5).

Analysis of the tandem mill vibration spectrum shows that the main chatter frequency peak (100–120 Hz) has many side-band peaks ($\pm k \cdot f_{\text{BUR}}$, k = 1,2...5), which correspond to harmonics of backup rolls rotation frequency (Fig. 7.8). Right before chatter onset, the interrelation between the main peak and side-band peaks changes. In the time domain, vibration signals demonstrate a greater amplitude of modulation (Fig. 7.5).

The new algorithm for online chatter diagnostics and tandem mill control is proposed, which allows the chatter detection earlier than by known methods (based on spectrum amplitude within a narrow band). In the new method, the

control signal is generated at the moment preceding the resonant vibration, the occurrence of which is determined based on the joint or separate fulfilment of the following conditions:

$$\sigma_n \le \sigma_{\max};\ K_{XY_j} > \left[K_{XY_j}\right]_{\max};\tag{7.6}$$

where σ_n – current root-mean-square deviation of the values of the frequencies of the maxima of the spectrum of vibration acceleration signals in a given range along the mill stands, Hz, determined by the dependence:

$$\sigma_n = \sqrt{\frac{1}{n}\sum_{i=1}^{n}\left(F_i - F_{\text{mean}}\right)^2},\tag{7.7}$$

where F_i – the current value of the frequency of the maximum spectrum of the vibration acceleration signal of the i-th stand in the mill, Hz; n – the number of stands, starting from the last of N stands, $2 \le n \le N$; F_{mean} – the current average value of the frequencies of the maxima of the spectrum of the vibration acceleration signals along the n mill stands, Hz; defined as:

$$F_{\text{mean}} = \frac{1}{n}\sum_{i=1}^{n} F_i,\tag{7.8}$$

where $\sigma_{\max}$ – permissible root-mean-square deviation of the frequencies of the maxima of the spectrum of the vibration acceleration signals along the n mill stands, Hz; determined from the condition:

$$\sigma_{\max} \le \Delta f,\tag{7.9}$$

where $\Delta f = 1 / T$ – frequency step when calculating the spectrum, Hz; T is the period for recording vibration signals when calculating the spectrum, s, and the minimum frequency in the range when calculating the spectrum of vibration acceleration signals is taken based on the expression:

$$f_{\min} \ge 2 \cdot f_{WR},\tag{7.10}$$

where f_{WR} – the rotational frequency of the work rolls in the last stand of the mill at the maximum rolling speed and the minimum diameter of the rolls, Hz, and

the maximum frequency in the range when calculating the spectrum of vibration acceleration signals is taken based on the expression:

$$f_{\max} \le \frac{1}{(4...5)\cdot 2\cdot \Delta t}, \tag{7.11}$$

where Δt – sampling interval of signals in time, s; K_{XY} – correlation coefficients of vibration acceleration signals in the j-th pair of stands X and Y of the mill, $j = \begin{cases} 2,...,n-1 \to n>2 \\ 1 \to n=2 \end{cases}$, determined as:

$$K_{XY} = \left| \frac{\mathrm{Cov}(X,Y)}{\sigma_X \cdot \sigma_y} \right|, \tag{7.12}$$

where σ_X, σ_Y – current root-mean-square deviations of vibration acceleration signals in stands X and Y of the mill; $Cov(X, Y)$ – current covariance of vibration signals in stands X and Y of the mill, determined by the expression:

$$\mathrm{Cov}(X,Y) = \frac{1}{m}\sum_{i=1}^{m}(x_1-\mu_x)\cdot(y_1-\mu_y), \tag{7.13}$$

where μ_X, μ_Y – current average values of vibration acceleration signals in two stands X and Y of the mill, m is the number of discrete values of signals taken for calculation; $[K_{XY_j}]_{\max}$ – the maximum permissible value of the correlation coefficient of vibration acceleration signals before the onset of resonance, $[K_{XY_j}]_{\max} < 0.3$.

The onset of resonance vibration during stands' synchronization is determined 3–5 s earlier than the amplitude of the spectrum maxima in each stand separately begins to increase. This is because the shift of frequencies and phases begins even with insignificant exchanges of vibrational energy. The degree of synchronization of adjacent stands is determined by the current root-mean-square deviation of the frequencies of the spectral maxima in the stands according to expression (7.7) and by the current values of correlation coefficients of vibration signals, determined by dependence (7.12).

An increase in the average rolling speed and productivity of a multi-stand mill is achieved due to a smaller impact on the mill speed at the first signs of stands' synchronization, determined by expression (7.6). The amplitudes of vertical vibrations in the stands do not have time to reach a high level, at which a greater reduction in speed is required to exit the resonant rolling mode. The need to limit

the value by expression (7.9) is because the minimum value of the frequency difference in the signal spectrum is determined by the accuracy of the spectrum calculation, which is equal to the frequency step.

It was experimentally established that low-frequency oscillations of the amplitude of the spectrum maxima are determined by the beats of the backup and work rolls due to their unbalance and eccentricity, therefore, the value of the minimum frequency of the range according to expression (7.10) should exceed double the turnover frequency of the work rolls in the last stand at the maximum rolling speed and minimum diameter work rolls.

The maximum frequency of the range according to expression (7.11) is determined by the known theoretical provisions, according to which, for reliable spectral analysis, it is necessary to have 4–5 samples of the analogue signal for the oscillation period with the maximum frequency in the specified range $f_{max} = 1 / [(4...5)\ 2\ \Delta t]$, determined by the sampling interval of the signal in time Δt.

The use of the root-mean-square deviation of frequencies according to expression (7.6) instead of the values of the amplitude of the signal spectrum maxima and a reasonable choice of a given frequency range according to expressions (7.10), (7.11) also makes it possible to exclude the influence of fluctuations in the technological load and beating of the rolls. It was experimentally established that under normal conditions, the correlation coefficient of signals in adjacent stands varies within a range of 0.2...0.3 and does not depend on the vibration levels in the stands at different technical conditions of the rolls and mill equipment.

An increase in the reliability of the proposed method in comparison with known diagnostic methods is achieved through the use of a set of diagnostic features included in expression (7.6) in different versions. For example, to increase noise immunity, the moment of transition to resonant vibrations is determined by the simultaneous fulfilment of the conditions included in the expression (7.6), the logical "AND". If it is necessary to increase the sensitivity of the method, the diagnostics of the phase of transition to dangerous vibrations are carried out according to the fulfilment of any of the conditions included in logical "OR". It is possible to use the combined fulfilment of the conditions included in (7.6). For example, a combination of the first and second parts by "AND", and by "OR" with one of the sets of conditions of the second part, i.e. when the threshold value is simultaneously reached by the current RMS frequency values and one of the pair correlation coefficients.

When stands' synchronization appears, all technological parameters (electric drive current, strip tension, rolling force) exhibit oscillations at the same fre-

quency common to all adjacent stands. Although the resonant vibration can be detected by the proposed method with other process control sensors, the monitoring of vibration signals gives the earliest response to chatter amplification but requires additional sensors.

7.2. Torsional vibration control by the electric drive acceleration

Methods for dynamic load reduction are classified and analysed from the viewpoint of their applicability in the gear drivelines of heavy-duty industrial machines.

Introduction of feedback loops. Some new parameters can be used to create additional feedback loops in the control systems, e.g., by the torque signal in the drivelines. This solution has been known for a long time, but its practical implementation was hampered by the lack of a reliable torsional vibration meter with a permanent power supply for harsh conditions. The developed digital telemetric torque meter adapted for use in heavy industry makes it possible to solve this problem in practice. By this method, torsional vibration reduction of up to 50–100% can be achieved.

Changing the rise time of the load can be efficient in a narrow range when the frequency of input load enters the region of the lowest natural modes of the driveline. There are always technological restrictions on this method. In the hot rolling mills, changing the rise time and the amplitude of input load can be achieved by changing the temperature of the front strip edge due to regulating the hydraulic system for surface cleaning from the oxidation scale.

Passive damping of torsional shocks in the form of polymer liners instead of bronze pads, which do not require lubrication and have an increased service time are analysed in [418]. It is possible to significantly reduce the rotating spindle axis deviation by modernizing the articulation unit and introducing a centring element. There have been attempts to modify the material of the slip pads and directly replace them with polymer, which failed. Some other examples of damping polyamide pads combined with steel reinforcement elements are shown in Figures 7.9 and 7.10. For the advanced designs of damping spindles, elastic elements are made of polyurethane. The necessary mechanical characteristics of polyurethane elastomers have been determined in [419].

The studies of driveline dynamics with damping elements have shown that the design of shafts and choice of material should be made not only from the

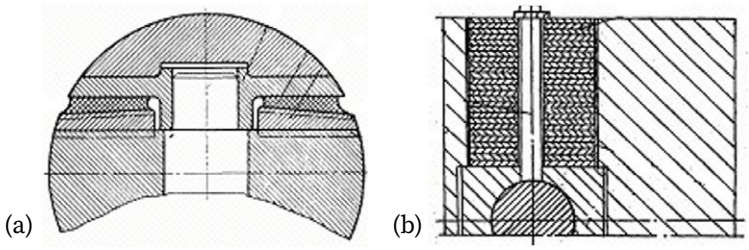

Fig. 7.9. Designs of damping elements: (a) polymer insert; (b) package of steel plates

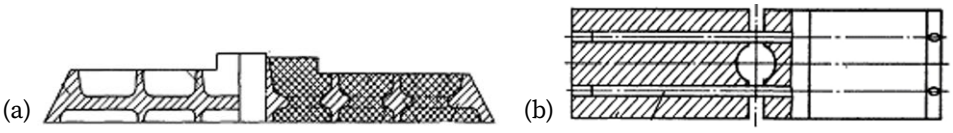

Fig. 7.10. Reinforcement elements: (a) metal frame; (b) insert elements

point of view of wear resistance and strength but also taking into account possible changes in the natural modes of torsional vibration. Lowering the stiffness reduces dynamics in the driveline, but at the same time the external disturbances (roll rotation frequency) must be taken into account. The increased compliance of spindles can lead to undesirable resonant vibration.

All the above-mentioned methods address dynamics control but not its origin – drivetrain wear. The ABB Company has developed backlash compensation along with new features addressing the reduction of the torsional dynamics. Some methods of backlash identification were tested involving periodic drive speed regulation. However, the spindle weight balancing units are not considered concerning torsional vibration control. The different known frictional or electromagnetic devices stopping one of the parts in a driveline for gaps closing are patented but not applied in industrial plants due to complexity or additional equipment.

Torsional vibrations control by the electric drive acceleration. The so-called “soft-start” method is known to reduce torsional oscillations in the drivelines with a speed-regulated electric drive, e.g., rolling mills, long conveyors and other industrial machines. Experimental testing of this method showed its high efficiency (TAF reduction by a factor of 2) in the drivelines with a single-stage

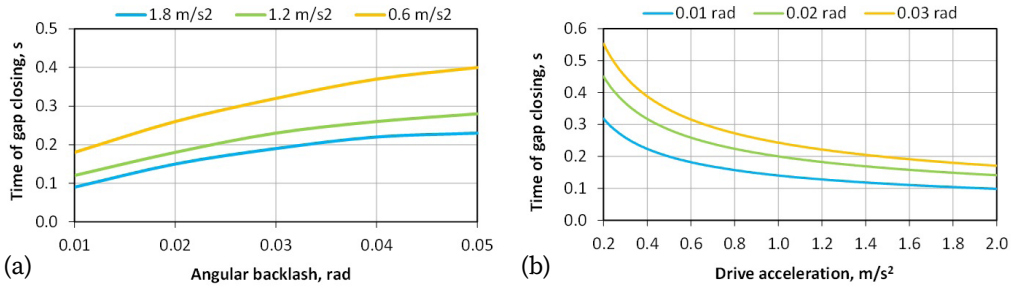

Fig. 7.11. Time of gap closing with: (a) the different accelerations; (b) gap sizes

gearbox. However, implementation in other industrial machines requires additional theoretical investigation and experimental testing [420].

To learn particular features of drive acceleration effect on transient torsional vibration, a dynamic simulation has been carried out for different drivetrains. The time required for backlash gaps closing estimated by the model is shown in Figure 7.11. It can be seen that under a constant acceleration rate, its value increasing in the range of 0.6–2.0 m/s^2 has little effect on gap closing time. Gap size variation in the range of 0.01–0.03 rad has also little effect on the closing time for more than 0.6 m/s^2 acceleration level. The lower acceleration limit is restricted by the drive control system (about 0.1 m/s^2). An implementation of the drive acceleration method for a non-reversal rolling stand with an edger (vertical rolls) is represented in Figure 7.12. The time interval between successive slabs is 30–40 s and the drive speed is 1–4 m/s. The first zone of drive speed regulation is assumed (below nominal value).

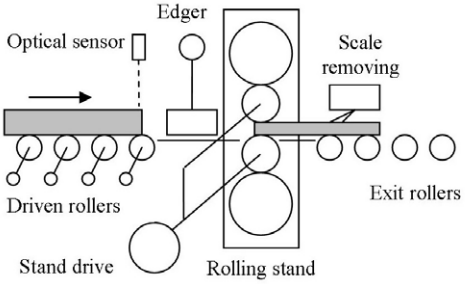

Fig. 7.12. Scheme of drive acceleration method implementation

Drive dynamic torque should have enough high level to enable backlash gap closing and overcoming reactions in the drivetrain:

$$T_{dyn\,ij} > \max\left(T_{Rij}, T_{\min\,ij}\right), \tag{7.14}$$

where $T_{dyn\,ij} = J_{ij}\,a$ – dynamic torque; J_{ij} – summary inertia of drive chain from the rolls to K_{ij} coupling; a – rotation acceleration referred to K_{ij} coupling; $T_{R\,ij}$ – reaction torque; $T_{\min\,ij}$ – minimal dynamic torque after first oscillation.

Two components are important to vibration control: angular gaps in the unbalanced spindles and radial gaps in gearbox bearings. Dynamic torque has to be greater than the reaction torque caused by the unbalanced spindle weight and torque produced by the middle gear wheel in a 2-stage gearbox. It is also desirable to provide positive load torque $T_{\min\,ij} > 0$ to keep the gap closed until the end of the transient process.

The drive speed control algorithm includes the following steps:

1) Slow down the drive speed after unloading.
2) Start drive acceleration by the signal of an optical sensor of metal position.
3) Stop drive acceleration after the electric motor current exceeds the nominal level.
4) Apply sequence (1)–(3) for every next loading cycle.

Incoming slab position may also be determined by the signals of drive current or speed of the nearest transportation roller or vertical edger.

The schematic time diagram of drive acceleration control is shown in Figure 7.13. The time intervals and critical points are as follows: t_0–t_2, t_3–t_5 – acceleration/deceleration intervals; t_1, t_4 – moments of drive loading and unloading (strip biting and releasing). Time interval t_0–t_1 should exceed a slight transient of gap closing and the t_1–t_2 interval should be longer than the main transient process du-

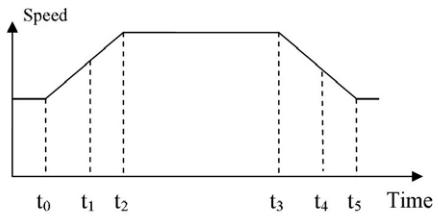

Fig. 7.13. Schematic time diagram of drive speed acceleration control

ration (about 4–5 periods of the main mode oscillations). Drive deceleration before unloading provides a reduction of shocks in the gearboxes. Worse tuning of weight balancing needs more drive acceleration to close backlashes in the heavy spindles.

Torque measurements have been carried out for evaluation of the drive acceleration method in the industrial hot rolling mill. The transient torques measured on the motor shaft in stand 4 are shown in Figure 7.14 when drive acceleration was switched off (normal mode) and applied (testing mode). It could be seen that motor acceleration allows the avoidance of repeated back shocks in the drivetrain which reduces the lifetime of tooth couplings significantly. Besides, torque modulation due to nearest natural frequencies $f_1 = 12$ Hz and $f_2 = 15$ Hz ($f_2/f_1 \ll 2$ – criterion of two close modes beating) is almost eliminated, which means one mode of torsional vibration has been suppressed.

Measurements in stand 4 were conducted with a synchronous speed increase of edger drive (small vertical rolls before the main stand). Experiments in stand 3 have been carried out with drive acceleration independently from the edger (constant speed) and no interference was observed between stand 3 and the edger because it has much less power of electric motor and small stiffness of the drivetrain. Consequently, it is possible to accelerate only the main stand drive without the speed control of the edgers. That makes implementation much simpler in the reversing universal stands equipped with two edgers at both sides or in the roughing stands with only one edger.

Optimization of drive control parameters. Measurements have been conducted with one level of drive acceleration in 2-high stand No. 0 (without backup rolls) and in 4-high stand No. 3. While five levels of acceleration were applied in 4-high stand No. 4. Motor acceleration has a positive effect not only on torsional dynamics but also on reducing shock vibrations in the bearings of the gearboxes. A relation of vibration peak value at the gearbox input shaft bearing and TAF at the motor shaft by the drive angular acceleration in stand No. 4 are shown in Figure 7.15.

It could be seen as an optimum near the 1.20 rot/s^2. This value is individual for every driveline and depends on total rotation inertia referred to as torque measurement point. A negative value of –0.20 rot/s^2 corresponds to drive deceleration, which has been applied in experiments to estimate the backlash effect on the transient process when the gap was completely opened. The fully opened gaps greatly increased TAF and vibration. However, drive deceleration plays a positive role in torsional dynamics reduction when applied just before load ending (strip releasing after rolling).

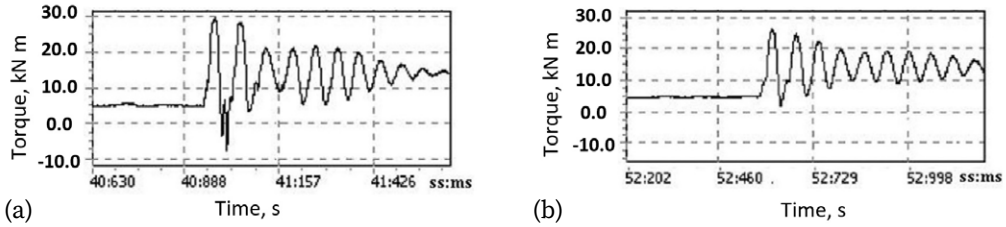

Fig. 7.14. Transient torques measured on the motor shafts with drive acceleration: (a) off; (b) on

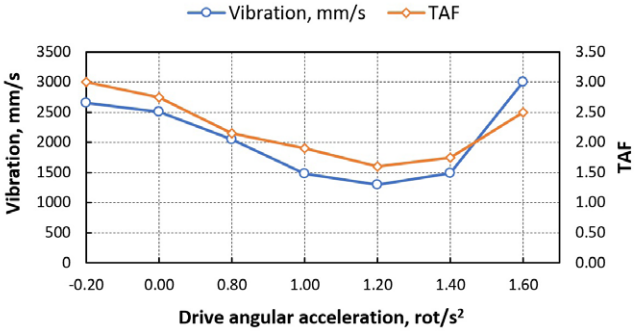

Fig. 7.15. Gearbox vibration and TAF for the different levels of drive acceleration

The average effect of TAF reduction was obtained as follows: 2% – in stand duo; 22% – in stand 3; 96% – in stand 4. This is in inverse proportion to the total inertia of drivelines. The stand duo had the highest inertial torque (about 40% of static technological load) although only two work rolls produced less inertial torque than in stands 3 and 4, which have pairs of big backup rolls (50 t each). Hence, the main contribution of inertial torque create rotating elements in the driveline.

To achieve maximum efficiency of the drive acceleration method in torsional dynamics reduction, the following conditions have to be fulfilled (see notations in Figure 7.12):

- Motor current should not exceed the overload limit assigned in its control system.
- Time interval $[t_0, t_1]$ should exceed the idle gap closing time to avoid overlap with a main transient.

- Time interval $[t_1, t_2]$ should be longer than the main transient to let torque attenuate within about 4–5 periods (0.5 s) of the lowest natural frequency (10 Hz).
- The time of maximum gap 0.05 rad closing is about 0.13 s, therefore the full time of control $[t_0, t_2]$ is less than 1 s for 1 rot/s^2 and the lowest modes 10–30 Hz.
- Acceleration should be finished below the working speed and nonlinear control is preferable to avoid exceeding this. Inertial torque should exceed the reaction produced by spindle unbalance and gear shaft weight until the transient end.
- Drive deceleration before the rolling end provides shocks reducing in the gearboxes.

The most important factors influencing dynamics are spindle weight balancing and drivetrain design, which influence summary acceleration dynamic torque. It is important to take into account second and higher modes of torsional vibration when designing control methods in the geared drivetrains of industrial machines.

The drive acceleration method could be effectively implemented in the drivelines with a gear ratio in the range of 1–7 where summary inertial torque will have less effect on TAF reduction. An intention to make less acceleration level with gearbox ratio 7–25 does not allow closing angular gaps due to low accuracy of spindles weight balancing.

The most advanced approach to transient torsional vibration control is the hydraulic weight balancing units with the position sensors of spindles. However, it requires costly additional actuators and position measurement instrumentation working in harsh conditions.

7.3. Modelling of plate front end bending in hot rolling

Almost in every thick plates hot rolling mills, as well as in the roughing stands of thin plates rolling mills, there is a problem of the front end bending up or down in the vertical plane, the so-called “ski” or “snake” effect. When the front end is bent upwards, especially when the work roll diameter is small, the steel plate entering the stand or the subsequent technological unit is dangerous or impossible. When the front end is bent down, the guiding and transportation rollers are subjected to shock impacts during the plate motion, thin sheets get stuck in the rollers, and it is impossible to grip the plate in the following stands or passes.

(a) (b) (c)

Fig. 7.16. (a) Plate rolling mill;
damages caused by front end bending (b) up; (c) down [426]

The direction and magnitude of the front-end bending of the plate are determined by a significant number of factors that cause asymmetric conditions for rolled metal in the upper and lower deformation zones. The general view of the investigated hot rolling mill and defected strip are shown in Figure 7.16a. In both cases of front-end bending, it causes severe damage to elements in the mill and long downtimes for its repair (Fig. 7.16b,c).

There are several research works [421–426] devoted to the study of front-end bending of sheets in hot rolling mills, and some approaches to solve this problem have been proposed. Formation of the front-end bending patterns depends on the

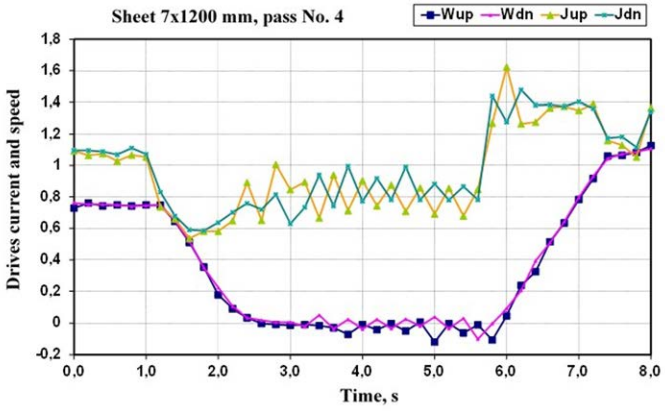

Fig. 7.17. Measured signals of current (J_{up}, J_{dn}) and rotation speed (W_{up}, W_{dn}) with out-of-phase oscillations of the top and bottom drives of the rolling stand with significant sheet waviness

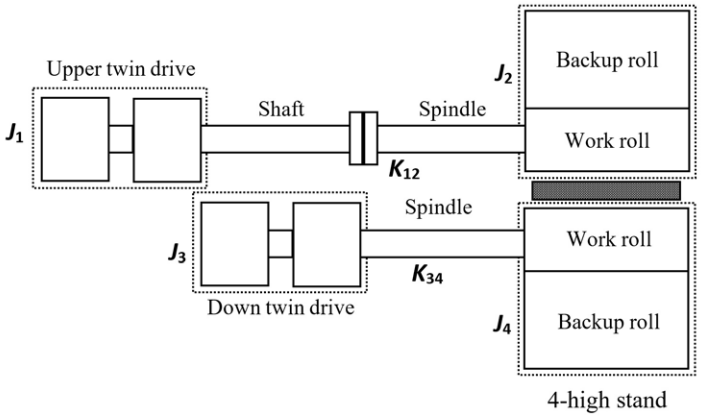

Fig. 7.18. Drivelines calculation diagram of the finishing stand in the plate rolling mill

difference in the diameters and speeds of the rolls, the difference in temperature and friction on both strip surfaces, torsional stiffness of the upper and lower drivelines.

During the period of metal capture by rolls, a transient process occurs in the form of fluctuations in the speed and load of electric drives. Depending on the rolling speed, it is superimposed on different lengths of both ends of the plate when the mill is reversed. With a phase shift of torsional vibrations of the upper and lower rolls and drives by 180°, dynamic processes affect the formation of metal waviness (Fig. 7.17). If there is an individual drive for every roll, it is possible to influence the curvature of the front end, to reduce or eliminate it. To do this, it is necessary to automatically set the calculated difference between the upper and lower rolls until the metal is captured and then smoothly reduce this difference after the stable rolling starts so as not to overload one of the drives due to unequal loading. Such an algorithm for controlling the main drives requires the use of modern automation and digital signal processing tools.

To analyse the dynamics of this system, a multi-mass model of drivelines has been developed and the natural modes of torsional vibration have been determined. For each roll driveline, the two-mass scheme is assumed in the form of "motors-spindle-rolls" (Fig. 7.18), where two paired motors are combined into separate masses (J_1 and J_3), and the backup rolls are combined with corresponding work rolls (J_2 and J_4). According to the diagram, the upper roll drive has two successive stiffnesses (intermediate shaft and spindle), whose equivalent stiffness is:

$$\frac{1}{K_{12}} = \frac{1}{K_1} + \frac{1}{K_2}, K_{12} = \frac{K_1 \cdot K_2}{K_1 + K_2} \tag{7.15}$$

The natural frequency of a two-mass system is determined by the formula:

$$\omega_{12} = \sqrt{\frac{K_{12}}{J_{12}}}, \tag{7.16}$$

where $J_{12} = \frac{J_1 + J_2}{J_1 \cdot J_2}$ – equivalent moment of inertia, kg m^2.

The natural frequency of the upper driveline (about 12 Hz) is slightly less than the lower one (about 15 Hz) due to the compliance of the additional intermediate shaft. As a result, the lower roll takes the load by 0.016 s faster and bends the sheet upwards. At a maximum rolling speed of 4 m/s (80 rpm), up to 80–100 mm of the plate will be rolled during this time and the front end is formed. After metal capture by rolls, this factor loses its value but the drivelines of the upper and lower rolls become joined via the rolled metal (nonlinear elastic-viscoplastic link) and the system begins to exhibit dynamic properties as a three-mass system, i.e. “upper drives – upper intermediate shaft and spindle – all rolls – lower spindle – lower drives”.

From the solution of the frequency equation for a three-mass system, the expression for natural frequencies has the form:

$$\beta_{1,2} = \sqrt{\left(a_0 \mp \sqrt{a_0^2 - 4a_1}\right)/2}, \tag{7.17}$$

where coefficients are as follows:

$$a_0 = \beta_{12}^2 + \beta_{23}^2, a_1 = \frac{K_{12}K_{23}\left(J_1 + J_2 + J_3\right)}{J_1 J_2 J_3}; \tag{7.18}$$

and partial frequencies of a three-mass system:

$$\beta_{12}^2 = \frac{K_{12}\left(J_1 + J_2\right)}{J_1 J_2}; \beta_{23}^2 = \frac{K_{23}\left(J_2 + J_3\right)}{J_2 J_3}. \tag{7.19}$$

In this three-mass system, the natural frequency is about 2 Hz for the first mode of oscillation (out-of-phase oscillations of the lower and upper motors with

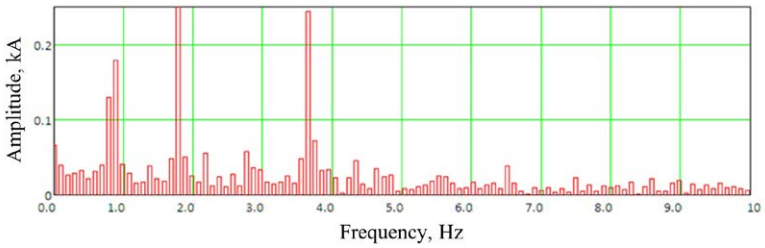

Fig. 7.19. Spectrum of the electric current of the upper work roll drive

an oscillation node between the rolls), and about 11 Hz for the second mode (synchronous oscillations of the upper and lower motors being out of phase with the rolls and two nodes of vibration in the spindles). When the waviness of the plate appears, out-of-phase oscillations of the upper and lower electric drive currents are observed (Fig. 7.17), i.e., torsional vibrations occur at the first mode.

Deviations in the shape of the rolls constitute an external kinematic disturbance in the stand. They were measured with a micrometer on a roll grinding machine.

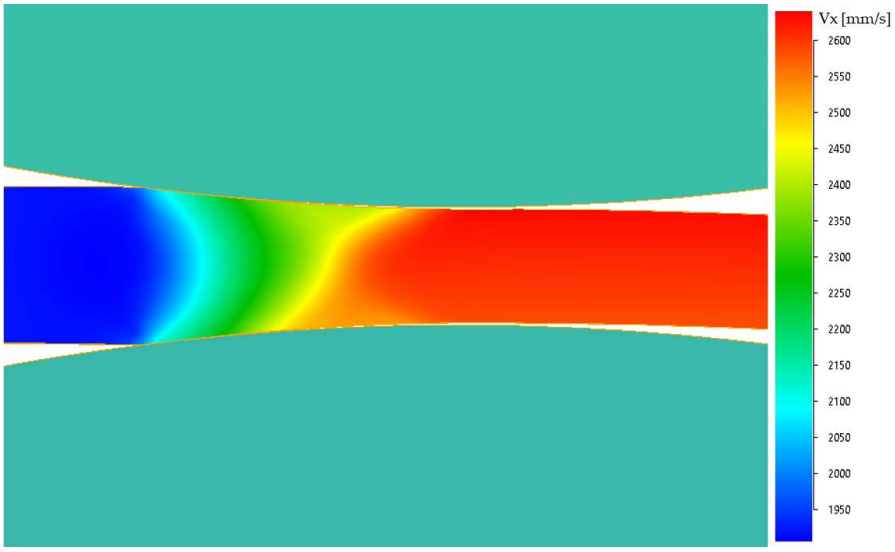

Fig. 7.20. The metal flow rate when rolling a sheet of 30 mm;
the mismatch of the roll speed –5%; the strain 25%;
bending of the sheet towards the faster lower roll

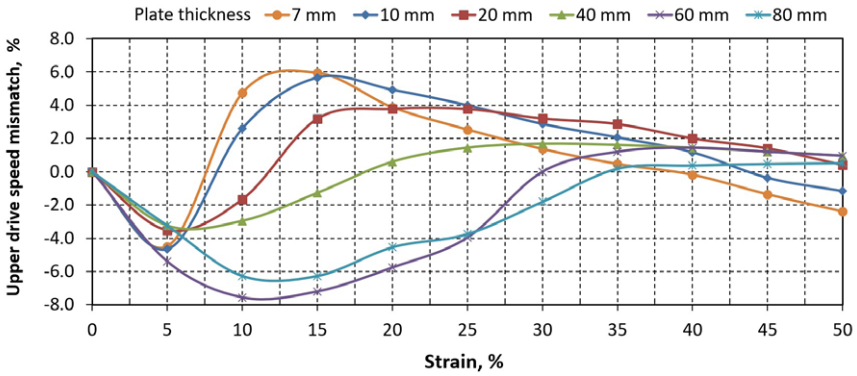

Fig. 7.21. The basic model of the required drive speed mismatch to compensate for the upward curvature of the front end of the plate for different plate thicknesses (7–80 mm)

On average, the values of the radial eccentricity are as follows: 50–60 μm for the backup rolls, and 20–30 μm for the work rolls. Frequency analysis of the measured signals of the electric drive currents shows the presence of the rotation frequency of the work rolls and its two even harmonics of about 2 and 4 Hz (Fig. 7.19).

During the rolling stand acceleration, the natural frequencies of the drivelines may coincide with the rotational speed of the work rolls (1 Hz at a speed of 3.14 m/s or 60 rpm with work rolls diameter of 1000 mm) and its double harmonic (about 2 Hz), which on its turn coincides with the main mode of the driveline natural oscillations. Hence, such a situation has to be avoided.

The main factors that explain the front-end bending of plates have been identified by using finite element modelling in a specialized software QForm. To develop a control model for individual drives by creating a drive speed asymmetry, a simulation of the rolling process is performed under different rolling conditions (metal thickness, strain rate, temperature, and contact friction). As a result of the numerical solution of the problem, the characteristics of the stress-strain state of the metal, the temperature field and the metal flow rate are determined. The example of simulation is shown in Figure 7.20.

Based on the simulations and driveline dynamics analysis, the control model is developed in the form of the required speed mismatch of the upper roll drive concerning the lower roll drive depending on metal strain for different input thicknesses (7–80 mm) of the plate in every pass, which is given in Figure 7.21.

7.4. Dynamics control of the hydraulic roof supports

The scope of this research is to study the transient dynamics of hydraulic roof support (one of two parallel cylinders) to determine a possible way for its high dynamics control by the regulation of the safety valve. The following tasks are formulated:

- find the natural frequency of free oscillations under shock impact;
- estimate time delay of piston displacement and pressure signal at the safety valve;
- find relations between peak pressure and time opening of the safety valve.

Control signals in the feedback loop can be supplied from any type of additional sensors (vibration, displacement or force) installed on a canopy of hydraulic prop. Their characteristics selection should be based on the results of experimental research taking into account the harsh operating conditions and the need for energy supply limited by explosive risk regulations. For this purpose, different autonomous energy harvesters can be used based on thermo- and piezoelectric principles or other sources.

In real work conditions, the prop height is always changing in time depending on static load over the roof supports section. The natural frequency of oscillation is variable:

$$\omega_n(t) = \sqrt{\frac{K(t)}{m}}, \tag{7.20}$$

where m is a join mass that changes for every impact in the conditions of an underground mine. Hence, all hydraulic props (with a pair of cylinders) are dynamical systems with variable parameters. This frequency depends on the initial piston position x_0 (Fig. 7.22). Then, in the case of safety valve opening under conditions of overloading, the hydraulic spring deforms to x_1 length and becomes nonlinear (piecewise softening characteristic). Further deformation depends on the flow rates $Q_i (Q_1 < Q_2 < Q_3)$ provided by the safety valve.

Some important features should be noted:

- pressure peaks are reduced with advance time lags;
- flow rate has a greater influence than time lag;
- dynamics related to frequency and shock duration ratio;
- with every next oscillation, the natural frequency changes;
- higher props have less stiffness and more shock damping.

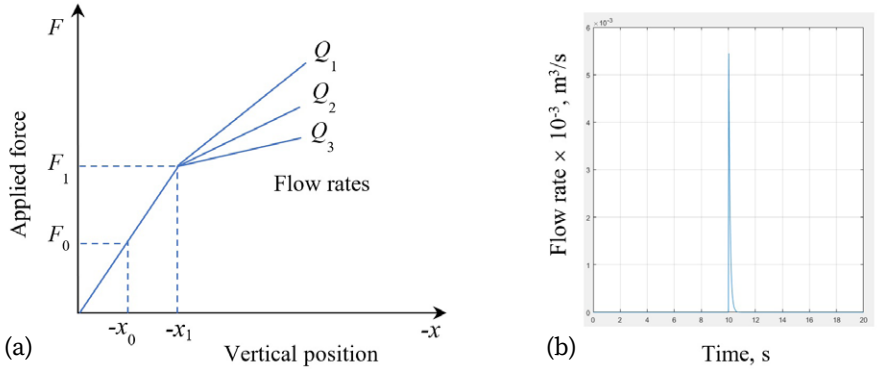

Fig. 7.22. Simulation of hydraulic cylinder parameters with the safety valve opening:
(a) stiffness characteristics; (b) flow rate

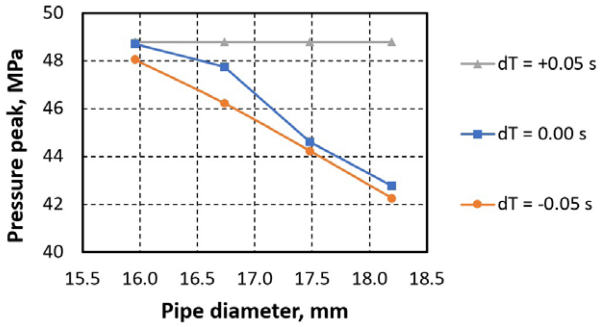

Fig. 7.23. Dynamic pressure peak amplitude by the pipe diameter
for different time of safety valve opening
(+0.05 – existing delay; 0.00 – without delay; –0.05 – in advance)

The greater flow rates Q correspond to softer stiffness characteristics above the fracture point in the graphs and better dynamics damping. On the other hand, big flow rates increase the risk of piston full contact at the bottom of the cylinder when fluid height becomes close to zero, especially after several subsequent oscillations above the pressure limit.

The signal of impact applied to the upper elements of the canopy can be detected in advance of time and used for shock damping. Results of model simulations are summarized in Figure 7.23 where pressure peaks are shown in relation to pipe diameter and time lags of safety valve control. Detection of load applica-

tion is possible by the use of additional sensors on the top of hydraulic prop housing. The physically allowable values of time lags for safety valve opening control are assumed.

This new approach of dynamic impact reduction based on a mathematical model and the use of additional signals to control safety valves has not yet been used in underground mining machines although well known in other applications, e.g. active disturbances damping in automotive suspension.

Model simulations showed that the time delay between force application on the top of the piston and pressure signal reaction at the safety valve position (near the bottom of the cylinder on the small section exhaust pipe) is about 0.02–0.05 s. However, it is enough to measure shock impact and generate a feedback signal to control the safety valve. In this way, the pressure peak can be reduced by 30% or even more.

Additional research is required to develop optimal control by the signals of additional sensors (vibration, displacement or force) and the selection of fast electrically regulated valves with minimum reaction time providing a high flow rate under high pressures. The «smart valve» with optimised control functions by the input signals from additional sensors (vibration, deformation, piston position) has to provide a fast reaction with a flow rate above 1000 L/min under pressures up to 100 MPa.

The existing automation and monitoring systems provide a basis for the smooth implementation of a new solution in the mining industry. The huge amount of hydraulic props ensures a great potential for application. This approach can also be applied in other hydraulic machines with long cylinders subjected to severe abrupt loading.

8. INDUSTRIAL APPLICATIONS

Operation of many industrial plants is associated with significant wear in elements where implementation of digital diagnostic tools is difficult due to harsh environments. Reliable vibration monitoring is very complicated due to inherent changes in technological regimes, treated material properties and drive speed. It appears more beneficial to monitor dynamic torques in addition to vibration signals, but this is restricted to the installation of strain gauges. The more acceptable approach is to monitor electric motor signals or vibration and, having identified multibody models, to control dynamical processes and calculate the remaining useful life (RUL) of machine elements. Based on this approach, the new monitoring systems are developed with integration into plant automation infrastructure. Adaptation of nonlinear dynamical model parameters (backlashes) and technological loads optimization is provided.

8.1. System of chatter vibrations control in the cold rolling mills

The first chatter monitoring systems were installed in the tandem mills in the 1990s. Some of them were designed by plant engineers and collect analogue signals from the pressure sensors in the HAGC hydraulics. Later, vibration monitoring systems were implemented, which provided mill operators with three levels of alarms and fulfilled automatic mill speed reduction when the chatter suddenly occurred.

The recently developed chatter monitoring system (Fig. 8.1) has 6 channels for vibration control and some additional channels for rolling parameters logging. Sensors installed in the last three stands Nos. 3, 4, 5 on the top and bottom backup rolls chocks on the operator side. Later, similar sensors were also installed in stands Nos. 1, 2 for diagnostic purposes. The complete set of the system hardware and software includes the following elements:

- Computer PC 1.8 GHz, RAM 2 GB, HDD 256 GB, MS Windows.
- PCI 6071E National Instruments ADC board installed on a PC.

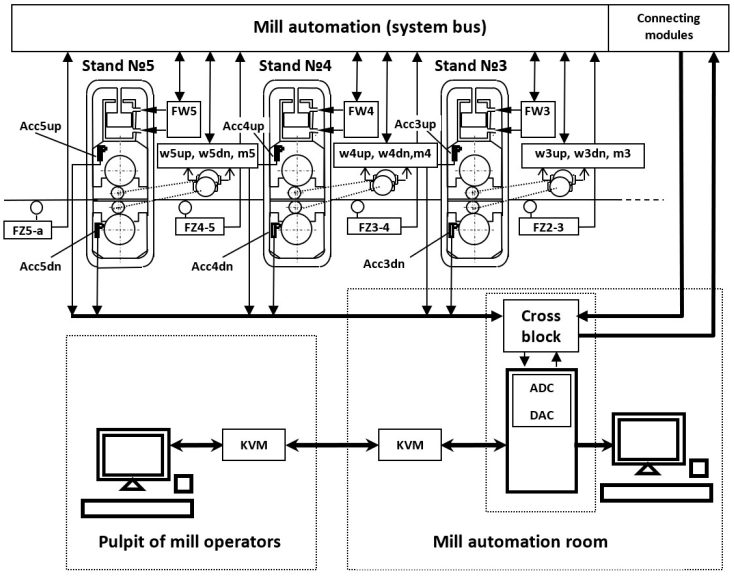

Fig. 8.1. Block diagram of a vibration control system
in a continuous cold rolling mill

- NI-DAQ software with ADC board drivers.
- Software module monitor_rt.
- SH100100 100-pin cable for signal input/output (shielded).
- SCB-100 I / O 100 pin connector for signals on the cross-block.
- Cross-block for input and output signals.
- Vibration signal transducers 4-ch 482A22 with power adapters 488A04.
- Vibration sensors (accelerometers) 603C01 ICP (2 sensors per stand).
- Magnetic mounts for each vibration sensor 080A133.
- Three-axis adapters for mounting vibration sensors 080A62.
- Shielded 042 STP cable (line length up to 150 m per channel).

A multi-channel National Instruments ADC/DAC board PCI 6071E includes 32 differential or 64 single-ended analogue inputs; 2 digital-to-analogue outputs for control signals; 8 digital inputs and 8 outputs.

Signal notations in Figure 8.1 are as follows: AccN_{up}, AccN_{dn} – vibration acceleration; FW_n – rolling forces; $FZ_{n\text{-}k}$ – strip tension; wN_{up}, wN_{dn} – drive rotations of the upper and lower rolls, mN are the torques of electric drives. KVM (Keyboard Video Mouse) is a device for two-way communication of a remote monitor, key-

(a) (b)

Fig. 8.2. Magnetic mount with adapter for: (a) accelerometer; (b) signal converter

board and mouse with a computer. Vibration sensors and signal conditioner are shown in Figure 8.2.

The developed vibration control system implements the following functions.

Tracking of kinematical frequencies. Vibration levels increase when some kinematical and natural frequencies match. Signals of angular speed and load of individual upper and low work roll drives are obtained from the mill automatic system. For the convenient kinematic analysis, the colour-scaled time-frequency diagram is realised in the monitoring system. As an example, Figure 8.3a shows

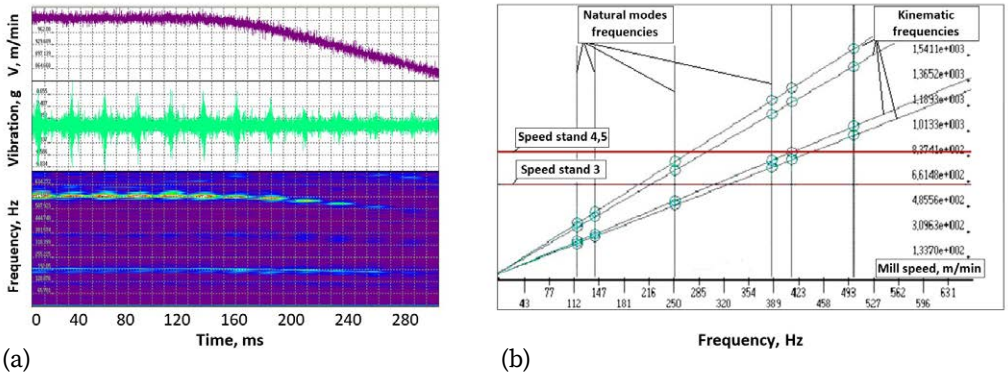

(a) (b)

Fig. 8.3. Kinematical frequency tracing:
(a) time series and time-frequencies diagram of gearbox meshing in stand No. 5;
(b) diagram for mill speed choosing to avoid resonances

a trace of gearbox teeth frequency during rolling speed changes. The main stand natural frequency is observed there as a horizontal line. Backup rolls beating intervals are reflected in the spectrum. Such elements of the drivelines as gear couplings for overload protection placed between motors and gearboxes are well heard by the sensors on the backup rolls chocks on the operator side. Therefore, the wear of such elements placed even far from rolls is important for chatter excitation. In addition, the gearbox meshing frequency is very noticeable in the signals on the stands. Although the spindles are the nearest to the stand elements, gear coupling frequency is visible in the spectrum only when their wear is large. It was discovered that stand vibration amplitude increases for speeds where bearing frequencies match with the main chatter peak in the spectrum (115–120 Hz). To avoid resonance ranges of speed, a frequency diagram was drawn (Fig. 8.3b). Operating at an even higher speed may be less dangerous for chatter. This diagram helps mill operators to go through the resonance ranges during mill acceleration and slowing down.

Rolling process parameters. Online control of rolling parameters in the vibration monitoring system allows the determination of some dynamic conditions that lead to mill instability. The first condition takes place when the neutral angle shifts beyond the contact zone (rolls slipping). Instability is caused by tension oscillations and other rolling parameters. The reliable method to achieve higher rolling speed is the decreasing of strip tensions, which makes connections softer between stands. In the series of experiments, specific tensions between the stands were reduced from 130–150 kN/mm^2 to 90–100 kN/mm^2. For strip thickness 0.5–0.6 mm, the mill speed increased by 50–100 m/min without chatter occurring. However, with tension 100 kN/mm^2 for stands No. 4–5, the strip lost stability and the roll surface was damaged. Hence, such a method has some technological restrictions.

Horizontal forces acting on the work rolls. The horizontal beating of work roll chocks occurs when the balance between strip tension forces, the horizontal component of a rolling force and drive torque is violated. Due to backlashes opening, work roll chocks begin to vibrate in the stand housing, which further leads to chatter in the whole tandem mill. To prevent such dynamic effect, the vibration monitoring system controls the balance of horizontal forces and gives an alarm signal when it is violated in any stand. This method is more advantageous than the hydraulic liners mentioned above, as it does not interfere with the HAGC system.

Measuring the high-frequency waviness of strip thickness. As mentioned above the high-frequency strip thickness variation appears in the mill even during normal rolling conditions (without chatter). The amplitude of the strip thickness wave may overcome standard deviation and cause product rejection by customers. It was assumed that the last stand vertical vibrations have the most influence on strip thickness variation. Therefore, such a method for periodical defect measuring was implemented based on vibration signals in the last stand. As the 3rd octave vibration chatter mode occurs for most cases, the joint motion of upper and low pairs of backup and work rolls is assumed.

Efficiency of automatic vibration control system. The new method of chatter detection is implemented in mill automation system for rolling speed optimal

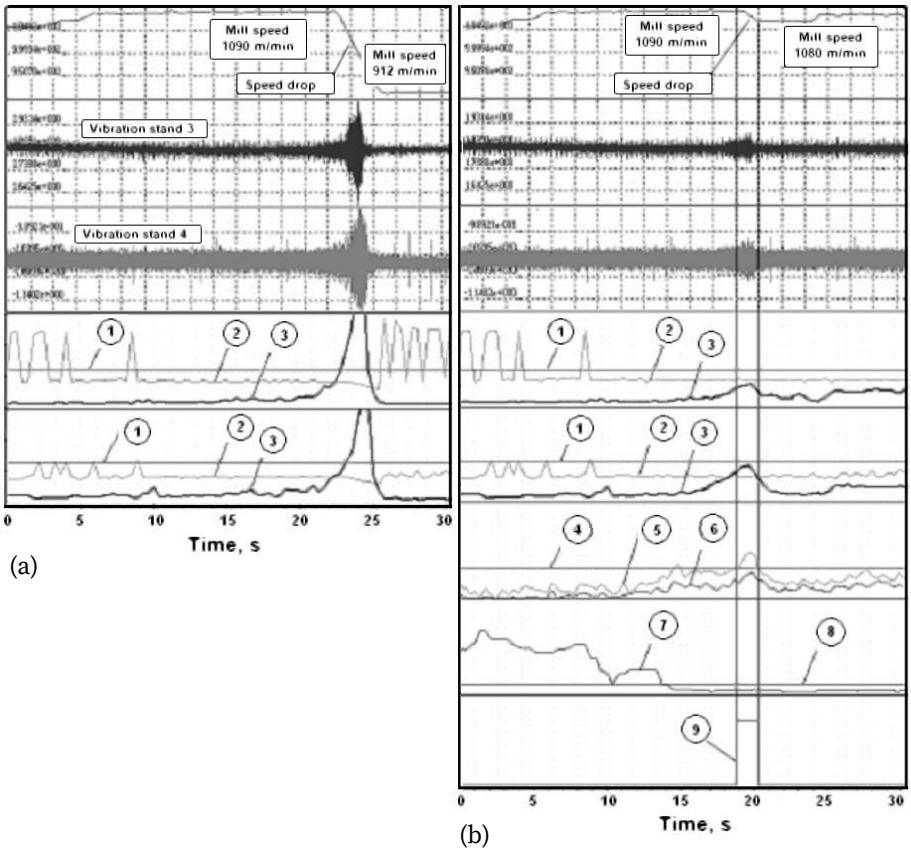

Fig. 8.4. Chatter control in the tandem mill: (a) manual control by mill operator; (b) automatic early detection of vibration excitation by the monitoring system

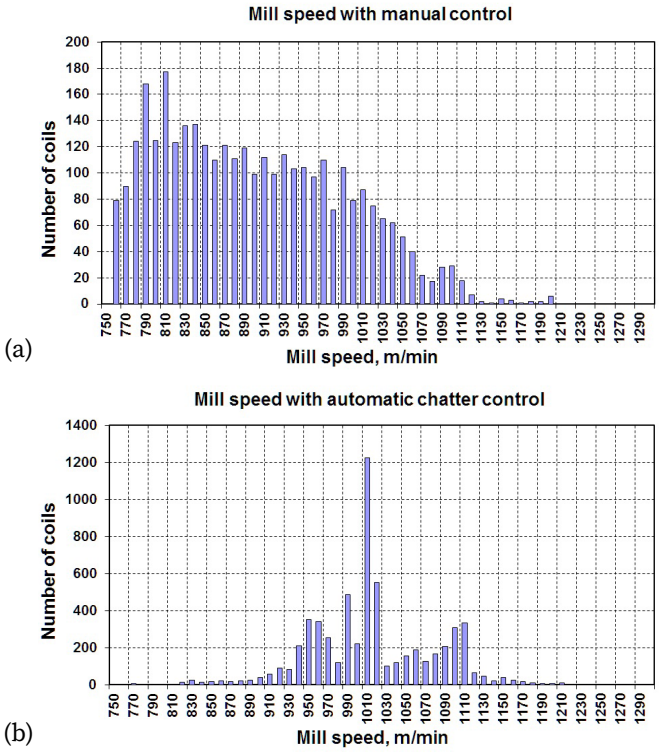

Fig. 8.5. Work speed distribution of tandem mill:
(a) under manual control by mill operator;
(b) under automatic control by the vibration monitoring system

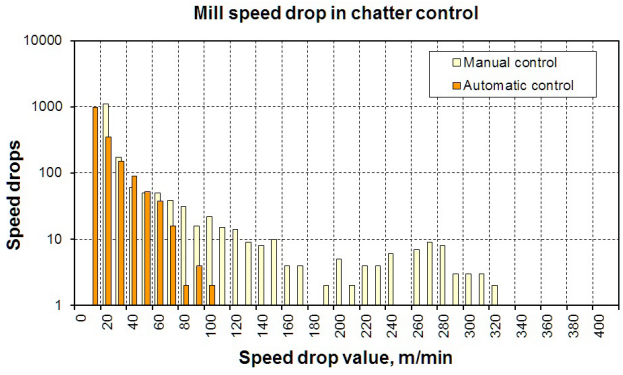

Fig. 8.6. Speed drop values distribution in tandem mill
with manual and automatic control

Table 8.1. Efficiency of tandem mill automatic control

Absolute parameters	Manual control				Automatic control			
	Apr.	May.	Jun.	Mean	Jul.	Aug.	Sep.	Mean
Average mill speed, m/min	862	901	895	886	1010	1006	926	980
Maximum mill speed, m/min	1137	1159	1197	1165	1274	1244	1257	1258
Speed drop value, m/min	107	94	39	80	13	60	92	55
Relative parameters	**Manual control**				**Automatic control**			
Average speed increasing, %	–	–	–	–	13.9	13.5	4.5	10.62
Maximum speed increasing, %	–	–	–	–	9.4	6.8	7.9	8.03
Speed drop decreasing, %	–	–	–	–	–83.8	–25.0	–15.0	–31.25

control. When chatter amplitude is still small, the speed drop value may be less than 5–10 m/min and it is enough to prevent a further vibration increase (Fig. 8.4). Notations in Figure 8.4: 1 – spectrum amplitude alarm level; 2 – spectrum peak frequency; 3 – spectrum peak amplitude; 4 – chatter index No. 2 alarm level; 5, 6 – chatter index No. 2 for stands Nos. 3, 4 (coefficient of correlation); 7 – chatter index No. 1 (main mode frequency deviation); 8 – chatter index No. 1 alarm level; 9 – mill speed control signal.

Performance parameters of automatic mill control are represented in Figures 8.5 and 8.6 and summarised in Table 8.1 covering several months of the new system operation. The basic period for analysis is April–June of the reference year under manual control. It is compared with the period July–September under the automatic mill control by the new monitoring system. The maximum mill speed increased by 11% and the average mill speed – by 8%.

8.2. System of plate front-end levelling in the hot rolling mill

The innovative automation system is developed for plate front-end levelling in the hot rolling mill. Before the plate rolling, the initial mismatch of the speed is

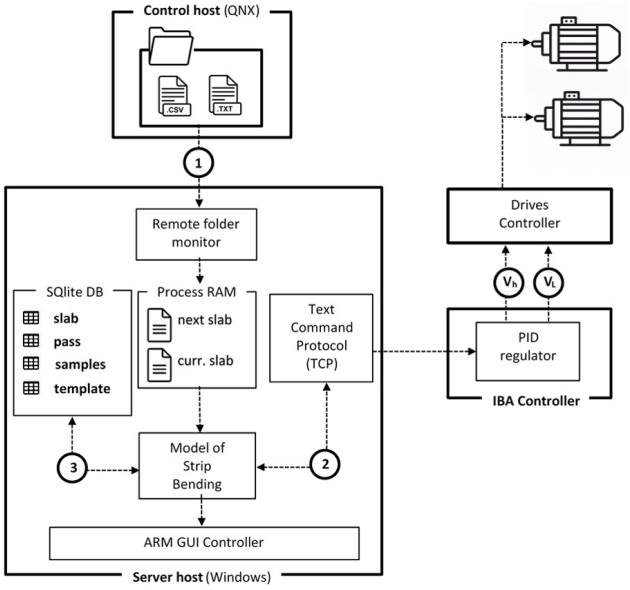

Fig. 8.7. Scheme of data exchange between the new system and mill control subsystems

generated and is further controlled along the several passes depending on the plate thickness. Visualization of the signals of the finishing mill stand and network communication with the server of the second level is provided. The scheme of data exchange and interaction with the existing rolling mill control subsystems is shown in Figure 8.7.

Taking into account the frequent cases of operation of the drives of one of the rolls in the generator mode with significant rolling asymmetry and the transition of the load torque through zero, the control algorithm in the digital controller provides only positive additions to the speed setting of one of the drives. This eliminates the opening of gaps in the drivelines when braking motors and the occurrence of dynamic processes in the drivelines.

At the first level, analogue-to-digital and digital-to-analogue conversion of signals is carried out using ibaNet750 components for interaction with the main control loops of the drives, and the digital controller itself is implemented in the ibaLogic software environment.

At the second level of control, a server operates, which interacts with the sheet tracking system at the workshop level. The server has the functions of monitor-

ing the parameters of the technological process and the actions of the operators to change the settings of the stand (the number of passes, reduction and sheet thickness, the end of rolling), synthesis of the developed model of control actions for the first-level controller in each pass, saving the calculated and actual parameters in the database, displaying system status and recommendations for mill operators. At idle running without load, the PI-controller coefficients were adjusted and the stability of the entire control system was checked when the digital subsystem was connected in parallel with the main control loops of the electric drives of the finishing mill stand.

The model of targeted front-end bending of the sheet is implemented as a separate module in the process automation system. The initial data about the current rolled sheet are read from the rolling mill database. Part of this information is transferred to the IBA controller. For this, a set of text commands is used and implemented over the TCP data transfer protocol. Next, the setpoints are calculated and transferred to the IBA controller. The final setpoints are calculated using a PID controller and transferred as additional analogue signals to the automation system, which directly controls the drives. After the plate has been rolled (in each pass), the controller transmits to the server the real parameters of the rolling process in the form of individual values or arrays of numbers. After receiving data on the completion of the pass, the automation system updates the information on the graphical user interface in the mill operator pulpit.

All information about rolled sheets is stored in the database. In addition to the sheet parameters, the parameters of all passes are saved. For each pass, various signals are measured, for example, the deviation of the sheet thickness from the target value. For each signal, its statistical characteristics are calculated and saved. In addition to storing information in the database, the server carries out full logging of all important events.

The perturbation for the developed digital regulator, which operates in parallel with the main control loops, is the natural drop in the speed of the electric drives. The speed drop of a more heavily loaded drive will be greater than that of a drive with a lower speed. The mill operators have the possibility of disabling the automatic mode at any time and switching to the manual setting to correct the speed mismatch.

The maximum speed difference is limited by overloading a drive with a higher speed, and completely unloading up to the generator mode of another drive with a lower speed. Empirically, the maximum allowable speed difference was

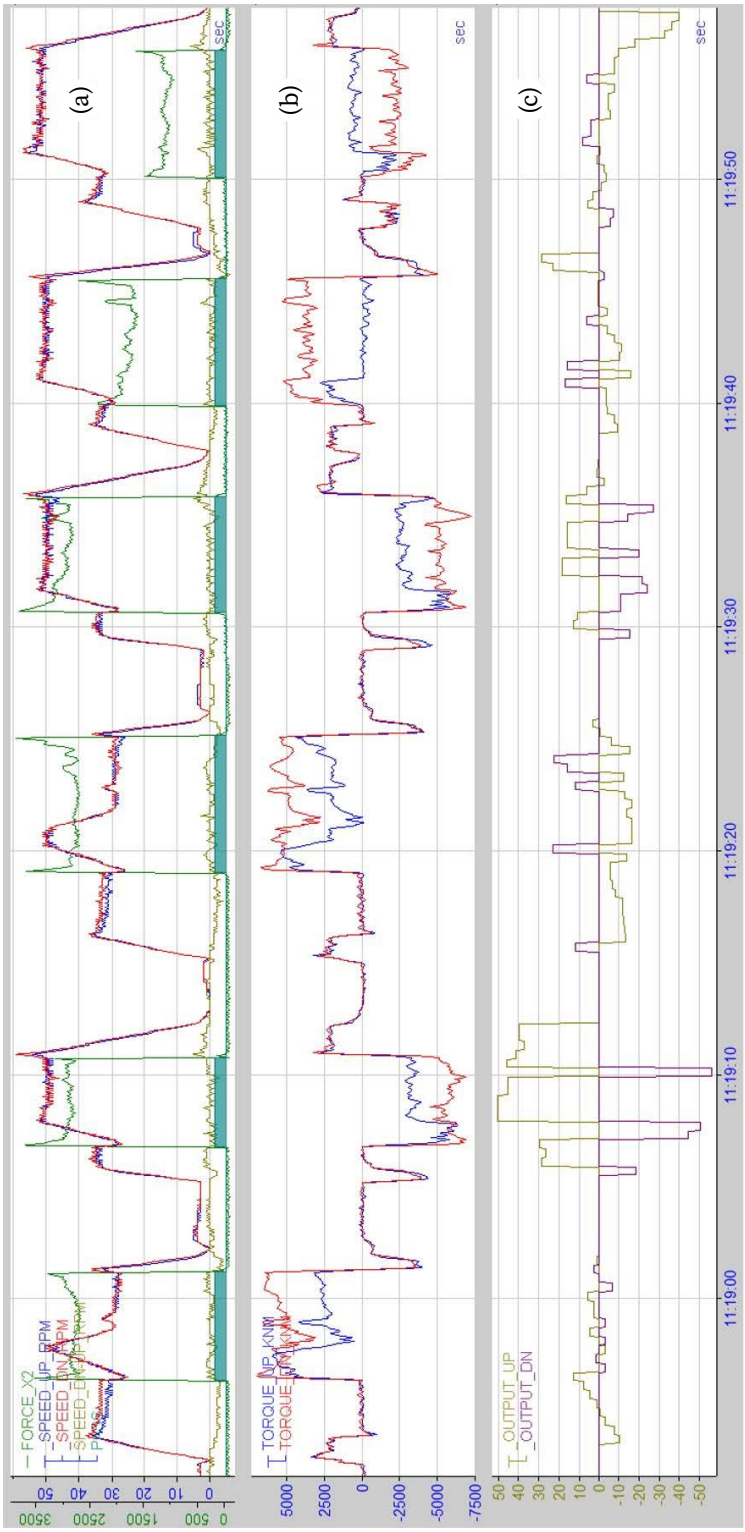

Fig. 8.8. An example of the automatic control system operation (see explanations in the text)

set to be 10% of the current average speed of the drives. This restriction is implemented when the operator assigns the controller parameters.

To improve the accuracy of working out the specified mismatch values, the range of the dead zone of the speed regulator was reduced to ±6 rpm. Reduced from 400 to 200 ms, the averaging time of the speed signal received at the input of the controller increased the time for working out the specified mismatch to 2 s with its smooth decrease from the initial value dWBite, effective during capture, to the second level dWRoll, effective during rolling of the main part of the sheet.

The example of system operation is shown in Figure 8.8. The upper graph (Fig. 8.8a) shows the rotation speeds of the upper and lower rolls (rpm), their difference and the rolling force (kN × 10^{-1}). The sections in the time series correspond to each reverse pass. The middle graph (Fig. 8.8b) shows the changes in the torques of the upper and lower drives (kN m). The third graph (Fig. 8.8c) shows the system output signals whose aim is to correct the rotation speed of the upper and lower drives (rpm).

It is noticeable that in passages 5 and 6 the moment of the top drive changes its sign, which means it operates for a short time in the generator mode. That is why the regulator works in such a way that it creates a given speed mismatch only by positive additions to the speed of one of the rolls to prevent the gaps from opening in the drivelines and not causing shocks in the driveline. From the graphs of the 1st pass, it is noticeable that after the pass start and mill acceleration, the system

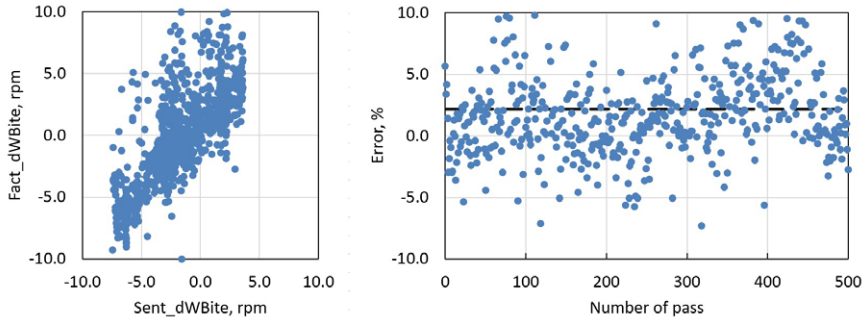

Fig. 8.9. (a) The relation between the assigned speed mismatch (Sent_dWBite) and the real difference in speeds (Fact_dWBite) of the upper and lower rolls; (b) error of regulation

creates a pre-calculated mismatch in the rolls' rotation speed. Then it smoothly decreases the speed difference to zero after the front-end rolling.

The statistical relation of assigned and real speed mismatch is shown in Figure 8.9. The mean value of error in speed mismatch regulation is about 2%. A noticeable spread is visible due to the delay in the existing control system. The deviation in the idle speed of the drives within ±1 rpm is due to the unbalanced heavy spindles beating in the driveline. Besides, the short time of the mill acceleration plays a role after reversing. The speed regulator switches on beyond the dead zone (±10 rpm) and keeps the two drives› speed difference until the metal gripping speed (22–24 rpm – in manual and semi-automatic mode and 33–34 rpm – in automatic mode).

The automatic system for the front-end bending control of thick plates is implemented with minimal changes to the existing analogue system of the individual drives. It has been put into permanent operation on the hot rolling mill. As a result of long-term operation, the system allowed a 25% reduction in the number of sheets with curvature, which required additional heating and levelling, hence, energy consumption was also reduced.

8.3. System for dynamic load monitoring and maintenance management

The multi-disciplinary research resulted in the development of an intelligent RUL monitoring system for hot rolling mills drivelines [427]. The approach is based on physical models and consistent with the recently introduced term of Dynamics Based Maintenance [428]. The developed CMMS incorporates such distinctive features as the relation of dynamic response and static load, rolling stands interaction; RUL prediction using physical degradation model; the influence of bearing clearances on dynamics; using modal analysis for wear assessment; online estimation of driveline dynamic properties; and fatigue analysis. Some simplifying assumptions (e.g., neglecting the influence of shaft misalignment on contact pressure in gears) do not restrict the proposed approach. It can be applied in any plants, e.g., heavy mining machinery working in non-stationary conditions.

The information structure of the developed CMMS is represented in Figure 8.10. Initial or rarely updated information, supplied on a daily or weekly basis and online signals are shown by the arrows in different colours: black, green and red, respectively.

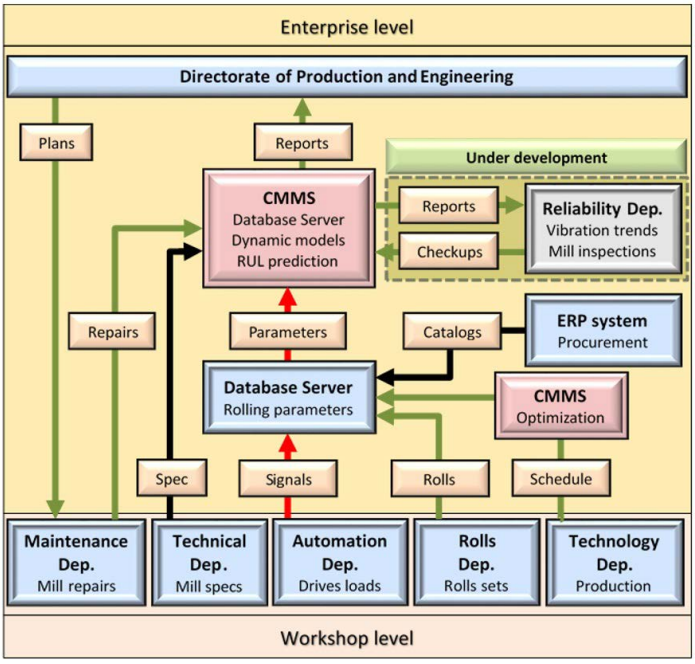

Fig. 8.10. Data flow chart of CMMS integration into ERP and data flows

Groups of main users and data sources are divided at the enterprise level: plant mechanical manager, reliability department, automation department; and workshop level: head of the production, rolls grinding workshop, technical department, mill maintenance mechanics and electricians. Department of plant equipment reliability can provide vibration trends from the vibration monitoring system recently installed on the mill.

Database of structural materials. The continuous hot rolling mill consists of 5 roughing stands with 3 edgers (side reduction vertical rolls) and 7 finishing stands. The driveline units included for RUL monitoring are bearings, spindles, gearboxes and couplings.

CMMS supports the hierarchical structure of mill equipment at four levels: stand – aggregate – unit – detail. Each type of element is associated with the place of its installation. Real exemplars of equipment are coded in corresponding catalogues to track them after replacement. Some details can be placed in a warehouse, and the system continues to accumulate load cycles after their reinstallation in the mill as a member of maybe another assembly unit and stand. This

important function of CMMS (warehouse support) is necessary for accurate RUL prediction.

CMMS contains a catalogue of materials with steel grades, and their properties (ultimate and yield stress, endurance limit, hardness). Different heat and chemical treatments of alloy steel are represented as additional records. Materials are linked to types of details. This is basic information for RUL prediction. Ultimate stress (S_U), yield stress (S_Y) and endurance limit (S_E) are taken, when available, from steel specifications or calculated from experimental Brinell hardness value (BHN) as:

$$S_U = a_1 BHN + a_0; \tag{8.1}$$

$$S_Y = b_1 BHN + b_0; \tag{8.2}$$

$$S_E = c_1 BHN + c_0, \tag{8.3}$$

where a_i, b_i, c_i – coefficients of a given grade of alloy steel. The fracture point of endurance limit on the S–N curve is taken equal to 5×10^6 cycles. Endurance limit for bending stress of carburized gear tooth with a hardened layer (23 mm) is considered for core material.

CMMS contains a catalogue of bearings with their static (C_0) and dynamic (C_1) load capacity. Properties of material are rarely known from suppliers, hence, standard high carbon, chromium steel is assumed. Bearings are differentiated by suppliers for the analysis of reliability.

Data on mill drives operation. The steel plant, where the hot rolling mill is operated, has a database server in the ERP system where data from different sources are stored with 1 s sampling. A much higher sampling frequency (100 Hz) is provided by the ibaPDA system, but only in the finishing stands of the mill.

The most important signals for CMMS operation are the electric drive rotational speed and rotor armature current. Three types of main drives are used in different stands: direct current and alternative current synchronous in roughing stands and variable frequency drive in finishing stands.

The pre-processing procedure includes electric motor current (A) conversion into torque (kN m), averaging and transforming static torque to work rolls taking into account electric losses and driveline efficiency. Technological rolling param-

eters are as well received and used for rolling force model verification in CMMS optimization application.

Data on mill maintenance. The time between scheduled repairs varies from 7 to 12 days with a general overhaul at the end of the year. Service personnel cannot repair a single stand while other stands of a continuous rolling mill are working. Hence, in the case of failure, the whole plant is stopped for urgent repair. The most critical severe failures of continuous hot rolling mills occur shortly after one of the stand overload causing 6–8 hours of downtime for the whole mill repair. In the majority of cases, these damages are the result of fatigue as it follows from material microstructure analysis after accidents.

Textual and graphical information on the maintenance actions of mill staff has been systematized and digitized following the structure of mill stands equipment. The CMMS catalogue of failures and maintenance actions has the following fields:

Object position:	stand, aggregate, unit, side, position.
Failure mode:	crack, deformation, wear, pitting, breakage, heating.
Maintenance action:	inspection, replacement, measurement, grinding, tightening.
Repair type:	urgent, scheduled, overhaul.
Element state:	installed, stored, supplied, scrap.

This is the only manual input of information in CMMS, which is not possible to avoid. The rest input data are automatically processed and visualized via the client's application.

Dynamical models of the drivelines. To obtain a dynamic response for different elements in the rolling stand, a detailed spring-mass model has been designed including hydraulics. This model allows the simulation of any dynamic processes and determining loads in roll bearings to predict their RUL. After each slab rolling, the recorded torques are applied as an input disturbance into the corresponding models of the stand and driveline. Rolling force is calculated by the drive torque, strip geometry and material reduction in the stand, which are received from the mill automation system.

The following assumptions are admitted in the physical models of drivelines:

- Axial forces on roll bearings account wear of liners in the stands.
- Work roll bending is accounted for by average values (not measured).
- Torques in lower and upper spindles are calculated separately.
- Gap opening in spindles depends on weight balancing (roll position).

- Gaps in gears are considered closed before strip biting by rolls.
- Two parallel parts of gearbox meshing are considered as a whole stiffness.
- Gear shaft inclination is accounted by a coefficient of bearings wear.
- Gear shaft bolting is pre-loaded by screws tightening forces.
- The speeds of the transportation table and vertical rolls are adjusted to stands.
- Mechanical damping and electrical motor losses are constant.
- The influence of lubrication volume deviation on specific wear rates is neglected.

Models of wear. During the normal process of mill operation, the wear of elements in stands and drivelines gradually increases with different rates depending on the position in units and the history of loading. Degradation of contact surfaces resulted in angular and radial backlashes, which in turn increases torsional dynamics. Therefore, adaptation of dynamic models is required, and is based on known wear models [429]:

$$w = k p s, \tag{8.4}$$

where w – wear (mm); k – coefficient of material and contact conditions; p – contact pressure (MPa); s – sliding distance (mm). The same approach is used for spindle pads and bearings.

Known wear (mm) is then transformed into backlash (rad):

$$\Delta = \frac{w}{R}, \tag{8.5}$$

where R – radius of rotating part (mm).

Wear differs for pinion and wheel and is inversely proportional to the hardness of contact surfaces. The hardness of pinions is 550…630 BHN (case-hardening), and wheels – 320…470 BHN (inductive hardening). Sliding distance and contact pressure are calculated from the gear geometry. Contact ratio (overlap) describes tooth load sharing. Influence of gears degradation on contact pressure is neglected. The kinematic viscosity of lubricating oil and contact friction is assumed constant for every pair of gears. It is assumed that abrasive wear does not cause scuffing because pitting is a rare case in these drivelines.

Spindles are the most difficult for analysis elements due to complicated geometry and simultaneous torsional and bending stress. FEM simulation is used for the analysis of weight balancing force influence on the stress state of the spindle shaft

and head design optimization [430]. Intensive wear of bronze pads within 14–30 days modifies contact stress distribution, specific wear models are proposed in [431].

CMMS model of spindle wear is verified by numerous measurements of bronze pads' geometry in stands with a wide range of working conditions. Two failure modes are supposed for spindle parts: abrasive wear of bronze pads (up to 5–6 mm); and cyclic fatigue of heads.

CMMS runs the procedure of dynamical model parameters adaptation after every cycle of strip rolling and the database is updated before the next strip enters into the stand.

Contact and bending stresses of gears are determined by the real-time torque:

$$\tau = a\sqrt{T}, \tag{8.6}$$

$$\sigma = b\,T, \tag{8.7}$$

where a, b – coefficients of gear geometry. Since the spindle head is subjected to multi-axial stress, its equivalent value is calculated as:

$$\sigma_{eq} = \sqrt{\sigma^2 + 3\tau^2}, \tag{8.8}$$

To determine cyclic fatigue in elements of the rolling mill, the S–N diagrams (Wöhler's curves) are used. Typical transient torque and fatigue diagrams for structural alloy steel are shown in Figure 8.11. When torque is about zero, the

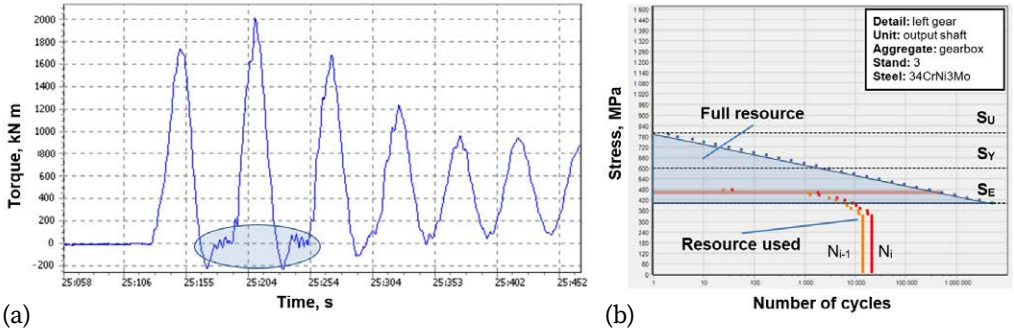

Fig. 8.11. Fatigue cycles in the driveline:
(a) transient torque; (b) S–N diagram for RUL estimation

backlash opens and loading cycles become symmetrical, which is more dangerous for gears. The system uses Goodman's law to process combined asymmetrical cycles and transforms them into equivalent reversed stress cycles. RUL's prediction is based on Miner's relation.

CMMS includes three software applications: server, client and optimization modules. They are the MS Windows applications developed during research projects.

The server application works online 24/7 independently from the other parts of CMMS and using disk space at the plant automation department. Its main functions are as follows:

- Automated search and statistical processing of electric drive loads.
- Time synchronization of electric drive loads with product processing.
- Calculation of dynamic loads and accumulated damages in elements.
- Support of maintenance database on repairs, failures and changes.
- Estimation of RUL in elements based on the historical data.

Retrieval of online data on electric motor loads, speeds and rolling parameters by stands is carried out by SQL queries from the plant automation database. The server has a minimal user interface allowing it to start, load parameters of calculation from the configuration file and install network connection with databases and client applications.

The client application of CMMS has the following user-oriented functions:

- Visualization of loads for the selected elements.
- Visualization of elements failures.
- Manual updating of maintenance database.
- Visualization of accumulated fatigue cycles for the selected elements.
- Generating reports on overloads, failures and RUL.

Reports on driveline elements overloading include the following parameters: time of mill operation, number of cycles above the limit, maximal/minimal values, and absolute/relative deviation over the limit. Some of the screenshots from the client application are shown in Figure 8.12. The linear trend is used for RUL prediction. The probability of an element's failure by overloading is estimated by the tails' overlap of stress and material strength distributions. Material properties deviation is estimated, e.g., by gear tooth hardness due to imperfect heat treatment process.

In many software applications, the calendar time or working hours are used for RUL, which is a simple and proven way for stationary working conditions.

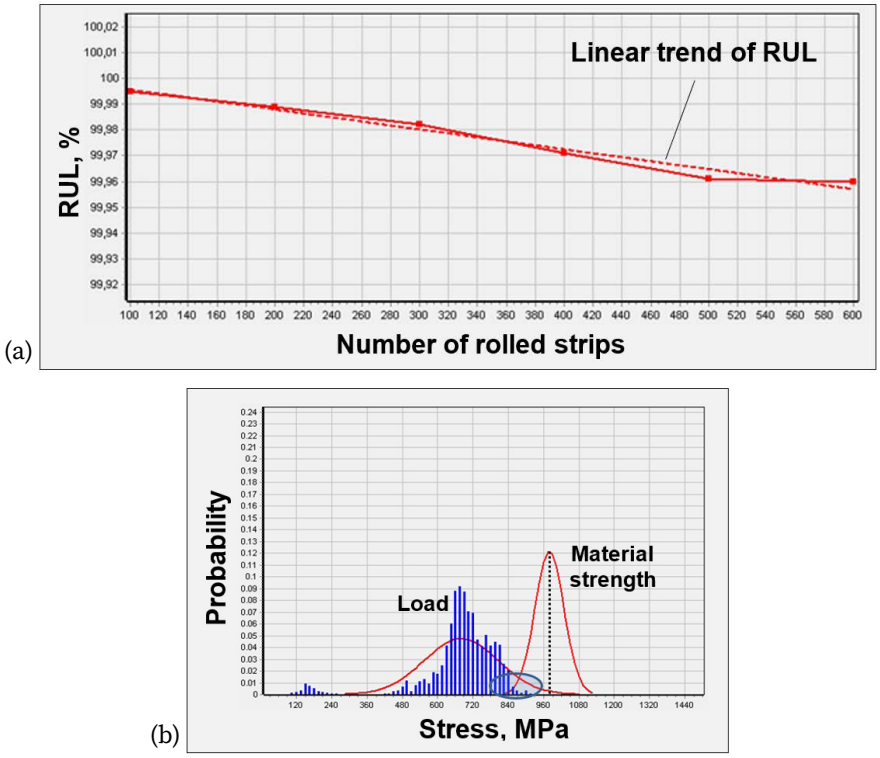

Fig. 8.12. (a) Trend of RUL reduction during operation;
(b) distributions of load stress and material strength of machine element

In rolling mills, RUL can also be expressed in: tonnage of the product; length of rolled strips; and their number.

CMMS represents RUL for future periods expressed both in calendar days and a number of strips approximated by daily mill output. This is a quite reasonable approach for continuous steel production because maintenance staff needs to plan the next scheduled repair, while the technology department builds a production plan by rolling cycle (about 30 s).

The optimization application is designed as an offline module with the following functions:

- Adaptation of rolling force models by measured drive loads in stands.
- Verification of models by the actual plan of the rolled product.
- Calculations of rolling process parameters using adapted models.
- Calculations of fatigue in the rolling mill equipment.

- RUL prediction for virtual rolling plans with initial values from CMMS.
- Optimization of rolling schedules according to RUL-related criteria.

The technological department of the hot rolling mill, having such a software tool, can correct rolling schedules before some troubles happen in stands due to overloading in the real production process. Besides, they can estimate what effect will have on the new steel grades or critical reductions in the overall mill reliability. Users can assign various batches of the existing and planned assortment, especially wide thin strips of hard-to-deform steels. The optimization module uses information from the plant and CMMS on the current RUL of elements, but the user can assign any initial values, e.g., after gear replacement (RUL = 100%).

The generalized criterion of optimal rolling schedule is proposed, namely the deviation of rolled strips numbers with constraints on strength capacity by torques and minimal RUL values:

$$\min_{0\le k_i \le 1} SD\left(N_i\right); T_i < T_{\max_i}; RUL_{ij} > RUL_{\min}, \tag{8.9}$$

where N_i – number of rolled strips; i – stand number; j – element number; k_i – load share coefficients; T_i – rolling torque in the stand; $T_{\max_i}$ – strength capacity limit in the stand; RUL_{ij} – remaining useful life of elements in stands; $RUL_{\min}$ – minimum value (set at 10%).

CMMS optimization module accounts for constraints imposed by strength capacity and RUL in stands, then adjusts reductions in mill stands by load share coefficients ($k_i = 0…1$).

In addition, a useful function is also available to rearrange reductions in stands in the case of one stand being out of work ($k_i = 0$), e.g., due to its abrupt failure, and on-the-go repair.

CMMS deployment consists of several stages. In the first stage, users need to design catalogues of equipment, materials, maintenance actions and model parameters. Then, determine the degree of wear and RUL values for all considered in calculations elements currently installed in the mill. This procedure is based on expert assessments and historical data for a representative amount of strips (by size and steel grades) with corresponding S–N curves for elements. This is some kind of retrospective simulation of the real process.

In the second stage, CMMS begins to accumulate S–N data based on real signals. Wear measurements and mill inspections are used for model adaptation on historical data since the previous installation of elements. Statistical analysis of

RUL prediction accuracy is possible after a given period of operation when the full-service time becomes available after CMMS starts.

Although some simplified assumptions are made, they do not decrease the system validity, because dynamical models are verified by measurements. The CMMS is applicable in any industrial plant, e.g., heavy mining machinery working in non-stationary conditions. It provides equalization of loads and safe operation of a series of industrial machines.

9. SUMMARY

Based on the conducted experimental and theoretical studies, a unified approach to the implementation of dynamical models in condition monitoring of heavy-duty industrial machines has been developed. It comprises efficient diagnostic methods with complementary measurement tools and data processing techniques.

During normal operation, mining and metallurgical equipment is subjected to frequent changes in technological regimes and severe impacts from processed materials that cause non-stationary and non-Gaussian distribution of applied loads and noise in the measured signals. These impacts from treated materials including friction instability are represented by the wide-band frequency spectrum, which excites the main natural modes of dynamical systems.

Almost all types of industrial machines work with unavoidable and hardly controllable wear, which result in angular and radial backlashes. These kinds of deterioration of machine parts are considered the main factors affecting excessive dynamic loads and subsequent failures of separate parts and assembly units (gearboxes, shafts with bearings, cardan couplings) inside the machines and their technological complexes. The main idea of the research was to measure backlashes, predict the increase of dynamic loading and high vibration and undertake appropriate actions before severe damage occurs.

The spectrum of significant natural modes of multibody heavy industrial machines during their torsional and spatial vibrations rarely exceeds several hundred hertz or even less. These specific features of their design (spring and mass values combination) make it possible to efficiently apply the low degree-of-freedom (DOF) dynamical models with lumped parameters in condition monitoring. To describe various dynamic phenomena in machines, different classes of models should be considered and appropriately used based on linear, nonlinear or parametric differential equations.

The modal analysis is applied as a useful technique for dynamical systems analysis combined with the frequency response functions (FRF). The represen-

tation of the measured and simulated signals by the phase space plots (PSP) and trajectories of motion (orbits) gives some advantages in online diagnostics of vibrating machines. These methods do not require high-frequency sampling of data and are suitable for condition monitoring, e.g. vibrating sieving screens.

Non-stationary loading of machines makes less efficient an implementation of the standard vibration diagnostic methods. On the other hand, these regimes can be used for the diagnostics of backlashes that do not exhibit their action under stable static loading. The nonlinear features such as the deviations of frequencies, amplitudes and phases of the natural modes, dependence of dynamical response on the static load, and transient signal damping rate can be successfully used for condition monitoring.

The design of instrumentation and sensors developed for torsional torques and angular backlashes measurements takes into account harsh working environments and is applicable for continuous condition monitoring of mining and metallurgical machines.

Bolts loosening and plastic deformation, as a type of nonlinear stiffness characteristics, are quite difficult to detect and time-consuming by visual inspections. Using intelligent measurement techniques and special tools applied in structural health monitoring is complicated due to multi-bolt joints and the harsh working conditions of heavy-duty machines. Therefore, the developed methods of bolts loosening are based on vibration signals measured by the standard sensors.

The diagnostics of helical springs supporting vibrating machines for bulk materials processing is a complicated technical problem. Therefore, model-based methods applicable in condition monitoring systems contribute to this less represented in the maintenance practice domain. Besides, the model-based approach to bolt loosening detection can solve this problem frequently occurring in vibrating machines. This is certainly a new feature, which is not represented in the literature and is absent in condition monitoring systems.

Combining hydraulic and mechanical units of industrial machines constitutes dynamical systems with variable parameters. The stiffness of elements in such systems is changed by the position of the piston in a cylinder. The sudden destruction of high-pressure cylinders and tubes constitutes a danger for personnel. Hydraulic impact estimation in tubes testing rig required a multi-disciplinary approach for potential damage estimation, which has advantages against FEM simulation in the case of numerous variants of loading and disintegration of masses. Regarding the rotating and vibrating industrial machines, FEM simulations are mainly applicable

at the design stage. Modelling of angular and linear backlashes and wear of elements, namely, changes of contact geometry, disintegration and collisions of inertial masses, appearing during machines' operation meet remarkable difficulties.

The pressure release via the safety valves used in hydraulic roof supports and other hydraulic machines makes the dynamical system nonlinear with softening stiffness characteristics, which reduces peak loading and prevents severe failures. An alternative approach based on smart safety valves controlled by the signals from additional sensors is proposed but needs further development to provide higher flow rates and short delays in safety valves.

The same problem exists in the application of hydraulic cylinders for chatter vibration damping in cold rolling mills, which is restricted by the flow rates and delays in the servo valves. Therefore, the new approach is proposed and implemented in the condition monitoring system based on the phenomenon of several oscillators (rolling stands) synchronisation via the elastic links (strip), which was not previously considered in the literature for such application.

The presented results improved the understanding of the multi-motor drive systems (MMDS) concerning load equalisation and branched parts interaction by the gear couplings. An analysis of small deviations of electric motor parameters and angular backlashes cause out-of-phase oscillations accompanied by parametric resonances. The use of spur gears in MMDS is not desirable and phasing of parallel gears plays an important role in dynamics.

The branched drivelines with only one motor and changeable structure like in reducing-sizing mill or transmission of articulated underground vehicles impose additional limitations related to out-of-phase torsional oscillations of terminal masses. The design of such systems should account for the interaction of separate branches and higher dynamics due to gaps playing.

Passive vibration damping requires embedding certain elements or modification of contact surfaces or whole parts of machines with non-metallic materials. Taking into account size restrictions and design change complications, this approach has little potential for a significant reduction of machine dynamics. Instead, ubiquitous digitalisation makes methods of active vibration damping and dynamics control more efficient in the prevention of overloading and technological process interruption.

Active damping of torsional oscillations and spatial vibrations is a promising approach for industrial machines. Under certain conditions, which are determined in the research, electric drive acceleration can be used for dynamic torque reduction

not only in the simple drivelines (motor and load) but also in the multibody systems including gearboxes as the intermediate rotating inertia. The load balance regulation between the individual electric drives made it possible to solve an important problem of front-end bending of hot rolled plates. Moreover, this regulation is realised during the short period of drive acceleration.

The random variations of treated material properties or scheduled replacement of large-scale machine parts during maintenance have little influence on the natural frequencies of a machine but can shift the nodes of either spatial or torsional modes of vibration. That is, in turn, a reason for the dynamical behaviour change of the whole system when other neighbouring inertial parts start to oscillate out of phase (gears, rolls). This node shifting greatly affects nonlinear systems when it coincides with backlashes in the couplings but dynamical models can accurately predict the cases that are difficult to detect by monitoring with sensors.

The stochastic shock loads acting on the mining and metallurgical machines can be represented not only by the standard statistical distributions but also as spectra in the frequency domain. In this case, the time of load rising is considered as a half-period of input impact. Combining frequency response functions by different channels in industrial machines together with the spectra of external loads indicates the ways of dynamics reduction. In addition, the calculation of internal dynamic loads in nonlinear systems with backlashes, which is quite difficult even on the FEM models, made it possible to obtain relations of system response from the statistical parameters of stochastic impacts.

The logical continuation of dynamical models (digital twins) utilisation is the continuous monitoring of loading cycles in the machine parts where force, torque or deformation sensors are not available for installation. The collected data constitute the basis for Remaining Useful Life (RUL) prediction and on this basis the maintenance strategy development, i.e., further migration from condition monitoring based on local defect detection to monitoring of accumulated fatigue cycles and RUL-based maintenance planning. This approach can only be implemented with the high-level integration of software applications and database of CMMS into the ERP systems. It is mostly applicable to machines working under non-stationary conditions where standard methods are difficult or impossible to implement because of continuous transient processes.

Finally, the scientific findings on complicated technical problems are reflected in the industrial condition monitoring or plant automation systems: chatter vibrations control system, torsional loads monitoring and maintenance planning

system, front-end levelling system of plate rolling mill, and vibrating screen monitoring system. The novelty of the developed methods of condition monitoring and automation systems has been proven by the patents and publications in peer-reviewed indexed journals.

The future directions of research include the development of non-invasive methods of wear (backlashes) detection in industrial machines based on vision data recorded by the standard cameras installed in the inspection drones. Another aim is the creation of optimal motion control of heavy-duty vibrating machines and operators' assistance for dynamic loads reduction in remotely controlled or autonomous vehicles for dangerous mining applications.

REFERENCES

[1] UPKEEP, 2020, *Maintenance Statistics: Predictive & Preventive, Labor & Costs*, https://upkeep.com/learning/maintenance-statistics/ [Accessed: 2024-03-07].

[2] OHLERT J., SPROCK A., SUDAU P., 2016, *Digitalization in hot and cold rolling mills*, Mat. Science Forum, 854, 215–224, https://doi.org/10.4028/www.scientific.net/MSF.854.215

[3] LEI Y., LI N., GUO L., LI N., YAN T., LIN J., 2018, *Machinery health prognostics: A systematic review from data acquisition to RUL prediction*, Mechanical Systems and Signal Processing, 104, 799–834, https://doi.org/10.1016/j.ymssp.2017.11.016

[4] BACHSCHMID N., PENNACCHI P., VANIA A., 2003, *Identification of multiple faults in rotor systems*, J. of Sound and Vibration, 254(2), 327–366, https://doi.org/10.1006/jsvi.2001.4116

[5] ROTHERAC A., JELALI M., SÖFFKER D., 2015, *A brief review and a first application of time-frequency-based analysis methods for monitoring of strip rolling mills*, J. of Process Control, 35, 65–79, https://doi.org/10.1016/j.jprocont.2015.08.010

[6] DONNOLI M., 2010, *On line detection of faults in a rolling mill process a method for detecting faults in a rolling mill process using multivariate SPC and system identification*, Int. Symposium on Power Electronics, Electrical Drives, Automation and Motion (SPEEDAM 2010), Pisa, Italy, 1640–1644, https://doi.org/10.1109/SPEEDAM.2010.5542069

[7] CINQUEMANI S., ROSA F., OSTO E., 2015, *Bearing faults simulations through a parametric model of a gearbox*, [in:] C. Niezrecki (ed.), *Structural Health Monitoring and Damage Detection*, Conf. Proc. of the Soc. for Experimental Mech. Series, Springer, Cham, 7, 1–9, https://doi.org/10.1007/978-3-319-15230-1_1

[8] LABIB A., 2008, *Computerised maintenance management systems*, [in:] K. Kobbacy, D. Murthy (eds.), *Complex System Maintenance Handbook*, Springer Series in Reliability Engineering, Springer, London, 417–435, https://doi.org/10.1007/978-1-84800-011-7_17

[9] SIKORSKA J.Z., HODKIEWICZ M., MA L., 2011, *Prognostic modelling options for remaining useful life estimation by industry*, Mechanical Systems and Signal Processing, 25(5), 1803–1836, https://doi.org/10.1016/j.ymssp.2010.11.018

[10] JARDINE A.K.S., LIN D., BANJEVIC D., 2006, *A review on machinery diagnostics and prognostics implementing condition-based maintenance*, Mechanical Systems and Signal Processing, 20, 1483–1510, https://doi.org/10.1016/j.ymssp.2005.09.012

[11] CHEN J., WAN Z., PAN J., ZI Y., WANG Y., CHEN B., SUN H., YUAN J., HE Z., 2016, *Customized maximal-overlap multiwavelet denoising with data-driven group threshold for condition monitoring of rolling mill drivetrain*, Mechanical Systems and Signal Processing, 68–69, 44–67, https://doi.org/10.1016/j.ymssp.2015.07.022

[12] ZIMROZ R., BARTELMUS W., 2012, *Application of adaptive filtering for weak impulsive signal recovery for bearings local damage detection in complex mining mechanical systems working under condition of varying load*, Solid State Phenomena, 180, 250–257, https://doi.org/10.4028/www.scientific.net/SSP.180.250

[13] GELMAN L., ZIMROZ R., BIRKEL J.F., LEIGH-FIRBANK H., SIMMS D., WATERLAND B., WHITEHURST G., 2005, *Adaptive vibration condition monitoring technology for local tooth damage in gearboxes*, Insight – Non-Destructive Testing and Cond. Monitoring, 47(8), 461–464, https://doi.org/10.1784/insi.2005.47.8.461

[14] BEKTAS O., 2018, *An adaptive data filtering model for remaining useful life estimation.* PhD Thesis. University of Warwick, UK.

[15] ZHENG Y., 2019, *Predicting remaining useful life based on Hilbert–Huang entropy with degradation model*, J. of Electrical and Computer Eng., ID 3203959, 11.

[16] USMANI N.I., VELISETTI S., TIWARI P.K., MISHRA S.K., KUMAR S., PATNAIK U.S., 2018, *Chatter detection using principal component analysis in cold rolling mill*, Diagnostyka, 19(1), 73–81, https://doi.org/10.29354/DIAG/81692

[17] PETIT B., DECREQUY D., JAKUBOWSKI A., BERTOLINI F., PERRET J., GOUTTEBROZE S., 2005, *Global approach of 3rd octave chatter vibrations at Arcelor Mardyck cold rolling mill and analysis of technological interactions*, Metallurgical Research & Technology., 102(7–8), 535–541, https://doi.org/10.1051/metal:2005150

[18] KOZHEVNIKOV A.V., 2021, *Sheet rolling under conditions of unsteady dynamic loading. Operation and management*, Cherepovets State University, Russia. ISBN 978-5-85341-899-8.

[19] MACKEL I.J., 2000, *Maintenance and quality related condition monitoring in rolling mills*, AISE Annual Convention, Chicago, Illinois, USA.

[20] RADIONOV A.A., GASIYAROV V.R., TVERSKOI M.M., KHRAMSHIN V.R., LOGINOV B.M., 2017, *Implementation of telemetric online monitoring system of elastic torque of rolling mill line of shafting*, IEEE 2nd International Ural Conf. on Measurements (UralCon), Chelyabinsk, Russia, 450–455, https://doi.org/10.1109/URALCON.2017.8120750

[21] SWIATONIOWSKI A., GREGORCZYK R., RABIASZ S., 2008, *Modular monitoring system for pilger mill drive*, Mechanics, AGH University of Sci. and Technology, 27(4), 172–178.

[22] FAGARASAN I., TALEB S., LESECQ S., GENTIL S., STUECHER R., 2004, *Signal-based diagnosis of torsional vibration of a hot rolling mill main drive*, IFAC Proc. Volumes, 37(15), 185–190, https://doi.org/10.1016/S1474-6670(17)31021-2

[23] WU Z. (2009), *Study on torsional vibration fault physics diagnose model of large rotation shaft*, Proc. 8th Int. Conf. on Reliability, Maintainability and Safety (ICRMS), July 20–24, 2009. Chengdu, China, 844848, https://doi.org/10.1109/ICRMS.2009.5269953

[24] CHEN Z., WANG T., GU F., HARAM M., BALL A., 2012, *Gear transmission fault diagnosis based on the bispectrum analysis of induction motor current signatures*, J. of Mech. Eng., 48(21), 84–90.

[25] TRAN V.T., ALTHOBIANI F., BALL A.D., CHOI B., 2013, *An application to transient current signal based induction motor fault diagnosis of Fourier–Bessel expansion and simplified fuzzy ARTMAP*, Expert Systems with Applications, 40(13), 5372–5384, https://doi.org/10.1016/j.eswa.2013.03.040

[26] GHARAIBEH N.S., MATARNEH M.I., 2014, *Loading decrease in metallurgical machines*, Research Journal of Applied Sciences, Engineering and Technology, 8(12), 1461–1464, https://doi.org/110.19026/RJASET.8.1122

[27] MAZUR V., ARTYUKH V., ARTIUKH G.V., TAKADZHI M., 2012), *Current views on the detailed design of heavily loaded components for rolling mills*, Engineering Designer, 37(1), 26–29.

[28] RADIONOV A.A., GASIYAROV V.R., KARANDAEV A.S., KHRAMSHIN V.R. 2018, *Use of automated electric drives for limiting dynamic loads in shaft lines of roll mill stands*, The 9th Int. Conf. on Power Electronics, Machines and Drives (PEMD 2018), Journal of Engineering, 2019(17), 3578–3581, https://doi.org/10.1049/joe.2018.8135

[29] KOZHEVNIKOVA I., KOZHEVNIKOV A.V., SOROKIN G.A.. MARKUSHEVSKII N.A., 2016, *Damping of vibrations in the primary drives of cold-rolling mills*, Steel in Translation, 46(10), 739–741.

[30] BELLI P., et al. (2004), *Active control of torsional vibrations in hot rolling mills*, IFAC Proceedings, 37(15), 113–118, https://doi.org/10.3103/S096709121610003X

[31] YANG X., HU C., PENG K., TONG C., 2013, *Load distribution of evolutionary algorithm for complex-process optimization based on differential evolutionary strategy in hot rolling process*, Math. Prob. in Eng., 675381, 8, https://doi.org/10.1155/2013/675381

[32] HEIDARI A., FOROUZAN M.R., 2013, *Optimization of cold rolling process parameters in order to increasing rolling speed limited by chatter vibrations*, J. of Advanced Research, 4(1), 27–34, https://doi.org/10.1016/j.jare.2011.12.001

[33] GUO Z.Q., XU Z.L., 2014, *Finite element analysis of the influence of balance mode on rolling mill universal spindle strength*, Applied Mechanics and Materials, 548–549, 449–453, https://doi.org/10.4028/www.scientific.net/AMM.548-549.449

[34] NETPU S., SRICHANDR P., 2012, *Failure analysis of a helical gear in a gearbox used in a steel rolling mill*, Journal of Materials Science & Engineering: B, 2(4), 289–294.

[35] SAGAR H.N., ARUN KUMAR K.B., 2019, *Minimization and controlling of bearing failure in rolling mill stand*, International Research Journal of Engineering and Technology (IRJET), 6(1), 491–496.

[36] PALIT P., JUGADE H., JHA A.K., DAS S., MUKHOPADHYAY G., 2015, *Failure analysis of work rolls of a thin hot strip mill*, Case Studies in Engineering Failure Analysis, 3, 39–45, https://doi.org/10.1016/j.csefa.2015.01.001

[37] ZYL van G., AL-SAHLI A., 2013, *Failure analysis of conveyor pulley shaft*, Case Studies in Engineering Failure Analysis, 1(2), 144–155, https://doi.org/10.1016/j.csefa.2013.04.011

[38] ZIMROZ R., KRÓL R., 2009, *Failure analysis of belt conveyor systems for condition monitoring purposes*, Mining Science, 128(36), 255–270.

[39] KAZILBASH S., 2020, *Drilling down into underground mining equipment*, https://www.engineering.com/story/drilling-down-into-underground-mining-equipment, [Accessed: 2024-03-07].

[40] STEFANIAK P., KOPERSKA W., SKOCZYLAS A., STACHOWIAK M., 2022, *Application of spectral entropy in haul truck joint damage detection*, Sensors, 22(19), 7358, https://doi.org/10.3390/s22197358

[41] SZURGACZ D., BRODNY J., 2020, *Adapting the powered roof support to diverse mining and geological conditions*, Energies, 13(2), 405, https://doi.org/10.3390/en13020405

[42] RUMICHE F., NORIEGA A., LEAN P., FOSCA C., 2020, *Metallurgical failure analysis of a welded drive beam of a vibrating screen*, Engineering Failure Analysis, 118, 104936, https://doi.org/10.1016/j.engfailanal.2020.104936

[43] WODECKI J., KROT P., WRÓBLEWSKI A., CHUDY K., ZIMROZ R., 2023, *Condition monitoring of horizontal sieving screens—a case study of inertial vibrator bearing failure in calcium carbonate production plant*, Materials, 16(4), 1533, https://doi.org/10.3390/ma16041533

[44] DĄBEK P., KROT P., WODECKI J., ZIMROZ P., SZREK J., ZIMROZ R., 2022, *Measurement of idlers rotation speed in belt conveyors based on image data analysis for diagnostic purposes*, Measurement, 202, 111869, https://doi.org/10.1016/j.measurement.2022.111869

[45] WODECKI J., GÓRALCZYK M., KROT P., ZIĘTEK B., SZREK J., WORSA-KOZAK M., ZIMROZ R., ŚLIWIŃSKI P., CZAJKOWSKI A., 2020, *Process monitoring in heavy duty drilling rigs—data acquisition system and cycle identification algorithms*, Energies, 13, 6748, https://doi.org/10.3390/en13246748

[46] INTERNATIONAL ORGANISATION OF STANDARDIZATION, 1996, *Mechanical vibration – evaluation of machine vibration by measurements on non-rotating parts*, ISO 10816:1996.

[47] INTERNATIONAL ORGANISATION OF STANDARDIZATION, 2009, *Mechanical vibration – Evaluation of machine vibration by measurements on rotating shafts – Part 3: Coupled industrial machines*, ISO 7919-3:2009.

[48] LI Y., PENG S., LI Y., JIANG W., 2020, *A review of condition-based maintenance: Its prognostic and operational aspects*, Frontiers of Eng. Management, 7, 323–334, https://doi.org/10.1007/s42524-020-0121-5

[49] ROSMAINI A., SHAHRUL K., 2012, *A review of condition-based maintenance decision-making,* European J. of Industrial Engineering, 6(5), 519–541, https://doi.org/10.1504/EJIE.2012.048854

[50] TUNG T.V., YANG B.-S., 2009, *Machine fault diagnosis and prognosis: the state of the art,* Int. J. of Fluid Machinery and Systems, 2(1), 61–71, https://doi.org/10.5293/IJFMS.2009.2.1.061

[51] KICKI J., DYCZKO A., 2010, *The concept of automation and monitoring of the production process in an underground mine*, [in:] V. Bondarenko, I. Kovalevska, R. Dychkovskiy (eds.) *New Techniques and Technologies in Mining: School of Underground Mining*, CRC Press, 245–253.

[52] RALSTON J.C., HAINSWORTH D.W., McPHEE R.J., REID D.C., HARGRAVE C.O., 2003, *Application of signal processing technology for automatic underground coal mining machinery*, IEEE Int. Conf. on Acoustics, Speech, and Signal Processing (ICASSP-03), Hong Kong, China, 2, 249–252, https://doi.org/10.1109/ICASSP.2003.1202341

[53] McBAIN J., TIMUSK M., 2012, *Software architecture for condition monitoring of mobile underground mining machinery a framework extensible to intelligent signal processing and analysis*, IEEE Conference on Prognostics and Health Management (PHM-2012), 18–21 June, Denver, CO, USA, 1–12, https://doi.org/10.1109/ICPHM.2012.6299543

[54] STEFANIAK P., KOPERSKA W., SKOCZYLAS A., WITULSKA J., ŚLIWIŃSKI P., 2023, *Methods of optimization of mining operations in a deep mine-tracking the dynamic overloads using IoT sensor*, IEEE Access, 11, 79384–79396, https://doi.org/10.1109/ACCESS.2023.3291080

[55] RASHVAND H.F., ABEDI A. (eds.), 2017, *Wireless sensor systems for extreme environments: space, underwater, underground, and industrial*, John Wiley & Sons. ISBN: 978-1-119-12646-1.

[56] LI J.-G., ZHAN K., 2018, *Intelligent mining technology for an underground metal mine based on unmanned equipment,* Engineering, 4(3), 381–391, https://doi.org/10.1016/j.eng.2018.05.013

[57] MARSHALL J., BARFOOT T., LARSSON J., 2008, *Autonomous underground tramming for center-articulated vehicles*, J. of Field Robotics, 25(6–7), 400–421, https://doi.org/10.1002/rob.20242

[58] JUNG J., CHOI Y., 2017, *Measuring transport time of mine equipment in an underground mine using a bluetooth beacon system*, Minerals, 7(1), 1–10, https://doi.org/10.3390/min7010001

[59] SKOCZYLAS A., ROT A., STEFANIAK P., ŚLIWIŃSKI P., 2023, *Haulage cycles identification for wheeled transport in underground mine using neural networks*, Sensors, 23(3), 1331, https://doi.org/10.3390/s23031331

[60] LAN J., XIANG Y., WANG L., SHI Y., 2011, *Vehicle detection and classification by measuring and processing magnetic signal*, Measurement, 44, 174–180, https://doi.org/10.1016/j.measurement.2010.09.044

[61] YANG S.K., LIU T.S., CHENG Y.C., 2008, *Automatic measurement of payload for heavy vehicles using strain gages*, Measurement, 41, 491–502, https://doi.org/10.1016/j.measurement.2007.07.003

[62] CHU D., LI Z., WANG J., WU C., Hu Z., 2018, *Rollover speed prediction on curves for heavy vehicles using mobile smartphone*, Measurement, 130, 404–411, https://doi.org/10.1016/j.measurement.2018.07.054

[63] LI X., SONG X., CHAN C., 2014, *Reliable vehicle sideslip angle fusion estimation using low-cost sensors*, Measurement, 51, 241–258, https://doi.org/10.1016/j.measurement.2014.02.007

[64] GUSTAFSON A., SCHUNNESSON H., GALAR D., KUMAR U., 2013, *The influence of the operating environment on manual and automated load-haul-dump machines: a fault tree analysis*, Int. J. of Mining, Reclamation and Environment, 27(2), 75–87, https://doi.org/10.1080/1755182X.2011.651371

[65] TIMUSK M.A., LIPSETT M.G., McBAIN J., MECHEFSKE C.K., 2009, *Automated operating mode classification for online monitoring systems*, J. of Vibration and Acoustics, Trans. of the ASME, 131(4), 041003, https://doi.org/10.1115/1.3142871

[66] WODECKI J., STEFANIAK P., MICHALAK A., WYŁOMAŃSKA A., ZIMROZ R., 2018, *Technical condition change detection using Anderson–Darling statistic approach for LHD machines – engine overheating problem*, Int. J. of Mining, Reclamation and Environment, 32(6), 392–400, https://doi.org/10.1080/17480930.2017.1388336

[67] JAKKULA B., MANDELA G., CHIVUKULA M.S., 2018, *Improvement of overall equipment performance of underground mining machines – a case study*, Modelling, Measurement and Control C, 79(1), 6–11, https://doi.org/10.18280/mmc_c.790102

[68] WYLOMANSKA A., ZIMROZ R., 2014, *Signal segmentation for operational regimes detection of heavy duty mining mobile machines – a statistical approach*, Diagnostyka, 15(2), 33–42.

[69] WYLOMANSKA A., ZIMROZ R., 2015, *The analysis of stochastic signal from LHD mining machine*, [in:] A. Steland, E. Rafajłowicz, K. Szajowski (eds.), *Stochastic models, statistics and their applications*. Springer Proceedings in Mathematics & Statistics, Springer, Cham, 122, 469–478, https://doi.org/10.1007/978-3-319-13881-7_52

[70] POLAK M., STEFANIAK P., ZIMROZ R., WYŁOMAŃSKA A., ŚLIWIŃSKI P., ANDRZEJEWSKI M., 2016, *Identification of loading process based on hydraulic pressure signal*, [in:] Proc.

of 16th Int. Multidisciplinary Scientific GeoConference "Surveying Geology & Mining Ecology Management (SGEM 2016), 30 June–6 July 2016, Sofia, Bulgaria, 2, 459–466.

[71] STEFANIAK P., ZIMROZ R., OBUCHOWSKI J., SLIWINSKI P., ANDRZEJEWSKI M., 2015, *An effectiveness indicator for a mining loader based on the pressure signal measured at a bucket's hydraulic cylinder*, Procedia Earth and Planetary Science, 15, 797–805, https://doi.org/10.1016/j.proeps.2015.08.128

[72] SLIWINSKI P., ANDRZEJEWSKI M., KANIEWSKI T., HEBDA-SOBKOWICZ J., ZIMROZ R., 2019, *Selection of variables acquired by the on-board monitoring system to determine operational cycles for haul truck vehicle,* [in:] Proc. of the 39th Int Symposium APCOM 2019: Mining Goes Digital, Application of Computers and Operations Research in the Mineral Industry, Wroclaw, Poland, June 04–06, CRC Press, London, 525–533, https://doi.org/10.1201/9780429320774

[73] JABLONSKI A., BARSZCZ T., WICIAK P., 2014, *Non-clustering method for automatic selection of machine operational states,* [in:] G. Dalpiaz, et al. (eds.), Advances in Condition Monitoring of Machinery in Non-Stationary Operations. Lecture Notes in Mechanical Engineering, Springer, Berlin, Heidelberg, 5, 419–427, https://doi.org/10.1007/978-3-642-39348-8_36

[74] WODECKI J., STEFANIAK P., ŚLIWIŃSKI P., ZIMROZ R., 2018, *Multidimensional data segmentation based on blind source separation and statistical analysis,* [in:] Timofiejczuk A., et al. (eds.), Advances in Condition Monitoring of Machinery in Non-Stationary Operations (CMMNO 2016). Applied Condition Monitoring, Springer, Cham, 9, 353–360, https://doi.org/10.1007/978-3-319-61927-9_33

[75] QI Z., GU Q., MENG Y., BAI G., DING D., 20123, *The load-haul-dump operation cycle recognition based on multi-sensor feature selection and bidirectional long short-term memory network*, Measurement and Control, 56(9–10), 1523–1533, https://doi.org/10.1177/00202940231161569

[76] STEFANIAK P.K., ZIMROZ R., SLIWINSKI P., ANDRZEJEWSKI M., WYŁOMANSKA A., 2014, *Multidimensional signal analysis for technical condition, operation and performance understanding of heavy duty mining machines,* [in:] F. Chaari, et al. (eds.), Advances in Condition Monitoring of Machinery in Non-Stationary Operations (CMMNO 2014). Applied Condition Monitoring, Springer, Cham, 4, 197–210, https://doi.org/10.1007/978-3-319-20463-5_15

[77] WEN B., 2008, *Recent development of vibration utilization engineering,* Frontiers of Mechanical Engineering in China, 3(1), 1–9, https://doi.org/10.1007/s11465-008-0017-2

[78] PENG L.P., JIANG H., CHEN X., LIU D., FENG H., ZHANG L., ZHAO Y., LIU C., 2019, *A review on the advanced design techniques and methods of vibrating screen for coal preparation*, Powder Technology, 347, 136–147, https://doi.org/10.1016/j.powtec.2019.02.047

[79] STANDISH N., BHARADWAJ A., HARIRI-AKBARI G., 1986, *A study of the effect of operating variables on the efficiency of a vibrating screen*, Powder Technology, 48(2), 161–172, https://doi.org/10.1016/0032-5910(86)80075-4

[80] ZAHEDI S.A., BABITSKY V., 2016, *Modeling of autoresonant control of a parametrically excited screen machine*, Journal of Sound and Vibration, 380, 78–89, 2016, https://doi.org/10.1016/j.jsv.2016.06.011

[81] KUZIO I.V., LANETS O.V., GURSKY V.M., 2013, *Substantiation of technological efficiency of two-frequency resonant vibration machines with pulse electromagnetic disturbance*, Naukovyi Visnyk Natsionalnoho Hirnychoho Universytetu, 3, 71–77.

[82] WU X.Q., LI Z., XIA H., TONG X. 2018, *Vibration parameter optimization of a linear vibrating banana screen using DEM 3D simulation*, Journal of Engineering Technology Science, 50, 346–363, https://doi.org/10.5614/j.eng.technol.sci.2018.50.3.3

[83] YANG X., WU J., JIANG H., QIU W., LIU C., 2019, *Dynamic modeling and parameters optimization of large vibrating screen with full degree of freedom*, Shock and Vibration, 2019, ID 1915708, 12, https://doi.org/10.1155/2019/1915708

[84] GONG S., OBERST S., WANG X., 2020, *An experimentally validated rubber shear spring model for vibrating flip-flow screens*, Mechanical Systems and Signal Processing, 139, 106619, https://doi.org/10.1016/j.ymssp.2020.106619

[85] ENE G., SPOREA N., 2016, *Approaches regarding the calculus of the elastic system of the initial vibrating screens*, Revista de Chimie (Bucharest), 67(2), 308–313, https://doi.org/10.37358/Rev.Chim.1949

[86] RACZKA W., SIBIELAK M, KOWAL J, KONIECZNY J., 2013, *Application of an SMA spring for vibration screen control*, Journal of Low Frequency Noise, Vibration and Active Control, 32(1–2), 117–132, https://doi.org/10.1260/0263-0923.32.1-2.117

[87] LLANO-VIZCAYA L.D., RUBIO-GONZÁLEZ C., MESMACQUE G., CERVANTES-HERNANDEZ T., 2006, *Multiaxial fatigue and failure analysis of helical compression springs*, Engineering Fatigue Analysis, 13(8), 1303–1313, https://doi.org/10.1016/j.engfailanal.2005.10.011

[88] GURSKY V., KUZIO I., 2016, *Strength and durability analysis of a flat spring at vibro-impact loadings*, Eastern-European J. of Enterprise Technologies, 5(7–83), 4–10, https://doi.org/10.15587/1729-4061.2016.79910

[89] KROT P., BOBYR S., DEDIK M., 2017, *Simulation of backup rolls quenching with experimental study of deep cryogenic treatment*, Int. J. of Microstructure and Materials Properties, 12(3/4), 259–275, https://doi.org/10.1504/IJMMP.2017.091105

[90] KROT P., ZIMROZ R., MICHALAK A., WODECKI J., OGONOWSKI S., DROZDA M., JACH M. 2020, *Development and verification of the diagnostic model of the sieving screen*, Shock and Vibration, 2020, ID 8015465, https://doi.org/10.1155/2020/8015465

[91] ONOFREI R., DOBRE G.M., MIRICĂ R.F., PALI M.2013, *On measurement and processing data of the real loading: application to cement equipment components,* [in:] G. Dobre (ed.) Power Transmissions, Mechanisms and Machine Science, Springer, Dordrecht, 13, 701–713, https://doi.org/10.1007/978-94-007-6558-0_57

[92] CAI Z., XU Y., DUAN Z., 2018, *An alternative demodulation method using envelope-derivative operator for bearing fault diagnosis of the vibrating screen,* J. of Vibration and Control, 24(15), 3249–3261, https://doi.org/10.1177/1077546317739117

[93] LIU J., 2020, *A dynamic modelling method of a rotor-roller bearing-housing system with a localized fault including the additional excitation zone,* Journal of Sound and Vibration, 469, 115144, https://doi.org/10.1016/j.jsv.2019.115144

[94] WYLOMANSKA A., ZIMROZ R., JANCZURA J., OBUCHOWSKI J., 2016, *Impulsive noise cancellation method for copper ore crusher vibration signals enhancement,* IEEE Trans. on Ind. Electronics, 63(9), 5612–5621, https://doi.org/10.1109/TIE.2016.2564342

[95] MICHALAK A., WODECKI J., WYŁOMAŃSKA A., ZIMROZ R., 2019, *Application of cointegration to vibration signal for local damage detection in gearboxes,* Applied Acoustics, 144, 4–10, https://doi.org/10.1016/j.apacoust.2017.08.024

[96] OBUCHOWSKI J., ZIMROZ R., WYŁOMAŃSKA A., 2015, *Identification of cyclic components in presence of non-Gaussian noise – application to crusher bearings damage detection,* J. Vibroeng., 17(3), 1242–1252. URL: https://www.extrica.com/article/15965

[97] PENG L.-P., LIU C., SONG B., WU J., WANG S., 2015, *Improvement for design of beam structures in large vibrating screen considering bending and random vibration,* Journal of Central South University, 22(9), 3380–3388, https://doi.org/10.1007/s11771-015-2878-y

[98] SOROKIN V.S., 2020, *Vibrations of a non-linear stochastic system with a varying mass under near resonant excitation,* Journal of Vibration and Control, 26(17–18), 1435–1444, https://doi.org/10.1177/1077546319898304

[99] DETYNA J., 2010, *Stochastic models of particle distribution in separation processes,* Arch. Civil Mech. Eng., 10, 15–26, 10.1016/S1644-9665(12)60127-7

[100] PENG L.P., RUNXIN F., HUIHUI F., ZHANG L., WENDA M., XIAO-DI H., 2018, *A more accurate dynamic model for dual-side excitation large vibrating screens,* J. Vibroeng., 20, 858–871, https://doi.org/10.21595/JVE.2018.18811

[101] RODRIGUEZ C.G., MONCADA M., DUFEU E., RAZETO M., 2016, *Non-linear model of vibrating screen to determine permissible spring deterioration for proper separation,* Shock and Vibration, ID 4028583, 7, https://doi.org/10.1155/2016/4028583

[102] LIU Y., MENG G., SUO S., LI D., WANG A., CHENG X., YANG J., 2019, *Spring failure analysis of mining vibrating screens: numerical and experimental studies,* Appl. Sci., 9, 3224, https://doi.org/10.3390/APP9163224

[103] PENG L., LIU C., Li J., WANG H.B., 2014, *Static-deformation based fault diagnosis for damping spring of large vibrating screen*, Journal of Central South University, 21(4), 1313–1321, https://doi.org/10.1007/s11771-014-2068-3

[104] PIENAAR S., 2024, *Sensitivity study of dynamic features for vibrating screen isolator condition monitoring*. MSc Thesis, University of Pretoria, SAR.

[105] JIANG Y.-Z., HE K.-F., DONG Y.-L, YANG D., SUN W., 2019, *Influence of load weight on dynamic response of vibrating screen*, Shock and Vibration, 2019, ID 4232730, 8, https://doi.org/10.1155/2019/4232730

[106] MONCADA M., RODRIGUEZ C.G., 2018, *Dynamic modeling of a vibrating screen considering the ore inertia and force of the ore over the screen calculated with discrete element method*, Shock and Vibration, 2018, ID 1714738, 13, https://doi.org/10.1155/2018/1714738

[107] BATKO W., KORBIEL T., PAWLIK P., 2012, *Analiza eksperymentalna przydatności trajektorii fazowych do diagnostyki maszyn wirujących*, Problemy Eksploatacji, 1, 7–15.

[108] WANG W.J., CHEN J., WU X.K., WU Z.T., 2001, *The application of some non-linear methods in rotating machinery fault diagnosis*, Mechanical Systems and Signal Processing, 15(4), 697–705, https://doi.org/10.1006/mssp.2000.1316

[109] BOVSUNOVSKY A.P., BOVSUNOVSKY O., 2007, *Crack detection in beams by means of the driving force parameters variation at non-linear resonance vibrations*, Key Engineering Materials, 347, 413–420, https://doi.org/10.4028/www.scientific.net/KEM.347.413

[110] GELMAN L.M., 2007, *Piece-wise model and estimates of damping and natural frequency for a spur gear*, Mechanical Systems and Signal Processing, 21, 1192–1196, https://doi.org/10.1016/j.ymssp.2005.10.012

[111] PENG Y., CUI J., SUN J., ZHANG M., 2021, *Torsional vibration for rolling mill with the drive system shaft axis deviations*, Arabian Journal for Science and Engineering, 46, 12165–12177, https://doi.org/10.1007/s13369-021-05684-7

[112] WEISHAAR B., STAMBERGER K., GOGATE R., 1998, *Dynamic behavior of rolling mill main drives having various motor-gearbox designs*, Iron and Steel Engineer, 75, 45–52.

[113] WRIGHT J., 1981, *Tuning mill drives to minimize dynamic torques*, Iron and Steel Engineer, May, 35–37.

[114] DOI K., ISHIKAWA K., TSUKUDA H., YAMAMOTO K., SUGANUMA N., NAITO T., 1987, *Analysis and control systems for shaft vibration in steel rolling processes*, Kawasaki Steel Tech Report, 17, 73–80. URL: https://www.jfe-steel.co.jp/archives/en/ksc_giho/no.17/e17-073-080.pdf

[115] HORI Y., ISEKI H., SUGIURA K., 1994, *Basic considerations of vibration suppression and disturbance rejection control of multi-inertia system using SFLAC (state feedback and load*

acceleration control), IEEE Trans. Ind. Applications, 30(Jul/Aug), 4, 889–896, https://doi.org/10.1109/28.297904

[116] ZHANG R., CHEN Z., YANG Y., TONG C., 2007, *Torsional vibration suppression control in the main drive system of rolling mill by state feedback speed controller based on extended state observer*, IEEE International Conference on Control and Automation (ICCA 2007), 2172–2177, https://doi.org/10.1109/ICCA.2007.4376745

[117] WANG L., FRAYMAN Y., 2002, *A dynamically generated fuzzy neural network and its application to torsional vibration control of tandem cold rolling mill spindles*, Engineering Applications of Artificial Intelligence, 15(6), 541–550, https://doi.org/10.1016/S0952-1976(03)00006-X

[118] SZABAT K., ORLOWSKA-KOWALSKA T., DYRCZ K., 2006, *Extended Kalman filters in the control structure of two-mass drive system*, Bulletin of the Polish Academy of Sciences, Tech. Sciences, 54(3), 315–325. URL: http://bluebox.ippt.pan.pl/~bulletin/(54–3)315.pdf

[119] GURIAN S., 2001, *Resonance compensation of large AC drivetrains with significant time lag*, MSc Thesis, Polytechnic Institute of the State University, Blacksburg, Virginia, USA. URL: http://hdl.handle.net/10919/31061

[120] BUTLER D.H.E., CHURCHES M.A., ANBE Y., NAITOH H., 1992, *Compensation of a digitally controlled static power converter for the damping of rolling mill torsional vibration*, IEEE Transactions on Industry Applications, 28(March/April), 2, 427–433, https://doi.org/10.1109/28.126752

[121] BELLI P., BITTANTI S., MARCO De A., 2004, *On the origin of torsional vibrations in hot rolling mills and a possible remedy*, ASME J. Dynamic Systems, Measurement, and Control, 126(4), 811–823, https://doi.org/10.1115/1.1850531

[122] MJÖRNING L., 2005, *ABB drives and control system for hot flat rolling mills improves yield and quality*, 42º ABM Rolling Mill Seminary, 25–28 October, Santos, SP, Brazil.

[123] LEE Y., 2004, *Rod Bar Rolling: Theory and Applications (Manufacturing Engineering and Materials Processing)*, Marcel Dekker, New York, Basel.

[124] RADIONOV A.A., PETUKHOVA O.I., ERDAKOV I.N., KARANDAEV A.S., LOGINOV B.M., KHRAMSHIN V.R., 2022, *Developing an automated system to control the rolled product section for a wire rod mill with multi-roll passes*, J. Manuf. Mater. Process, 6, 88, https://doi.org/10.3390/jmmp6040088

[125] KIEFER B.V., SHORE T.M., 2007, *Recent innovations in high-speed rod and bars mills*, Millenium Steel, 151–155.

[126] ROY C., LEGER A., PARISEAN P., 1982, *Morgan compact mill, design parameters, applications and operational benefits*, Iron and Steel Engineer, 59(11), 25–30.

[127] WANG J., 1999, *Optional multi-ratio gear transmission system*. Patent US 5921152, F16H 37/06, Morgan Construction, Prior. 1999-07-13.

[128] HOFNER J., OLENICK J.E., FOLEY J.D., 1991, *Predictive maintenance for no-twist rod mills using vibration signature analysis*, Iron and Steel Engineer, 68, 55–61.

[129] SCHMIDT J.M., PLAYER R.E., QUIGLEY K.G., KOUMA S., 2002, *Continuous vibration monitoring of a 10stand rod block*, AISE Steel Technology, Jan., 44–45.

[130] SHI P., GAO H., YU Y., XU X., HAN D., 2022, *Intelligent fault diagnosis of rolling mills based on dual attention-guided deep learning method under imbalanced data conditions,* Measurement, 204, 111993, https://doi.org/10.1016/j.measurement.2022.111993

[131] ZHENG C., ZHIHAO W., 2014, *Online monitoring method for vibration state of reducing and sizing mill*, Patent CN 103769425A, B21B 38/00, Shanghai Baosteel Industry Technological, Prior. 2012-10-26.

[132] LUO H., 2011, *System and method for monitoring the condition of a drivetrain,* Patent US 20050284225A1, F16H 57/01, General Electric, Prior. 2004-06-28.

[133] MAO L., 2022, *Simulation analysis and optimal design of spinning head dynamic balance*, J. of Physics: Conference Series, 2390, 012098, https://doi.org/110.1088/1742-6596/2390/1/012098.

[134] BOROVSKY T., KYSLAN K., DUROVSKY F., 2017, *Material tracking with dynamic torque adaptation for tension control in wire rod mill*, Mechatronics, 15(2), 176–183, https://doi.org/10.15598/aeee.v15i2.2139

[135] GORBANEV A.A., BINKEVICH E.B., MAMUZIC I., 1998, *Regulation of forces in interstand spacings by rolling in finishing blocks of wire roll stands*, Metalurgija, 37(3), 153–157.

[136] TROEDER C., DIEKHANS G., PEEKEN H., 1979, *Torsional vibration studies on the power drive transmissions of a rod mill – model finding*, Stahl und Eisen, 99(22), 1232–1240.

[137] TROEDER C., DIEKHANS G., PEEKEN H., 1979, *Torsional vibration investigations on the power drive transmission of a wire rod mill – results of simulation of torsional vibration*, Stahl und Eisen. 99(24), 1372–1380.

[138] TANG N., ZHANG Q., WANG C., GAO L., 2023, *Hybrid fault diagnosis for high speed wire rod finishing mill*, 6th International Symposium on Autonomous Systems (ISAS2023), Nanjing, China, 1–6, https://doi.org/10.1109/ISAS59543.2023.10164300

[139] CHEN S.S., YANG P., 2010, *The failure diagnosis of the step-up gearbox in the finishing mill and the formation of its intelligent system*, Applied Mechanics and Materials, 33, 618–622, https://doi.org/10.4028/www.scientific.net/AMM.33.618

[140] PARSIAN A., 2013, *Stability prediction of multiple-teeth boring operations,* MSc Thesis, Blekinge Institute of Technology, School of Engineering, Sweden.

[141] YAN Y., XU J., WIERCIGROCH M., 2016, *Regenerative chatter in self-interrupted plunge grinding*, Meccanica, 51, 3185–3202, https://doi.org/10.1007/s11012-016-0554-4

[142] MORI H., TSUNASHIMA H., KOJIMA T., MATSUMOTO A., MIZUMA T., 2010, *Condition monitoring of railway track using in-service vehicle*, J. of Mech. Systems for Transportation and Logistics 3(1), 154–165, https://doi.org/10.1299/jmtl.3.154

[143] SCHLACHER K., FUCHSHUMER S., GRABMAIR G., HOLL J., KEINTZEL G., 2005, *Active vibration rejection in steel rolling mills,* IFAC Proceedings Volumes, 38(1), 1–6, https://doi.org/10.3182/20050703-6-CZ-1902.01679

[144] KRIMPELSTAETTER K., KEINTZEL G., 2015, *Elimination of third-octave mill chatter vibration in cold rolling – first successful pilot installation*, European Steel Technology and Application Days (METEC & ESTAD), 15–19 June 2015, Düsseldorf, Germany.

[145] EVANS P.R., 1996, *Rolling mill vibration control,* Patent WO 1996027454A1, B21B 37/007, Davy Mckee, Prior. 1996-06-03.

[146] BROWN R., SEIBERT M., MILLER D.L., FAIRLIE M., GAENSBAUER D., 2015, *Process damping of self-excited third octave mill vibration,* Patent EP 3169460B1, B21B 1/22, Novelis, 2015-07-15.

[147] KRÜGER M., 2018, *Active chatter damping for cold rolling mills*, Magazine (SMS Group), https://www.sms-group.com/insights/all-insights/active-chatter-damping-for-cold-rolling-mills Accessed 2024-03-07.

[148] VIGNOLO L., LUCA De A., NOBILE M., AMATI N., PRISTERA C., ROMEO G., TONOLI A., 2011, *Vibration damping system for a rolling mill with first and second passive hydraulic elements*, Patent EP 2624973A1, B21B 37/007, 2013-08-14.

[149] JIANG L., WANG T., HUANG Q.-X., 2023, *Resonance analysis of horizontal nonlinear vibrations of roll systems for cold rolling mills under double-frequency excitations*, Mathematics, 11, 1626, https://doi.org/10.3390/math11071626

[150] PAVLOV S.I., KUZNETSOV V.V., GARBER E.A., TIMOFEEVA M.A., 2009, *Method of continuous strip cold tension rolling*, Patent RU 2409432C1, B21B 1/28, Severstal, 2009-06-29.

[151] DONINI A., PAN G.D., 2002, *Method to eliminate the play between chocks and relative support blocks in four-high rolling stands and relative device*, Patent US 6354128 B1, Danieli, Publ. 2002-03-12.

[152] MACHIDA S., 1996, *Method for detecting chattering of rolling mill*, Patent JP 8108205, B21B 37/00, Sumitomo Metal Industries, Publ. 1996-04-30.

[153] WANG A.C., CHAN K.W., DUNLAP L.D., LUO J., STEWART D.F., BARRY M.L., LEE T.C., 1997, *Interruption of rolling mill chatter by induced vibrations*, Patent US WO1997027953A1, B21B 37/00, Aluminium Company of America, Publ. 1997-08-07.

[154] SAKURAI A., SUZUKI E., YONEZAWA T., 1996, *Method for suppressing vibration of material to be rolled*, Patent JP 8238510, B21B 37/48, Kobe Steel, Publ. 1996-09-17.

[155] SAKURAI A., YONEZAWA T., SUZUKI E., 1996, *Method for suppressing vibration of material to be rolled and device there for*, Patent JP 8238512, B21B 37/48, Kobe Steel, Publ. 1996-09-17.

[156] YONEZAWA T., SUZUKI E., SAKURAI A., 1996, *Method for suppressing vibration of material to be rolled*, Patent JP 8238511, B21B 37/48, Kobe Steel, Publ. 1996-09-17.

[157] LUO Z., WANG X., XUE X., WU B., YU Y., 2005, *Modeling and prediction of violent abnormal vibration of large rolling mills based on chaos and wavelet neural networks*, [in:] J. Wang, X.F. Liao, Z. Yi (ed.), *Advances in Neural Networks (ISNN 2005), Lecture Notes in Computer Science,* Springer, Berlin, Heidelberg, 3498, 827–832, https://doi.org/10.1007/11427469_131.

[158] WIERCIGROCH M., CHENG A.H.-D., 1997, *Chaotic and stochastic dynamics of orthogonal metal cutting*, Chaos, Solitons & Fractals, 8(4), 715–726, https://doi.org/10.1016/S0960-0779(96)00111-7.

[159] AL-REGIB E., 2000, *Machining systems stability analysis for chatter suppression and detection*, Ph.D. dissertation, University of Michigan, USA.

[160] HU P.H., EHMANN K.F., 2001, *Regenerative effect in rolling chatter*, Journal of Manufacturing Processes, 3(2), 82–93, https://doi.org/10.1016/S1526-6125(01)70123-5.

[161] CHEN Y., LIU S., SHI T., YANG S., LIAO G., 2002, *Stability analysis of the rolling process and regenerative chatter on 2030 tandem mill*, Proc. Inst. Mech. Eng., Part C: J. of Mechanical Eng. Science, 216(12), 1225–1235, https://doi.org/10.1243/095440602321029463.

[162] JOHNSON R.E., 1994, *The effect of friction and inelastic deformation on chatter in sheet rolling*, Proc. of the Royal Society of London Series A, 445, 479–499, https://doi.org/10.1098/rspa.1994.0073.

[163] GUO R.M., 1994, *Material damping effect in cold rolling process*, Iron & Steel Technology, 71(12), 2835.

[164] FOROUZAN M.R., KIYANI I., SALIMI M., GHASEMI A.R., 2008, *Analysis of chatter vibration in cold strip rolling.* Part I*: System equivalent damping*, Steel Research International, 79, 21–28.

[165] KHRAMSHIN V.R., KARANDAEV A.S., EVDOKIMOV S.A., 2015, *Reduction of the dynamic loads in the universal stands of a rolling mill*, Metallurgist, 59, 315.

[166] ZAWADA S. 1982, *Dynamic torque variation in the drive of a large slabbing mill*, J. of Mech. Working Technology, 7(1), 57–77, https://doi.org/10.1016/0378-3804(82)90094-8.

[167] DOBRUCKI W., GREGORCZYK R., ZAWADA S., 1989, *Modelling of the interaction of slabbing mills during the simultaneous rolling of slabs in both roll-pairs*, J. of Mech. Working Technology, 19(3), 275–283, https://doi.org/10.1016/0378-3804(89)90077-6.

[168] KHARCHENKO G.N., ZEMENKOV A.A., POPOV V.K., 1976, *Relationships of the roll speeds of the universal stand of a slabbing mill,* Metallurgist, 20(6), 410–412, https://doi.org/10.1007/BF01090886.

[169] SVETLICHNY A.V., ZEMLYANSKY A.I., KRIVTSOV A.I., 2013, *Limitation of the dynamic loads of a slabbing mill by means of an electric drive*, Metallurgical Processes and Equipment, 1, 28–37.

[170] KROT P.V., 2002, *Parametric oscillations in rolling mills*, Scientific Bulletin of the Dnipro National Mining University (NMU), 3(13), 15–21.

[171] KROT P.V., 2009, *Dynamic processes in a multi-path gear drive of slabbing mill*, Proc. of National Technical University Kharkov Polytechnic Institute. Series: Problems of Mechanical Drive, 19, 96–105.

[172] CHUDNOVSKY V.Y., 2005, *Dynamic problems of powerful multi-motor drives,* Problems of Mechanical Engineering and Machine Reliability, 5, 22–27.

[173] BOLSHAKOV V.I., KHOMENKO V.I., BUCUKIN V.V., 1993, *Experimental study of loads in a multi-motor tilt drive of converter with a support reducer*, Metallurgical and Mining Industry, 3, 56–59.

[174] GU Y.K., TONG X.X., LUO X.C., 2012, *The Dynamics analysis of full mounted converter vessel tilting mechanism*, Applied Mechanics and Materials, 128–129, 1242–1245, https://doi.org/10.4028/www.scientific.net/AMM.128-129.1242

[175] WEI J., SUN Q., SUN W., CAI J., ZENG J., 2013, *Dynamic analysis and load-sharing characteristic of multiple pinion drives in tunnel boring machine*, J. of Mechanical Science and Technology, 27(5), 1385–1392, https://doi.org/10.1007/s12206-013-0319-0

[176] SHU R., LIU Z., LIU C., LIN X., QIN D., (2015), *Load sharing characteristic analysis of short driving system in the long-wall shearer*, Journal of Vibroengineering, 17(7), 3572–3585.

[177] BARTELMUS W., ZIMROZ R., 2011, *Vibration spectra characteristic frequencies for condition monitoring of mining machinery compound and complex gearboxes*, Mining Science, 133(40), 17–34.

[178] SWIATONIOWSKI A., BAR A., 2003, *Parametrical excitement vibration in tandem mills-mathematical model and its analysis*, Journal of Materials Processing Technology, 134(2), 214–224, https://doi.org/10.1016/S0924-0136(02)01037-3

[179] ZHANG D., WANG S., 2015, *Parametric vibration of split gears induced by time-varying mesh stiffness*. Proc. of the Institution of Mech. Eng. Part C, J. of Mech. Eng. Science, 229(1), 18–25, https://doi.org/10.1177/0954406214531748

[180] HAN D.Y., SHI P.M., XIA K., 2014, *Non-linear torsional vibration dynamics behaviors of rolling mill's multi-DOF main drive system under parametric excitation*, J. of Appl. Math., 202686, 7, https://doi.org/10.1155/2014/202686

[181] AMER Y.A., EL-SAYED A.T., EL-BAHRAWY F.T., 2015, *Torsional vibration reduction for rolling mill's main drive system via negative velocity feedback under parametric excitation*,

J. of Mech Science and Technology, 29(4), 1581–1589, https://doi.org/10.1007/s12206-015-0330-8

[182] RAKHMANOV S.R., 2016, *Connecting-rod dynamics of the primary drive in a cold-rolling mill*, Steel in Translation, 46(4), 276–281, https://doi.org/10.3103/S0967091216040124

[183] LIU G., PARKER R.G., 2012, *Non-linear, parametrically excited dynamics of two-stage spur gear trains with mesh stiffness fluctuation*, Proc. of the Institution of Mechanical Engineering, Part C: Journal of Mechanical Engineering Science, 226(8), 1939–1957, https://doi.org/10.1177/0954406212447509

[184] GAWANDE S.H., KOKARE D.K., 2017, *Experimental investigations of vibration reduction in spur gear pair by method of phasing*, J. of Vibration Engineering and Technologies, 5(6), 573–585.

[185] DONG H., HU Y., 2018, *Dynamic load-sharing characteristic analysis of face gear power-split gear system based on tooth contact characteristics*, AIP Conference Proceedings, 1955, 030028-1, https://doi.org/10.1063/1.5033627

[186] ARTIUKH V., MAZUR V., KARGIN S., ZAKHAROVA L., 2018, *Adapters for metallurgical equipment*, MATEC Web of Conf., 170, 03028, https://doi.org/10.1051/matecconf/201817003028

[187] XUE S., HOWARD I., 2018, *Torsional vibration signal analysis as a diagnostic tool for planetary gear fault detection*, Mechanical Systems and Signal Processing, 100, 706–728, https://doi.org/10.1016/j.ymssp.2017.07.038

[188] RADIONOV A.A., GASIYAROV V.R., TVERSKOI M.M., KHRAMSHIN V.R., LOGINOV B.M., 2017, *Implementation of telemetrie online monitoring system of elastic torque of rolling mill line of shafting*, Proc 2nd Int Ural Conf on Measurements (UralCon2017), 450–455, https://doi.org/10.1109/URALCON.2017.8120750

[189] JEFTENIC B., BEBIC M., STATKIC S., 2006, *Controlled multi-motor drives*, IEEE Int Symposium on Power Electronics, Electrical Drives, Automation and Motion (SPEEDAM 2006), 53–59, https://doi.org/10.1109/SPEEDAM.2006.1649985

[190] VOLKOV D.V., STASHINOV Y., 2018, *Equalization of torques in multi motor electric drives with estimation of motors parameters*, IEEE Int. Multi-Conference on Industrial Engineering and Modern Technologies (FarEastCon2018), 1–5, https://doi.org/10.1109/FarEastCon.2018.8602838

[191] MICHAEL C.A., SAFACAS A.N., 2007, *Dynamic and vibration analysis of a multimotor DC drive system with elastic shafts driving a tissue paper machine,* IEEE Trans. on Ind. Electronics, 54(4), 2033–2046, https://doi.org/10.1109/TIE.2007.895149

[192] SYED F.U., KUANG M.L., YING H., 2009, *Active damping wheel-torque control system to reduce driveline oscillations in a power-split hybrid electric vehicle*, IEEE Trans. on Vehicular Technology, 58(9), 4769–4785, https://doi.org/10.1109/TVT.2009.2025953

[193] ZHAO N., WANG R.F., TAO L., JIA Q.J., 2012, *Load sharing of parallel shaft split torque transmission system*, Adv. Mat. Res., 490–495, 2231–2235, https://doi.org/10.4028/www.scientific.net/AMR.490-495.2231

[194] WU J.-S., CHEN C.-H., 2001, *Torsional vibration analysis of gear-branched systems by finite element method*, J. of Sound and Vibration, 240(1), 159–182, https://doi.org/10.1006/jsvi.2000.3197

[195] DONG H., LIU Z.-Y., ZHANG J.-W., 2019, *Inherent characteristic analysis of a dual power split gear train*, IOP Conference Series: Earth and Environmental Science, 233, 032007, https://doi.org/10.1088/1755-1315/233/3/032007

[196] WOREK C., KRZAK Ł., MROWKA R., BARSZCZ T., 2018, *Comparison of wireless technologies for rotating machinery diagnostics*, [in:] A. Timofiejczuk, B. Łazarz, F. Chaari, R. Burdzik (eds.), Advances in Technical Diagnostics (ICDT 2016), Applied Condition Monitoring, Springer, Cham, 10, 129–138, https://doi.org/10.1007/978-3-319-62042-8_12

[197] MARGIELEWICZ J., GASKA D., WOJNAR G., 2017, *Numerical modelling of toothed gear dynamics*, Scientific Journal of Silesian University of Technology. Series Transport, 97, 105–115, https://doi.org/10.20858/sjsutst.2017.97.10

[198] TRANSMISSION DYNAMICS, http://www.jrdltd.co.uk, [Accessed: 2024-03-10].

[199] SAVKOVIC M., DEDIC M., PAVLOVIC G., ARSIC M., STAMENIC Z., 2019, *Analysis of the drive shaft fracture of the conveyor belt for transport of coal*, Tehnicki vjesnik, 26(5), 1333–1338, https://doi.org/10.17559/TV-20181031162954

[200] CHEN X., FENG Z., 2017, *Time-frequency analysis of torsional vibration signals in resonance region for planetary gearbox fault diagnosis under variable speed conditions*, IEEE Access, 5, 21918–21926, https://doi.org/10.1109/ACCESS.2017.2763172

[201] MONES Z., ALQATAWNEH I., ZHEN D., GU F., BALL A.D., 2019, *Fault diagnosis for planetary gearbox using on rotor MEMS sensor and EMD analysis*, IEEE 25th Int. Conf. on Automation and Computing (ICAC), 1–6, https://doi.org/10.23919/IConAC.2019.8895155

[202] LIU S., LI W., SHUAI Z., CHEN M., 2019, *Vibration analysis of a single-cylinder reciprocating compressor considering the coupling effects of torsional vibration*, Shock and Vibration, 2019, 1–9, https://doi.org/10.1155/2019/3904595

[203] REN Y., WANG N., JIANG J., ZHU J., SONG G., CHEN X., 2019, *The application of downhole vibration factor in drilling tool reliability big data analytics – a review*, ASME J. Risk Uncertainty Part B, 5(1), 010801, https://doi.org/10.1115/1.4040407

[204] PAVKOVIĆ D., CIPEK M., PLAVAC F., ŠPRLJAN P., JURIŠIĆ G., 2019, *Damping optimum tuning of drill-string torque based torsional vibrations suppression system*, IEEE 18th Int Conference on Smart Technologies (EUROCON 2019), 1–6, https://doi.org/10.1109/EUROCON.2019.8861990

[205] MORSHEDLOU A., DEHGHANI H., HOSEINIE H.A., 2019, *Data driven decision making approach for long-wall mining production enhancement*, Mining Science, 26, 7–20, https://doi.org/10.37190/msc192601

[206] SILVA D., MENDES J.C., PEREIRA A.B., GÉGOT F., ALVES L.N., 2017, *Measuring torque and temperature in a rotating shaft using commercial SAW sensors,* Sensors, 17, 1547, https://doi.org/10.3390/s17071547

[207] GINZBURG V.B., 1970, *Magnetoelastic sensors*, Energy Publisher, Moscow, 72 pp.

[208] KALININ V., 2011, *Wireless physical SAW sensors for automotive applications,* IEEE International Ultrasonics Symposium, 212–221, https://doi.org/10.1109/ULTSYM.2011.0053

[209] EFREMOV L.V., 2007, *Theory and practice of torsional vibrations research of power plants with the use of computer technology*, Saint-Petersburg, Science Publisher, 276 pp.

[210] ZAPPALÁ D., BEZZICCHERI M., CRABTREE C.J., PAONE N., 2018, *Non-intrusive torque measurement for rotating shafts using optical sensing of zebra-tapes*, Measurement Science and Technology, 29(6), 065207, https://doi.org/10.1088/1361-6501/aab74a

[211] BOGDANOWICZ A., KNIAZIEWICZ T., 2019, *Bezprzewodowy pomiar torqueu obrotowego silnika okrętowego z wykorzystaniem układu mikrokontrolerowego*, XLVI Ogólnopolskie Symposjum Diagnostyka Maszyn, Politechnika Śląska, Wisła, 3–7 marca 2019, 12.

[212] PODKOVYRIN E.Y., 1969, *Contactless torque meter,* Proc. of Iron and Steel Institute, NAS of Ukraine, 31, 159–161.

[213] MARCINISZYN P.W., 2006, *Maximizing bearing life through proper installation and lubrication*. Pumps & Systems, https://www.pumpsandsystems.com/maximizing-bearing-life-through-proper-installation-and-lubrication, [Accessed 2024-03-09].

[214] MEYERS K.E., 2000, *Understanding bearing internal clearance*, https://www.machinedesign.com/motors-drives/article/21834658/understanding-bearing-internal-clearance [Accessed: 2024-03-09].

[215] BICKFORD J., 1998, *Handbook of bolts and bolted joints*, CRC Press, Boca Raton, USA, 911 pp.

[216] BOBYR S., KROT P., PARUSOV E., GOLUBENKO T., BARANOVS'KA O., 2023, *Increasing wear resistance of the structural alloy steel 38CrNi3MoV subjected to isothermal hardening and deep cryogenic treatment*, Applied Sciences, 13(16), 9143, https://doi.org/10.3390/app13169143

[217] KRAEMER F., KLEIN M., OECHSNER M., 2020, *Fatigue strength of metric steel screws depending on pre-load and nut type*, Engineering Failure Analysis, 112, 104484, https://doi.org/10.1016/j.engfailanal.2020.104484

[218] ARGATOV I., SEVOSTIANOV I., 2010, *Health monitoring of bolted joints via electrical conductivity measurements*, International Journal of Engineering Science, 48, 874–887, https://doi.org/10.1016/j.ijengsci.2010.05.009

[219] PAN Q., PAN R., CHANG M., SHAO C., LIU X., XU X., 2019, *Reliability evaluation of bolt fastening force based on ultrasonic measurement method*, IEEE Int. Conf. on Mechatronics and Automation (ICMA 2019), 2212–2217, https://doi.org/10.1109/ICMA.2019.8816545

[220] MBA D., 2002, *Applicability of acoustic emissions to monitoring the mechanical integrity of bolted structures in low speed rotating machinery: case study*, NDT E Int., 35, 293–300, https://doi.org/10.1016/S0963-8695(01)00053-6

[221] ZHANG Z., LIU M., LIAO Y., SU Z., XIAO Y., 2018, *Contact acoustic non-linearity (CAN)--based continuous monitoring of bolt loosening: hybrid use of high-order harmonics and spectral sidebands*, Mechanical Systems and Signal Processing, 103, 280–294, https://doi.org/10.1016/j.ymssp.2017.10.009

[222] ZHANG Z., XU H., LIAO Y., SU Z., XIAO Y., 2017, *Vibro-acoustic modulation (VAM)-inspired structural integrity monitoring and its applications to bolted composite joints*, Composite Structures, 176, 505–515, https://doi.org/10.1016/J.COMPSTRUCT.2017.05.043

[223] WANG F., CHEN Z., SONG G., 2020, *Monitoring of multi-bolt connection looseness using entropy-based active sensing and genetic algorithm-based least square support vector machine*, Mech. Systems and Signal Proc., 136, 106507, https://doi.org/10.1016/j.ymssp.2019.106507

[224] WANG C., WANG N., HO S.C., CHEN X., PAN M., SONG G., 2018, *Design of a novel wearable sensor device for real-time bolted joints health monitoring*, IEEE Internet of Things J., 5, 5307–5316, https://doi.org/10.1109/JIOT.2018.2852653

[225] HUYNH T.-C., DANG N.-L., KIM J.-T., 2018, *Preload monitoring in bolted connection using piezoelectric-based smart interface*, Sensors, 18, 2766, https://doi.org/10.3390/s18092766

[226] PARK J.-H., HUYNH T.-C., CHOI S.-H., KIM J., 2015, *Vision-based technique for bolt-loosening detection in wind turbine tower*, Wind and Structures, 21, 709–726, https://doi.org/10.12989/was.2015.21.6.709

[227] ZHANG Y., SUN X., LOH K.J., SU W., XUE Z., ZHAO X., 2020, *Autonomous bolt loosening detection using deep learning*, Structural Health Monitoring, 19, 105–122, https://doi.org/10.1177/1475921719837509

[228] HUYNH T.-C., PARK J.-H., JUNG H.-J., KIM J.-T., 2019, *Quasi-autonomous bolt-loosening detection method using vision-based deep learning and image processing*, Automation in Construction, 105, 102844, https://doi.org/10.1016/j.autcon.2019.102844

[229] CHA Y.-J., YOU K., CHOI W., 2016, *Vision-based detection of loosened bolts using the Hough transform and support vector machines*, Automation in Construction, 71, 181–188, https://doi.org/10.1016/j.autcon.2016.06.008

[230] WANG C., WANG N., HO S.-C., CHEN X., SONG G., 2020, *Design of a new vision-based method for the bolts looseness detection in flange connections*, IEEE Trans. Ind. Electron., 67, 1366–1375, https://doi.org/10.1109/TIE.2019.2899555

[231] XU C., HUANG C.-C., ZHU W.-D., 2019, *Bolt loosening detection in a jointed beam using empirical mode decomposition–based non-linear system identification method*, Int. Journal of Distributed Sensor Networks, 15(9), 13, https://doi.org/10.1177/1550147719875656

[232] ZHANG T., BISWAL S., WANG Y., 2020, *SHMnet: Condition assessment of bolted connection with beyond human-level performance*, Structural Health Monitoring, 19, 1188–1201, https://doi.org/10.1177/1475921719881237

[233] WANG T., SONG G., LIU S., XIAO H., 2013, *Review of bolted connection monitoring*, Int. Journal of Distributed Sensor Networks, 9(12), 8, https://doi.org/10.1155/2013/871213

[234] DEKA A., RAO A., KAMATH S., GAURAV A., GANGADHARAN K.V. 2020, *Modeling and experimental studies on the dynamics of bolted joint structure: Comparison of three vibration-based techniques for structural health monitoring*, [in:] S. Dutta, E. Inan, S. Dwivedy (eds.), Advances in Rotor Dynamics, Control, and Structural Health Monitoring. Lecture Notes in Mech. Eng., Springer Singapore, 301–313, https://doi.org/10.1007/978-981-15-5693-7_21

[235] WANG Z., LIU M., ZHU Z., 2019, *Clamp looseness detection using modal strain estimated from FBG based operational modal analysis*, Measurement, 137, 82–97, https://doi.org/10.1016/j.measurement.2019.01.051

[236] YOU R., REN L., SONG G., 2020, *A Novel comparative study of European, Chinese and American codes on bolt tightening sequence using smart bolts*, Int. Journal of Steel Structures, 20, 910–918, https://doi.org/10.1007/s13296-020-00331-7

[237] TODD M.D., NICHOLS J.M., NICHOLS C.J., VIRGIN L.N., 2004, *An assessment of modal property effectiveness in detecting bolted joint degradation: Theory and experiment*, J. Sound Vib., 275, 1113–1126, https://doi.org/10.1016/j.jsv.2003.10.037

[238] HU Y.-J., GUO W., JIANG C., ZHOU Y., ZHU W., 2018, *Looseness localization for bolted joints using Bayesian operational modal analysis and modal strain energy*, Adv. Mech. Eng., 10(11), 110, https://doi.org/10.1177/1687814018808698

[239] KOSTEK R., LANDOWSKI B., MUSLEWSKI L., 2015, *Simulation of rolling bearing vibration in diagnostics*, Vibroeng. Procedia, 6, 335–340. URL: https://www.extrica.com/article/16696

[240] GEORGIADIS A., GONG X., MEIER N., 2018, *Vibration analysis based on the spectrum kurtosis for adjustment and monitoring of ball bearing radial clearance*, MATEC Web Conf., 211, 06006, https://doi.org/10.1051/matecconf/201821106006

[241] OMAR R., ABDUL RANI M.N., YUNUS M.A., 2020, *Representation of bolted joints in a structure using finite element modelling and model updating,* J. Mech. Eng. Sci., 14, 7141–7151, https://doi.org/10.15282/jmes.14.3.2020.15.0560

[242] KUMAR A., JAISWAL H., AHMAD F., PATIL P., 2014, *Dynamic vibration characteristics analysis of truck transmission gearbox casing with fixed constraint of vehicle frame based on FEA,* Procedia Eng., 97, 1107–1115, https://doi.org/10.1016/j.proeng.2014.12.389

[243] XIANLONG H., TIANLI S. (2019), *A new identification method for bolt looseness in wind turbine towers,* Shock Vib., 2019, 6056181, https://doi.org/10.1155/2019/6056181

[244] NGUYEN T.C., HUYNH T.-C., YI J.-H., KIM J., 2017, *Hybrid bolt-loosening detection in wind turbine tower structures by vibration and impedance responses,* Wind Struct., 24, 385–403, https://doi.org/10.12989/was.2017.24.4.385

[245] CHEN G., CHEN Y., CHEN Y., JI S., 2020, *Dynamics modeling and experimental modal analysis of bolt loosening for lightning rod,* J. Vibroengineering, 22, 657–671, https://doi.org/10.21595/jve.2019.20918

[246] BRONS M., THOMSEN J.J., SAH S.M., TCHERNIAK D., FIDLIN A., 2020, *Analysis of transient vibrations for estimating bolted joint tightness,* [in:] G. Kerschen, M. Brake, L. Renson (eds.), Non-linear Structures and Systems: Proc. of the 37th Conf. and Exposition on Structural Dynamics (IMAC 2019), Springer, Cham, 1, 21–24, https://doi.org/10.1007/978-3-030-12391-8_3

[247] SAH S.M., THOMSEN J.J., BRØNS M., FIDLIN A., TCHERNIAK D., 2018, *Estimating bolt tightness using transverse natural frequencies,* J. Sound Vibration, 431, 137–149, https://doi.org/10.1016/j.jsv.2018.05.040

[248] BRONS M., THOMSEN J.J., SAH S.M., TCHERNIAK D., FIDLIN, A., 2021, *Estimating bolt tension from vibrations: Transient features, non-linearity, and signal processing,* Mech. Syst. Signal Process., 150, 107224, https://doi.org/10.1016/j.ymssp.2020.107224

[249] LI Q., JING X., 2021, *A novel second-order output spectrum based local tuning method for locating bolt-loosening faults,* Mech. Syst. Signal Process., 147, 107104, https://doi.org/10.1016/j.ymssp.2020.107104

[250] MIAO R., SHEN R., ZHANG S., XUE S., 2020, *A review of bolt tightening force measurement and loosening detection,* Sensors, 20, 3165, https://doi.org/10.3390/s20113165

[251] GUARINO J., HAMILTON R., FISCHER W., 2009, *Acoustic detection of bolt detorquing in structures,* 157th Meeting Acoustical Society of America, 6, 065002, https://doi.org/10.1121/1.3167485

[252] BRUAND G., CHATELAIN F., GRANJON P., 2020, *Reconstructing shaft orbit using angle measurement to detect bearing faults*, Mech. Syst. Signal Process., 139, 106561, https://doi.org/10.1016/j.ymssp.2019.106561

[253] ZHANG H., ZHANG H., BORGHESANI P., SMITH W.A., RANDALL R.B., SHAHRIAR R., PENG Z. (2021). *Tracking the natural evolution of bearing spall size using cyclic natural frequency perturbations in vibration signals*. Mechanical Systems and Signal Processing, *151*, 107376, https://doi.org/10.1016/j.ymssp.2020.107376

[254] PNEVMATIKOS N.G., BŁACHOWSKI B., HATZIGEORGIOU G.D., SWIERCZ A., 2016, *Wavelet analysis based damage localization in steel frames with bolted connections*, Smart Struct. Syst., 18, 1189–1202, https://doi.org/10.12989/sss.2016.18.6.1189

[255] GELMAN L., PATEL T.H., 2015, *Novel rolling bearing diagnosis technology using spectral kurtosis and the wavelet higher-order spectra*, Insight – Non-Destructive Testing and Condition Monitoring, 57(8), 452–456, https://doi.org/10.1784/insi.2015.57.8.452

[256] BARTELMUS W., ZIMROZ R., 2009, *A new feature for monitoring the condition of gearboxes in non-stationary operating conditions*, Mech. Syst. Signal Process., 23, 1528–1534, https://doi.org/10.1016/j.ymssp.2009.01.014

[257] WODECKI J., MICHALAK A.M., ZIMROZ R., 2021, *Local damage detection based on vibration data analysis in the presence of Gaussian and heavy-tailed impulsive noise*, Measurement, 169, 108400, https://doi.org/10.1016/j.measurement.2020.108400

[258] WODECKI J., KRUCZEK P., BARTKOWIAK A., ZIMROZ R., WYŁOMAŃSKA A., 2019, *Novel method of informative frequency band selection for vibration signal using Nonnegative Matrix Factorization of spectrogram matrix*, Mech. Syst. Signal Process., 130, 585–596, https://doi.org/10.1016/j.ymssp.2019.05.020

[259] INTERNATIONAL ORGANISATION OF STANDARDIZATION (2009), *Rolling bearings – Internal clearance* – Part 1: *Radial internal clearance for radial bearings*, ISO 5753-1:2009.

[260] INTERNATIONAL ORGANISATION OF STANDARDIZATION (2002), *Condition monitoring and diagnostics of machines – Vibration condition monitoring*, ISO 13373:2002-2017 (all parts).

[261] INTERNATIONAL ORGANISATION OF STANDARDIZATION (2003), *Condition monitoring and diagnostics of machines – Data processing, communication and presentation* – Part 1: *General guidelines*, ISO 13374-1:2003.

[262] INTERNATIONAL ORGANISATION OF STANDARDIZATION, 2003, *Condition monitoring and diagnostics of machines – Data interpretation and diagnostics techniques*, ISO 13379:2003-2015 (all parts).

[263] INTERNATIONAL ORGANISATION OF STANDARDIZATION, 2015, *Condition monitoring and diagnostics of machines – Prognostics* – Part 1: *General guidelines*, ISO 13381-1:2015.

[264] INTERNATIONAL ORGANISATION OF STANDARDIZATION, 2018, *Condition monitoring and diagnostics of machines — General guidelines*, ISO 17359:2018.

[265] MITCHEL J., 1989, *Diagnostic maintenance expert system for the hydraulic subsystem of a continuous miner*, IEEE Trans. on Industry Applications, 25, 841–845, https://doi.org/10.1109/28.41246

[266] CAWLEY J.C., 1991, *Online diagnostic maintenance systems for continuous mining machines,* Mining Engineering, 43(12), 1444–1448. URL: https://www.osti.gov/etdeweb/biblio/5684602

[267] TALLFORS M., 2005, *Parameter estimation and model based control design of drivetrain systems*, BSc Thesis, KTH University, Stockholm, Sweden.

[268] SARKAR N., ELLIS R.E., MOORE T.N., 1997, *Backlash detection in geared mechanisms: modeling, simulation, and experimentation*, Mech. Systems and Signal Process., 11(3), 391–408, https://doi.org/10.1006/mssp.1996.0082

[269] KIM T.C., 2003, *Analysis of clearance non-linearities and vibro-impacts in torsional systems,* Ph.D. Thesis, Ohio State University, USA.

[270] VERENEV V.V., 2007, *Diagnostics and dynamics of rolling mills,* Dnepr, IMA-press, 144 pp.

[271] PODKOPAEV V.V., PODKOPAEV S.V, 1987, *The method of determining the wear of the main transmission line of vehicles*, Patent SU 1422055 A1, G01M 13/02, Prior. 1987-03-30.

[272] CHISTYAKOV Y.P., RYAZANTSEV A.N. , BROWN A.E. , TIKOTSKY A.E., 1998, *A device for determining wear in friction pairs of a stand pressure device*, Patent RU 2147474C1, B21B 38/00, OJSC "Ural Heavy Engineering Plant", Prior. 1998-06-07.

[273] GROMAKOVSKY D.G., AVERKIEVA V.I., YAFYASOV R.A., SMIRNOV B.I., RUZHAN V.M., GORLOV V.V., 1987, *Method of diagnosing friction units*, Patent SU 1441255A1, G01N 03/56, Prior. 1987-04-13.

[274] FEDOROV P.F., NOSOV V.L., URUIMAGOV A.D., 2002, *Determination of the technical condition of the mill stands 2500 of OJSC MMK according to the results of the study of the quality factor of oscillations of the roll system*, Production of Rolled Products, 5, 20–22.

[275] VERENEV V.V., YUNAKOV O.M., DALICHUK A.P., PUTNOKI O.Y., MATSKO S.V., BORSCHOV O.V., BUDAKVA S.A., 2003, *Method of determining technical condition of driveline in rolling stand*. Patent UA 70137A. G01M 7/00. Prior, 2003-12-26.

[276] ADAMIA R.S., 1978, *Optimization of dynamic loads of rolling mills,* Metallurgy Publishing, Moscow, 232 pp.

[277] KROT P.V., 2010, *Dynamics and diagnostics of the rolling mills drivelines with non-smooth stiffness characteristics,* Proc. of the 3rd Int. Conf. on Non-linear Dynamics (ND-KhPI 2010), 2124 Sep. 2010, Kharkiv, Ukraine, 115–120.

[278] KIM T.C., ROOK T.E., SINGH R., 2003, *Effect of smoothening functions on the frequency response of an oscillator with clearance non-linearity*, J. Sound and Vibration, 263(3), 665–678, https://doi.org/10.1016/S0022-460X(02)01469-4

[279] ADAMS D.E., ALLEMANG R.J., 2000, *Polynomial, non-polynomial, and orthogonal polynomial generating functions for non-linear system identification*, Proc. of Int. Conf. on Noise and Vibration Eng. (ISMA25), 13–15 Sep., Belgium.

[280] BOLOTIN V.V., 1964, *The dynamic stability of elastic systems*, Holden-Day, Inc., San Francisco, USA, 1964.

[281] BOLOTIN V.V., 1984, *Random Vibration of Elastic Systems*, Springer-Verlag, Berlin, 468 pp.

[282] TJAHJOWIDODO T., AL-BENDER F., BRUSSEL van H., 2007, *Quantifying chaotic responses of mechanical systems with backlash component*, Mech. Systems and Signal Processing, 21, 973–993, https://doi.org/10.1016/j.ymssp.2005.11.003

[283] ANISHCHENKO V.S., ASTAKHOV V.V., NEIMAN A.B., VADIVASOVA T.E., SCHIMANSKY-GEIER L., 2002, *Non-linear dynamics of chaotic and stochastic systems: Tutorial and Modern Developments (Springer Series in Synergetics)*, 2nd Edition, Springer-Verlag, Berlin, https://doi.org/10.1007/978-3-540-38168-6

[284] DOKUKIN A.V., KRASNIKOV Y.D., KHURGIN Z.Y., 1978, *Statistical dynamics of mining machines*, Mashinostroenie Publishing, Moscow, 238 pp.

[285] WERON R., 1996, *On the Chambers-Mallows-Stuck method for simulating skewed stable random variables*, Statistics and Probability Letters, 28, 165–171, https://doi.org/10.1016/0167-7152(95)00113-1

[286] BLEKHMAN I.I., DZHANELIDZE G.Y., 1964, *Vibrational transportation*, Nauka, Moscow.

[287] LIQIN W., LI C., DEZHI Z., LE G., 2008, *Non-linear dynamics behaviors of a rotor roller bearing system with radial clearances and waviness considered*, Chin. J. Aeronaut., 21, 86–96, https://doi.org/10.1016/S1000-9361(08)60012-6

[288] TIWARI M., GUPTA K., PRAKASH O., 2000, *Effect of radial internal clearance of a ball bearing on the dynamics of a balanced horizontal rotor*, J. Sound Vibration, 238, 723–726, https://doi.org/10.1006/jsvi.1999.3109

[289] KAPPAGANTHU K., NATARAJ C., 2011, *Non-linear modeling and analysis of a rolling element bearing with a clearance*, Communications in Nonlinear Science and Numerical Simulation, 16, 4134–4145, https://doi.org/10.1016/j.cnsns.2011.02.001

[290] BARTELMUS W., 2014, *Object and operation supported maintenance for mining equipment*, Mining Science, 21, 7–21.

[291] FILATOV A.A., GARTSMAN S.D., ZHUKOV A.A., KHREBIN V.N., 2003, *Determination of dynamic loads in pinion stands and reduction gears of rolling mills*, Stal', 8, 41–45.

[292] KORENNOY V.V., 2015, *Simulation of dynamic processes in gearboxes of rolling stands,* Metallurgical and Mining, Industry, 7, 127–132.

[293] ZHOU S., REN Z., SONG G., WEN B., 2015, *Dynamic characteristics analysis of the coupled lateral-torsional vibration with spur gear system,* Int. J. Rotating Mach., 2015, 371408, https://doi.org/10.1155/2015/371408

[294] CHEN Y., GAO Q., GUAN Z., 2017, *Self-loosening failure analysis of bolt joints under vibration considering the tightening process,* Shock and Vibration, 2017, 2038421, https://doi.org/10.1155/2017/2038421

[295] KASEI S., 2007, *A study of self-loosening of bolted joints due to repetition of small amount of slippage at bearing surface,* J. Advanced Mech. Design, Systems, and Manufacturing, 1, 358–367, https://doi.org/10.1299/jamdsm.1.358

[296] NASSAR S.A., HOUSARI B.A., 2007, *Study of the effect of hole clearance and thread fit on the self-loosening of threaded fasteners,* J. Mechanical Design, 129, 586–594, https://doi.org/10.1115/1.2717227

[297] BRAKE M.R.W. (ed.), 2018, *The Mechanics of Jointed Structures. Recent Research and Open Challenges for Developing Predictive Models for Structural Dynamics*, Springer International Publishing, Cham, Switzerland, 702 pp., https://doi.org/10.1007/978-3-319-56818-8

[298] ZHOU J., LIU J., OUYANG H., CAI Z., PENG J., ZHU M., 2019, *Self-loosening behavior of bolted joints subjected to dynamic shear load*, Int. J. Mod. Phys. B, 33, 1940009, https://doi.org/10.1142/S0217979219400095

[299] KROT P., SLIWINSKI P., ZIMROZ R., GOMOLLA N., 2020, *The identification of operational cycles in the monitoring systems of underground vehicles*, Measurement, 151, 107111, https://doi.org/10.1016/j.measurement.2019.107111

[300] TRUSHIN N., ANTSEV A., 2020, *Combined torque converter for mining machines*, IOP Conf. Series: Earth and Environmental Science, 459, 042078, https://doi.org/10.1088/1755-1315/459/4/042078

[301] SLIWINSKI P., KANIEWSKI T., HEBDA-SOBKOWICZ J., ZIMROZ R., WYLOMAŃSKA A., 2020, *Analysis of dynamic external loads to haul truck machine subsystems during operation in a deep underground mine,* [in:] Proc. 39th Int. Symp. on Appl. of Computers and Operations Research in the Mineral Ind. (APCOM-2019), 515–524, https://doi.org/10.1201/9780429320774

[302] ZIMROZ, R., WODECKI, J., KRÓL, R., ANDRZEJEWSKI, M., SLIWINSKI, P., STEFANIAK, P., 2013, *Self-propelled mining machine monitoring system – data validation, processing and analysis,* [in:] C. Drebenstedt, R. Singhal (eds.), Mine Planning and Equipment Selection. Proc. of the 22nd MPES Conf., Springer, Cham, 1285–1294, https://doi.org/10.1007/978-3-319-02678-7_124

[303] KROT P., ZIMROZ R., SLIWINSKI P., GOMOLLA N. (2022), *Safe operation of underground mining vehicles based on cyclic fatigue monitoring of powertrains,* [in:] G. Lesiuk, M. Szata, W. Blazejewski, A.M. de Jesus, J.A. Correia (eds.), Structural Integrity and Fatigue Failure Analysis (VCMF 2020), Structural Integrity, Springer, Cham, 25, 283–292, https://doi.org/10.1007/978-3-030-91847-7_26

[304] YOSHIDA K., TAKAMATSU H., MATSUMOTO S., 2016, *Non-linear identification of torsional driveshaft vibrations in a full-scale automotive vehicle during acceleration,* Non-linear Dynamics, 86, 711–721, https://doi.org/10.1007/s11071-016-2917-8

[305] WANG Y., ZHU G., ZHANG F., 2013, *Powertrain control parameter optimisation using HIL simulations of a heavy-duty vehicle,* Int. J. of Powertrains (IJPT), 2(1), 24, https://doi.org/10.1504/IJPT.2013.052662

[306] GALVAGNO E., VELARDOCCHIA M., VIGLIANI A., 2016, *Torsional oscillations in automotive transmissions: experimental analysis and modelling,* Shock and Vibration, 2016, 5721960, https://doi.org/10.1155/2016/5721960

[307] BAI J., WU X., GAO F., LI H., 2017, *Analysis of powertrain loading dynamic characteristics and the effects on fatigue damage,* Applied Sciences, 7(10), 1027, https://doi.org/10.3390/app7101027

[308] AZADI M. (2016), *Failure analysis and prevention in powertrain systems,* [in:] A.S. Hamdy, M.M. Aliofkhazraei (eds.), *Handbook of materials failure analysis with case studies from the aerospace and automotive industries,* Butterworth-Heinemann, 471–492, https://doi.org/10.1016/B978-0-12-800950-5.00021-1

[309] NEERUKATTI R.K., LIU K.C., KOVVALI N., CHATTOPADHYAY A., 2014, *Fatigue life prediction using hybrid prognosis for structural health monitoring,* J. of Aerospace Information Systems, 11(4), 211–232, https://doi.org/10.2514/1.I010094

[310] ASL H.A., AZAD N. L., McPHEE J., 2012, *Modeling torque converter characteristics in automatic drivelines: lock-up clutch and engine braking simulation,* Proc. ASME Int. Design Eng. Technical Conf., Computers and Inform., Chicago, IL, USA, 6, 359–367, https://doi.org/10.1115/DETC2012-70222

[311] KANIEWSKI T., ŚLIWIŃSKI P., HEBDA-SOBKOWICZ J., ZIMROZ R., 2019, *Comprehensive, experimental verification of the effects of the lock-up function implementation in LHD haul trucks in the deep underground mine,* [in:] Proc. of the 39th Int. Symposium on Application of Computers and Operations Research in the Mineral Industry (APCOM-2019), Taylor and Francis, 506–514, https://doi.org/10.1201/9780429320774

[312] GIPSER M., 2007, *FTire – the tire simulation model for all applications related to vehicle dynamics,* Vehicle System Dynamics, 45, 139–151, https://doi.org/10.1080/00423110801899960

[313] VERBAS V.V., NAUMENKO A.P., 2010, *To the formation of a calculation-experimental model of a safe wheel mover*, Issues of Chemistry and Chemical Technology, 3, 89–94.

[314] REGULA J., 2019, *How to successfully prepare and complete a hydrostatic test*. https://www.mcwaneductile.com/blog/how-to-successfully-prepare-and-complete-a-hydrostatic-test, [Accessed 2024-03-10].

[315] ENERPROM, (2024), *Stand for testing tubes with hydrostatic pressure*, https://www.enerprom-spb.com/catalog/ispytatelnoe-oborudovanie/gidroispytaniya, [Accessed 2024-03-10].

[316] URAL ENGINEERING CENTRE, 2024, *Press for hydraulic testing of tubes with a diameter 530–1420 mm of main gas pipelines*, http://www.cheltec.ru/tubes, [Accessed 2024-03-10].

[317] AMERICAN PETROLEUM INSTITUTE, 2018, *Casing and tubing*, API 5CT: 2018.

[318] INTERNATIONAL ORGANISATION OF STANDARDIZATION, 2007, *Petroleum and natural gas industries – equations and calculations for the properties of casing, tubing, drill tube and line tube used as casing or tubing*, ISO/TR 10400:2007.

[319] WLODARCZYK E., SARZYNSKI M., (2017), *Strain energy method for determining dynamic yield stress in Taylor's test*, Eng. Trans., 65(3), 499–511, https://doi.org/10.24423/engtrans.378.2017

[320] LEU M.C., MENG P., GESKIN E. S., TISMENESKIY L., 1998, *Mathematical modeling and experimental verification of stationary waterjet cleaning process*, ASME J. Manuf. Sci. Eng., 120(3), p.571–579, https://doi.org/10.1115/1.2830161

[321] LIU H., KANG C., ZHANG W., ZHANG T., 2017, *Flow structures and cavitation in submerged waterjet at high jet pressure*, Experimental Thermal and Fluid Science, 88, 504–512, https://doi.org/10.1016/j.expthermflusci.2017.07.003

[322] SHIMADA N., HIBARA H., ISHIBASHI Y., SUMIDA M., SUDO K., 2004, *Analysis of submerged water jets by visualization method*, Journal of Visualization, 7, 281–289, https://doi.org/10.1007/BF03181532

[323] IBATULOV K.A., 1972, *Hydraulic machines and mechanisms in the oil industry*, Nedra, Moscow.

[324] LINDELL J.E., MOORE W.P., KING H.W., 2018, *Handbook of hydraulics*, 8th ed., McGraw-Hill Education.

[325] VILNER Y.M., KOVALEV Y.T., NEKRASOV B.B. (eds.), 1976, *Reference manual for hydraulics, hydraulic machines and hydraulic drives,* Higher School, Minsk.

[326] PANOVKO Y.G., 1990, *Fundamentals of the applied theory of vibrations and shock*, Politechnika, Leningrad.

[327] KULAK G.L., FISHER J.W., STRUIK J.H.A., 2001, *Guide to design criteria for bolted and riveted joints*, 2nd edition, American Institute of Steel Construction.

[328] KROT P.V., ZIMROZ R., 2020, *Failure analysis and modernization of high-pressure hydraulic press for drilling tubes testing*, Engineering Failure Analysis, 117, 104772, https://doi.org/10.1016/j.engfailanal.2020.104772

[329] KRÓL R., ZIMROZ R., STOLARCZYK L., 2009, *Failure analysis of hydraulic systems used in mining machines operating in copper ore mine KGHM Polska Miedz S.A.*, Mining Science, 128(36), 127–139.

[330] BARCZAK T.M., 2017, *Research developments that contributed to the landscape of longwall roof support design over the past 25 years*, [in:] S.S. Peng (ed.), Woodhead Publ. Series in Energy, Advances in Coal Mine Ground Control, 1–34, https://doi.org/10.1016/B978-0-08-101225-3.00001-3

[331] HEREZY Ł., JANIK D., SKRZYPKOWSKI K., 2018, *Powered roof support – rock strata interactions on the example of an automated coal plough system*, Studia Geotechnica et Mechanica, 40(1), 46–55, https://doi.org/10.2478/sgem-2018-0007

[332] JUÁREZ-FERRERAS R., MENÉNDEZ-DÍAZ A., ÁLVAREZ-VIGIL A.E., ÁLVAREZ-FERNÁNDEZ M.I., 2009, *Forensic analysis of hydraulic props in longwall workings*, Engineering Failure Analysis, 16(7), 2357–2370, https://doi.org/10.1016/j.engfailanal.2009.03.025

[333] GONZÁLEZ-NICIEZA C., MENÉNDEZ-DÍAZ A., ÁLVAREZ-VIGIL A.E., ÁLVAREZ-FERNÁNDEZ M.I., 2008, *Analysis of support by hydraulic props in a longwall working*, Int. J. of Coal Geology, 74(1), 67–92, https://doi.org/10.1016/j.coal.2007.10.001

[334] LANGOSCH U., RUPPEL U., 2006, *New method for dimensioning of shield support to improve longwall roof control*, J. Mines Met. Fuels, 54(8), 179–184.

[335] ZHU D., TU S., TU H., YANG Z., 2019, *Mechanisms of support failure and prevention measures under double-layer room mining gobs – A case study: Shigetai coal mine*, Int. J. of Mining Sci. and Technology, 29(6), 955–962, https://doi.org/10.1016/j.ijmst.2018.06.006

[336] BIAŁY W., HĄBEK P., 2018, *Quality engineering tools in analysis of failure of longwall mining complex,* Mining – Informatics Automation and Electrical Engineering, 56(3), 33–39, http://dx.doi.org/10.7494/miag.2018.3.535.33

[337] MARK C., STEPHAN R.C., AGIOUTANTIS Z., 2020, *Analysis of mine roof support (AMRS) for US coal mines*, Mining, Metallurgy & Exploration, 37, 1899–1910.

[338] ISLAVATH S.R., DEB D., KUMAR H., 2019, *Life cycle analysis and damage prediction of a longwall powered support using 3D numerical modelling techniques*, Arab Journal of Geosciences, 12, 441, https://doi.org/10.1007/s12517-019-4574-y

[339] RAJWA S., 2020, *The influence of the geometrical construction of the powered roof support on the loss of a longwall working stability based on the practical experience*, Arch. Min. Sci., 65(3), 511–529, https://doi.org/10.24425/ams.2020.134132

[340] WARZYŃSKA U., SIWULSKI T., 2021, *Influence of boundary conditions on the accuracy of pulsation dampers characteristics in analytical models*, Int. J. of Fluid Power, 21(3), 363–382, https://doi.org/10.13052/ijfp1439-9776.2134

[341] SIWULSKI T., 2021, *Comparative Studies of the dynamic response of hydraulic cylinders with different hydraulic supply systems design*, [in:] J. Stryczek, U. Warzyńska (eds.), *Advances in Hydraulic and Pneumatic Drives and Control (NSHP 2020)*, Lecture Notes in Mechanical Engineering, Springer, Cham, 301–310, https://doi.org/10.1007/978-3-030-59509-8_27

[342] ŚWIĄTEK J., JANOSZEK T., CICHY T., STOIŃSKI K., 2021, *Computational fluid dynamics simulations for investigation of the damage causes in safety elements of powered roof supports—a case study*, Energies, 14(4), 1027, https://doi.org/10.3390/en14041027

[343] SZURGACZ D., BRODNY J., 2018, *Analysis of load of a powered roof support's hydraulic leg*, E3S Web of Conferences, 71, 1–5, https://doi.org/10.1051/e3sconf/20187100002

[344] PYTLIK A., 2015, *Process characteristics of hydraulic legs equipped with safety valves at dynamic load caused by a mining tremor*, Arch. Min. Sci., 60(2), 595–612, https://doi.org/10.1515/amsc-2015-0039

[345] SZARUGA W.S., 1985, *The rotary multi-plate valve as an integrated control system of a longwall roof support*, IFAC Proceedings Volumes, 18(6), 45–47, https://doi.org/10.1016/S1474-6670(17)60487-7

[346] VATAVU S., 2019, *The study of the influence of the hydro-pneumatic accumulator within the operation of hydraulic assemblies used for the supply of longwall roof supports*, 19th Int. Multidisciplinary Scientific GeoConference (SGEM 2019), 685–692, https://doi.org/110.5593/sgem2019/1.3/S03.087

[347] ZHAO G., WANG H., SONG Y., ZHANG C., 2020, *Dynamic characteristics study on the two-stage safety valve used on hydraulic support under impact loading*, J. of Theoretical and Applied Mechanics, 58(3), 623–635, https://doi.org/10.15632/jtam-pl/116576

[348] OSTROJ, 2024, *Powered Roof Supports*, http://www.ostroj.cz/en/powered-roof-supports [Accessed 2024-03-10].

[349] KLISHIN V.I., 2002, *Adaptation of mechanized supports to the dynamic loading conditions*. Novosibirsk, Nauka, 199 pp.

[350] BUEVICH V.V., GABOV V.V., ZADKOV D.A., VASILEVA P.A., 2015, *Adaptation of the mechanized roof support to changeable rock pressure*, Eurasian Mining, 2, 11–14, https://doi.org/10.17580/em.2015.02.03

[351] RUDZKI P., KROT P., 2021, *Dynamics control of powered hydraulic roof supports in the underground longwall mining complex*, IOP Conference Series: Earth and Environmental Science, 942, 012014, https://doi.org/10.1088/1755-1315/942/1/012014

[352] FENG H., DU Q., HUANG Y., CHI Y.B., 2017, *Modelling study on stiffness characteristics of hydraulic cylinder under multi-factors*, Journal of Mech. Eng., 63(7–8), 447–456, https://doi.org/10.5545/SV-JME.2017.4313

[353] KOZHEVNIKOV S.N., 1986, *Dynamics of non-stationary processes in machines*, Naukova Dumka, Kyiv.

[354] SMIRNOV V.V., YAKOVLEV R.A., 1977, *Rolling mill drive mechanics*, Metallurgy, Moscow, 216 pp.

[355] VEITS V.L., KOCHURA A.E., TSAREV G.V., 1979, *Calculation of mechanical drive systems with clearances*, Mashinostroenie, Moscow, 183 p.

[356] KROT P.V., 2010, *Dynamic model of geared drive with changeable structure of high-speed wire rolling block,* The Bulletin of NTU "KhPI". Series "Mechanical Drive Problems", 27, 96–108. URL: http://library.kpi.kharkov.ua/files/Vestniki/2010_27.pdf

[357] SUN J.I.-I., PENG Y., LIU H.-M., 2010, *Non-linear vibration and stability of moving strip with time–dependent tension in rolling process*, Journal of Iron and Steel Research Int, 17(6), 11–15, https://doi.org/10.1016/S1006-706X(10)60106-9

[358] SUN J.I.-I., PENG Y., LIU H.-M., JIANG G.-B., 2010, *Vibration of moving strip with distributed stress in rolling process,* J Iron Steel Research Int., 17(4), 24–30, https://doi.org/10.1016/S1006-706X(10)60081-7

[359] TANG H.P., DING R., WU Y.X., ZHONG J., 2002, *Investigation for parametric vibration of rolling mill*, Trans of Nonferrous Metals Society of China, 12(3), 485–488.

[360] PRAZDNIKOV A.V., 1975, *Automation of continuous small-section mills*, Metallurgy, Moscow.

[361] LUNDBERG S.E., 2007, *A vision of wire rod rolling technology for the twenty first century*, Advanced Materials Research, 23, 39–44, https://doi.org/10.4028/www.scientific.net/AMR.23.39

[362] FABRIS R., HEIN O., MOSHAMMER K., PALZENBERGER J., TROJACHER J., 2001, *Advanced solutions for bar and wire-rod mills*, Revue De Métallurgie, 98(7–8), 689–698, https://doi.org/10.1051/metal:2001116

[363] VERENEV V.V., 2015, *Dynamic processes in cold strip mills*, Lira Publishing, Dnipro.

[364] PANJKOVIC V., 2015, *Chatter in steel rolling*, [in:] Encyclopedia of iron, steel and their alloys, G.E. Totten, R. Colas (eds.), 1st edition, CRC Press, https://doi.org/10.1081/E-EISA-120050422

[365] MEEHAN P.A., 2002, *Vibration instability in rolling mills: Modeling and experimental results*, J. of Vibration and Acoustics, Trans. of the ASME, 124(2), 221–228, https://doi.org/10.1115/1.1456457

[366] CHEFNEUX L., FISCHBACH J.-P., J-P., GOUZOU J., 1984, *Study and industrial control of chatter in cold rolling*, Iron and Steel Eng., 61(11), 17–26,

[367] ARCULIS G.E., SHVARTSMAN Z.M., FAIZULLIN V.Kh., 1972, *Auto-vibrations in a cold rolling mill*, Stal', 8, 727–728.

[368] BOLLINGER L.A., RAPSINSKI T.S., 1994, *Winding reel involvement in temper mill chatter*, Iron and Steel Eng., 71(12), 27–29.

[369] GASPARIC J.J., 1991, *Vibration analysis identifies the causes of mill chatter*, Iron and Steel Eng., 68(2), 27–29.

[370] NESSLER G.L., CORY J.F., 1989, *Cause and solution of fifth octave backup roll chatter on 4-h cold mills and temper mills*, Iron and Steel Eng., 10, 23–27.

[371] ROBERTS W.L., 1978, *Four-h mill stand chatter on fifth octave mode*, Iron and Steel Eng., 55(4), 41–47.

[372] KLEPIKOV V.B., 1986, On a frictional auto-vibrations in the electrical drives, J. Electricity, 4, 5462.

[373] TANG H.P., WANG D.Y., ZHONG J., 2002, *Investigation into the electromechanical coupling instability of a rolling mill*, J. of Materials Processing Technology, 129(1–3), 294–298, https://doi.org/10.1016/S0924-0136(02)00679-9

[374] KOLPAKOV S.S., PIMENOV V.A., TSUKANOV Y.A., RUBANOV V.P., 1993, *Vibration research in the 5-stand mill 2030*, Stal', 1, 47–52.

[375] PIMENOV V.A., 1990, *On the causes of non-stable cold rolling*, Izvestiya VUZov. Chornaia Metallurgy, 8, 36–38.

[376] HARDWICK B.R., 1994, *Identification and solution of chatter vibration on roll grinding machines*, Iron and Steel Eng., 71(7), 41–46.

[377] BENHAFSI Y., 2006, *The use of vibration analysis tools to solve chatter problems on rolling mills and roll grinding machines*, Proc. of Steel Rolling 2006, the 9th Int. and 4th European Conf., June 19–21, 2006, Paris, France.

[378] NIEB J.R., NICOLAS V.T., 1991, *Automated monitoring and control of vibrations and chatter in rolling processes*, Iron and Steel Eng., 68(7), 33–42.

[379] MARJUTA A.N., 1993, *The frictional vibrations in the mechanical systems*, Nedra Publishing, Moscow.

[380] MARJUTA A.N., KROT P.V., 1997, *High frequency rolling mills chatter – mathematical identification and simulation*, 1st Int. Symposium on Multi-Body Dynamics Monitoring and Simulation Techniques (MBD MST 97), March 25–27, University of Bradford, UK, 407–419.

[381] BAR A., BAR O., 2005, *Types of mid-frequency vibrations appearing during the rolling mill operation*, J of Mat Proc Technology, 162–163, 461–464, https://doi.org/10.1016/j.jmatprotec.2005.02.063

[382] BAR A., SWIATONIOWSKI A., 2004, *Interdependence between the rolling speed and non-linear vibrations of the mill system*, J. of Materials Processing Technology, 155–156, 2116–2121, https://doi.org/10.1016/j.jmatprotec.2004.04.422

[383] DRZYMALA Z., SWIATONIOWSKI A., BAR A., 2003, *Non-linear vibrations in cold rolling mills*, Mecanique & Industries, 4(2), 151–158, https://doi.org/10.1016/S1296-2139(03)00033-2

[384] WU Y.X., DUAN J.A., 2002, *Frequency modulation of high-speed mill chatter*, J. of Materials Processing Technology, 129(1–3), 148–151, https://doi.org/10.1016/S0924-0136(02)00599-X

[385] ZHONG J., YAN H., DUAN J., XU L., WANG W., CHEN P., 2002, *Industrial experiments and findings on temper rolling chatter*, J. of Materials Processing Technology, 120(1–3), 2002, 275–280, https://doi.org/10.1016/S0924-0136(01)01181-5

[386] SWIATONIOWSKI A., 1996, *Interdependence between rolling mill vibrations and the plastic deformation process*, Journal of Materials Processing Technology, 61(4), 354 364, https://doi.org/10.1016/S0924-0136(96)02271-6

[387] SWIATONIOWSKI A., THOMSON P.F., 1996, *Theoretical study of the dynamic effect on the warping of rolled strip and loss of flatness*, Journal of Materials Processing Technology, 61(4), 373–381, https://doi.org/10.1016/S0924-0136(96)02273-X

[388] JOHNSON R.E., QI Q., 1994, *Chatter dynamics in sheet rolling*, Int. J. of Mech. Sciences, 36(7), 617–630, https://doi.org/10.1016/0020-7403(94)90017-5

[389] EHMANN K.F., WU S.M., 1980, *Forecasting control of machining chatter*, Computer Applications in Manufacturing Systems: Planning, Control and Robots, Winter Annual Meet of ASME, Chicago, IL, USA, 37–52.

[390] GARBER E.A., KOZHEVNIKOV A.V., 2005, *Method for strip rolling with tension in the tandem mill*, Patent RU 2259896, B21B 1/28, Severstal, Publ. 2005-09-10.

[391] PRYKHOD'KO I.Y., NASTICH V.P., CHERNOV P.P., 2004, *Method for cold rolling of strips in multistand mill*, Patent RU 2225272, B21B 1/28, NLMK, Publ. 2004-03-10.

[392] HELEKAL G., SPINDLER G., LUFTENSTEINER R., RIEGLER C., AIGNER H., 2002, *Automatic vibration analysis and trending for complex drives*, Steel Technology, 10, 43–49.

[393] BOULTON G., DOMANTI T., EDWARDS J., MEEHAN P., WALLACE G., 2000, *Modeling and suppression of rolling mill chatter*, Trans. Association of Iron and Steel Engi-neers.

[394] HOLL J., SCHLACHER K., KEINTZEL G., EISENKOCK N., 2003, *Analysis and active rejection of chatter in rolling mills*, PAMM – Proc. Appl. Math. Mech., 3, 134–135, https://doi.org/10.1002/pamm.200310344

[395] KONG T., YANG D.C.H., 1993, *Modeling of tandem rolling mills including tensional stress propagation*, Proc. Inst. Mech. Eng., Part E: J. of Process Mech. Eng., 207, p. 143–150, https://doi.org/10.1243/PIME_PROC_1993_207_217_02

[396] PIMENOV V.A., KOLPAKOV S.S., TSUKANOV Y.A., RUBANOV V.P., 1999, *Automatic vibration diagnostics and mill speed control in the 2030 cold rolling mill*, Rolling Technology Journal, 11, 42–48.

[397] KROT P.V., 2009, *Statistical dynamics of the rolling mills*, IUTAM Symposium on the Vibration Analysis of Structures with Uncertainties. July 6–10, 2009, IUTAM Bookseries, 27(4), 429–442, https://doi.org/10.1007/978-94-007-0289-9_31

[398] KROT P.V., PRYKHODKO I.Y., CHERNOV P.P., 2008, *Regenerative chatter vibrations control in the tandem cold rolling mills*, Proc of the 4th European Conf. on Structural Control (ECSC 2008), 428–437. URL: https://www.ipme.ru/ipme/conf/4ecsc/_english/ECSC2008_ScientificProgram.pdf

[399] KROT P.V., 2019, *Dynamical processes in a multi-motor gear drive of heavy slabbing mill*, J. of Vibroengineering, 21, 2064–2081, https://doi.org/10.21595/jve.2019.20973

[400] ZIETEK B., KROT P., BORKOWSKI, 2020, *An overview of torque meters and new devices development for condition monitoring of mining machines*, IOP Conference Series: Earth and Environ Sc, 684, 012019, https://doi.org/10.1088/1755-1315/684/1/012019

[401] KROT P., KORENNOI V., ZIMROZ R., SZREK J., 2023, *Angular backlashes monitoring in heavy industrial machines*, [in:] A. Puchalski, B.E. Łazarz, F. Chaari, I. Komorska, R. Zimroz (eds.), Advances in Technical Diagnostics II (ICTD 2022), Applied Condition Monitoring, Springer, Cham, 21, 212–228, https://doi.org/10.1007/978-3-031-31719-4_22

[402] KROT P.V., 2008, *Non-linear vibrations and backlashes diagnostics in the rolling mills drivetrains*, Proc. of the 6th EUROMECH Non-linear Dynamics Conference (ENOC 2008), 360–366. URL: http://lib.physcon.ru/doc?id=ef36ccc625d1

[403] BOLSHAKOV V.I., KROT P.V., KORENNOI V.V., SOLOVIOV K.V., DALICHUK A.P., 2007, *Method of wear diagnostics of transmission elements of rolling stands*, Patent UA 79859, Iron and Steel Institute of Ukraine, Publ. 2007-07-25.

[404] ZIMROZ P., KROT P., ZIMROZ R., 2023, *Statistical analysis of peak torque in drivelines of mining and metallurgical machines for clearances diagnostics*, [in:] A.D. Ball, H. Ouyang, J.K. Sinha, Z. Wang (eds.) Proceedings of the UNIfied Conference of DAMAS, IncoME and TEPEN Conferences (UNIfied 2023). Mechanisms and Machine Science, Springer, Cham., 152, 725–739, https://doi.org/10.1007/978-3-031-49421-5_59

[405] IVANCHENKO F.K., KRASNOSHAPKA V.A., 1983, *Applied problems of machine dynamics*. Vishcha Shkola, Kyiv.

[406] BOLSHAKOV V.I., KROT P.V., KORENNOI V.V., SOLOVIOV K.V., DALICHUK A.P., 2007, *Method for monitoring fluctuations of load on the drive mechanism of rolling mill*, Patent UA 79682. Publ. 2007-07-10.

[407] KROT P., KORENNOI V., ZIMROZ R., 2020, *Vibration-based diagnostics of radial clearances and bolts loosening in the bearing supports of the heavy-duty gearboxes*, Sensors, 20, 7284, https://doi.org/10.3390/s20247284

[408] BOLSHAKOV V.I., KROT P.V., KORENNOY V.V., SOLOVIOV K.V., DALICHUK A.P., 2005, *Method for diagnostics of bearing supports of the main drive line of a rolling mill*, Patent UA 79681, G01M 13/00, Publ. 2007-07-10.

[409] KROT P., SHIRI H., DĄBEK P., ZIMROZ R., 2023, *The diagnostics of bolted joints in vibrating screens based on a multi-body dynamical model*, Materials, 16(17), 5794, https://doi.org/10.3390/ma16175794

[410] PRYKHODKO I.Y., KROT P.V., 2006, *Vibration monitoring system and the new methods of chatter early diagnostics for tandem mill control*, Proc. of Int. Conf. "Vibration in rolling mills", Inst. of Materials, Minerals and Mining, London, UK, 87–106, https://doi.org/10.13140/RG.2.1.2534.5125

[411] KIMURA Y., SODANI Y., NISHIURA N., IKEUCHI N., MIHARA Y., 2003, *Analysis of chatter in tandem cold rolling mills*, J. of Iron and Steel Institute of Japan (ISIJ International), 43(1), 77–84, https://doi.org/10.2355/isijinternational.43.77

[412] WIERCIGROCH M., BUDAK E., 2001, *Sources of non-linearities, chatter generation and suppression in metal cutting*, Philosophical Trans. of the Royal Society of London, Math., Phys. & Eng. Sc., 359, 663–693, https://doi.org/10.1098/rsta.2000.0750

[413] FARLEY T.W.D., ROGERS S., NARDINI D., 2006, *Understanding mill vibration phenomena*, Proc. of Int. Conf. "Vibration in rolling mills", Inst. of Materials, Minerals and Mining, London, UK, 9 Nov, 5–10.

[414] DONGPING H., HUIDONG X., WANG T., REN Z., 2020, *Nonlinear time-delay feedback controllability for vertical parametrically excited vibration of roll system in corrugated rolling mill*, Metall. Res. Technol., 117, 210, https://doi.org/10.1051/metal/2020020

[415] GOLOVANOV P.N., STEPANENKO V.V., VERKHORUBOV A.A., PAVLOV S.I., 2002, *Method for determining critical vibrations in strip rolling mills*, Patent RU 2239501C2, B21B 37/00, Severstal, Prior. 2002-12-31.

[416] ANTONOV P.V., ADIGAMOV R.R., ZHILENKO S.V., KOZHEVNIKOV A.V., 2018, *Method for determining occurrence of initial stage of critical vibration in working stand of rolling mill*, Patent RU 2734360C2, B21B 38/00, Severstal, Prior. 2018-12-21.

[417] KROT P.V., PRIKHODKO I.Y., PARSENYUK E.A., PIMENOV V.A., SOLOVYOV K.V., DOLMATOV A.P., AKISHIN V.V., SHALAKHOV S.G., 2008, *Method of diagnosing of sympathitic vibration and control of multi-stand cold rolling mill and device for implementation of diagnosing*, Patent RU 2338609, B21B 37/00, NLMK, Prior. 2007-01-09.

[418] KROT P.V., NIZNIK N.V., 2006, *The problems of development of wear-resistant damping pads for spindles of the strip rolling mills,* Fundamental and Applied Problems of Ferrous Metallurgy, Proc. of the Iron and Steel Institute, NAS of Ukraine, 13, 298–306.

[419] ARTIUKH V., KARLUSHIN S., SOROCHAN E., 2015, *Peculiarities of mechanical characteristics of contemporary polyurethane elastomers,* Procedia Engineering, 117, 933–939, https://doi.org/10.1016/j.proeng.2015.08.180

[420] KROT P.V., 2009, *Transient torsional vibrations control in the geared drivetrains of the hot rolling mills,* 3rd IEEE Multi-conference on Control Appl. (CCA) and Intel. Control (ISIC) – MSC 2009, 1368–1373, https://doi.org/10.1109/CCA.2009.5280933

[421] KAWALEK A., DYJA H., KNAPINSKI M., BANASZEK G., KWAPISZ M., 2014, *Analysis of the asymmetric plate rolling process in the finishing stand 3600,* Archives of Metallurgy and Materials, 59(4), 1533–1538, https://doi.org/10.2478/amm-2014-0259

[422] SEO J.H., TYNE van C.J., MOON Y.H. (2016), *Prediction of turn down warping during hot plate rolling based on a Gaussian function,* Int. J. Mater. Form., 9, 705, https://doi.org/10.1007/s12289-015-1261-8

[423] KNIGHT C.W., HARDY S.J., LEES A.W., BROWN K.J., 2005, *Influence of roll speed mismatch on strip curvature during the roughing stages of a hot rolling mill,* J. Mater. Process Technology, 168, 184–188, https://doi.org/10.1016/j.jmatprotec.2004.09.094

[424] PHILIPP M., SCHWENZFEIER W., FISCHER F.D., WÖDLINGER R., FISCHER C., 2007, *Front end bending in plate rolling influenced by circumferential speed mismatch and geometry,* J Mater Proc Technology, 184, 224–232, https://doi.org/10.1016/j.jmatprotec.2006.11.027

[425] KIEFER T., KUGI A., 2008, *Model-based control of front-end bending in hot rolling processes,* IFAC Proceedings, 41(2), 1645–1650, https://doi.org/10.3182/20080706-5-KR-1001.00280

[426] ANDERS D., MUNKER T., ARTEL J., WEINBERG K., 2012, *A dimensional analysis of front-end bending in plate rolling applications,* J. Materials Processing Technology, 212, 1387–1398, https://doi.org/10.1016/j.jmatprotec.2012.02.005

[427] KROT P., PRYKHODKO I., RAZNOSILIN V., ZIMROZ R., 2020, *Model based monitoring of dynamic loads and remaining useful life prediction in rolling mills and heavy machinery,* [in:] A. Ball, L. Gelman, B. Rao (eds.), Advances in Asset Management and Condition Monitoring. Smart Innovation, Systems and Technologies, Springer, Cham, 166, 399–416, https://doi.org/10.1007/978-3-030-57745-2_34

[428] TINGA T., LOENDERSLOOT R., 2019, *Physical model-based prognostics and health monitoring to enable predictive maintenance,* [in:] Lughofer E., Sayed-Mouchaweh M. (eds.),

Predictive Maintenance in Dynamic Systems, Springer, Cham, 313–353, https://doi.org/10.1007/978-3-030-05645-2_11

[429] ONISHCHENKO V., 2008, *Tooth wear modeling and prognostication parameters of engagement of spur gear power transmissions,* Mechanism and Machine Theory, 43(12), 1639–1664, https://doi.org/10.1016/j.mechmachtheory.2007.12.005

[430] LEE H.-S., LEE Y.-S., 2008, *Optimal contact design and allowable limit on spindle assembly of aluminum hot rolling process,* J. of Mech. Sc. and Techology, 22, 240–246, https://doi.org/10.1007/s12206-007-1111-9

[431] ANTSUPOV A.V., 2019, *Model of failure due to wear process for mill rolls universal spindle couplings,* [in:] A. Radionov, O. Kravchenko, V. Guzeev, Y. Rozhdestvenskiy (eds.), Proc. of the 4th Int. Conference on Industrial Engineering (ICIE 2018), Lecture Notes in Mechanical Engineering. Springer, Cham, 1339–1346, https://doi.org/10.1007/978-3-319-95630-5_141

This book contains results of the theoretical and experimental research of mining and metallurgical machines aimed at developing new methods for condition monitoring, active vibration damping and process control. The main goals are to reduce machine dynamics, avoid abrupt failures, predict resonance phenomena and provide process stability, estimate the remaining useful life of elements, and diminish operational and maintenance costs.

Instead of the usually used data-driven approach, the proposed methodology is based on several known classes of dynamical models, of which some appropriate ones have been implemented for certain types of industrial machines and technological processes (articulated loaders and dump trucks, sieving screens, hydraulic machines, different steel rolling mills). The standard vibration sensors are used and in parallel special instrumentation is developed and tested for wireless torque monitoring and backlash measurement in the drivelines of machines.

The main idea of research is to use the non-stationary regimes, which excite natural modes of vibrations in multibody systems, and apply transient signals processing in conjunction with modal analysis for diagnosing wear of main elements, namely, angular backlashes in drivelines, radial clearances in the bearings, stiffness changes in supports and loosening of bolted joints. The influence of nonlinearities on the machine dynamics is highlighted including statistical distribution analysis and spectral representation of loads. The nonlinear features of multibody systems are utilised as the diagnostic parameters, which provide robustness to external non-Gaussian noise and impulsive disturbances.

The developed model-based condition monitoring and diagnostics methodology is realized in online computerized maintenance management systems and process automation implemented in different industrial plants.

Wydawnictwa Politechniki Wrocławskiej
są do nabycia w sprzedaży wysyłkowej:
zamawianie.ksiazek@pwr.edu.pl
ISBN 978-83-7493-279-0